Nils Trapp

Novel Salts of Weakly Coordinating Perfluorinated Alkoxyaluminate Anions and their Parent Lewis Acids – Design, Synthesis and Possible Applications

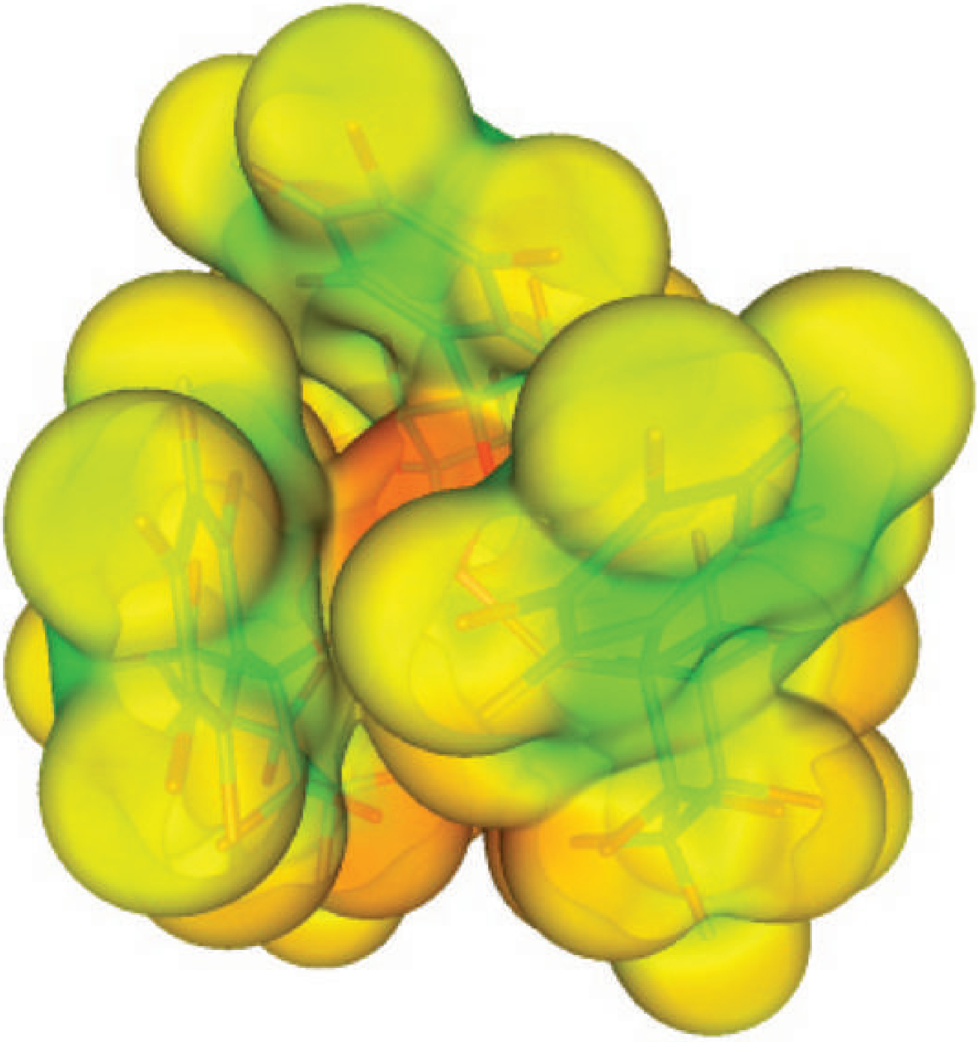

Cuvillier Verlag Göttingen

Novel Salts of Weakly Coordinating Perfluorinated Alkoxyaluminate Anions and their Parent Lewis Acids - Design, Synthesis and Possible Applications

INAUGURALDISSERTATION

Zur Erlangung des akademischen Grades eines

Doktors der Naturwissenschaften (Dr. rer. nat.)

der Fakultät für Chemie, Pharmazie und Geowissenschaften
an der Albert-Ludwigs-Universität zu Freiburg

vorgelegt von

Dipl. Chem. Nils Trapp
aus Heidelberg

Juli 2008

Bibliografische Information der Deutschen Nationalbibliothek
Die Deutsche Nationalbibliothek verzeichnet diese Publikation in der Deutschen Nationalbibliografie; detaillierte bibliografische Daten sind im Internet über http://dnb.ddb.de abrufbar.
1. Aufl. - Göttingen : Cuvillier, 2008
Zugl.: Freiburg, Univ., Diss., 2008

978-3-86727-768-6

Die vorliegende Arbeit entstand in der Zeit von April 2004 bis Juli 2008 an der Universität Karlsruhe (TH), der École Polytechnique Fédérale de Lausanne und der Albert-Ludwigs-Universität zu Freiburg im Breisgau unter Anleitung von Prof. Dr. Ingo Krossing.

Dekan:	Prof. Dr. A. Bechthold
Vorsitzender des Promotionsausschusses:	Prof. Dr. R. Schubert
Referent:	Prof. Dr. I. Krossing
Korreferentin:	Prof. Dr. C. Röhr
Datum der Promotion:	30. Oktober 2008

Nonnenstieg 8, 37075 Göttingen
Telefon: 0551-54724-0
Telefax: 0551-54724-21
www.cuvillier.de

1. Auflage, 2008
Gedruckt auf säurefreiem Papier

978-3-86727-768-6

Meinen Eltern gewidmet

Ich möchte an dieser Stelle die Gelegenheit ergreifen, den Kollegen und Freunden herzlich zu danken, die zum Gelingen dieser Arbeit beigetragen haben:
I would like to take the opportunity to sincerely thank the colleagues and friends who contributed to this work:

Meinem Doktorvater Prof. Ingo Krossing für die fortwährende Unterstützung, interessante Aufgabenstellung und die großen Entscheidungsfreiräume, die er mir gewährt hat.

Meiner Auszubildenden Kristin Guttsche für ihre Hilfe bei experimentellen Arbeiten und den guten Geist in meinem Labor.

Den Praktikanten Thorsten Walther, Hannes Böhrer, Peter Reiser, Anna Lehner und Raimund Rother für ihre Beiträge zu den experimentellen Teilen dieser Arbeit.

Den wissenschaftlichen Mitarbeitern des Arbeitskreises Krossing, insbesondere Dr. Ines Raabe, Dr. Marcin Gonsior, Dr. Lutz Müller, Dr. Andreas Reisinger, Dr. Werner Deck, Dr. Harald Scherer, Dr. Gunther Steinfeld, Petra Klose, Fadime Bitgül und Katrin Wagner für ihre Hilfe und das gute Arbeitsklima.

Den Kollegen der Arbeitskreise Schnöckel (Karlsruhe), Fenske (Karlsruhe), Röhr (Freiburg), Hillebrecht (Freiburg), Janiak (Freiburg) und Merbach (Lausanne) für das angenehme Arbeitsklima.

Dr. Daniel Himmel und Dr. John Slattery für wissenschaftliche Anregungen und zahlreiche Diskussionen.

Tobias Köchner und Philipp Eiden, die mich sehr entlastet haben. Tobias zusätzlich für die erfolgreiche Fortführung der Chemie mit meinen Anionen.

Dr. Gregor Stösser, der mir alles über Linux beigebracht hat.

Vera Bruksch, Gerda Probst, Monika Kayas, Sylvia Soldner und Christina Zamanos-Epremian für Hilfe mit der Bürokratie.

Den Mitarbeitern der Haustechnik und Werkstätten in Karlsruhe, Lausanne und Freiburg für die Anfertigung teilweise komplexer Spezialgeräte sowie zahlreiche Reparaturen, insbesondere Bernd Schucker, Roger Ith, Renato Bregonzi, Harald Große, Markus Melder und Christian Roll.

Bernd Herold und Albert Mörder für die zuverlässige Versorgung mit flüssigem Stickstoff und unzähliges mehr.

Den Glasbläsern Tim Oelsner, Kalam Keilhauer und Peter Neuenschwander für die Anfertigungen und Reparaturen unzähliger Spezialglasgeräte.

Patrick Favre und Klaus Bickel für die Anfertigung und Reparatur von Elektrogeräten.

Den Mitarbeitern der Chemikalienausgaben Jacques Gremaud, Gabi Kuhne, Gladys Pache, Giovanni Petruzzi, Friedbert Jerg, Berthold Lenhard und Monika Völker für den schnellen und zuverlässigen Service.

Dr. Harald Scherer, Prof. Lothar Helm, Dr. Manfred Keller, Dr. Eberhard Matern, Sibylle Schneider und Helga Berberich für die Aufnahme von NMR-Spektren, Hilfe bei der Interpretation, sowie die Einführung in die Methode.

Petra Hauser, Boumahdi Benkmil und Dr. Rosario Scopelliti für die Durchführung von Röntgenstrukturanalysen. Prof. Gervais Chapuis und seinen Mitarbeitern für die Vermittlung der Grundlagen. Prof. Caroline Röhr für ein offenes Ohr und ihre Hilfe bei Diffraktometer- und Kristallstruktur-Problemfällen. Dr. Lee Daniels und Dr. Nav Dhaliwal (Rigaku) für ihre Hilfe bei Problemen mit CrystalClear. Dr. Michael Ruf (Bruker AXS) für seine Hilfe mit der APEX-II Suite.

Dr. Stuart Hayes und Dr. Raphael Berger für GED Untersuchungen meiner Alkohole.

Prof. Ivo Leito und seinen Mitarbeitern für die Bestimmung von Gasphasenaciditäten.

Den Mitarbeitern von Prof. Reinhard Ahlrichs und Cosmologic für Unterstützung bei Problemen mit TURBOMOLE, insbesondere Dr. Dmitrij Rappoport und Dr. Uwe Huniar. Dr. Egbert Keller für SCHAKAL und Prof. Louis Farrugia für ORTEP.

Dr. Daniel Himmel, Tobias Köchner, Dr. Harald Scherer und Eva Trapp für das Korrekturlesen dieser Arbeit.

Meinen Kommilitonen und Assistenten Ari, Betti, Ben, Christian, Ralf, Jens, Kai, Sonja, Michael, Simon, Andi, Christoph, Patrick, Robert, Ulf, Jochen, Gregor, Daniel, Tom, Olli, Kalle, Simone, Aneta, Julia und Melanie für die schöne Studienzeit und die daraus entstandene Freundschaft.

Meinen Eltern und meiner Schwester Eva für die großartige Unterstützung während des Studiums und der Promotion.

Table of contents

1. Chemistry with weakly coordinating anions - Introduction and overview

"Begin at the beginning," the King said, very gravely, "and go on till you come to the end: then stop."

A very important aspect in the field of chemistry deals with understanding the fundamental nature of interactions between atoms, ions and molecules. While quantum chemical simulations often deliver reliable predictions and are already quite cost-effective, larger systems or systems containing weak interactions still pose problems. For example, it is unimaginable to run molecular dynamics simulations with highly flexible basis sets on the coupled cluster level of theory, simply because the memory and time requirements cannot be met by modern computers. Thus, chemical experiments are necessary because of hardware limitations and inaccuracies in the models. The work of experimentalists is needed to shed some light on selected systems in order to improve the theories.

Among these systems are highly electrophilic cations or complex cations that are held together by extremely weak interactions. These can often be observed in the gas phase in a mass spectrometer, in a solid argon matrix, or predicted by ab-initio calculations. The challenge posed to the synthetic chemist by spectroscopists and theoreticians is to reproduce their results under laboratory conditions, thereby checking if the models are feasible. Pushing the boundaries is not only of academic interest, but makes syntheses of so far inaccessible reactive species possible that could find their way into practical applications. Some prominent examples include the $C(CH_3)_3^+$ cation[1-3] and the halocarbonium ions CX_3^+,[4-7] which are well known in the gas phase[8-10] and could recently be fully characterized in solution by NMR and in the solid state by X-ray diffraction with the help of weakly coordinating anions. An example for a weakly bound Lewis-acid-Lewis-base complex cation is $[Ag(P_4)_2]^+$. This ion has been characterized in 1995 through mass spectrometry, and subsequent calculations predicted a minimum geometry with η^1 coordination of the P_4 units.[11] However, this is not true in the solid state, as could be shown by the crystal structure of a salt of the same cation, in which P_4 is η^2-coordinated.[12, 13] This example shows that conclusions drawn from gas phase studies should be validated in the solid state, if possible.

Further spectacular results, many of which have found their way into modern textbooks, include the stabilizations of cations like Xe_2^+,[14] N_5^+[15] and HC_{60}^+[16].

It becomes clear that such cations must be partnered with a suitable anion that is ideally non-coordinating and not distorting the cation´s geometry. Unfortunately, true non-coordination is not possible, because any confined system must be charge-neutral. For every positive charge created, an equal negative charge must exist somewhere; everybody intuitively understands that opposed charges interact with each other. Yet it is possible to find anions which help to replace few strong cation-anion interactions by many very weak ones, ideally placing the cation in a field of weak interactions that mostly cancel each other out. These are called "*w*eakly *c*oordinating *a*nions" (WCAs) and are sometimes also referred to as "spectator anions" because ideally, they play no role in reactions of their partner cation. To be weakly coordinating, an anion must possess a very low nucleophilicity and basicity. A high stability versus oxidation and strong electrophiles is necessary to prevent degradation, thus the WCA should be formed of chemically robust moieties. Finally, its negative charge should be delocalized over a large surface, because sites that offer a significantly higher charge concentration than the rest of the surface would be primary locations of electrophilic attack.

Several classes of weakly coordinating anions are known, which shall be briefly introduced in the following sections along with a short description of their suitability for various applications.

Fluorometallate anions

Anions of the type $[MF_6]^-$ (M = Sb, As) can be introduced by metathesis with their Li^+ or Ag^+ salts, which are prepared by reacting M_2O_3 with bromine trifluoride and LiF or AgF.[17] A more practical approach is the in situ generation of fluoride bridged fluorometallates, as MF_5 are among the strongest Lewis acids; in weakly basic media like anhydrous HF, SO_2, SO_2ClF or SbF_5, larger and less coordinating oligomeric species of the general type $[M_nF_{5n+1}]^-$ can be directly obtained by fluoride abstraction (Fig. 1). The $[As_2F_{11}]^-$ anion has been known for a long time, but was only recently structurally verified.[18-22]

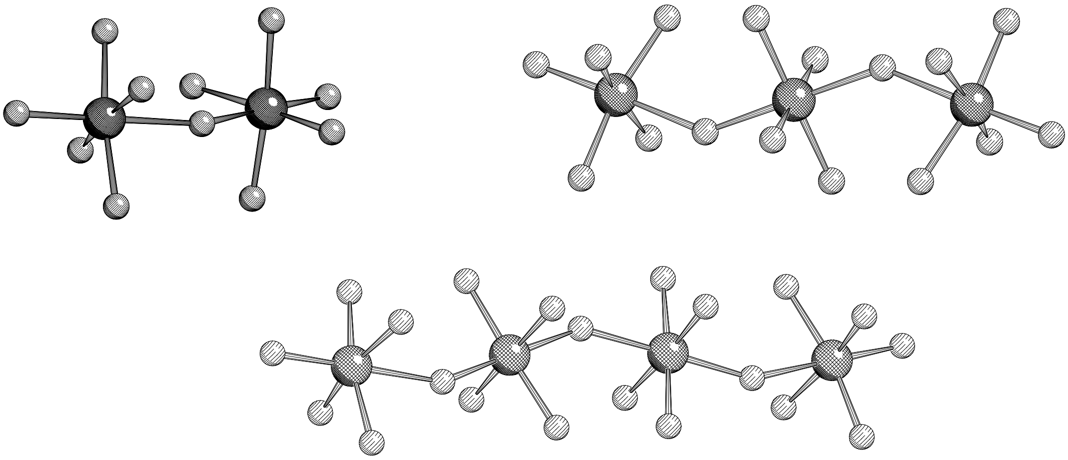

Fig. 1: Structures of $[Sb_2F_{11}]^-$ (top left), $[Sb_3F_{16}]^-$ (top right) and $[Sb_4F_{21}]^-$ (below).

Anions of this type are very robust against decomposition and a variety of extremely electrophilic cations could be stabilized with their help, including Br_2^+[23] and Xe_2^+[14], as well as weakly bound adducts like $[Au(Xe)_n]^+$ (n = 1, 2, 4).[24, 25] However, $[M_nF_{5n+1}]^-$ salts can only be handled in specialized fluorine laboratories, restricting application to the elucidation of textbook cations. Furthermore, $[M_nF_{5n+1}]^-$ exist in solution only as mixtures with varying n (1-4), leading to difficulties during crystallization. The free Lewis acids MF_5 act as strong oxidizing agents, which may give rise to unwanted side reactions.

Borate and related anions

Another type of WCAs consists of boron-centered anions, which can be very stable because boron forms very strong B-C bonds with a large variety of ligands. Among the most well-known complex anions in this class are tetrafluoroborate $[BF_4]^-$ and tetraphenylborate $[BPh_4]^-$. Both are strongly coordinating and suffer from a low stability; $[BF_4]^-$ tends to decompose into F^- and BF_3 and $[BPh_4]^-$ is prone to hydrolysis.[26, 27] These problems can be overcome if fluorinated groups are introduced as in the $[B(C_6F_5)_4]^-$[28] and $[BAr^F_4]^-$ ($Ar^F = C_6H_3$-3,5-$(CF_3)_2$)[29, 30] anions (Fig. 2); several salts of both are commercially available. Especially the $[BAr^F_4]^-$ anion is widely used, e.g. in homogenous catalysis.[31]

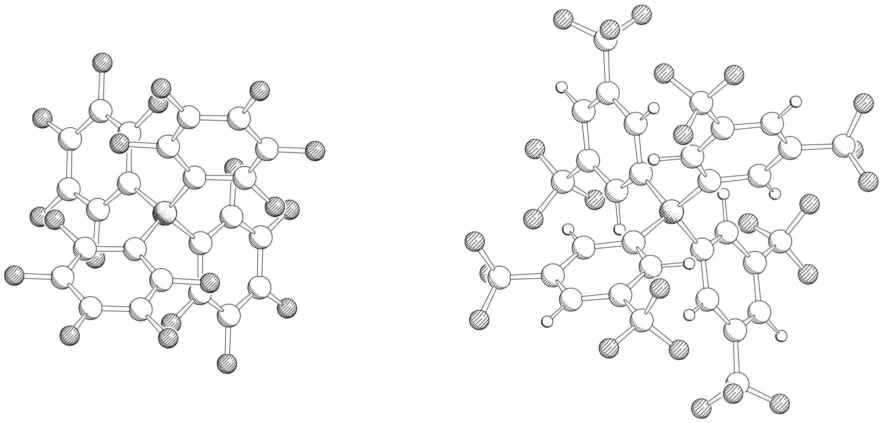

Fig. 2: Structures of the $[B(C_6F_5)_4]^-$ (left) and $[BAr^F{}_4]^-$ ($Ar^F = C_6H_3$-3,5-$(CF_3)_2$, right) anions.

The ligands can be modified to achieve higher stability, weaker coordination and better solubility in unpolar solvents, resulting in anions like $[B((C_6H_3)\text{-}3,5\text{-}(R^F)_2)_4]^-$ (R^F = perfluorinated alkyl group),[32, 33] $[B(C_6F_4(CF_3))_4]^-$,[34] $[B(C_6F_4(Si(^iPr)_3))_4]^-$,[35, 36] $[B(C_6F_4(SiMe_2{}^tBu))_4]^-$[35, 36] or $[B(C_6F_4(CF(C_6F_5)_2)]^-$.[37] It is also possible to exchange the boron atom for aluminum or gallium, but the resulting anions are very unstable versus hydrolysis, and the aluminum species tend to be explosive.[38] Another approach is to react the parent Lewis acid $B(C_6F_5)_3$ with a strong nucleophile X^- like CN^-[39], NH_2^-[40], or $C_3N_2H_3$[41] to obtain boron-bridged anions of the type $[X(B(C_6F_5)_3)_2]^-$ (Fig. 3), which are very stable and easily prepared.

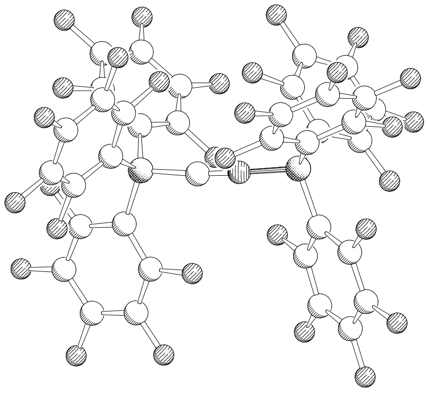

Fig. 3: Structure of the $[(F_5C_6)_3B(\mu\text{-}CN)B(C_6F_5)_3]^-$ anion.

Smaller borate anions include $[FB(CF_3)_3]^-$[42-45], $[B(CF_3)_4]^-$[46-48] and tetracyanoborate $[B(CN)_4]^-$[49, 50] (Fig. 4), the latter being able to stabilize $[C_6F_5Xe]^+$.[49] $[B(CF_3)_4]^-$ is very stable (against Na in liquid ammonia and against elemental fluorine in anhydrous HF) and its coordinative strength is small enough to form $[Ag(CO)_n]^+[B(CF_3)_4]^-$ (n = 3, 4) from the silver salt at high CO pressure.[46]

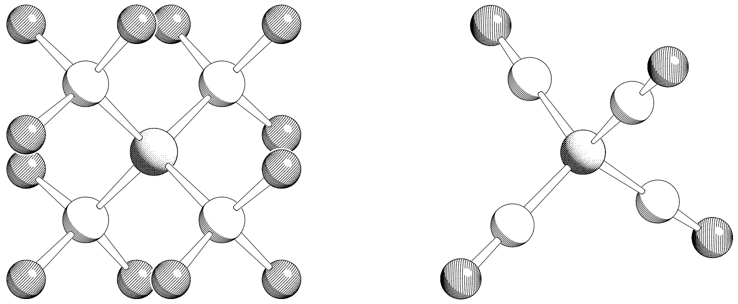

Fig. 4: Structures of the $[B(CF_3)_4]^-$ (left) and $[B(CN)_4]^-$ (right) anions.

Alkoxy- and aryloxymetallates

Similar in structure to the borate anions are metallates of the general formula $[M(OR^F)_n]^-$ (Fig. 5, R^F = poly- or perfluorinated alkyl or aryl group, M = Al^{III}, Nb^V, Ta^V, Y^{III}, La^{III}).[51-56]

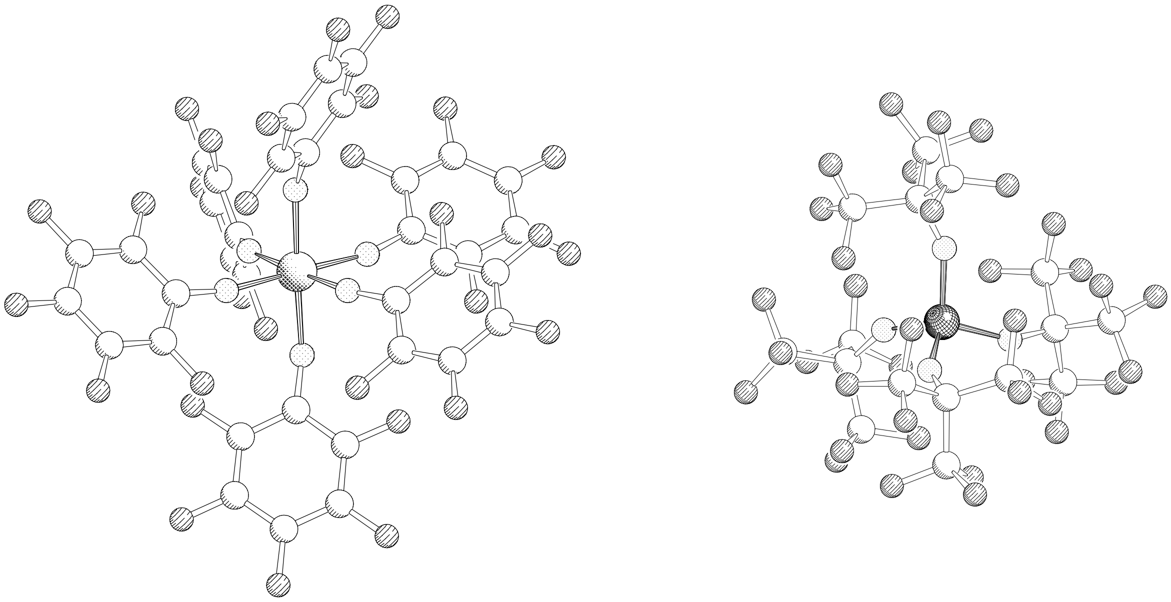

Fig. 5: Structures of $[Nb(OC_6F_5)_6]^-$ (left) and $[Al(OC(CF_3)_3)_4]^-$ (right).

Salts of $[M(OR^F)_n]^-$ are easily accessible even in larger scales. Some of these anions have successfully been tested as counterions in cationic polymerization reactions.[34, 57, 58] Especially the introduction of sterically demanding ligands like $OC(CF_3)_3$, $OC(CH_3)(CF_3)_2$ or $OCH(CF_3)_2$ has lead to alkoxyaluminate anions that are well suited for many purposes.[53, 54] $[Al(OC(CF_3)_3)_4]^-$ is among the most weakly coordinating anions currently known (due to the high number of peripheral C-F bonds), comparable with the carboranate $[CB_{11}(CF_3)_{12}]^-$ (cf. later in this chapter), which has the disadvantage of being explosive and suffers from an extremely tedious synthetic route with low yields.[59] The Li^+ salt of the aluminate is available in 100 g scale with over 95 % yield from commercially available starting materials and is even stable in water and boiling aqueous nitric acid (35 weight %).[53] This high stability arises from the steric shielding of the basic oxygen atoms by the bulky ligands with perfectly interlocking $-CF_3$ groups and the electronic stabilization resulting from perfluorination. Consequently, the $[Al(OC(CF_3)_3)_4]^-$ anion can be used to stabilize very reactive cations like $[H(OEt_2)_2]^+$,[60] CI_3^+,[4] $[Ag(P_4)_2]^+$,[12] PX_4^+, $P_2X_5^+$, $P_5X_2^+$ (X = Br, I),[61, 62] $AsBr_4^+$[63] and many more. In analogy to the bridging in $[M_nF_{5n+1}]^-$ and some borates, the stability is further improved in the fluoride-bridged $[F\{Al(OC(CF_3)_3)_3\}_2]^-$ anion (Fig. 6), in which the negative charge is distributed across 54 peripheral C-F bonds.[64] This species was first discovered as a decomposition product from $[Al(OC(CF_3)_3)_4]^-$ in reactions with very reactive cations like PX_2^+ (X = Cl, Br, I),[62, 65] but can also be synthesized directly in a planned synthesis in 100 g scale. As will be discussed later in this chapter, the increase in size also induces a lower coordinative strength compared to $[Al(OC(CF_3)_3)_4]^-$. Alkoxyaluminate anions of various types were almost exclusively used in the practical work presented in this thesis, and some of their characteristics will be described in more detail in later chapters.

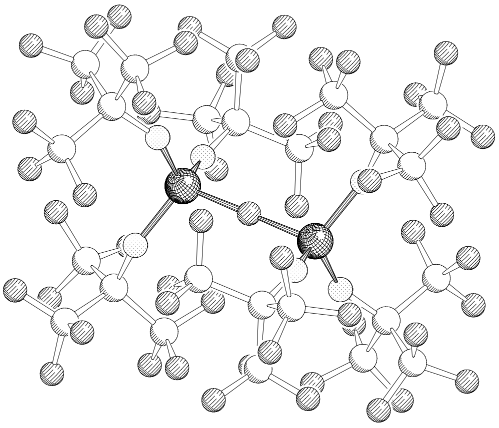

Fig. 6: Structure of the fluoride-bridged $[F\{Al(OC(CF_3)_3)_3\}_2]^-$ anion.

Carboranate anions

Carboranates are formally derived from the closo-boranates $[B_{12}H_{12}]^{2-}$ by replacing one B-H unit with C-H, thereby reducing the negative charge by one. The charge in the resulting $[CB_nH_{n+1}]^-$ anions is very well-delocalized over the polyhedron, and the exohedral B-H bonds are already very stable and weakly coordinating. However, these anions are prone to oxidation. This problem can be overcome by substitution of H atoms with halogen atoms, methyl or trifluoromethyl groups, which also decreases the coordinative strength. Among the resulting anions of the general formula $[CB_{11}X_nH_{12-n}]^-$ (Fig. 7; n = 0-12, X = F, Cl, Br, I, CF_3, CH_3)[59, 66-71] are the most robust and weakly coordinating anions known today, as shown by some of the extremely reactive species they are able to stabilize: $[Mes_3Si]^+$ (Mes = 2,4,6-trimethylphenyl),[72] $[Me_3Si]^+$,[73] $H_5O_2^+$,[74] C_{60}^+, HC_{60}^+,[16, 75] $C(CH_3)_3^+$,[2] protonated benzene[76] and toluene.[77] $H[CHB_{11}Cl_{11}]$[78] is currently the strongest published isolable Brønsted acid, possibly only surpassed by its perfluorinated analog $H[CHB_{11}F_{11}]$.[79, 80]

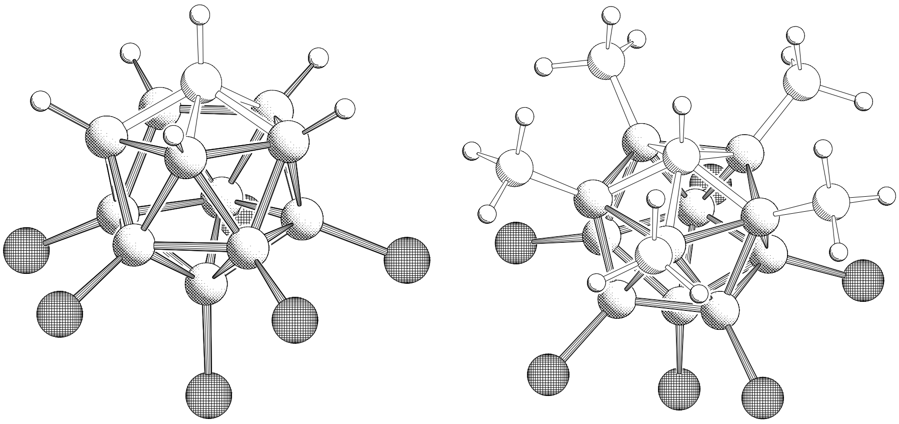

Fig. 7: Structures of $[CB_{11}H_6Cl_6]^-$ (left) and $[CB_{11}Me_5Cl_6H]^-$ (right).

It is possible to introduce up to five ethyl substituents to $[CB_{11}H_{12}]^-$[81] or an alkyl group in the 1-position of perfluorinated carboranes.[79] $[1\text{-Et-}CB_{11}F_{11}]^-$ (Fig. 8) is currently the least coordinating chemically robust carboranate, as shown by the extreme low-field ^{29}Si-NMR shift of its $[Si^iPr]^{\delta+}$ derivate.[67] Consequently, it can be used to stabilize extremely unstable cations like the non-classical carbonyls $[M(CO)_n]^+$ (M = Rh, Cu; n = 1-4)[71, 82] or $[Me_3Si]^+$.[83] The $[1\text{-Et-}CB_{11}F_{11}]^-$ salt of the latter obeys the definition of an ionic liquid with a melting point of 75 °C and a conductivity of 2.5 m S cm^{-1}; the melt is even stable up to 220°C.

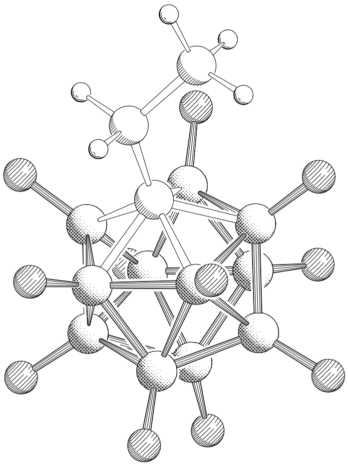

Fig. 8: Structure of the $[1\text{-Et-CB}_{11}F_{11}]^-$ anion.

$[1\text{-Et-CB}_{11}F_{11}]^-$ is surpassed in its low coordinative strength by $[CB_{11}(CF_3)_{12}]^-$,[59] which is explosive due to steric crowding of the CF_3 substituents and the energy gain associated with B-F bond formation.

Carboranates of the various types are obviously very well-suited for the elucidation of textbook cations, yet they suffer from extremely expensive and time-consuming syntheses with very low yields (in many cases < 2%), severely limiting their range of applications.

Teflate-based anions

Substitution of fluorine in $[BF_4]^-$ or $[MF_6]^-$ with -OTeF_5 ligands leads to the larger and more robust teflate anions $[B(OTeF_5)_4]^-$[49, 84] and $[M(OTeF_5)_6]^-$ (M = As,[85] Sb,[86, 87] Bi,[85] Nb).[86, 88] The negative charge in these anions is delocalized over 20, respectively 30 fluorine atoms (Fig. 9).

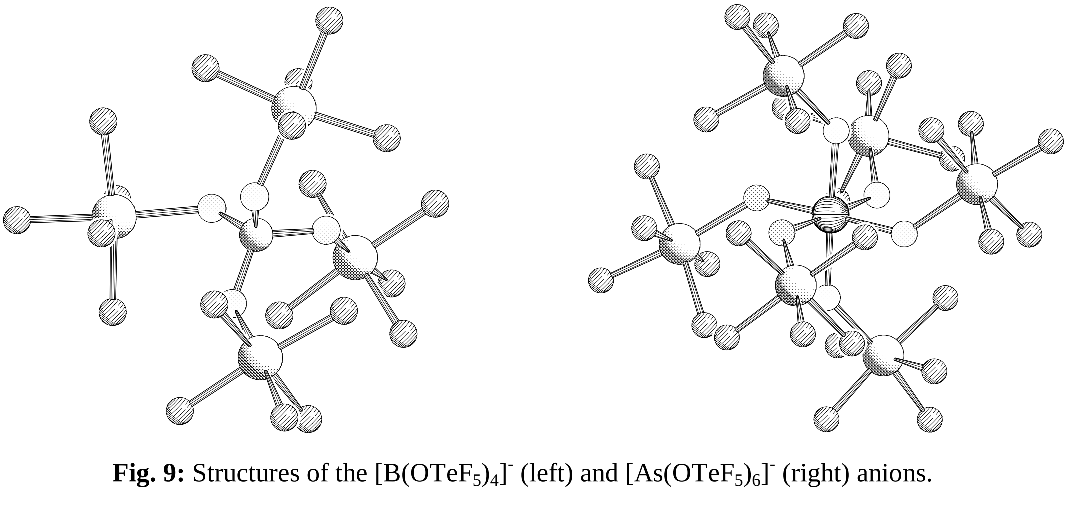

Fig. 9: Structures of the $[B(OTeF_5)_4]^-$ (left) and $[As(OTeF_5)_6]^-$ (right) anions.

The pentavalent metallates appear to be more stable than $[B(OTeF_5)_4]^-$, which slowly loses a ligand in the presence of Ag^+ or Tl^+ under formation of silver/thallium teflate and volatile $B(OTeF_5)_4$.[84] All teflate anions are decomposed by even small traces of water, making synthesis difficult. For the same reason they are unsuitable for many applications like catalysis; but the borate, arsenate and antimonite anions were used successfully in the stabilization of metal ion adducts with weak Lewis bases, such as $[Ag(CO)_2]^+$[89] and reactive cations like CX_3^+(X = Cl, Br, $OTeF_5$),[90] $[XeOTeF_5]^+$[90], AsX_4^+[91] and SbX_4^+ (X = Cl, Br).[92]

Sulfonated imides and methanides ("triflimides" and "triflides")

The triflimides $N(SO_2F)_2^-$ and $N(SO_2CF_3)_2^-$, which are derived from the corresponding amines,[93, 94] along with the analogous triflides $[C(SO_2F)_3]^-$ and $[C(SO_2CF_3)_3]^-$[95, 96] (Fig. 10), are often used in electrochemical applications.[97-100] They are chemically very robust, stable in water[101] and prove to be very good counterions in many catalytic reactions, such as electrophilic aromatic substitutions (acylations or nitrations),[102-104] or Diels-Alder reactions.[105-107]

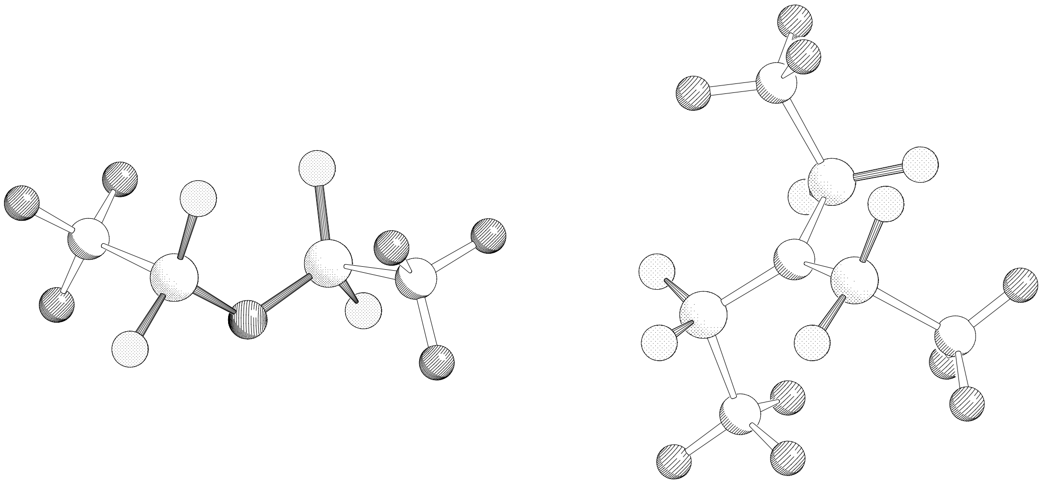

Fig. 10: Structures of $N(SO_2CF_3)_2^-$ (left) and $C(SO_2CF_3)_3^-$ (right).

Since strong coordination with the oxygen atoms limits their suitability for many catalytic reactions and for the stabilization of reactive cations, the most promising field of their application is probably chemistry in and with ionic liquids (cf. later in this chapter).[100, 108, 109]

Possible future candidates for WCAs

There are some candidates for WCAs that do not fit into any of the preceding categories. Some of them have even been discovered as unexpected side products, such as the surprisingly stable $[Ag(CF_3)_4]^-$ anion (Fig. 11),[110-114] or the similar $[Ag(CF_2H)_4]^-$,[115] which can also be obtained in a directed synthesis as Ag(I) salts in good yields.[110, 115] $[Ag(CF_3)_4]^-$ has been known since 1986, but no systematic studies of its suitability as a WCA have been carried out yet. Albeit very small, these anions are weakly coordinating and very robust due to strong electrostatic stabilization by the four CF_3 substituents. Additionally, all ligands interlock perfectly, and the fluorine atoms form two regular hexagons that shield the central silver atom. Although certainly not suitable for large-scale applications, because the silver salts are synthesized through trifluoromethylation of Ag(I) compounds with $Cd(CF_3)_2$ followed by oxidation, this type of anion may well prove to be suitable for the stabilization of unstable cations or for catalysis.

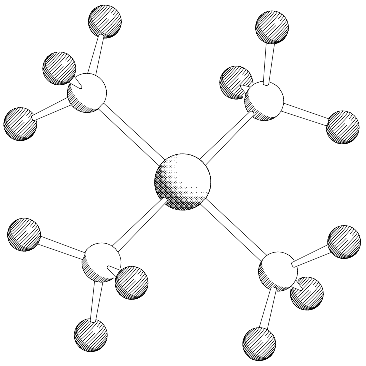

Fig. 11: Structure of the $[Ag(CF_3)_4]^-$ anion.

Other examples of new WCA are oxalates of the type $[B(C_2O_4)_2]^-$,[116-118] $[BF_2(C_2O_4)]^-$[117] $[PF_4(C_2O_4)]^-$[117] and $[P(C_2O_4)_3]^-$ (Fig. 12).[119] Because of their wide electrochemical windows and their high solubility in aprotic solvents, lithium salts of these or related anions find or may soon find their way into application as electrolytes in new Li-ion batteries. The protonated ether salt $[H(Et_2O)_2]^-[P(C_2O_4)_3]^-$ can cheaply and easily be obtained in large scale from oxalic acid and PCl_5 in Et_2O. This compound is a very strong acid and has successfully been tested as a catalyst in Friedel-Crafts reactions. The Li^+ salt can be obtained in a trivial quantitative neutralization with LiH.[119]

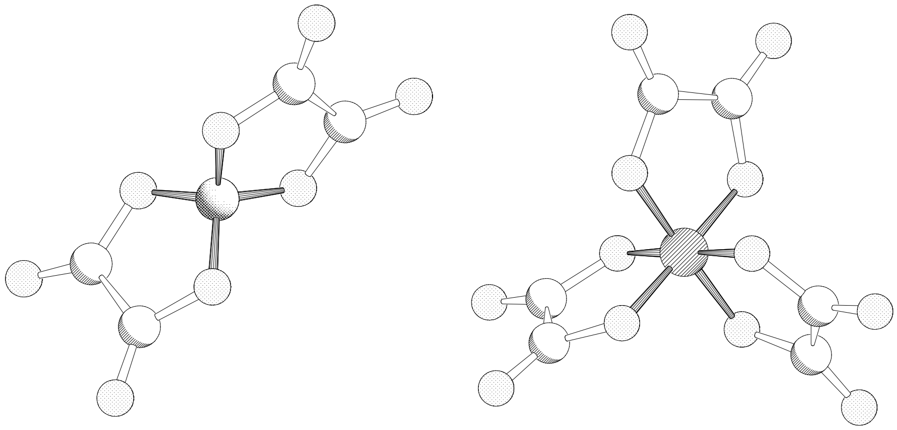

Fig. 12: Structures of $[B(C_2O_4)_2]^-$ (left) and $[P(C_2O_4)_3]^-$ (right).

With so many different WCAs available, the question arises which qualities are needed to stabilize specific target cations, or in other words, to make the anion suitable for a specific application. The quality of WCAs for certain tasks can be judged by some criteria which also allow the chemist to rationalize and plan their design. These concepts, which are based on simple thermodynamic considerations, will be briefly discussed in the following.

The effect of ion size on lattice energy

Comparing the sizes of WCAs, one notices that over time, the focus has shifted towards bigger anions in many applications. But why is a larger size desirable if one wants to minimize ionic interactions? This is due to the fact that the coulombic force is inversely proportional to the square distance of two separated charges:

$$F = \frac{1}{4\pi\varepsilon_0}\frac{q_1 \cdot q_2}{r^2} = \frac{1}{4\pi\varepsilon_0}\frac{z_1 z_2 \cdot e^2}{r^2}$$

(Eq. 1)

q_1, q_2 = point charges; z_1, z_2 = ion charges; r = distance between charges; e = elemental charge;

ε_0 = vacuum permittivity.

From this equation follows the coulomb attractive energy for a 1:1 ion pair in a vacuum as:

$$E = \int_{\infty}^{d} F dr = -\frac{1}{4\pi\varepsilon_0}\frac{z^2 \cdot e^2}{d}$$

(Eq. 2)

z = ion charge; d = contact distance between cation and anion; ε_0 = vacuum permittivity.

For singly charged ions and distances given in pm this amounts to approximately

$$E = -\frac{143730}{d}\, pm \cdot kJ \cdot mol^{-1}$$

(Eq. 3)

This yields a rather drastic effect on the strength of cation-anion interactions, as can be depicted for the simplified case of singly charged anions paired with Li^+ in a vacuum (Fig. 13):

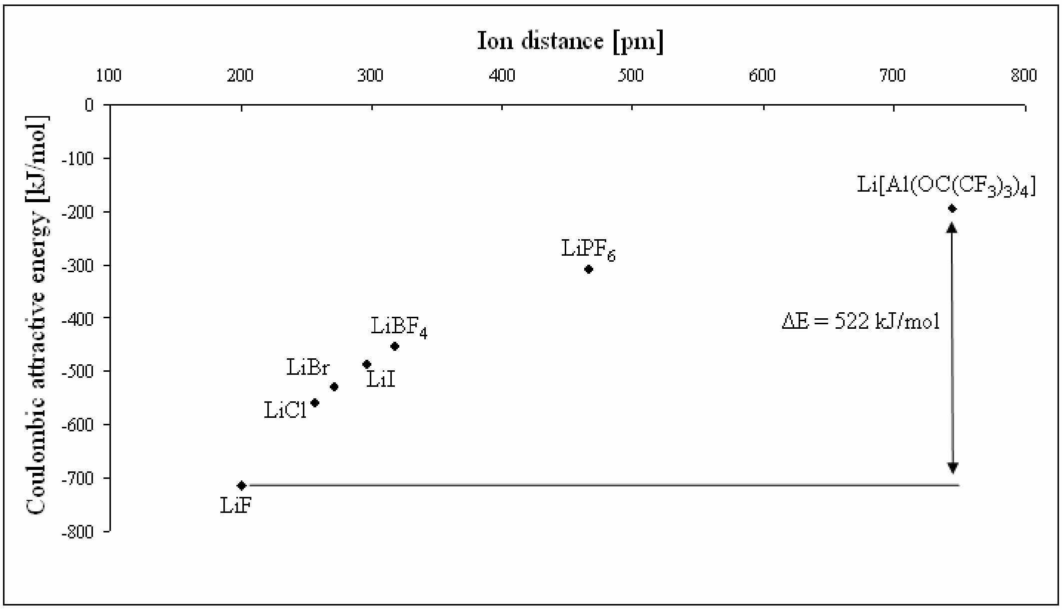

Fig. 13: Calculated dependence of coulomb attraction energy on anion size for ion pairs in the gas phase. Ionic radii have been taken from Shannon´s scale;[120, 121] in the case of the complex anions they were calculated from crystal structures.[52, 122, 123]

Large WCA approach diameters in the nanometer scale ($[Al(OC(CF_3)_3)_4]^-$: 1.25 nm,[53] $[Sb(OTeF_5)_6]^-$: 1.20 nm).[86] Comparing $[Al(OC(CF_3)_3)_4]^-$ with tetrafluoroborate, which can be considered a “classic” WCA, this corresponds to a reduction in coulomb attraction by 258 kJ mol^{-1}. This difference becomes more than twice as large (522 kJ mol^{-1}) in comparison with the strongly coordinating fluoride anion. This is oversimplified because the model completely neglects all condensed phase interactions (e.g. the ionic radius in a crystal lattice is larger than in the gas phase) as well as effects arising from the chemical composition, but it clarifies why size is a major factor in the design of new anions.

In the gas phase in low concentrations, the interaction between different cation-anion pairs can be neglected, which is no longer the case in the solid state. When charges are forced into close contact, strong electrostatic fields influence the interactions of matter. The quantity that describes these interactions is called the lattice potential energy. For a long time, the simple Kapustinskii equation (Eq. 4) has successfully been used to approximate values of the lattice energy for inorganic salts of varying complexity based on thermochemical radii.[124, 125]

$$U_L = -120250 \frac{v \cdot \left|z^+\right| \cdot \left|z^-\right|}{r^+ + r^-}\left(1 - \frac{34.5}{r^+ + r^-}\right) kJ \cdot mol^{-1}$$

(Eq. 4)

U_L = lattice energy; r^+, r^- = cation and anion radii in pm; v = number of ions in the unit cell;

z^+, z^- = cation and anion charges.

Calculated thermochemical radii have been reported for many ions.[126] To get an estimate of the lattice energy for new components, the (r^+ + r^-) term of the Kapustinskii equation can be equated to the shortest anion-cation contact distance found in a crystal structure.[122] If the radius of one of the ions is known, this distance can also be used to calculate the thermochemical radius of the counterion. The Kapustinskii equation has later been generalized by Jenkins, Passmore et. al.,[122] who used empirical parameters obtained from fits on experimental data to correlate U_L directly with the thermochemical volume (Eq. 5).

$$U_L = z^+ \cdot z^- \cdot n \cdot \left(\frac{\alpha}{\sqrt[3]{V_{therm}}} + \beta\right) kJ \cdot mol^{-1}$$

(Eq. 5)

U_L = lattice energy; n = number of ions in the unit cell; z^+, z^- = cation and anion charges;

V_{therm} = thermochemical volume; α,β = empirical constants.

Another empirical approach that works very well, at least for 1:1 salts, is based on molecular volumes and became known as Bartlett´s equation[127] (Eq. 6):

$$\Delta H_L = \left(\frac{232.8nm}{\sqrt[3]{V}} + 110\right) kJ \cdot mol^{-1}$$

(Eq. 6)

ΔH_L = Lattice enthalpy change; V = molecular volume in nm^3.

ΔH_L is the lattice enthalpy change associated with the conversion of the solid into its gaseous ions. This equation can often provide a more convenient prediction of the lattice enthalpy than the original Kapustinskii equation and has the additional advantage of using more fundamental crystallographic parameters, which can help if only powder data is available.

The lattice potential energy of a salt can be calculated from ΔH_L by a simple equation[128] (Eq. 7):

$$U_L(M_pX_q) = \Delta H_L - \left(p\left(\frac{n_M}{2} - 2\right) + q\left(\frac{n_X}{2} - 2\right)\right)RT$$

(Eq. 7)

n_M, n_X = 3 for monatomic ions, 5 for linear polyatomic ions, and 6 for polyatomic nonlinear ions.

This is based on the approximation that the vibrational degrees of freedom are equally excited in both the crystal and the gaseous ions, while applying corrections for rotational degrees of freedom only in the gas phase.

The lattice energy is a major structure-determining factor in the solid state that is at least one order of magnitude stronger than dispersive van-der-Waals or dipole-dipole interactions. Many WCAs have poly- or perfluorinated surfaces, which further diminishes dispersive interactions because fluorine atoms and element-fluorine bonds show a very low polarizability. From eq. 4-6 it becomes clear that an increase in the size of the anion leads to a decrease in lattice energy. For a large weakly coordinating anion, the lattice energy can approach the sublimation enthalpy of a molecular solid of comparable atomic weight. This indicates that the environment of the cation in the WCA´s proximity more closely resembles gas phase conditions or conditions in a molecular solid than the situation in the strong electrostatic field usually found in typical ionic compounds (Tab. 1). Comparing for example the calculated lattice energy of the WCA salt $Ag(S_8)_2^+[Al(OC(CF_3)_3)_4]^-$[129] (M = 1588 g mol^{-1}) of 326 kJ mol^{-1} with that of C_{60} or C_{70} as representatives of molecular solids with large molecular weights, this effect becomes very clear: the fullerenes have lattice energies in the same order of magnitude, namely 175 and 200 kJ mol^{-1}[121, 130, 131] (M = 721 (C_{60}) and 841 (C_{70}) g mol^{-1}).

Tab. 1: Thermochemical volumes and lattice potential energies of several 1:1 salts.

Compound	**V_{therm} [Å^3]**	**U_L [kJ mol^{-1}]**
Li^+F^-	27	1036[a]
Cs^+F^-	43	740[a]
$Cs^+[AsF_6]^-$	128	568[b]
$Li^+[Al(OC(CF_3)_3)_4]^-$	760	361[b]
$Cs^+[Al(OC(CF_3)_3)_4]^-$	776	362[b]
$Ag(S_8)_2{}^+[Al(OC(CF_3)_3)_4]^-$[129]	1169	326[b]

[a] experimental values;[121, 130, 131] [b] calculated from the thermochemical volumes.[122]

The same can be deduced by comparing the lattice energies of Cs^+ and Li^+ salts with the same anions. For CsF and LiF, this difference amounts to 296 kJ mol^{-1}, which results only from cation size, while in Li^+ and Cs^+ salts of the large $[Al(OC(CF_3)_3)_4]^-$ WCA it approaches zero. Generally, large and possibly highly fluorinated weakly coordinating anions provide environments in the solid state that resemble the gas phase closely enough to be called "pseudo gas-phase conditions".[129]

The effect of size on solvation energy

For solvation to occur, energy is required to release individual ions from the crystal lattice, thereby breaking interionic attractions. In other words, the solid´s lattice energy must be overcome through association of ions with solvent molecules. If one wants to approximate gas phase conditions, the solvation energy of a salt should be low. Traditionally, solvation free energies have been calculated with Born´s equation (cf. later in this chapter),[132] which essentially describes the difference between the properties of one mole of ions in an ideal gas and in an ideal solution. As this is dependent on the dielectric constant (relative permittivity) ε_r of the solvent, one has to differentiate between systems of high and low polarity. Salts of smaller anions are often only soluble in highly polar solvents such as water ($\varepsilon_r = 81$), ethanol ($\varepsilon_r = 24$) or acetonitrile ($\varepsilon_r = 35$), whereas WCA salts with larger anions, due to the considerations above, have small lattice energies and thus small solvation free energies. This makes them soluble in less polar solvents like toluene ($\varepsilon_r = 2.4$) or dichloromethane ($\varepsilon_r = 8.9$).[121]

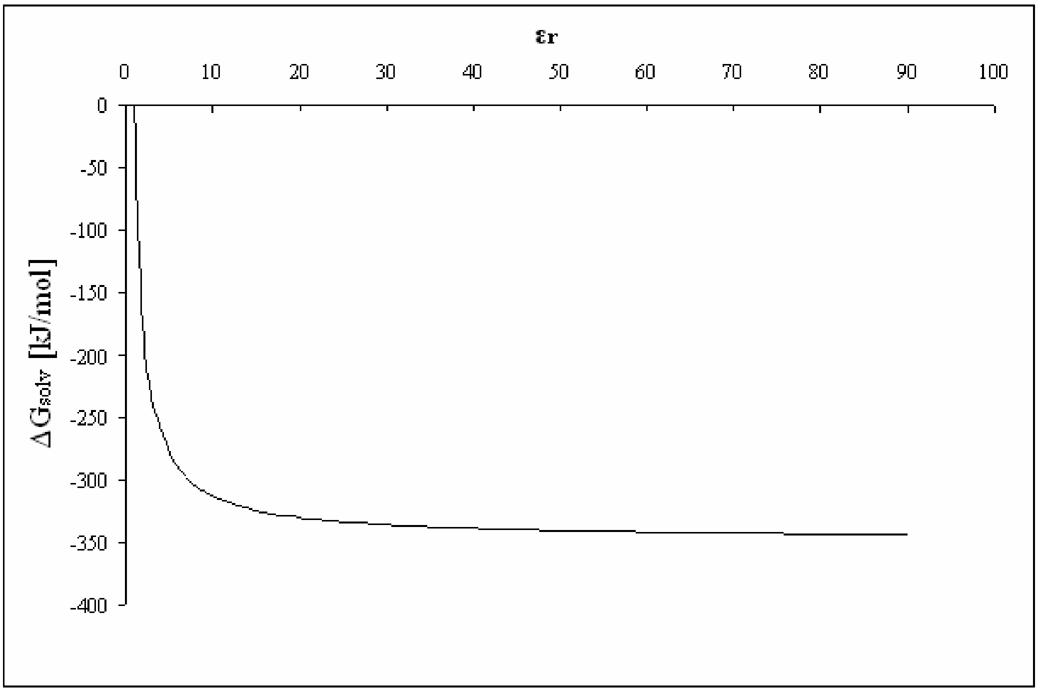

Fig. 14: Plot of the solvation free energy for an univalent ion of radius 200 pm vs. ε_r of the solvent.

As can be seen in Fig. 14, the stabilization of ions by solvation steeply decreases with the dielectricity constant for solvents with $\varepsilon_r < \sim 10$, thereby approximating gas phase conditions. This means the term "pseudo gas-phase conditions" can also be applied to solutions of WCA salts in low dielectric media.[129] It should be noted that the polarity of a solvent is dependent on temperature (Fig. 15). Electrophilic cations are stabilized by polar media, so if the WCA salt of a given cation is not stable at ambient conditions, the polarity can be slightly tuned by a change in temperature.

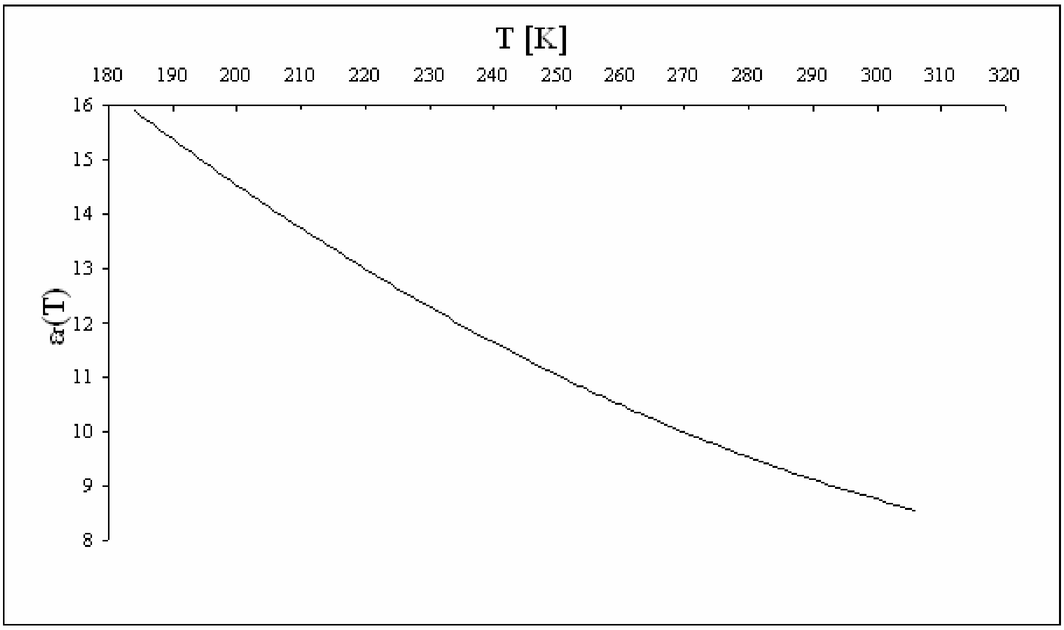

Fig. 15: Dependence of ε_r on temperature for CH_2Cl_2.[121]

The high solubility of WCAs results from their decreased lattice energy. A salt is soluble if the sum of Gibbs free energies of solvation for both the cation and anion exceeds the lattice enthalpy of the salt A^+X^-, as can be depicted by a simple Born-Haber-Fajans cycle (Fig. 16).

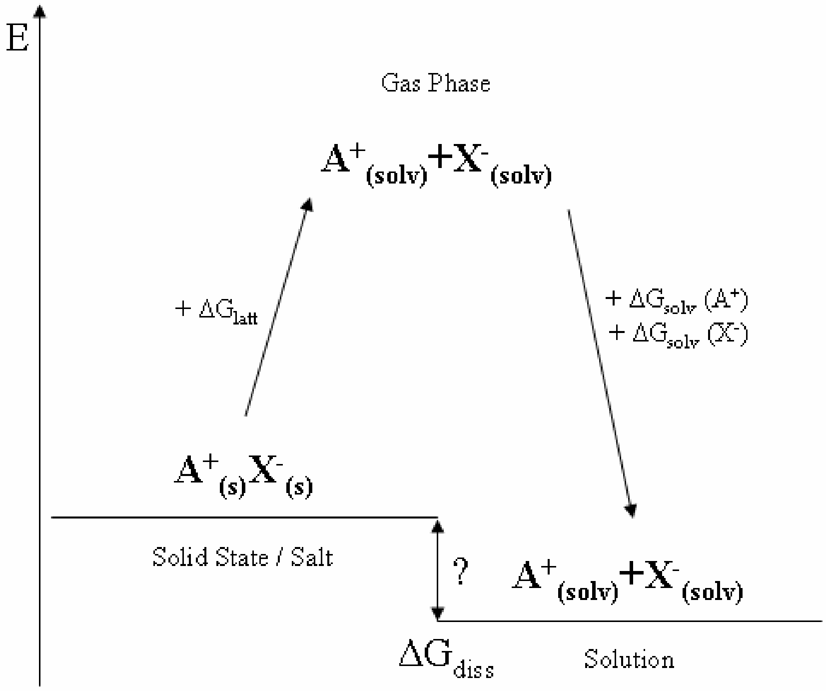

Fig. 16: Born-Haber-Fajans cycle for the dissolution of a soluble salt A^+X^-.

A very large WCA X^- yields a lattice enthalpy that is smaller than the negative sum of Gibbs solvation energies, hence the WCA salt is soluble. As an example, consider a cation A^+ of roughly the size of a K^+ or Ag^+ ion in a solvent with low polarity (r_{K+} = 1.38 Å). The size of the anion X^- is then varied between the size of very small halide anions and large WCAs, and the sum of the Gibbs energies of solvation for the cation and the anions is calculated and compared with the lattice energy (Fig. 17).

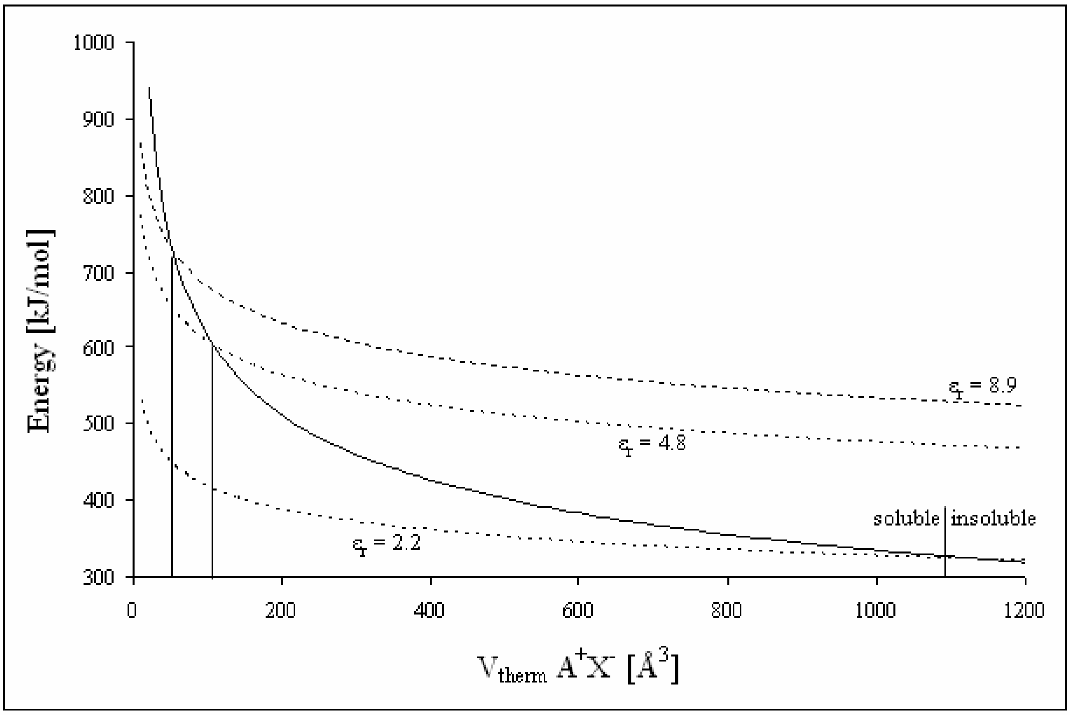

Fig. 17: Lattice energy (solid line) and $-(\Delta G_{solv}(A^+)+\Delta G_{solv}(X^-))$ (dashed lines; at different solvent permittivities) for a salt A^+X^-; $r(A^+)$ kept constant at 1.38 Å). Intersections between solid and dashed lines mark the threshold between solution and precipitation.

In this example, the lattice energy was calculated with the Jenkins-Passmore equation.[122] Lattice energy and Gibbs free energy of solvation are directly compared for simplicity, because the entropic effects are small in the solid state, yielding a negligible error. The Gibbs free energies of solvation for both the anion and the cation were approximated with the Born equation[132] (Eq. 8) for three solvents (toluene, ε_r = 2.4; chloroform, ε_r = 4.8 and dichloromethane, ε_r = 8.9).

$$\Delta G_{solv} = -\left(\frac{z^2 \cdot e^2 \cdot N_A}{8\pi \cdot e_0 \cdot r}\right)\left(1 - \frac{1}{\varepsilon_r}\right)$$

(Eq. 8)

z = ion charge; N_A = Avogadro constant; ε_0 = vacuum permittivity;
ε_r = dielectric constant/relative permittivity of the solvent medium; r = ionic radius.

With all constants and conversion factors considered, the Born equation amounts to approximately

$$\Delta G_{solv} = -694.4 \cdot \frac{z^2}{r}\left(1 - \frac{1}{\varepsilon_r}\right) kJ \cdot mol^{-1}$$

(Eq. 9)

Simplified formula for the Gibbs energy of solvation of an ion; distance r given in Å.

This yields values of -447, -398 and -274 $kJmol^{-1}$ for the cation at ε_r = 8.9, 4.8 and ε_r = 8.9, which were then added to the ΔG_{solv} values of the anion at variable radii. Fig. 17 shows a rapid decline in both the lattice and solvation energies with increasing size of the anion. However, the lattice energy decreases much faster, thus the indicated intersections between lattice and solvation energies are highly sensitive to changes in the anion size. These intersections mark the points of solvation for the different solvents, indicating that an A^+X^- salt of an anion with a volume of approximately 1100 $Å^3$ (cation size neglected) would be soluble in the rather unpolar toluene. For more polar solvents, the minimum anion size can be a lot less (e.g. approximately 60 $Å^3$ in dichloromethane). In agreement, univalent metal salts of $[Al(OC(CF_3)_3)_4]^-$ (V_{therm} = 762 $Å^3$) exhibit at least some solubility in toluene, while salts of $[BF_4]^-$ (V_{therm} = 77 $Å^3$) are only soluble in dichloromethane. These considerations neglect covalent solvation effects, dispersive interactions, temperature etc.; but a general trend can be seen: Salts with large WCAs are soluble in solvents with a rather low dielectric constant, often even at low temperatures.

WCAs in catalysis

Apart from fundamental chemistry, WCAs can be used in many industrial applications, such as homogenous catalysis.[33, 51, 133]

Electrocyclic organic reactions such as Diels-Alder type reactions, 1,4-conjugate additions or pericyclic rearrangements are usually performed in $Li[ClO_4]$ solutions, the Li^+ cation acting as catalyst.[134-139] This limits the reactions to polar solvents and introduces potentially explosive perchlorate salts in large scale. Both problems can be overcome by using stable salts in which the Lithium cation is weakly coordinated. Li^+ salts of $[Al(OR^F)_4]^-$ ($R^F = C(Ph)(CF_3)_2$),[55] $[B(Ar^F)]^-$ ($Ar^F = C_6H_3(CF_3)_2$),[29] $[CB_{12}Me_{12}]^-$[139] and other anions[140-142] have been successfully tested in such reactions. Ag^+ can also be used to catalyze some Diels-Alder type reactions.[138, 143] It could be shown that $[Ag(PPh_3)^+][CB_{11}H_6Br_6]^-$, an air- and moisture stable salt of a very weakly coordinating carboranate anion, is the best catalyst for such reactions,[133] but much simpler and more readily available compounds like silver triflate also demonstrate sufficient activity.[143]

Other important reactions which can be catalyzed include olefin polymerizations and hydrogenations.[31, 144-147] Ziegler-Natta polymerizations utilize cationic metallocene complexes of the type $[cp_2MMe]^+$ (cp = C_5H_5; M = Zr, Ti), which are only active when paired with a sufficiently weakly coordinating anion. In practice the catalyst is generated in situ from cp_2MX_2 (X = Cl, I, CH_3) and the strong alkylating agent and Lewis acid MAO (methylalumoxane, $[MeAlO]_n$, n = 5-10) (Eq. 10).

$$cp_2MMe_2 + MAO \longrightarrow [cp_2MX]^+[MAO\text{-}Me]^-$$

(Eq. 10)

$[MAO\text{-}X]^-$ can already be considered a fairly weakly coordinating anion and has the additional advantage that MAO is very straightforward to synthesize, e.g. by hydrolysis of trimethylaluminum. Because MAO is oligomeric, the negative charge of the generated anion is delocalized over a large surface; however the obtained catalytically active system is not well-defined. While the crystal structure of the $[Al_7O_6Me_{16}]^-$ anion could be determined,[148] a complete structural model for the various possible MAO oligomers has still not been found, although there is proof that they are probably cage structures.[149, 150] Catalyses with MAO require a thousand-fold excess of the catalyst. Alternatively, other parent Lewis acids (eg. $B(C_6F_5)_3$), as well as trityl or acidic ammonium salts of WCAs (e.g. $CPh_3[B(C_6F_5)_4]$), can be used to directly generate more reactive and ideally more controllable catalysts.[31, 151, 152] The catalytic activity rises with sinking coordinative strength of the anion.[41, 153, 154]

WCAs in ionic liquids

*I*onic *l*iquids (ILs) are by definition salts with melting points below 100°C. They were first developed as reaction media for electrochemistry or electrical deposition (e.g. the electroplatination of aluminum) and usually consist of asymmetrically substituted imidazolium, ammonium, pyridinium or phosphonium cations and a complex inorganic anion.[155-157] Traditionally used systems are based on chloroaluminates and $[PF_6]^-$. However, it was found that many WCAs form ionic liquids which are stable against hydrolysis. Prominent examples include the triflate and triflimide anions $CF_3SO_3^-$ and $(CF_3SO_2)_2N^-$, which were studied as IL counterions.[158] Carborane anions form ILs when paired with imidazolium cations;[159] some $[Al(OR^F)_4]^-$ based ILs are also known.[54] As liquid salt melts, these compounds are non-volatile, often non-flammable and thermally stable, which makes them ideal candidates for "green solvents". ILs or IL mixtures which contain catalytically active species as cations might not only be used as solvents, but also as catalysts at the same time, for example in Diels-Alder cycloadditions. ILs with WCAs were found to be suitable catalysts for hydrovinylation reactions, with anions like $[Al(OC(Ph)(CF_3)_2)_4]^-$ and $[B(C_6H_3(CF_3)_2)_4]^-$ inducing the best reactivities.[160]

Many "classic" IL cations introduce a high toxicity, and good anions are often fluorinated, which leads to high production costs. In industry-scale reactions, it may prove difficult to separate the products and by-products from the IL; yet long life cycles of the solvent are necessary to justify the high costs of IL production, recycling and disposal. Because of other properties like tuneable viscosity, thermal and electrical conductivity and a high microwave absorption threshold, ILs are also interesting for applications like lubricants,[161-163] sensor technology (in ion, gas or biosensors)[164, 165] and as reaction media for the synthesis of nanoparticles.[166-168] Gases exhibit strongly varying solubilities in ILs; apart from applications in sensors it is possible to store reactive gases like trifluoroborane, phosphine or arsine in IL solutions under sub-ambient pressure.[169] The extremely low solubility of hydrogen in ILs is exploited during the compression of gas in filling stations, where a body of ionic liquid can be used instead of a mechanical piston. Recently, a method to predict the properties of ILs based on the thermochemical volume of the ions was established.[170, 171] This could facilitate the design of the perfect IL for a given task, if suitable WCAs are available.

WCAs in electrochemistry

Cyclovoltammetry (CV) measurements are usually carried out in non-aqueous media with the help of supporting electrolytes. These electrolytes are typically of the type $NR_4^+X^-$ (R = alkyl; X = ClO_4^-, PF_6^-, BF_4^-, $CF_3SO_3^-$).[172, 173] Many of the commonly used anions have too small so-called “electrochemical windows”, which means they are not stable enough against oxidation and reduction and can be decomposed by the generated oxidized species.[172] The solubility of these salts in weakly polar solvents (e.g. dichloromethane) is often too low; more polar solvents like acetonitrile tend to be too reactive.[174] Additionally, precipitation of anion decomposition products can occur on the electrodes. All these problems could be avoided by introducing larger and more robust WCAs, like in the salts $NBu_4^+[B(C_6F_5)_4]^-$[175, 176] or $NBu_4^+[B(C_6H_3(CF_3)_2)_4]^-$,[177-179] which can keep the species formed at the anode in solution and are were reported to be very stable towards oxidation (reduction may still be a problem because of the electron-depleted aromatic ligands).

WCAs in lithium ion batteries

Lithium ion batteries are now commonly used in many appliances such as power tools, hybrid car batteries, cell phones, laptop computers, cameras, etc. Compared to classical batteries, they have several advantages: lower weight, high current and very high energy density of up to 120 W h kg^{-1}. Modern lithium ion batteries reach nominal voltages of 3.6 V, which is three times as much as in a nickel metal hydride battery.[180] Today, $Li[PF_6]$ is commonly used as conducting agent in ethylene carbonate or propylene carbonate solution; yet there is much room for improvement. Total discharges decrement the capacity of $Li[PF_6]$-based batteries quickly and even when unused, the electrolyte degrades over time. A damaged cell can lead to local heat buildup, followed by a rise in pressure due to vaporization of the solvent. The result can be a violent explosion of the battery because the solvent is inflammable. Also the ideal operating temperature of these batteries is commonly given as between 0 and 40°C, limiting the range of applications especially at low temperatures, when the internal resistance rises quickly. It becomes clear that with the increasing demand for electric storage capacity, e.g. in electrically powered cars, better systems are needed. To improve the mobility of the charge-transporting Li^+ cation, thereby increasing the maximum possible battery current, very small and weakly coordinating anions are needed, which ideally should be chemically very stable and available in very large scale at low cost. Considering the gigantic production scale, these anions should also be non-toxic, stable against hydrolysis and easy to decompose into recyclable products. Likely, but by far not perfect candidates reported in the literature include $[F_{4-n}B(CF_3)_n]^-$,[181] $[F_{6-n}P(CF_3)_n]^-$,[182-184] $[F_3P(C_2F_5)_3]^-$,[185] and $[B\{O(C(CF_3)_2)_2O\}_2]^-$.[186]

Extraction of lanthanide(III) ions

Lanthanide ions "Ln(III)" can be extracted from HNO_3 solutions into an organic phase when partnered with a suitable extractant. The distribution between organic and aqueous phase can be enhanced by orders of magnitude when a $[B(C_6H_3(CF_3)_2)_4]^-$ salt is used as extractant.[187] This anion can also be used for a selective separation of Am(III) from lanthanide(III) ions.[188]

2. Objectives of the thesis

“Then it doesn´t much matter which way you go,” said the Cat.
“...so long as I get somewhere,” Alice added as an explanation.
“Oh, you´re sure to do that,” said the Cat, “if you only walk long enough.”

2.1. Design and synthesis of new WCAs and strong Lewis acids

As already depicted in the previous chapter, the $[Al(OC(CF_3)_3)_4]^-$ or “$[Al(pftb)_4]^-$” (tetra-*p*er*f*luoro-^{t}*b*utoxy-aluminate) anion has all of the characteristics of a very good WCA.[52, 53] It is available in a straightforward synthesis in the form of its lithium salt from lithium aluminum hydride and nonafluoro-^{t}butanol in almost quantitative yields:

$$LiAlH_4 + 4\ (CF_3)_3COH \xrightarrow[-\ 4\ H_2]{\text{pentane}} Li[Al(OC(CF_3)_3)_4]$$

(Eq. 11)

Although the stability of this anion is very high, extremely electrophilic cations can still decompose it. In many decomposition reactions, e.g. with $SiCl_3^+$ or PCl_2^+[62, 64, 65] the bridged anion $[F\{Al(OC(CF_3)_3)_3\}_2]^-$ is formed, which is slightly more stable than $[Al(pftb)_4]^-$ and less coordinating because of its larger size. In some cases, a salt of the desired cation with $[F\{Al(OC(CF_3)_3)_3\}_2]^-$ as the counterion can directly be obtained, along with side products of the decomposition. But even with this approach, currently known alkoxyaluminate-based anions are not quite as stable as some carboranates or teflates, limiting their application. While for example the electrophilic cation salt $CI_3^+[Al(pftb)_4]^-$ could be stabilized and fully characterized, the same was not yet possible with CBr_3^+ or CCl_3^+, which can both be obtained as salts of the $[Sb(OTeF_5)_6]^-$ anion.[90, 189] The goal in the design of new aluminate-based anions must thus be to develop WCA which conserve the advantages of low price and straightforward synthesis with high yields, while at the same time approaching the stability and low coordinative strength of carboranates. Using the $[Al(pftb)_4]^-$ anion as a starting point, one quickly realizes how this can be done by analyzing the main pathways of electrophilic attack. Fig. 18 points out the largest gap in the shell formed by C-F bonds on the anion´s surface, revealing the oxygen atoms. Note that the picture shows the CF_3 units in an interlocked conformation, which can often be observed in crystal structures; these groups are rotating in solution, opening up the gap even more. The lone electron pairs of the oxygen atoms form the most basic sites and are therefore most likely to be coordinated by small electrophiles. Thus, closing up the external shell and sterically shielding the oxygen atoms stabilizes the anion against ligand abstraction.

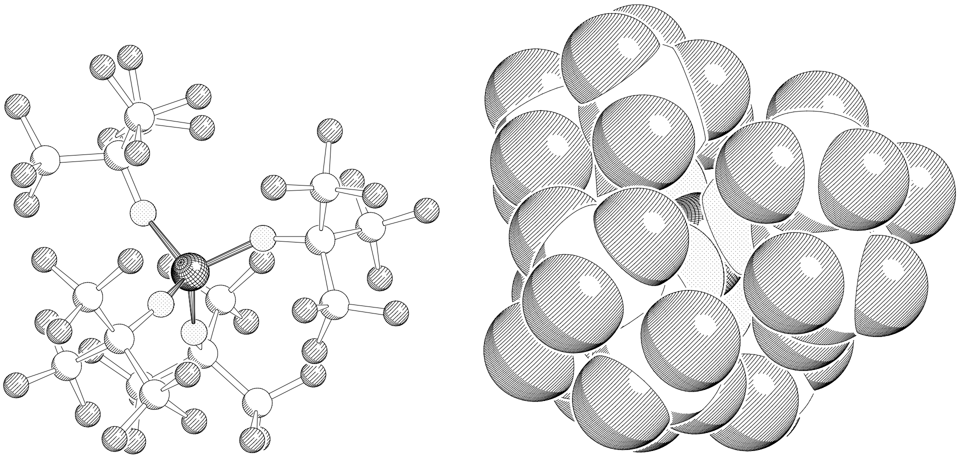

Fig. 18: Ball-and stick (left) and space-filling models (right) of the $[Al(OC(CF_3)_3)_4]^-$ ($[Al(pftb)_4]^-$) anion, showing the most accessible opening for electrophilic attack on the basic oxygen positions.

The second decomposition pathway begins with a fluoride abstraction by the cation in a S_n2-type reaction with resulting formation of the stable and very volatile epoxide C_4F_8O, which makes the whole reaction irreversible (Eq. 12).

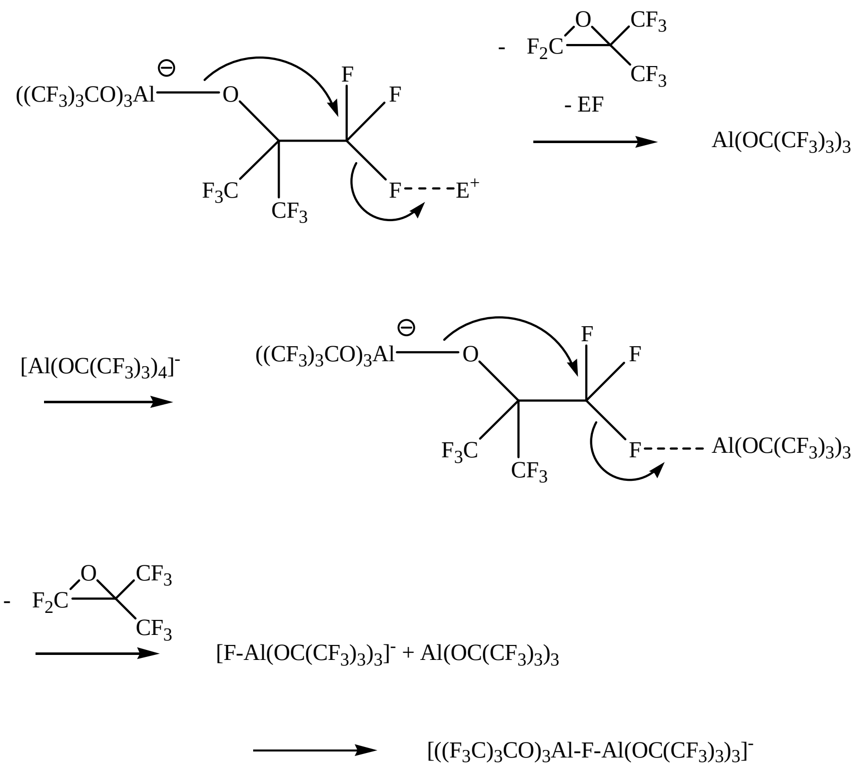

(Eq. 12)

In the first step, the very strong Lewis acid $Al(OC(CF_3)_3)_3$ is formed as an intermediate, immediately separating a fluoride from another $[Al(pftb)_4]^-$ anion. Finally, a reaction of $[FAl(OC(CF_3)_3)_3]^-$ with the Lewis acid yields the fluoride bridged anion. If an electrophile is strong enough to cleave a C-F σ bond, the only possibility of stabilization is to increase the number of fluorine atoms on the anion surface, thus introducing more, but weaker interactions into the system.

Other problems of the known alkoxyaluminate anions often emerge during crystal structure analysis. $[Al(OC(CF_3)_3)_4]^-$ is highly symmetric, closely approaching S_4 symmetry (in some crystal structures, the central aluminum even rests on a $\bar{4}$ axis), and its surface can be considered orb-shaped. In combination with small cations of lower symmetry, this often leads to pseudomerohedral twinning, which in turn can cause problems during data reduction or cell determination. Modern crystallographic software can often, but not always, overcome this. From the point of view of a synthetic chemist, it would often be easier to reduce the symmetry of the WCA, as in $[Al(OC(H)(CF_3)_2)_4]^-$ ("$[Al(hfip)_4]^-$", tetra-*h*exa*f*luoro-^{i}*p*ropoxy-aluminate).[53] Yet in this anion, the gap in the shell becomes too large, allowing coordination with the basic oxygen atoms. This effect, along with the reduced number of fluorine atoms, makes $[Al(hfip)_4]^-$ considerably stronger coordinating than $[Al(pftb)_4]^-$. A better solution would be to introduce a rigid perfluorinated building block that is larger than CF_3 to break up symmetry, while at the same time preserving the shielding of the anion´s core. Reducing the number of CF_3 groups has another benefit: disorder arising from their rotation can be significantly lessened. The same can be achieved by measuring at lower temperatures with a helium or nitrogen crystal cooling apparatus, but this can also lead to unexpected phase transitions or icing problems. With these considerations in mind, introducing perfluorinated phenyl groups C_6F_5 seems to be a good option. Their rigidity and steric demand helps to break up symmetry, and they should increase solubility in aromatic solvents. At the same time, crystallization can be promoted by π-stacking effects and the aromatic system offers a weak but robust coordination site for small metal cations. In applications where a high mobility of the cation is required, such as electrochemistry with Li^+ salts, this mode of coordination is more desirable than the rather strong coordination of the metal ion with oxygen.

Many of these considerations also hold for the design of new aluminum-centered strong Lewis acids. It could be shown in previous theoretical work that $Al(OC(CF_3)_3)_3$ is stabilized by coordination with two fluorine atoms of opposing CF_3 groups (Fig. 19).[190]

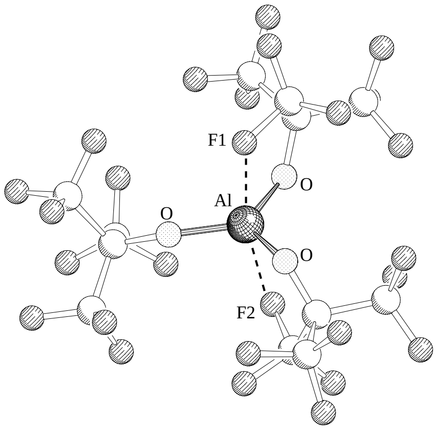

Fig. 19: Al-F coordination in the Lewis acid $Al(OC(CF_3)_3)_3$.

While donor-free $Al(OC(CF_3)_3)_3$ is only stable in solution at -10° C, insertion of a carefully chosen ligand that provides weak Al-F coordination without cleavage of C-F bonds could lead to a strong Lewis acid, which is stable at room temperature but still reactive. The practical work described in this thesis focuses on the 1,1,1,3,3,3-*h*exa*f*luoro-2-*p*entafluorophenyl-^{i}*p*ropoxy ("hfpp", $OC(CF_3)_2(C_6F_5)$) and 2,2,3,3,4,4,5,5,6,6-decafluoro-1-*p*entafluorophenyl-^{cyclo}*hex*anoxy ("phex", $OC(C_5F_{10})(C_6F_5)$) ligands (Fig. 20), which have 11, respectively 15 C-F bonds and should fulfill the criteria described above. The latter species is very rigid and contains no CF_3 groups, which should lead to very well-defined crystal lattices with no disorder in the corresponding anions and parent Lewis acids.

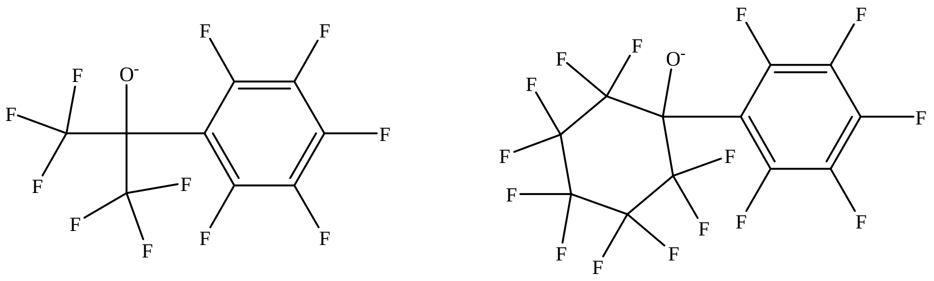

Fig. 20: Structural formulae of the hfpp (left) and phex (right) ligands.

Along with new strong Lewis acids and WCAs based on these ligands, related starting materials will be presented.

2.2. Applications of new WCAs and strong Lewis acids

Applications of new WCAs explored in this thesis focus on salts of very electrophilic or weakly bound cations. Apart from being of fundamental interest, some of these salts may find practical use in synthesis or serve as starting materials for further research.

The stabilisation of reactive cations relies heavily on specialized experimental techniques developed to handle this sensitive chemistry, as well as on extensive quantum chemical calculations which give reliable estimates for the thermodynamics of a reaction and physical observables such as vibrational frequencies and chemical shifts. The majority of research groups relies on fluorometallate WCAs ($[AsF_6]^-$, $[Sb_nF_{5n+1}]^-$) as counterions, whose drawbacks were already described in chapter 1. While syntheses of reactive cations that are incompatible with common inorganic solvents and can only exist in a very weakly basic environment are still a challenge, aluminate WCAs like $[Al(pftb)_4]^-$ allow the chemist to avoid the use of potentially very harmful inorganic solvents such as anhydrous HF. In this thesis, WCA salts of highly electrophilic carbocations of the type $X_3C_2S_2^+$ and XCS^+ (X = Cl, Br, I) will be investigated with ab initio and DFT methods, and in selected cases also experimentally in the condensed phase. Homologous species have so far been unknown in the solid state or in solution, with the exception of $ClCO^+$, which has been characterized by ^{13}C-NMR and vibrational spectroscopy.[191, 192] XCO^+ cations with X = Cl-I have been observed at -78°C in superacidic media.[193] The related acyl cations RCO^+ (R = alkyl or aryl) are proposed as intermediates in Friedel-Crafts acylations.[194] It could be shown in mass spectrometer experiments that XCO^+ (X = F, Br, Cl) cations can activate C-H bonds in simple aromatic compounds like benzene, thiophene, pyrrole, furane and some derivates by electrophilic addition followed by HX elimination, thereby forming acyl cations.[195] If WCA salts of XCE^+ (or $X_3C_2E_2^+$, which can be interpreted as adducts of XCE^+ and X_2CE, E = S, O) can be stabilized under controllable conditions, they would be promising synthons for compounds so far inaccessible through known organic reactions.

Unstable cations, which have already been obtained as salts of other anions, can serve as benchmarks for new WCAs based on the hfpp and phex ligands. Suitable candidates include the ^{t}butyl cation $[C(CH_3)_3]^+$,[14-16] CX_3^+ (X = Cl, Br, I)[4-6] and $[Ag(P_4)_2]^+$.[20, 21] Only if these or similar known cations can be stabilized with a given new anion, its ability for very weak coordination and thus its usability in the elucidation of even more reactive species can be proven. The same holds for much simpler cations like univalent metal ions (e.g. Li^+, Ag^+) that can be used in catalysis or in electrochemistry (see chapter 1). Catalytic activity and conductivity benefit from weak coordination of the cation, so M^+ salts of new WCAs should be thoroughly analyzed with respect to the coordination around the metal ion.

Finally, new Lewis acids can be applied in the generation of salts of heteroleptic WCAs. Especially with bulkier ligands, the steric strain around the central aluminum atom in a $[Al(OR^F)_4]^-$ anion can lead to a low stability against ligand abstraction. Starting from a parent Lewis acid, a second, smaller ligand can be introduced, creating a smaller but potentially more stable WCA of the type $[Al(OR^F)_3R']$ (R' = F, Cl, Br, alkoxy-, (per-)fluoroalkoxy-, etc.) (Eq. 13).

$$\begin{aligned} Al(OR^F)_3 + LiOR' &\longrightarrow Li^+[Al(OR^F)_3R']^- \\ Al(OR^F)_3 + Cat^+X^- &\longrightarrow Cat^+[Al(OR^F)_3R']^- \end{aligned}$$

(Eq. 13)

In catalysis, this strategy is widely used to generate catalytically active cations from stable reagents in situ (see chapter 1). With a stable and easily accessible Lewis acid at hand, it is also a good strategy to quickly access a wide range of new WCAs or even WCA salts of reactive cations, eliminating the need to isolate and purify the WCA first.

3. Design of new WCAs and strong Lewis acids with perfluorinated ligands

“One side will make you grow taller, and one side will make you grow shorter.”
“One side of what? The other side of what?” thought Alice to herself.
“Of the mushroom,” said the Caterpillar, just as if she had asked it aloud; and in another moment it was out of sight.

3.1. New starting materials for WCAs and Lewis acids

3.1.1. Perfluorinated alcohols

One main goal of this thesis is the synthesis of novel fluorinated alcohols as starting materials for the preparation of $[Al(OR^F)_4]^-$, related types of WCAs, and their parent Lewis acids $Al(OR^F)_3$. For maximum anion stability, the target ligands R^F should be able to sterically shield the oxygen atoms better than $C(CF_3)_3$. The use of exclusively (perfluoro-)alkyl- or aryl-substituted alkoxides is desirable, because these ligands most tightly bind to the central atom of the WCA, i.e. to aluminum for $[Al(OR^F)_4]^-$. This is due to the higher electronegativity of the OR^F ligand compared to a non-fluorinated OR, leading to highly polar Al-O bonds. In a stable WCA, this effect must outbalance the higher steric requirement of the fluorinated alkoxy ligands, which is associated with a larger strain upon formation of Al-O bonds. Increasing WCA stability correlates with higher Brønsted acidity of the parent alcohol (Tab. 2). The acidity is quantified by the *g*as phase *a*cidity GA, which is defined as the Gibbs free energy associated with the deprotonation of one molecule in the gas phase (Eq. 14, the proton affinity equals the reaction enthalpy of the same process). It is a property that can be directly measured by FT-ICR (*F*ourier *t*ransform *i*on *c*yclotron *r*esonance) mass spectrometry.

$$ROH_{(g)} \rightleftharpoons H^+_{(g)} + RO^-_{(g)}$$

(Eq. 14)

Tab. 2: Comparison of the gas phase acidities (GAs) of selected alcohols and acids.

Compound	**GA (exp.)[196, 197]**	**GA (calc.)[a]**
$(CH_3)_3COH$	1539	1556
$(CF_3)_2(CH_3)COH$	1425	1428
$(CF_3)_2CHOH$	1416	1424
CH_3COOH	1423	1416
$(CF_3)_2(C_6F_5)COH$	-	1367
$(CF_3)_3COH$	1355	1366
$C_6F_5(C_6F_{10})OH$	-	1343
CF_3COOH	1322	1339

[a] MP2/TZVPP level.

The calculated energies in Tab. 2 are close to experimental values (largest error 17 kJ mol^{-1}). It can be deduced that the gas phase basicity of $(CF_3)_2(C_6F_5)COH$ and $(C_6F_5)C_6F_{10}OH$ is similar to perfluoro-^{t}butanol. As a more accessible measure of acidity, pK$_a$ values in water have been reported for many perfluorinated alcohols.[54, 198, 199]

Tab. 3: Experimental pK$_a$ values of selected alcohols.

Compound	**pK$_a$ (exp.)[54, 198, 199]**
$(CH_3)_3COH$	19.2
$(CF_3)_2C_6H_{10}OH$	10.3
$(CF_3)_2(CH_3)COH$	9.6
$(CF_3)_2CHOH$	9.3
$(CF_3)_2(C_6H_5)COH$	8.8
$(CF_3)_2(C_6F_5)COH$	7.9
$(CF_3)_3COH$	5.4

Indeed, an almost linear dependence of Lewis basicity of $[Al(OR)_4]^-$ anions on the pK$_a$ value of the parent alcohol has been determined by other authors by measuring their coordinative strength towards Li$^+$.[54] It becomes clear that a higher number of fluoroalkyl groups leads to a higher acidity, e.g. in the extreme case of ^{t}butanol, perfluorination results in an increase in acidity of 14 orders of magnitude. For fluorinated aromatic ligands, the effect is much less pronounced; replacing just one CF_3 group with a pentafluorophenyl group decreases the pK$_a$ from 5.4 to 7.9. This is due to the surprisingly low electronegativity of the pentafluorophenyl group, which has been explained by a destabilization of negative charge on the fluorinated aromatic ring by interaction with non-bonding p-electron density on fluorine atoms.[200]

Very extensive studies have been reported on hydrogen bonding in fluorinated alcohols.[201-204] In summary, the presence of electron-withdrawing groups adjacent to the hydroxyl function makes the oxygen a weaker donor, while the proton is a stronger Lewis acceptor. However, this higher Lewis acidity does not compensate for the reduced basicity of the oxygen atom. As a result, there is weaker intermolecular hydrogen bonding between fluorinated alcohols, but stronger interaction between the alcohol and a donor molecule (such as an ether), than is the case in the absence of fluorination. For example, hexafluoroisopropanol forms a discrete complex with tetrahydrofurane and other basic solvents.[205]

Synthetic aspects

Perfluorophenyl groups can be introduced by a Grignard-type reaction (Eq. 15), thereby avoiding the use of erratically explosive C_6F_5Li.[206, 207] The Grignard reagent C_6F_5MgBr has the additional advantage of being stable at ambient conditions.

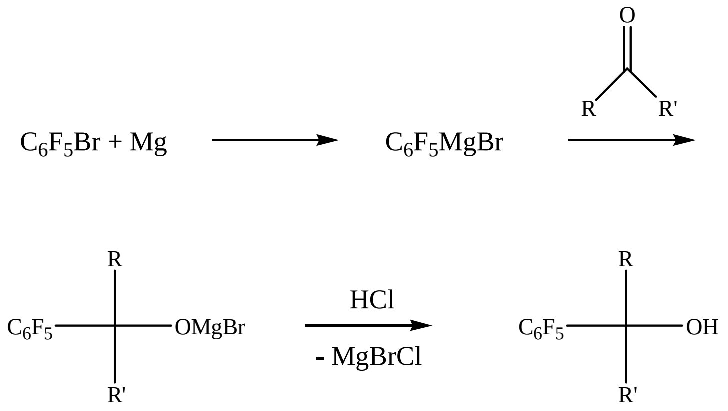

(Eq. 15)

3.1.2. Synthesis and characterization of $C_6F_5(CF_3)_2COH$

Synthesis

1,1,1,3,3,3-hexafluoro-2-pentafluorophenyl-^{i}propanol $C_6F_5(CF_3)_2COH$ **1** can be prepared as described in chapter 3.1.1 (Eq. 15) by reacting C_6F_5MgBr with gaseous hexafluoroacetone in diethylether, followed by protonation with aqueous HCl solution. The resulting liquid ether adduct $C_6F_5(CF_3)_2COH\text{-}OEt_2$ is very stable and partly stays intact in a simple fractioned distillation. The ether can only be fully removed by distilling the adduct from concentrated H_2SO_4 in vacuo. **1** is obtained as a colorless liquid with total yields of up to 65%.

NMR spectroscopy

Carbon, fluorine and proton NMR spectra were recorded and exhibit good agreement with calculated chemical shifts (Tab. 4).

Tab. 4: Experimental and calculated chemical shifts of **1**.

	shift (exp.) [ppm][a]	**shift (calc.) [ppm][b]**	**assignment[c]**
$\delta^{13}C$	79.1	86.6	a
	105.4	106.9	c
	121.6	131.4	b
	138.3	138.5	f
	142.6	143.6	g
	146.3	145.3	d, e
$\delta^{19}F$	-76.2	-76.5	b
	-132.8	-117.6	d
	-138.4	-143.0	e
	-148.9	-146.1	g
	-160.2	-155.3	f
$\delta^{1}H$	4.13	2.71	-

[a] in $CDCl_3$; [b] on BP86/def-SV(P) level, C_1 symmetry, referenced on CH_4 and CF_4; [c] see Fig. 21.

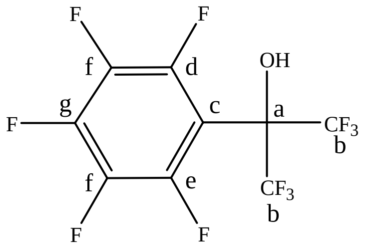

Fig. 21: Assignment of NMR signals for **1**.

However, there are significant deviations between the prediction and the measurements for the proton signal, which is low-field shifted significantly by 1.4 ppm in the experiment, as well as for one fluorine atom in the ortho position of C_6F_5. The proton signal is less broadened than could be expected for a dimeric or oligomeric structure (singlet with FWHM = 9 Hz), indicating that little or no intermolecular hydrogen bonding is taking place. In the calculated structure of the monomer, contacts between the proton and two fluorine atoms occur, one in the ortho position of the pentafluorphenyl group, the other in a CF_3 group (Fig. 22). Both H-F contacts are shorter than the sum of van der Waals radii of 290 pm (H-F_{CF3}: 246 pm, O-F_{CF3}: 271 pm, H-F_{C6F5}: 184 pm, O-F_{C6F5}: 260 pm), and the F-O contacts range between the F-F distance in $(HF)_6$ (253 pm) and the O-O distance in $(H_2O)_x$ (275 pm)[208] as models for typical asymmetric hydrogen bonds.

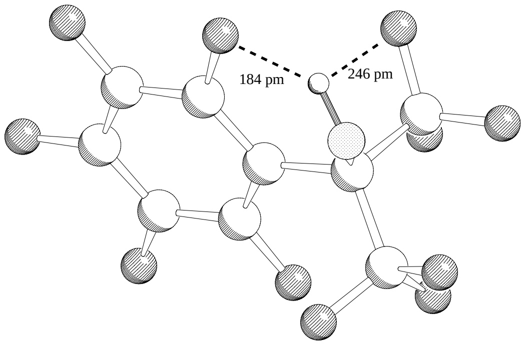

Fig. 22: H-F contacts in **1** (geometry calculated at the MP2/TZVPP level, C_1 symmetry).

The shorter H-F_{C6F5} contact can be observed indirectly in the ^{19}F NMR spectrum (Fig. 23); the two fluorine atoms in the ortho position of C_6F_5 (d and e in Fig. 21) are not equivalent and their ^{19}F signals are considerably broadened (FWHM = 300 Hz). Correspondingly, the calculated chemical shifts deviate from the measurement by 4.5 and 14.8 ppm, respectively.

Because the signals are too broad, H-F coupling cannot be observed directly, yet it can be concluded that the free rotation of the pentafluorophenyl ring in **1** is significantly hindered even in solution, either by H-F or F-F contacts. The CF_3 signal is a triplet ($^5J_{F,F}$ = 14.5 Hz), arising from coupling with the fluorine atoms in ortho position of the aromatic C_6F_5 group (see COSY spectrum below).

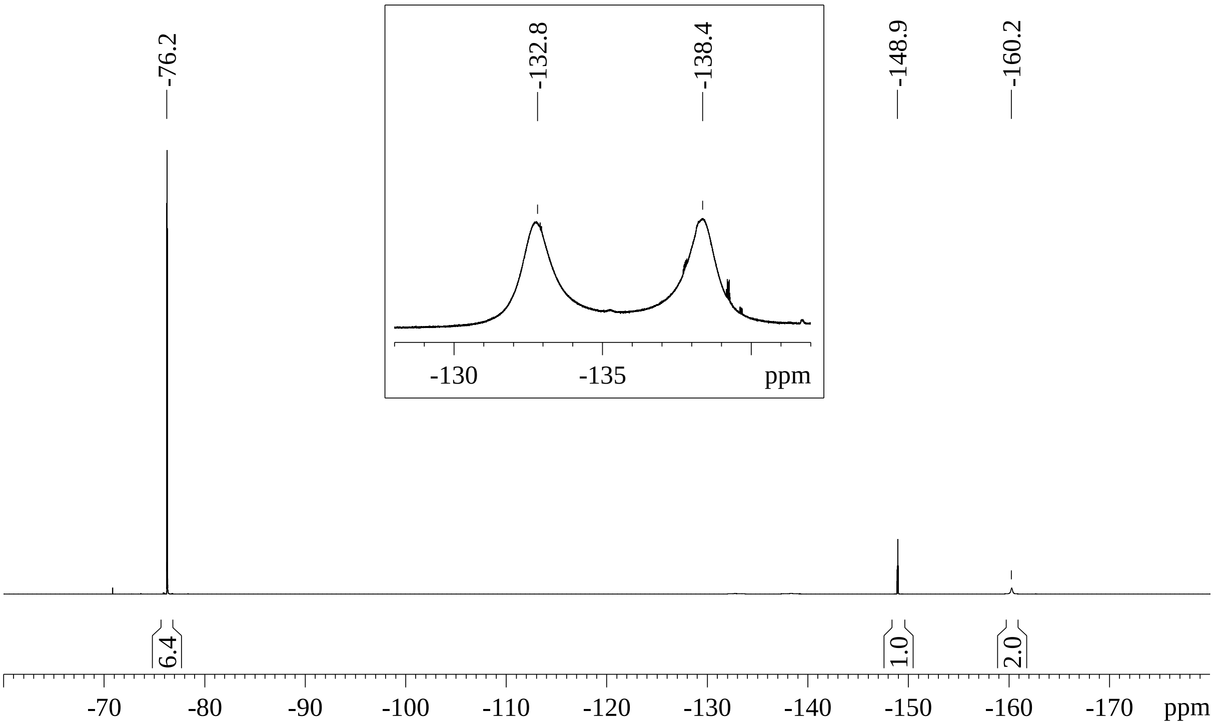

Fig. 23: ^{19}F-NMR spectrum of **1**, recorded at room temperature in $CDCl_3$. The peaks in the ortho position of the fluorinated phenyl ring are broadened and only visible in the magnification.

To check if the inhibited rotation of the pentafluorophenyl group is really the result of a H-F interaction, a ^{19}F,^{19}F COSY spectrum was recorded (Fig. 24). The spectrum shows a weak crosspeak between the CF_3 group and one of the fluorine atoms in the ortho position of the aromatic ring (132.8 ppm, d in Tab. 4), proving at least a partial influence of F-F interactions on C_6F_5 rotation. The calculation predicts the shortest F_{CF3}-F_{C6F5} contact at 252 pm (c.f. double van-der-Waals radius of fluorine: 294 pm). The signal at -138.4 ppm can be assigned to the fluorine atom in ortho position pointing away from the hydroxyl function (e in Fig. 21).

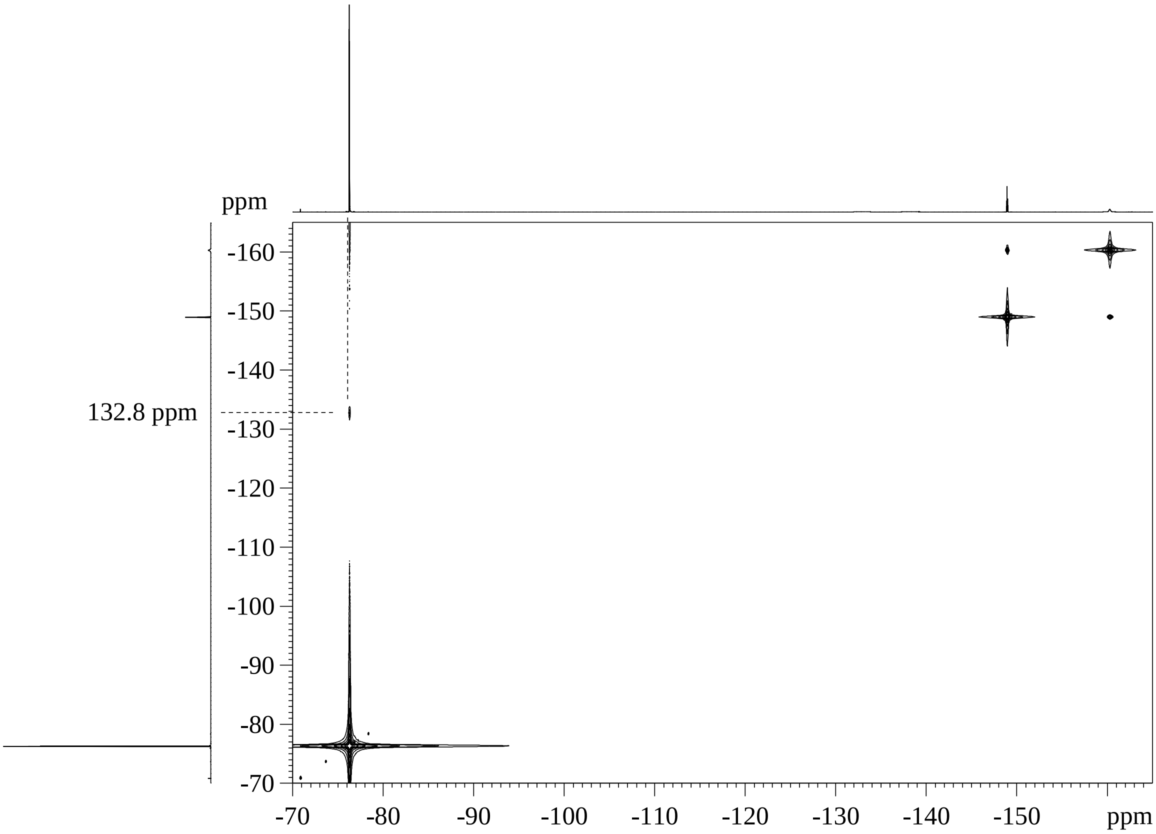

Fig. 24: ^{19}F, ^{19}F COSY spectrum of **1**, recorded at room temperature in $CDCl_3$.

Accordingly, while a ^{13}C NMR spectrum of **1** (Fig. 25) shows the expected $^1J_{F,C}$, $^2J_{F,C}$ and $^3J_{F,C}$ coupling for the carbon atoms in the ortho and meta positions, only $^1J_{F,C}$ coupling can be resolved in the ortho position (Tab. 5) and the signals are broadened (FWHM = 37 Hz) due to chemical exchange.

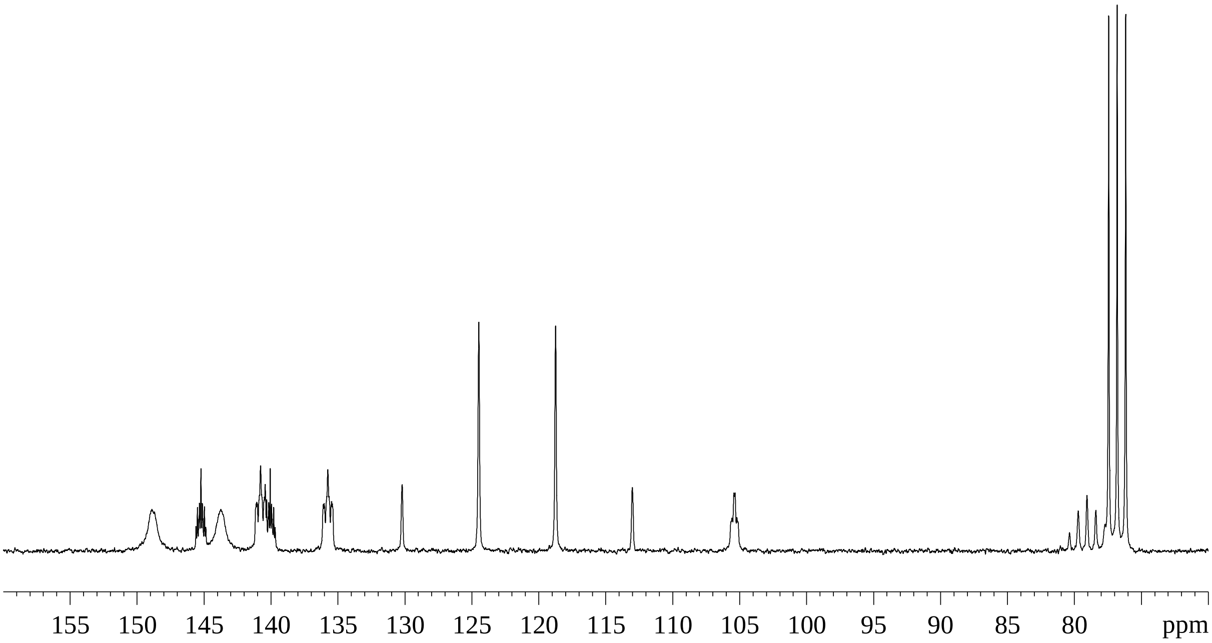

Fig. 25: $^{13}C[^{1}H]$ NMR spectrum of **1**, recorded at room temperature in $CDCl_3$.

Tab. 5: C, F coupling constants in the $^{13}C[^{1}H]$ NMR spectrum of **1**.

shift (exp.) [ppm][a]	assignment[b]	$^{1}J_{C,F}$ [Hz]	$^{2}J_{C,F}$ [Hz]	$^{3}J_{C,F}$ [Hz]
79.1	a	-	33	-
105.4	c	-	11	4
121.6	b	288	-	-
138.3	f	253	15	3
142.6	g	260	13	6
146.3	d, e	259	-	-

[a] in $CDCl_3$; [b] see Fig. 21.

Additionally ^{19}F, ^{13}C correlation spectra (HSQC) were recorded, which support the assignments given above.

Gas phase electron diffraction

1 was studied by S. Hayes and R. Berger of Bielefeld University with GED (gas phase electron diffraction). Tab. 6 shows a comparison between the resulting refined distances and the calculated geometry.

Tab. 6: Comparison of GED and calculated distances in pm.

	GED[a]	HF/TZVPP[b]	MP2/TZVPP[b]
F5-H	*198(16)*	*184.5*	*184.1*
F20-H	*235(12)*	*250.0*	*246.1*
C1–C2	141.3(3)	140.7	139.9
C2–C7	140.0(2)	139.8	139.0
C1–C12	153.9(6)	155.1	135.2
C12–C13	156.1(6)	158.8	156.3
C12–C17	154.9(5)	157.5	154.8
C2–F3	133.7(2)	133.9	132.8
C–F8	133.7(2)	133.9	132.7
C–F5	135.6(2)	135.9	134.5
C–F14	133.4(2)	133.4	132.6
C–F15	134.4(2)	135.3	133.6
C–F16	133.9(2)	134.9	133.1
C–F18	133.6(2)	134.5	132.8
C–F19	134.1(2)	135.1	133.3
C–F20	134.9(3)	136.2	134.2
C–O	140.7(5)	140.5	139.8

[a] Assigment see Fig. 26; [b] C_1 symmetry.

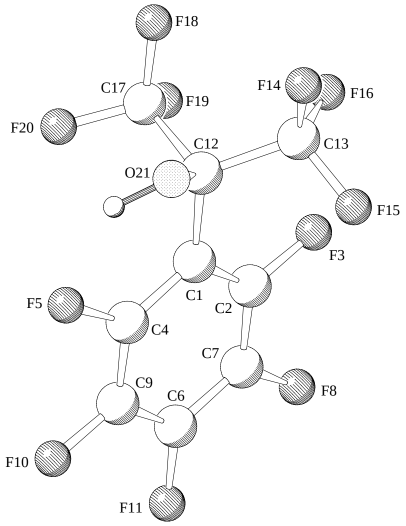

Fig. 26: Calculated minimum geometry of **1** (MP2/TZVPP), showing the atom numbering used in the GED refinement.

Generally, the results from GED are consistent with the geometry predicted by ab initio methods. The predicted H-F contact lengths deviate slightly from the experimentally determined values (GED: H-F_{CF3} 237 pm, H-F_{C6F5}: 198 pm, MP2/TZVPP: H-F_{CF3} 246 pm, H-F_{C6F5}: 184 pm), but exhibit large error limits (this can be expected due to the low scattering cross-section of hydrogen). For a more comprehensive report see sections 6.3.5 and 6.10.

IR spectroscopy

Fig. 27 shows the infrared spectrum of neat liquid **1**, which is in good agreement with calculated bands (cf. section 6.6, Tab. 38). The O-H band appears at 3610 cm^{-1}, which is shifted by 68 cm^{-1} with respect to the calculation (3542 cm^{-1}), probably due to intermolecular hydrogen bridging.

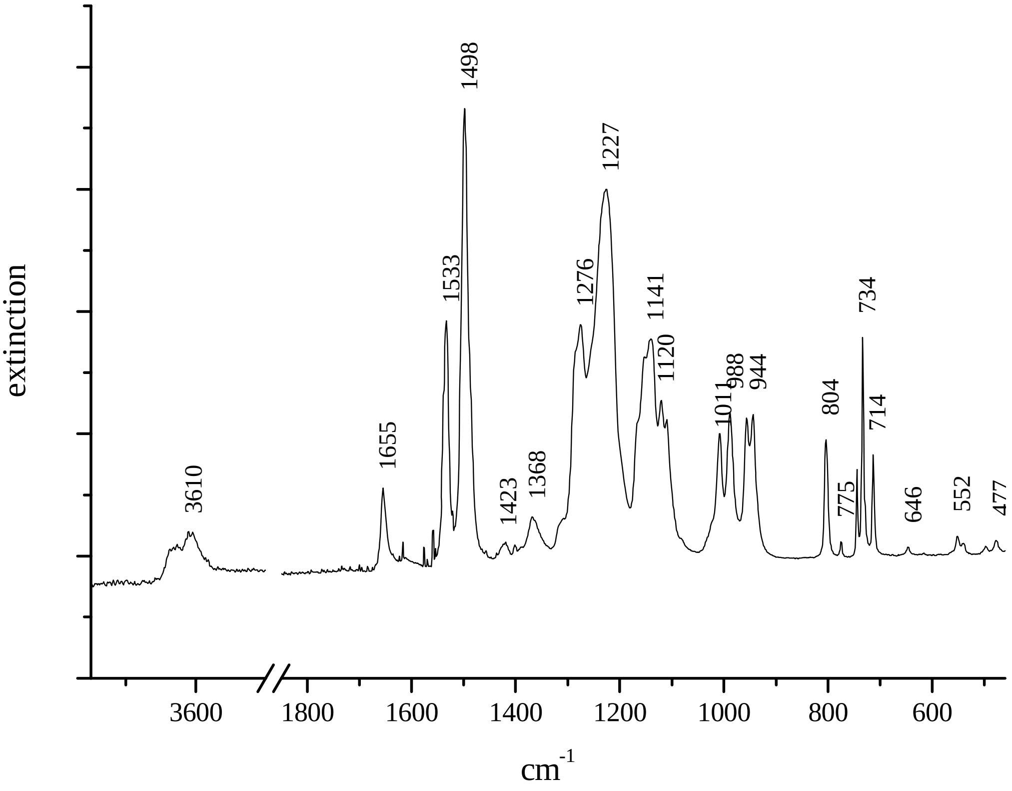

Fig. 27: IR spectrum of liquid **1**.

3.1.3. Synthesis and characterization of $C_6F_5(C_6F_{10})OH$

Synthesis

2,2,3,3,4,4,5,5,6,6-decafluoro-1-pentafluorophenyl-cyclohexanol $C_6F_5(C_6F_{10})OH$ **2** is formed in a Grignard-type reaction from perfluorocyclohexanone and C_6F_5MgBr in diethylether (Eq. 15). After hydrolysis of $C_6F_5(C_6F_{10})OMgBr$ with concentrated hydrochloric acid, the alcohol can be conveniently sublimed in vacuo (10^{-2} mbar) at ambient or slightly elevated temperatures and is obtained water- and ether-free with total yields of up to 85%. The product is a colorless solid (m.p. 52°C) which shows no tendency to form an ether adduct and shows poor solubility in alkanes, $CHCl_3$, $CHCl_2$ and water. It is soluble in 1,2- difluorbenzene, monofluorobenzene and toluene.

A further method to introduce the C_6F_5 ligand with the possibility of better yields was tested, using pentafluorophenyltrimethylsilane $C_6F_5SiMe_3$ as transfer agent. However, even when adding CsF or tetrabutylammonium fluoride as a catalyst, no reaction is observed, the reactivity of the silane being too low. Addition of water-free tetramethylammonium fluoride yields polymeric 1-$H(C_6F_4)_nF$ already at -80°C, as other authors have found simultaneously.[209]

Acidity

The acidity of **2** in acetonitrile was determined in Leito´s group at the University of Tartu (Estonia). In their self-consistent acidity scale in CH_3CN,[210, 211] **2** (pK_a = 22.0 +/- 0.2) is a slightly weaker acid than $(CF_3)_3COH$ (20.6 +/- 0.1), which is probably due to the reduced inductive effect (number of beta fluorines in **2** = 4 vs. 9 in $(CF_3)_3COH$). Another reason might be a stabilizing solvent effect, as the interactions between the anionic center in the alkoxide and the solvent molecules are governed by the degree of steric shielding of the oxygen atom. This shielding is less pronounced in $(CF_3)_3CO^-$ (Fig. 28), allowing more CH_3CN molecules to cluster around the oxygen, so the alkoxide is better stabilized than in $C_6F_5(C_6F_{10})O^-$.

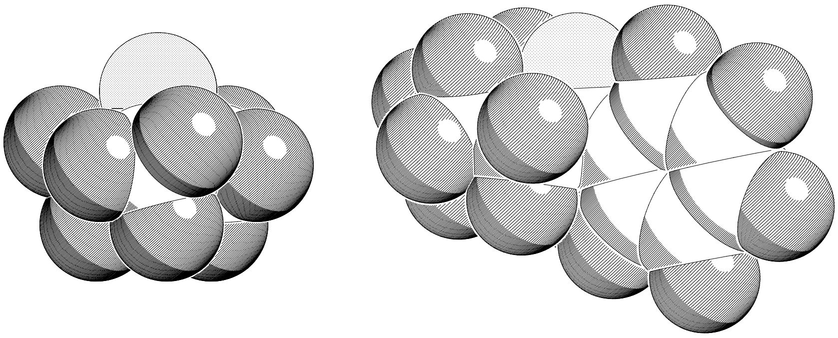

Fig. 28: Space-filling models of $(CF_3)_3CO^-$ and $C_6F_5(C_6F_{10})O^-$, optimized at MP2/TZVPP level.

Gas phase basicity/acidity studies might be more conclusive, because these properties depend more on size and polarizability. Measurements are currently carried out by Prof. Masaaki Mishima´s group at Kyushu University (Japan).

NMR spectroscopy

2 was extensively studied by ^{19}F, ^{13}C and ^{1}H spectroscopy (Tab. 7).

Tab. 7: Experimental chemical shifts of **2**.

	shift (exp.) [ppm]	**coupling constant [Hz]**	**assignment**[c]
δ^{13}C[a]	78.9	$^{2}J_{C,F} = 26$	a
	108.1	-[d]	3
	109.0	-[d]	2
	111.9	-[d]	1
	138.0	$^{1}J_{C,F} = 247$	c
	142.2	$^{1}J_{C,F} = 260$	d
	146.5	$^{1}J_{C,F} = 258$	b
δ^{19}F[a]	-113.6	$^{2}J_{F,F} = 275$, $^{5}J_{F,F} = 53$	1a
	-117.6	$^{2}J_{F,F} = 275$	2a
	-121.3	$^{2}J_{F,F} = 284$	3a
	-131.1	$^{2}J_{F,F} = 275$	1e
	-132.8	$^{5}J_{F,F} = 53$	b
	-135.8	$^{2}J_{F,F} = 275$	2e
	-140.6	$^{2}J_{F,F} = 284$	3e
	-146.6	$^{3}J_{F,F} = 22$, $^{4}J_{F,F} = 7$	d
	-159.0	$^{3}J_{F,F} = 22$, $^{4}J_{F,F} = 7$	c
δ^{1}H[b]	4.20	$J_{H,F} = 6.2$	-

[a] in toluene-D_8; [b] in $CDCl_3$; [c] see Fig. 29; [d] not resolved.

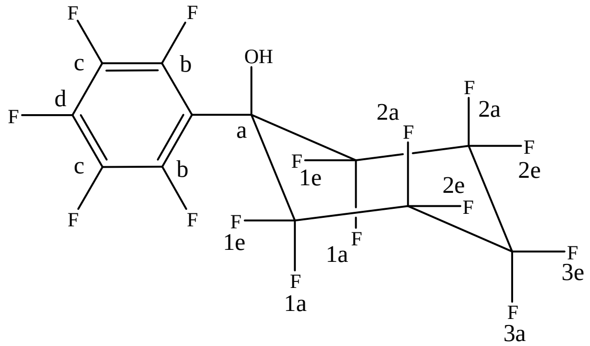

Fig. 29: Assignment of NMR signals for **2**; in the aliphatic ring: e = equatorial, a = axial.

The proton spectrum shows a triplet at 4.2 ppm (FWHM = 8 Hz, J = 6 Hz), probably arising from $^{4}J_{H,F}$ coupling with two fluorine atoms (b or 1a in Fig. 29). However, because of the very complicated F-F coupling pattern, the same coupling constant cannot clearly be assigned in the corresponding ^{19}F signals at -113.6 ppm. The triplet is not observed in saturated solutions of **2**, indicating intermolecular exchange or a formation of dimers (cf. crystal structure, see below). Less inhibited rotation of the aromatic ring than in **1** is indicated by the ^{19}F signal of the two fluorine atoms in ortho position, which is not split (but broadened, see below). The calculated molecular minimum structure is not consistent with the triplet signal of the hydroxyl group. An asymmetric monomer is predicted in the gas phase, which shows two H-F contacts with distances of H-F$_{\mathrm{C6F10}}$: 234 pm (Fig. 30, O-F$_{\mathrm{C6F10}}$: 269 pm) and H-F$_{\mathrm{C6F5}}$: 203 pm (O-F$_{\mathrm{C6F5}}$: 250 pm). For this geometry, a doublet of doublets in the proton NMR and a splitting of the signals for the fluorine atoms in ortho positions of the C_6F_5 unit and in 1-position of the aliphatic group would be expected, but are not observed. Both contacts are significantly shorter than the H-F$_{\mathrm{CF3}}$ distance in **1** (246 pm), but longer than the H-F$_{\mathrm{C6F5}}$ distance in the same compound (183 pm). Thus the H-F interaction and the repulsive F-F interactions between the aromatic and aliphatic rings (255 and 243 pm, Fig. 30) are probably too weak to completely prevent the rotation of the aromatic C_6F_5 group. Another, C_s symmetric local minimum structure is found on the potential energy hypersurface (Fig. 31), which is only 13 kJ mol^{-1} higher in energy than the absolute minimum structure. In this geometry, a rotation of the aromatic ring is only hindered by two weak repulsive F-F interactions with the aliphatic group, but not by a H-F interaction. The H-F contacts with the aliphatic ring are shorter (H-F$_{\mathrm{C6F10}}$: 210 pm) than in the absolute minimum structure, while the F-F contacts stay almost unchanged (F$_{\mathrm{C6F5}}$-F$_{\mathrm{C6F10}}$: 245 pm, cf. double van-der-Waals radius of fluorine: 294 pm). In summary, NMR spectra show a slightly inhibited rotation of the C_6F_5 ring, which is in agreement with both the C_1- and C_s-symmetric gas phase geometries.

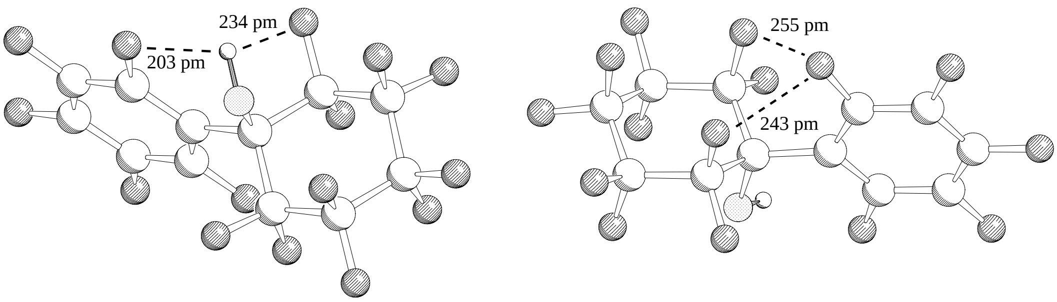

Fig. 30: H-F contacts (left) and F-F contacts (right) in the global minimum geometry of **2** (MP2/TZVPP level, C_1 symmetry).

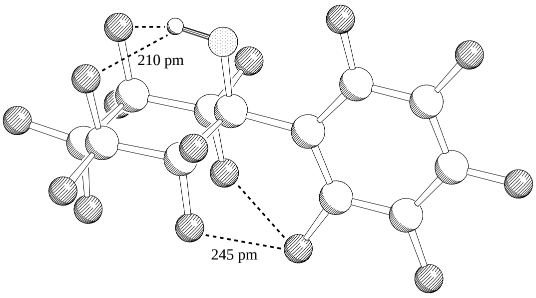

Fig. 31: H-F and F-F contacts in **2** (local minimum geometry, MP2/TZVPP level, C_s symmetry).

The triplet splitting in the proton NMR appears only in diluted solutions of **2**, indicating that in higher concentrations intermolecular H-bonding is preferred.

Fig. 32 shows the ^{19}F NMR spectrum of **2**, which is characteristic for all compounds containing the phex ligand. The assignments in Tab. 7 are based on coupling constants and integrals as well as ^{19}F, ^{19}F NOESY and COSY spectra.

All six signals arising from the aliphatic fluorine atoms are split due to geminal coupling with typical coupling constants (Tab. 7). As already discussed, there is only a single signal of the fluorine atoms in the ortho position of the aromatic ring (b in Fig. 29), indicating a free rotation of the aromatic ring. The signal is a triplet with a coupling constant of 53 Hz, which can also be found in the signal at -113.6 ppm, corresponding to the two axial fluorine atoms 1a in Fig. 29. Additionally, the associated correlation is found in the COSY spectrum (Fig. 33). The ^{13}C chemical shifts were assigned with the help of a HSQC spectrum (Fig. 34).

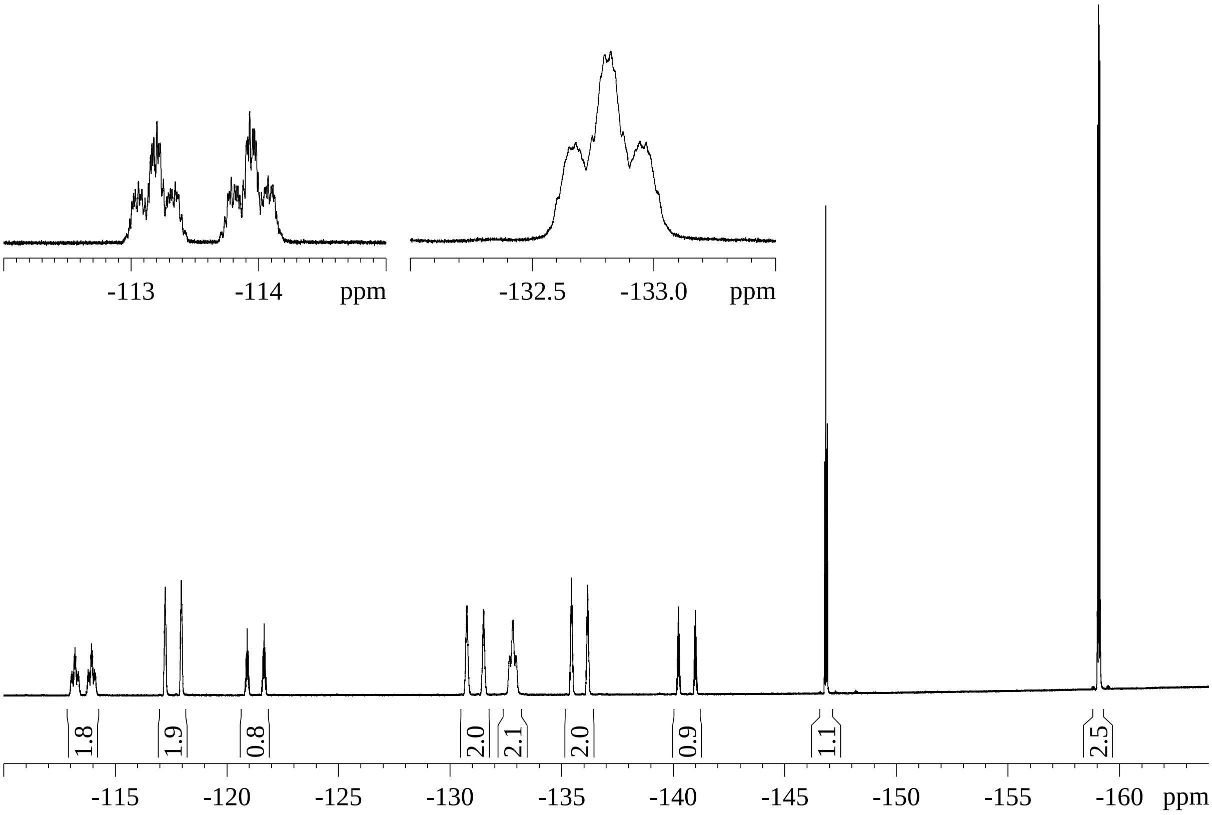

Fig. 32: ^{19}NMR spectrum of **2**. Note that the integral value for the peak at -159.0 ppm is overestimated because it coincides with the signal region of the NMR probehead.

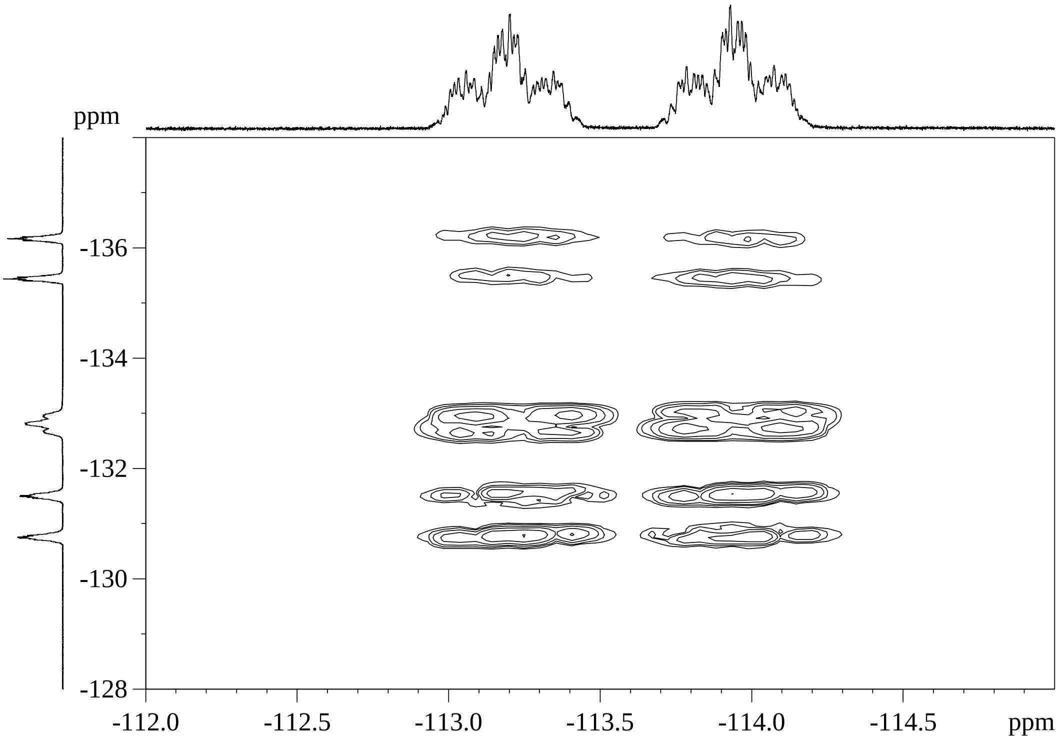

Fig. 33: Magnification of the ^{19}F, ^{19}F COSY spectrum of **2**, showing the correlation between the fluorine atom in ortho position of the C_6F_5 group and two axial fluorine atoms in the C_6F_{10} group.

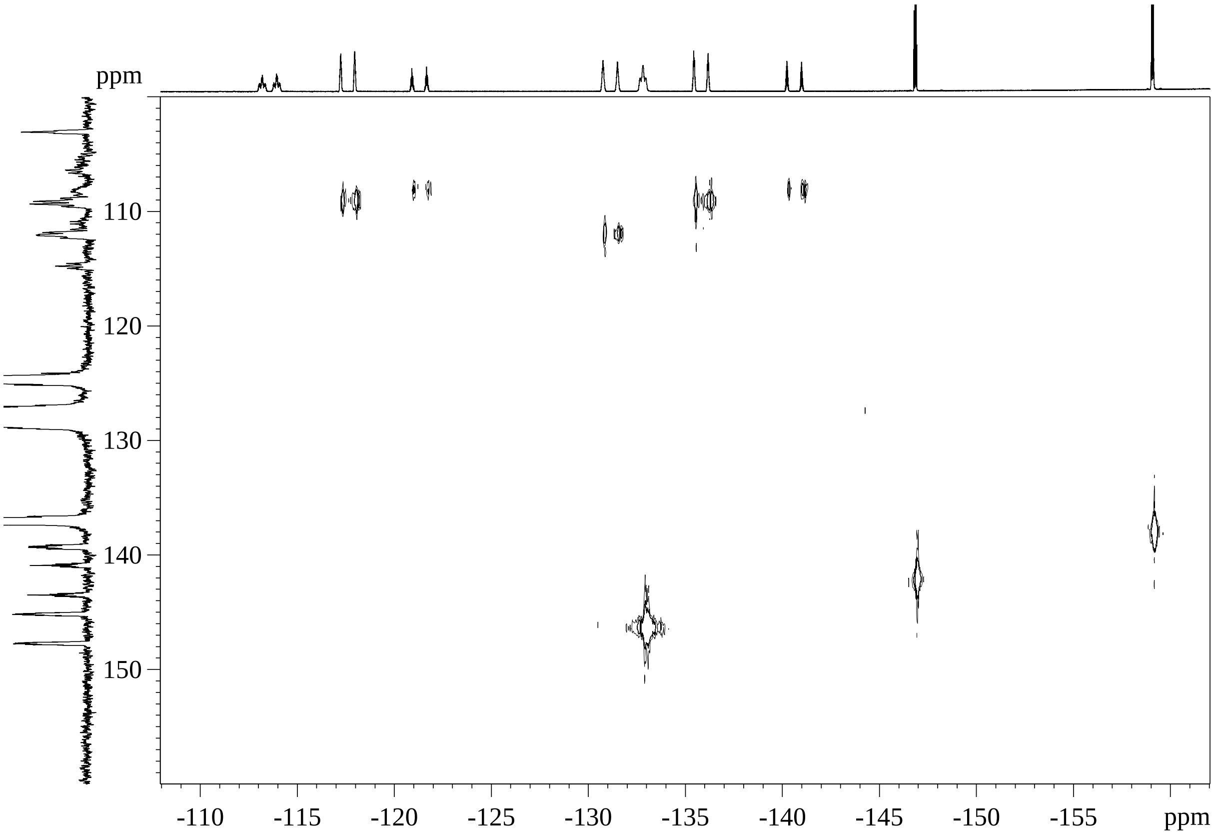

Fig. 34: ^{19}F, ^{13}C HSQC NMR spectrum of **2** in toluene.

Vibrational spectroscopy

Fig. 35 and Fig. 36 show the infrared and Raman spectra of solid **2**, which are in good agreement with calculated bands (cf. section 6.6, Tab. 39). The O-H band appears only in the IR spectrum at 3623 cm^{-1}, and is shifted by 81 cm^{-1} with respect to the calculation (3543 cm^{-1}). This is probably the result of strong intermolecular hydrogen bridging, which is also observed in the crystal structure (see below).

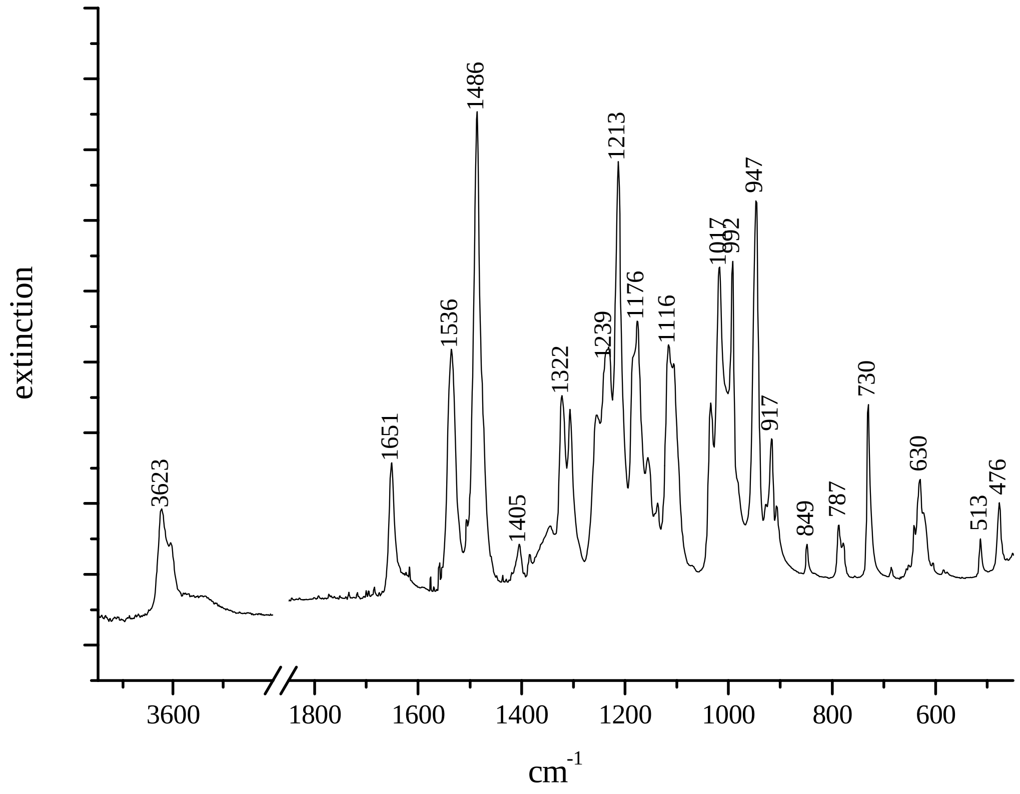

Fig. 35: IR spectrum of **2**.

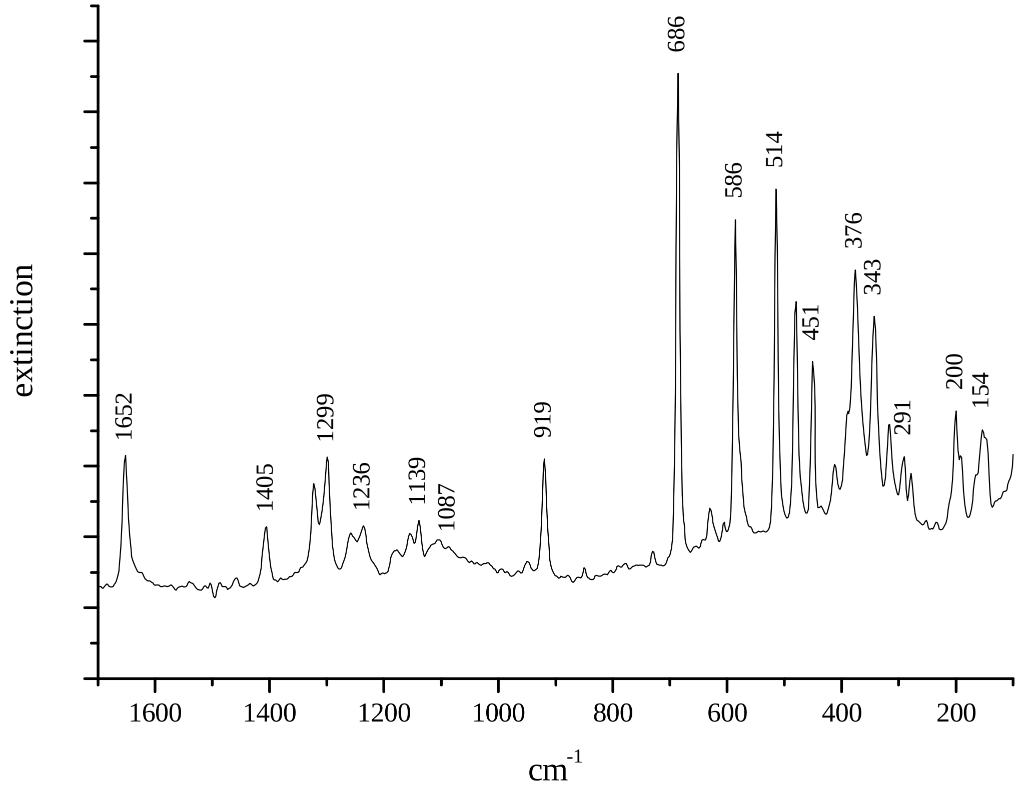

Fig. 36: Raman spectrum of **2**.

Crystal structure determination

2 slowly crystallizes at room temperature from hexane in the form of colorless needles. The space group was determined as monoclinic $P2_1/n$ with a = 12.05 Å, b = 15.16 Å, c = 15.66 Å, β = 110.9° and Z = 8. For a detailed report of the structural parameters see section 6.11, Tab. 61.

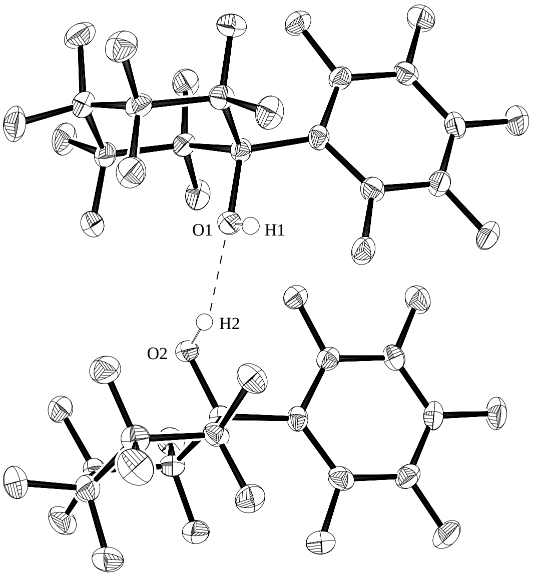

Fig. 37: Asymmetric unit of the crystal structure of **2**. Thermal ellipsoids drawn at 50% probability level. Distances in pm, libration-corrected distances are indicated by an asterisk: O1-O2 301.2(1) pm, O1-H1 93.4(2)*, O2-H2 93.6(3)*, O1-C 141.7(1), O2-C 140.0(1). O1-H2-O2 166.3(2)°.

The asymmetric unit contains a dimer of **2** (Fig. 37) connected by an asymmetric hydrogen bridge. All contacts fall into the characteristic range for weak O-H---O bridges[212, 213] with H2---O1: 223.3(1) pm, H2-O2: 93.6(3) pm (libration corrected, because the bond distances of hydrogen atoms found on the difference Fourier map are often too short, uncorrected distance 79.6(2) pm), O1---O2: 301.2(1) pm and an O-H-O angle of 166.3(2)°. The H atom not involved in the H bonding exhibits a slightly shorter O1-H1 distance of 93.4(2) pm (libration corrected, uncorrected: 73.8(1) pm). Both hydrogen atoms were found on the Fourier map and refined without positional constraints. The H1 proton points away from the hydrogen bridge with a H-O-H angle of 119.1(1)°. This peculiar bonding scenario is the result of the considerations in chapter 3.1.1. Perfluorinated alcohols tend to be poor donors for intermolecular H bonding. In the absence of a donor and in combination with the high steric demand of the $C_{12}F_{15}$ moiety, this leads to the formation of only a single weak hydrogen bridge. Correspondingly, in the molecule which acts as hydrogen donor, the C_6F_5 group is rotated by 81.7° with respect to the C_6F_{10} group, while in the other both groups are orthogonal with an angle of 89.7°. Expectedly, in the MP2/TZVPP calculation of the monomer without any hydrogen bonding, the angle lies between both values with 85.0°. The contacts between the fluorine atoms in the ortho position of the C_6F_5 ring and the 2-position of the C_6F_{10} ring range between 243 and 263 pm, which is in good accordance with the ^{19}F NMR results and the MP2 calculation (243 and 255 pm). The H1 proton, which is not involved in the intermolecular hydrogen bond, exhibits two H-F contacts at 220 pm (with the fluorine atom in ortho position of C_6F_5, O-F: 250 pm) and 232 pm (with a fluorine atom in C_6F_{10}, O-F: 273 pm). These interactions are comparable to the H-F interactions in **1** (H-F (calc.): 246 and 184 pm, O-F (calc.) 271 and 260 pm) and in excellent agreement with the MP2/TZVPP minimum geometry (which features O-F distances of 250 and 269 pm, respectively).

As a side note, crystals of **2**, and generally all crystals of compounds containing the phex ligand, dissolve slowly in perfluoroether oils. It is advisable to prepare samples in motor oil or at low temperatures.

Another crystal structure of **2** was obtained as a side product of a failed attempt to synthesize $N(^{n}Bu)_4[FAl(phex)_3]$ (see 3.2.5). **2** co-crystallizes with ^{n}butylammonium bromide and one water molecule, forming colorless crystalline platelets of $C_6F_5(C_6F_{10})OH\cdot(^{n}C_4H_9)_4NBr\cdot H_2O$ **2a** in the monoclinic space group C2/c with a = 29.32 Å, b = 11.14 Å, c = 23.69 Å, β = 119.9° and Z = 8. For a more detailed report of the structural parameters see section 6.11, Tab. 61.

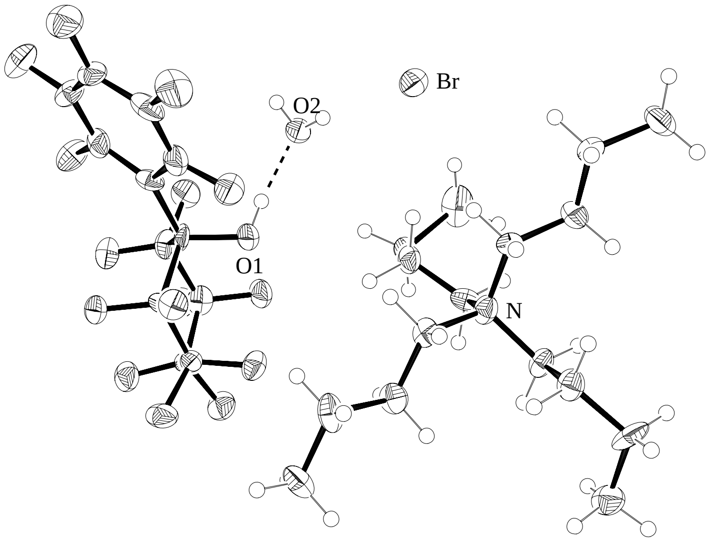

Fig. 38: Asymmetric unit of the crystal structure of **2a**. Thermal ellipsoids drawn at 50% probability level. Distances in pm: O1-O2 254.0(1), O1-C 139.1(1), H(bridge)-O2 171.1(1), N-C 151.4(1)-153.9(1). Angles in °: O1-H-O2 169.2(1), C-N-C 106.6(1)-111.4(1).

2a exhibits is a pronounced rotation of the C_6F_5 group with respect to the C_6F_{10} group with an angle of 51.6° between the two (cf. in **2**: 81.7 and 89.7°). This might be attributed to a rather short hydrogen bond with the water molecule (OH---O: 171.1(1) pm, O-O: 253.9(1) pm).

3.1.4. New perfluorinated metal(I) alkoxides

Main group and transition metal alkoxides are widely used in organometallic synthesis or as precursors for ceramic materials.[214-216] Despite their lack of a conventional donor site, fluoroalkoxides can act as functional groups via short secondary M-F bonds to electrophilic metals such as alkaline earth metals or lanthanides, strongly modifying the reactivity around the metal centre.[217] Fluorinated ligands often improve volatility, making them interesting targets for CVD precursor systems because they form metal fluorides upon decomposition. The most familiar examples for fluorinated alkoxides are the $(CF_3)_2(H)CO^-$ (hfip), $(CF_3)_2(CH_3)CO^-$ (hftb) and $(CF_3)_3CO^-$ (pftb) groups, of which various metal derivates were recently developed (Na, Zr, Ba,[218] Y,[219] La, Pr, Eu).[220, 221] In the case of group 11 transition metal alkoxides, research has been restricted to Cu(I) compounds and only $CuOCR_3$ (R = CH_3, C_6H_5) has been structurally characterized.[222-225] The only known homologous Ag or Au compounds were phosphine adducts of the metal trimethylsiloxanes.[226] Recently the first donor-free, structurally characterized Ag(I) alkoxide $AgOC(CF_3)_3$ was published,[227, 228] which, as a volatile silver compound, is an interesting CVD precursor candidate.

Alkali metal alkoxides can be prepared in straightforward syntheses from ROH and MH (M = Li, Na, K) in good yields.[218, 229, 230]

$$\text{LiH} + \text{HO-R}^F \xrightarrow[-\,H_2]{Et_2O} \text{Li-OR}^F$$

$$\text{Li-OR}^F + \text{AgX} \xrightarrow[-\,\text{LiX}]{CH_2Cl_2} \text{Ag-OR}^F \qquad X = F,\ BF_4$$

(Eq. 16)

Starting from the lithium alkoxide (Eq. 16), the silver alkoxides can be obtained by metathesis with AgF or $AgBF_4$. $AgBF_4$ is generally preferable and leads to better yields because of its higher solubility.

A possible route to directly obtain silver alkoxides containing the C_6F_5 group is the reaction of pentafluorophenylsilver AgC_6F_5 with ketones (Eq. 17).

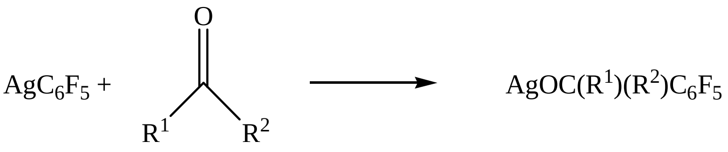

(Eq. 17)

Pentafluorophenylsilver is formed in quantitative yields in a facile synthesis from silver fluoride and pentafluorophenyltrimethylsilane (Eq. 18).[231]

$$C_6F_5SiMe_3 + AgF \xrightarrow{\text{RT, EtCN}} AgC_6F_5 + FSiMe_3$$

(Eq. 18)

Li and Ag alkoxides are interesting reagents for the synthesis of new WCA from metal halides (Eq. 19).

$$(n+1)\ A\text{-}OR^F + M^nX_n \xrightarrow{-\ n\ AX} A^+[M^n(OR^F)_{n+1}]^-$$

A = Li, Ag; M = Al, B, Sb, Nb, ...

(Eq. 19)

Silver alkoxides could enable the synthesis of Ag^+ salts of WCA that are not accessible through lithium alkoxides. For example, $SbCl_5$ reacts with only four equivalents of $LiOC(H)(CF_3)_2$ under formation of $Li[SbCl_2(OR^F)_4]$. However, $AgOTeF_5$ can be used in the synthesis of teflate-based homoleptic WCA salts with $SbCl_5$ or $NbCl_5$.[86] Furthermore, reactions of $AgOR^F$ with strong Lewis acids (Eq. 20) would directly lead to silver salts of homoleptic or heteroleptic WCA without formation of side products or the problems associated with metathesis reactions (solubility, lattice energy).[232]

$$Ag\text{-}OR^F + M^n(OR^{F'})_n \longrightarrow Ag^+[M^n(OR^F)(OR^{F'})_n]^-$$

M = Al, B, Sb, Nb, ...

(Eq. 20)

3.1.5. Synthesis and characterization of $LiOC(CF_3)_3 \cdot 2THF$

Synthesis

Commercially available nonafluoro-^{t}butanol was reacted with lithium borohydride in an attempt to synthesize a lithium salt of a boron-centered WCA according to (Eq. 21).

$$4\ (CF_3)_3COH + LiBH_4 \xrightarrow[-\ 4\ H_2]{\text{hexane}} Li[B(OC(CF_3)_3)_4]$$

(Eq. 21)

However, the expected reaction does not take place. The product (white powder) proved insoluble in CH_2Cl_2, but could be identified as $LiOC(CF_3)_3$ by IR spectroscopy. When recrystallizing from THF, the adduct $LiOC(CF_3)_3 \cdot 2THF$ **3** is formed. The mass balance clearly shows that only the first equivalent of the alcohol reacts (Eq. 22), indicating that apart from hydrogen, BH_3 is formed and the target WCA is not an intermediate.

$$(CF_3)_3COH + LiBH_4 \xrightarrow[\substack{-\ H_2 \\ -\ BH_3}]{\text{hexane}} LiOC(CF_3)_3$$

(Eq. 22)

NMR spectroscopy

The proton NMR of **3** shows no signals apart from THF, indicating that the reaction is quantitative and the solution contains no residual alcohol. No signal is observed in the ^{11}B spectrum of isolated **3**, supporting the assumption that boron was removed from the reaction in the form of BH_3. The ^{13}C NMR spectrum shows the expected signals of the perfluorinated ^{t}Bu group with two ^{13}C signals at 122.5 ppm ($^1J_{C,F} = 292$ Hz) and 52.8 ppm ($^2J_{C,F} = 28$ Hz). Only a single ^{19}F signal at -77.0 ppm is observed.

IR spectroscopy

The IR spectrum of **3** exhibits the typical bands of a perfluoro-^{t}Bu group in the range between 400 and 1320 cm^{-1}. They may easily be assigned by comparison with other compounds that contain these groups,[53, 60] as well as with the calculated vibrational frequencies of the donor-free tetrameric alkoxide $\{LiOC(CF_3)_3\}_4$.[228] All remaining bands can be assigned to THF.[233] For a complete list of IR bands see section 6.6, Tab. 40.

Crystal structure determination

The crystal structure of donor-free $LiOC(CF_3)_3$ has recently been published.[228] **3** crystallizes in small colorless blocks from concentrated solutions in 1:1 CH_2Cl_2/THF. The space group was determined as monoclinic $P2_1/n$ with a = 8.95 Å, b = 10.29 Å, c = 17.60 Å, β = 96.5° and Z = 4. For a detailed report of the structural parameters see section 6.11, Tab. 61.

In the solid state structure, two equivalents of the alkoxide form a centrosymmetric, almost square planar ring (Fig. 39) with Li-O bond distances of 193.1(3) and 195.3(4) pm. The O-Li-O angle (93.7(2)°) is larger than the Li-O-Li angle (86.2(2)°). The two remaining coordination sites of the tetrahedrally coordinated lithium atoms are occupied by THF molecules with longer Li-O bond distances of 197.4(4) and 200.5(4) pm. There are no Li-F contacts which are significantly shorter than the sum of van-der-Waals radii (329 pm) in the structure (shortest contact: 294.2(3) pm).

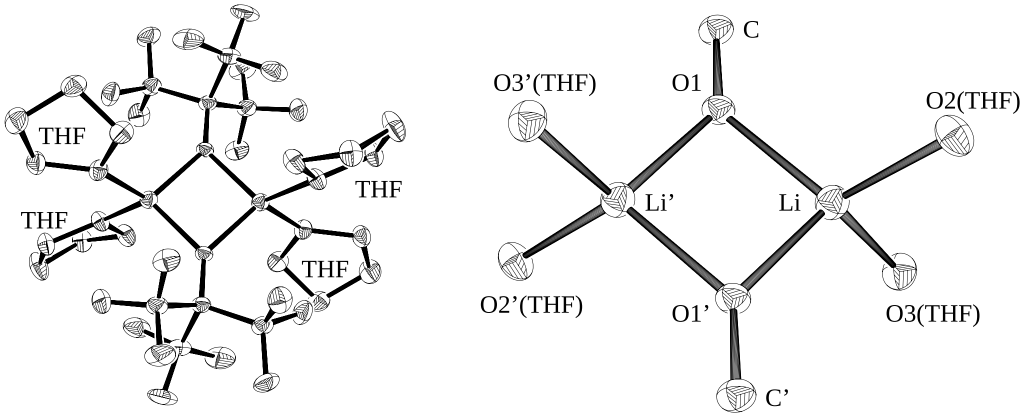

Fig. 39: Crystal structure of **3**. Thermal ellipsoids drawn at 50% probability level.
Hydrogen atoms were omitted for clarity. Symmetry equivalent atoms are indicated by an inverted comma.
Distances in pm: Li-O1 195.3(4), Li-O1' 193.1(3), Li-O2 200.5(4), Li-O3 197.4(4), O1-C 134.7(2).
Angles in °: Li'-O1-Li 86.3(2), O1-Li-O1' 93.7(2), O2-Li-O3 107.7(2).

3.1.6. Synthesis and characterization of $AgO(C_6F_{10})C_6F_5{\cdot}EtCN$

Synthesis

Pentafluorophenylsilver was prepared as described in the literature[231] and reacted with an excess of perfluorocyclohexanone. After removal of the solvent in vacuo, no reaction can be observed in CH_2Cl_2, diethyl ether or pure perfluorocyclohexanone, as detected by evaluation of the mass balance. In propionitrile, the reaction proceeds after short ultrasonic activation, forming the ocher, light-sensitive propionitrile adduct $AgO(C_6F_{10})C_6F_5{\cdot}EtCN$ **4**. The donor is strongly bound to the silver atom and can not be removed, even in vacuo at 80°C. Above this temperature, decomposition occurs.

NMR spectroscopy

The ^{19}F and ^{13}C NMR spectra of **4** in CD_2Cl_2 exhibit the typical signals expected for the phex ligand (see Tab. 8 and section 3.1.3). However, small amounts of residual AgC_6F_5 (peaks at -98.7, -157.4 and -145.0 ppm)[231] and $C_6F_{10}O$ can be found in the ^{19}F spectrum. The signal-to-noise ratio of the ^{13}C spectrum is poor because of the low solubility of **4** in CD_2Cl_2, but signals in the typical regions of 108-120 and 140-155 ppm can be observed. The proton NMR spectrum shows only one signal set for the coordinated propionitrile at 2.52 (quartet) and 1.32 ppm (triplet) (cf. pure propionitrile: 2.35 and 1.31 ppm).

Tab. 8: Experimental chemical shifts of **4** and comparison with **2**, signals of AgC_6F_5 and $C_6F_{10}O$ omitted.

	shift (4) [ppm][a]	**shift (2) [ppm][b]**	**assignment[c]**
$\delta^{13}C$	10.5	-	EtCN
	11.0	-	EtCN
	89.3	78.9	aromatic C
	-[d]	108.1	aliphatic C
	-[d]	109.0	aliphatic C
	-[d]	111.9	aliphatic C
	125.9	-	EtCN
	142.0	138.0	aromatic C
	145.1	142.2	aromatic C
	150.6	146.5	aromatic C
$\delta^{19}F$	-110.1	-113.6	aliphatic F
	-114.9	-117.6	aliphatic F
	-120.8	-121.3	aliphatic F
	-131.3	-131.1	aromatic F
	-134.6	-132.8	aliphatic F
	-134.9	-135.8	aliphatic F
	-139.9	-140.6	aliphatic F
	-145.0	-146.8	aromatic F
	-162.1	-159.0	aromatic F
$\delta^{1}H$	1.31	-	EtCN
	2.52	-	EtCN

[a] in CD_2Cl_2; [b] in toluene-d8; [c] see Fig. 29; [d] not resolved.

Crystal structure determination

4 crystallizes in colorless needles from concentrated solutions in CH_2Cl_2. The space group was determined as monoclinic $P2_1/c$ with a = 10.32 Å, b = 19.05 Å, c = 18.07 Å, β = 93.2° and Z = 8. For a detailed report of the structural parameters see section 6.11, Tab. 62.

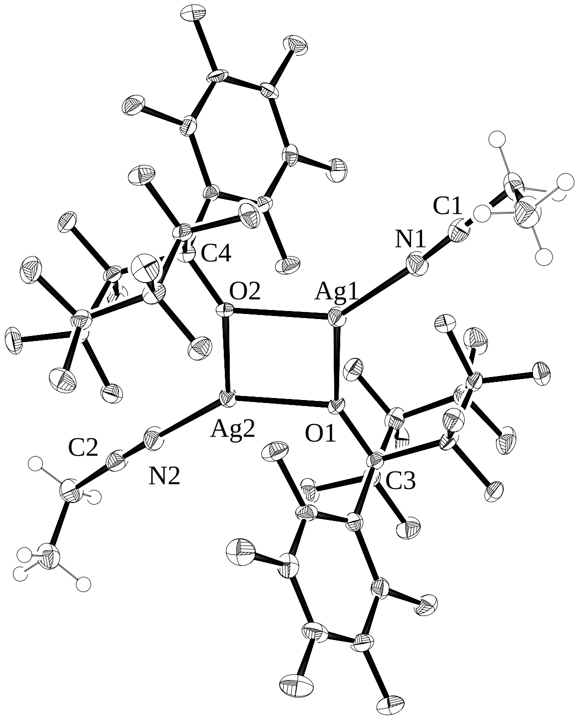

Fig. 40: Crystal structure of **4**. Thermal ellipsoids drawn at 50% probability level. Distances in pm: Ag1-O1 225.9(2), Ag1-O2 235.9(2), Ag2-O1 235.3(2), Ag2-O1 224.6(2), Ag1-N1 214.6(3), Ag2-N2 215.9(3), N1-C1 114.2(5), N2-C2 113.1(5), O1-C3 136.4(4), O2-C4 136.1(4). Angles in °: Ag1-O1-Ag2 96.3(1), Ag1-O2-Ag2 96.5(1), O1-Ag1-O2 83.4(1), O1-Ag2-O2 83.8(8), Ag-O-C 125.2(2)-132.7(2), Ag1-N1-C1 175.3(3), Ag2-N2-C2 178.4(3).

The asymmetric unit contains an almost planar, dimeric trapezoid unit of **4** (Fig. 40), in which each silver atom is trigonally coordinated by two oxygen atoms of the ligand and one propionitrile molecule. The nitrile groups almost form a plane with the silver atoms (Ag-N-C angles 175.3(3) and 178.4(3)°), with Ag-N bond lengths of 214.6(3) and 215.9(3) pm. The shortest contact Ag-F contact (289.4(2) pm, cf. sum of van-der-Waals radii: 319 pm) is formed between one silver atom and a fluorine atom in the ortho position of an attached C_6F_5 group. The contact distance is in the typical range of CF-Ag interactions (260-300 pm[234, 235]), but not particularly short.

3.1.7. Synthesis and characterization of $LiO(C_6F_{10})C_6F_5$

Synthesis

$LiO(C_6F_{10})C_6F_5$ **5** is obtained in quantitative yields in a simple reaction of the parent alcohol **2** with lithium hydride in diethyl ether. The product is a white solid with a melting point of 139°C.

NMR spectroscopy

Compound **5** is poorly soluble in many solvents, hence only a ^{19}F NMR spectrum was recorded. The signals are identical to the typical signal set of a phex ligand (Tab. 7). However, all signals are slightly broadened in comparison with the alcohol **2**. There are no residual proton signals of the alcohol in the ^1H NMR.

Vibrational spectroscopy

For a complete list of IR and Raman bands see section 6.6, Tab. 41. The IR bands of **5** are almost identical with the parent alcohol **2** (Fig. 41). The O-H band at 3623 is missing, indicating a quantitative reaction.

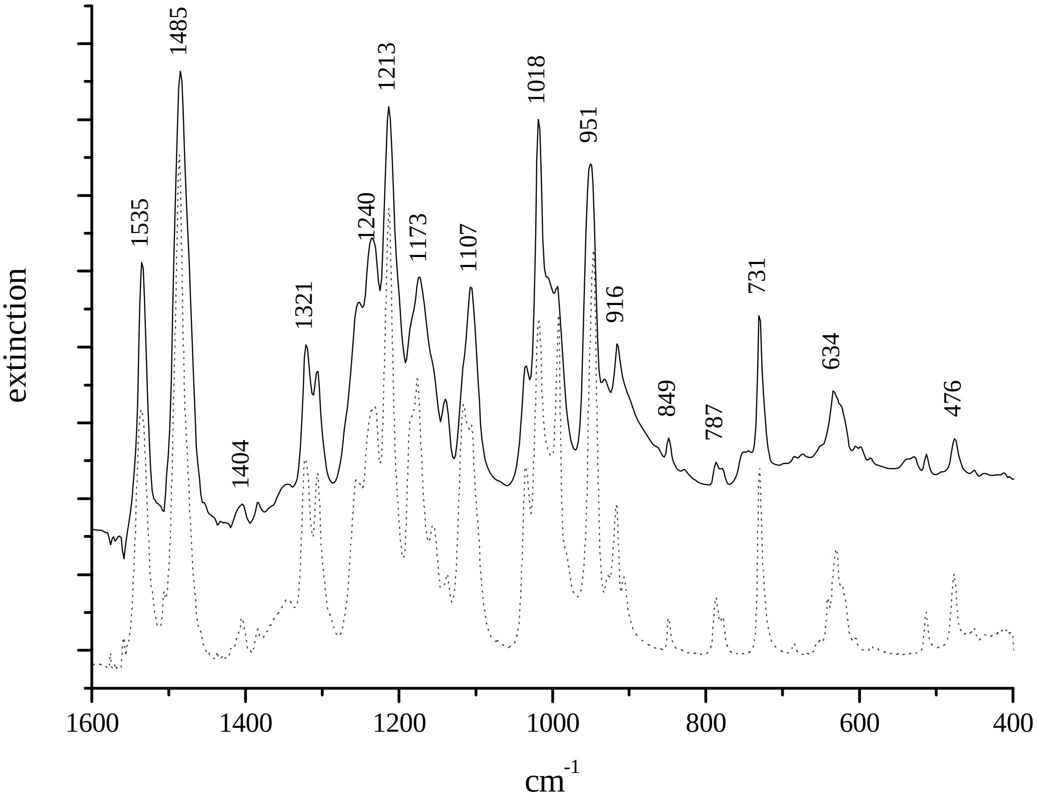

Fig. 41: IR spectrum of **5** (solid line). The dotted line shows the spectrum of the parent alcohol **2**.

Although crystals of **5** show a strong fluorescence and weaker Raman scattering than the parent alcohol **2**, almost all characteristic bands of the phex ligand can be observed in the Raman spectrum (Fig. 42). Although an aggregation of monomeric **5** to dimeric or oligomeric units can be expected, only very weak additional bands at 528, 752 and 827 cm^{-1} are observed in the region between 200 and 500 cm^{-1} (Raman and IR), that could be assigned to Li-O cage vibrations.

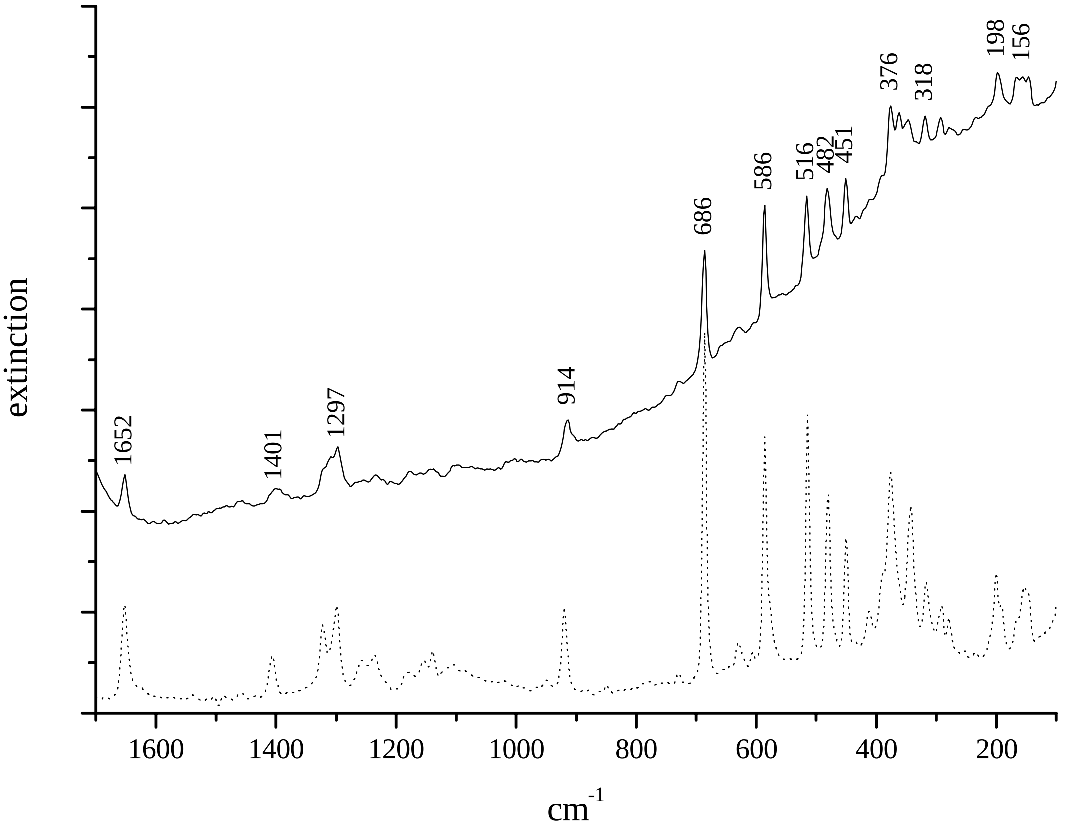

Fig. 42: Raman spectrum of **5** (solid line). The dotted line shows the spectrum of the parent alcohol **2**.

Crystal structure determination

5 crystallizes in colorless needles **5a** from concentrated solutions in toluene. The space group was determined as triclinic P1 with a = 11.37 Å, b = 12.28 Å, c = 17.71 Å, α = 75.9°, β = 71.5°, γ = 79.3° and Z = 2. For a detailed report of the structural parameters see section 6.11, Tab. 62. The presence of inversion symmetry was checked, but the structure contains a diffusely disordered toluene molecule which reduces the symmetry to P1. Additionally, the two molecules in the unit cell are not exactly identical and differ in various contact lengths (see below). In the crystal structure, six units of $LiO(C_6F_{10})C_6F_5$ form two trimeric $\{LiO(C_6F_{10})C_6F_5\}_3$ **5a** moieties (Fig. 43). In the **5a** molecules, all three aromatic ligands point in the same direction. The lithium and oxygen atoms form almost planar hexagons with O-Li-

O angles of 118.8(3) to 128.9(3)° and Li-O-Li angles 110.8(2) to 117.3(1)°. The Li-O bond distances are irregular and range between 178.1(1) and 196.8(1) pm, the O-C bond lengths between 133.8(1) and 139.8(1) pm.

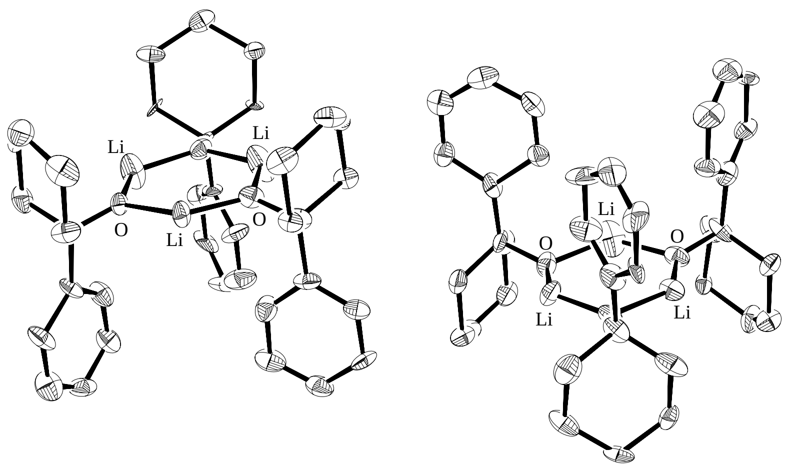

Fig. 43: Crystal structure of **5a**. Fluorine atoms omitted for clarity, thermal ellipsoids drawn at 50% probability level.

Each lithium atom is coordinated by one aromatic fluorine atom of the C_6F_5 group and three or four fluorine atoms of the aliphatic C_6F_{10} group (Fig. 44).

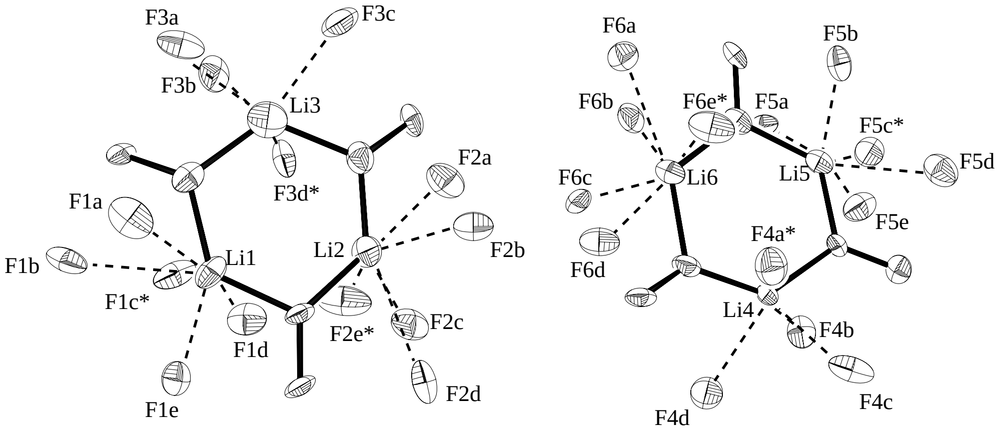

Fig. 44: Detail of the crystal structure of **5a**, showing the coordination of the lithium atoms. Thermal ellipsoids drawn at 50% probability level. Fluorine atoms of C_6F_5 groups are marked with an asterisk. Distances in pm: Li1-F1a 279.1(1), Li1-F1b 268.0(1), Li1-F1c* 211.2(1), Li1-F1d 213.6(1), Li2-F2a 275.1(1), Li2-F2b 214.7(1), Li2-F2c 287.6(1), Li2-F2d 269.8(1), Li2-F2e* 216.2(1), Li3-F3a 218.7(1), Li3-F3b 259.0(1), Li3-F3c 239.5(1), Li3-F3d* 215.0(1), Li4-F4a* 223.9(1), Li4-F4b 253.2(1), Li4-F4c 228.9(1), Li4-F4d 247.2(1), Li5-F5a 276.3(1), Li5-F5b 219.9(1), Li5-F5c* 213.7(1), Li5-F5d 257.8(1), Li5-F5e 267.4(1), Li6-F6a 257.3(1), Li6-F6b 271.9(1), Li6-F6c 209.6(1), Li6-F6d 269.1(1), Li6-F6e* 220.2(1).

The coordination with the aliphatic groups tend to be weaker with distances of 209.6 to 297.1 pm (av. 251.6 pm, sum of van-der-Waals radii of lithium and fluorine: 329 pm), while the Li-F contacts involving fluorine atoms in the ortho position of a pentafluorophenyl ring range between 211.2 and 223.9 pm (av. 216.7 pm). According to Plenio,[234] for hard metals it is better to evaluate M-F distances by other criteria than the sum of van-der-Waals radii, because the contacts are best described as interactions between a covalently bound fluorine atom with a metal cation. Instead, he proposes to use the sum d_{min} of the ionic radius of lithium as defined by Shannon[236] and the van-der-Waals radius of fluorine ($r_{ion}(Li^+)$ = 59 pm, $r_{vdw}(F)$ = 147 pm, d_{min} = 206 pm) as a minimum cutoff. The maximum distance d_{max} is defined as the sum of $r_{vdw}(F)$ and the ionic van-der-Waals radius of lithium as defined by Kollmann et al. ($r_{vdw}(Li^+)$ = 100 pm, d_{max} = 247 pm).[237, 238] Of the contacts shown in Fig. 44, all six involving aromatic fluorine atoms fulfill these criteria, while only 8 of the 21 contacts with aliphatic fluorine atoms are shorter than 247 pm. The shortest known intramolecular CF-Li contacts occur in the WCA salt $Li[Al(OC(C_6H_5)(CF_3)_2)_4]$[55] (198.4, 208.2, 209.8 and 235.2 pm). This shows that the coordination in **5a** is indeed very strong (cf. Li6-F6c 209.6(1) pm), owing to the high steric demand of the phex ligand which prevents the formation of larger Li-O cages. For example, the slightly less sterically demanding pftb ligand leads to the formation of distorted cubane-type tetramers in donor-free $LiOC(CF_3)_3$.[228]

From monofluorobenzene, **5** crystallizes in the form of colorless blocks **5b** in the triclinic space group $P\overline{1}$ with a = 7.16 Å, b = 11.05 Å, c = 11.65 Å, α = 94.2°, β = 96.4°, γ = 99.9 and Z = 2. For a detailed report of the structural parameters see section 6.11, Tab. 62. The unit cell contains a dimer $\{(C_6H_5F)LiO(C_6F_{10})C_6F_5\}_2$ **5b**, in which both lithium atoms are additionally coordinated by one molecule of monofluorobenzene (Fig. 45). Two Li and two O atoms form a planar ring, with Li-O bond lengths of 186.4(1) and 188.6(1) ppm and Li-O-Li angles of 85.6(1)° and O-Li-O angles of 94.4(1)°. The center of inversion resides on the center of the Li-O ring.

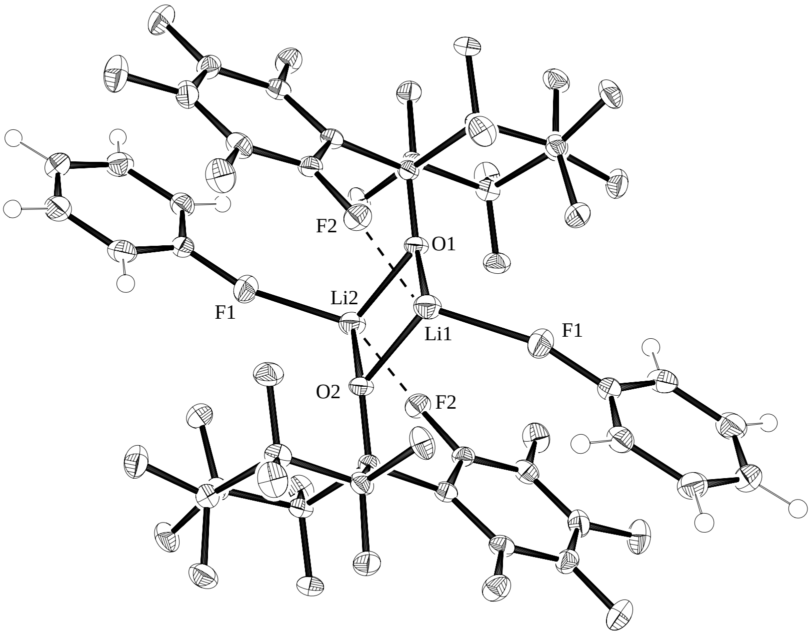

Fig. 45: Crystal structure of **5b**, thermal ellipsoids drawn at 50% probability level. Due to a center of symmetry in the Li-O ring, distances are not given for equivalent atoms. Distances in pm: Li1-O1 186.4(1), Li1-O2 188.6(1), Li-F1 201.4(1), Li-F2 208.1(1), F1-C 137.9(1), F2-C 135.7(1), O-C 135.2(1). Angles in °: Li-O-Li 85.6(1), O-Li-O 94.4(1), Li-F1-C 164.4(2), Li-F2-C 126.7(2), Li1-O1-C 133.7(1), Li2-O1-C 127.0(2).

The Li-F2 contacts involving the fluorine atoms in the ortho positions of the C_6F_5 group are very short (208.1(1) pm, cf. d_{min} = 206 pm, d_{max} = 247 pm).[234] The C-F bond of the coordinating fluorine (135.7(1) ppm) is not significantly longer than in the other C-F bonds of the perfluorophenyl group (133.5(1)-134.3(1) pm, av. 133.7 pm). There is no coordination with the aliphatic C_6F_{10} group (shortest Li-F contact 279.9 pm) or another dimer (282.1 pm). However, the strong coordination of fluorobenzene to lithium with a Li-F1 bond distance of only 201.4(1) pm is unique. While ortho-fluorophenyl ligands are known to form short Li-F contacts in some lithium silazides (e.g. Li-F: 198.2, 198.6 pm,[239] Li-F: 214.9 pm[240]) or in complexes with partially fluorinated macrocycles (Li-F: 203.5[241]), only one publication describes the coordination of lithium with a mono- or difluorobenzene.[242] In the therein described lithium hexamethyldisilazide (LiHMDS) complex $(LiHMDS)_2{\cdot}C_6H_5F$ (in which only one lithium atom of the LiHMDS dimer is coordinated by fluorobenzene), the Li-F contact distance is 186.6 pm. According to relatively low-level DFT calculations reported by other authors (B3LYP/6-31G*), the lighter alkali metal ions should coordinate the π-face of fluorobenzene, while for the heavier ones an equilibrium between π coordination and fluorine coordination occurs.[243, 244] A very shallow potential hypersurface can be expected for such M-F contacts,[245] so it is probable that the computational method is inadequate to describe the delicate bonding situation or the coordination mode is dominated by solid state packing effects.

5b can be expected to be very sensitive to moisture. Indeed, if stored in air for even a short time, crystals of **5b** exchange monofluorobenzene for water, forming colorless crystalline blocks of $\{(H_2O)LiO(C_6F_{10})C_6F_5\}_2$ **5c**. The compound crystallizes in the orthorhombic space group $P2_12_12$ (a = 19.17 Å, b = 9.84 Å, c = 15.70 Å and Z = 8), with two dimers in the asymmetric unit that are slightly different in some bond lengths (Fig. 46), but otherwise identical. For a detailed report of the structural parameters see section 6.11, Tab. 63.

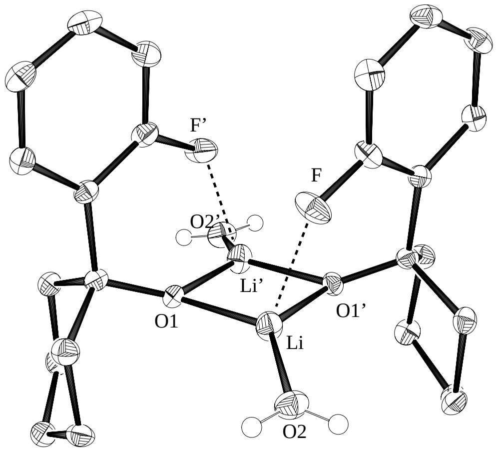

Fig. 46: Detail of the crystal structure of **5c**, showing only one of two symmetry-independent dimeric $\{(H_2O)LiO(C_6F_{10})C_6F_5\}_2$ units. Most fluorine atoms were omitted for clarity. Thermal ellipsoids drawn at 50 % probability level. Symmetry equivalent atoms are indicated by an inverted comma. Bond lengths and angles of the two symmetry-independent dimers are separated by a slash. Distances in pm: Li-O1 189.3(1) / 187.9(1), Li-O1’ 189.0(1) / 188.2(1), Li-O2 193.1(1) / 191.0(2), Li-F 219.8(1) / 238.4(1), O1-C 136.0(2) / 135.8(1). Angles in °: Li-O1-Li’ 86.1(1) / 86.2(1), O1-Li-O1’ 93.9(1) / 93.8(1), Li-F-C 130.8(1) / 128.9(1), Li-O1-C 136.2(1) / 137.4(1), Li’-O1-C 132.8(1) / 133.0(2).

Each of the two dimers exhibits a C_2 axis in the middle of an almost square planar ring formed by lithium and oxygen, which is normal to the plane. The Li-O bond lengths within the ring are 188.2(1) and 187.9(1), respectively 189.0(1) and 189.3(1) pm, and the bond Li-O lengths towards the coordinated water molecule are 191.0(1) and 193.1(1) pm. Each lithium atom is also coordinated by one fluorine atom in the ortho position of the C_6F_5 group of the phex ligand (Fig. 46), in one dimer the contact distance is significantly longer than in the other (238.4(1) vs. 219.8(1) pm, cf. d_{max} = 247 pm).

3.1.8. Synthesis and characterization of $NaO(C_6F_{10})C_6F_5$

Synthesis

The sodium alkoxide $NaO(C_6F_{10})C_6F_5$ **6** can be synthesized in a simple quantitative reaction of the parent alcohol **2** with an excess of NaOH in water. After removal of water in vacuo and extraction with hot toluene, the product is obtained in the form of colorless crystals.

Vibrational spectroscopy

For a complete list of IR and Raman bands see section 6.6, Tab. 42. The vibrational bands of **6** show good agreement with spectra of the parent alcohol **2** (Fig. 41). The O-H band at 3623 is missing in the IR spectrum, indicating a quantitative reaction. Both IR and Raman spectra show no bands of residual water, but contain characteristic bands of toluene between 2750 and 2970 cm^{-1}. Additionally, some weak bands appear in the Raman spectrum of **6**, which only exist in the IR spectrum of **2** and vice versa. This hints at a slightly distorted symmetry, because for some vibrational modes the selection rules applying for **2** are apparently no longer obeyed in the sodium alkoxide.

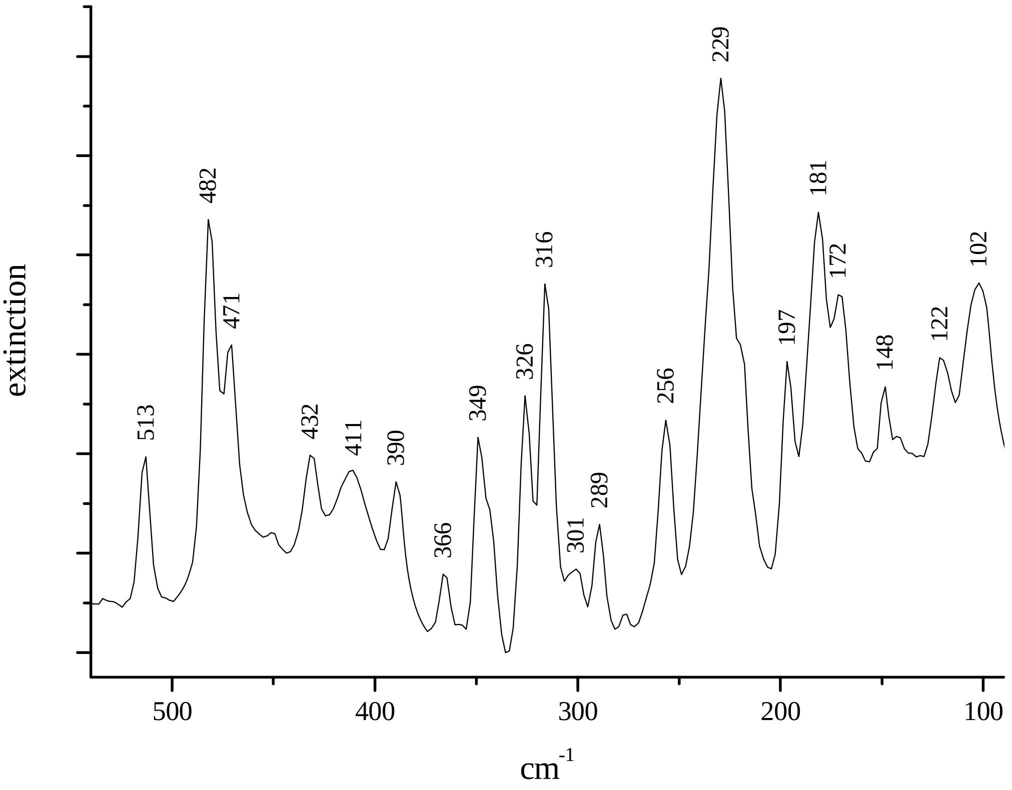

Fig. 47: IR spectrum of solid **6** in the region between 100 and 500 cm^{-1}.

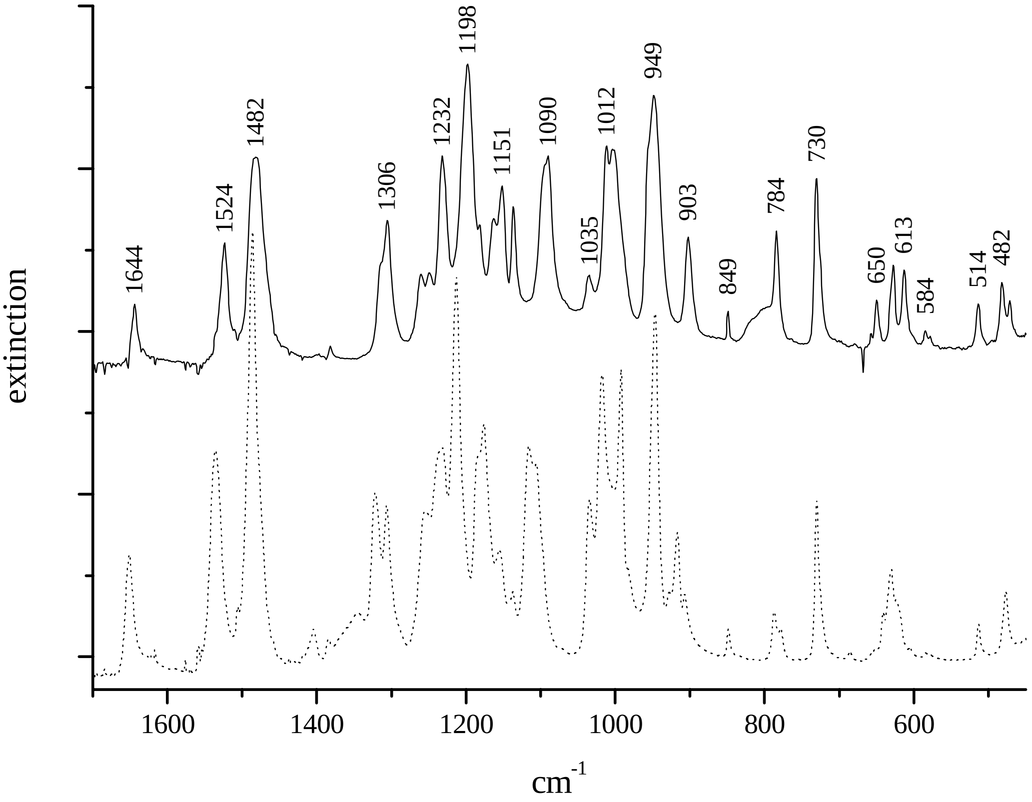

Fig. 48: IR spectrum of solid **6** in the region between 400 and 1700 cm^{-1} (solid line). One weak band of toluene at 2961 omitted for clarity. The dotted line shows the spectrum of the parent alcohol 2.

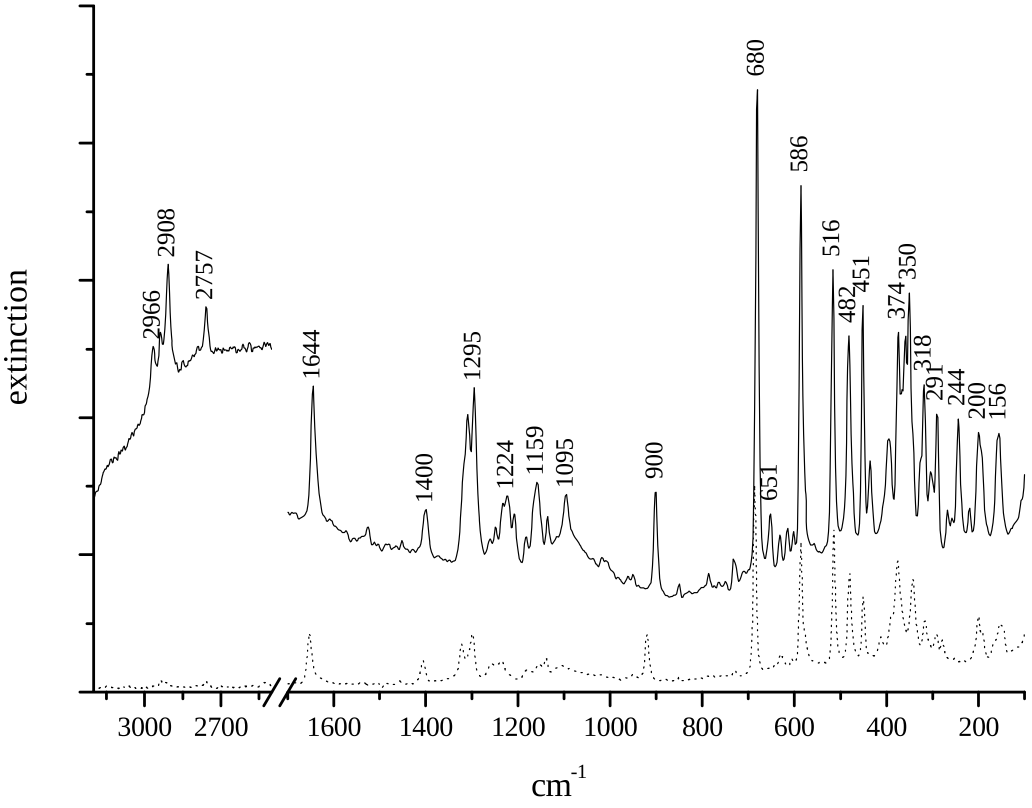

Fig. 49: Raman spectrum of crystalline **6** (solid line). The dotted line shows the spectrum of the parent alcohol **2**.

Crystal structure determination

6 crystallizes as thin colorless platelets from toluene in the monoclinic space group P2$_1$/c with the cell parameters a = 22.35 Å, b = 13.78 Å, c = 11.40 Å, β = 92.6° and Z = 4. The unit cell contains one solvent molecule (Fig. 50). **6** forms two-dimensional polymeric units $[\{NaO(C_6F_{10})C_6F_5\}_2]_n$ through intermolecular Na-F contacts, which commonly occur in fluorinated sodium alkoxides.[234] The four-membered ring formed by the oxygen and sodium atoms is almost planar (angle between O-Na-O planes: 4°) with Na-O bond lengths of 225.8(1) and 218.9(1) pm, Na-O-Na angles of 93.0(1)° and O-Na-O angles of 86.9(1)°.

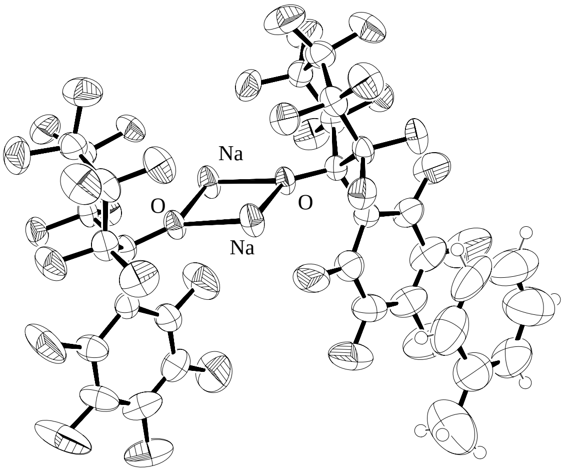

Fig. 50: Asymmetric unit of the crystal structure of **6**, showing a segment of the $[\{NaO(C_6F_{10})C_6F_5\}_2]_n$ polymer. Thermal ellipsoids drawn at 50% probability level.

Fig. 51 shows the eight-fold coordination of sodium, which is surrounded by 6 fluorine atoms and two oxygen atoms forming a distorted tetragonal antiprism. Four of the fluorine contacts are intramolecular with contact lengths of 257.0(1) to 297.7(1) pm ($r_{ion}(Na^+)$ = 102 pm, $r_{vdw}(F)$ = 147 pm, d_{min} = 249 pm, $r_{vdw}(Na^+)$ = 160 pm, d_{max} = 307 pm).[237, 238] The other two contacts are formed with one aliphatic and one aromatic fluorine atom of a neighboring $\{NaO(C_6F_{10})C_6F_5\}_2$ moiety (243.3(1) to 247.6(2) pm). From the contact lengths, no preference of Na-F coordination with aromatic fluorine atoms over the coordination with aliphatic fluorine atoms can be deduced. While the shortest distances are slightly longer than in other fluorinated sodium alkoxides (cf. shortest contact in $[NaOC(CF_3)(CH_3)_2]_4$: 233.2 pm[230], in $[NaOCH(CF_3)_2]_4$: 236.5 pm[218]), all CF-Na distances are well within the known range for such compounds.[234]

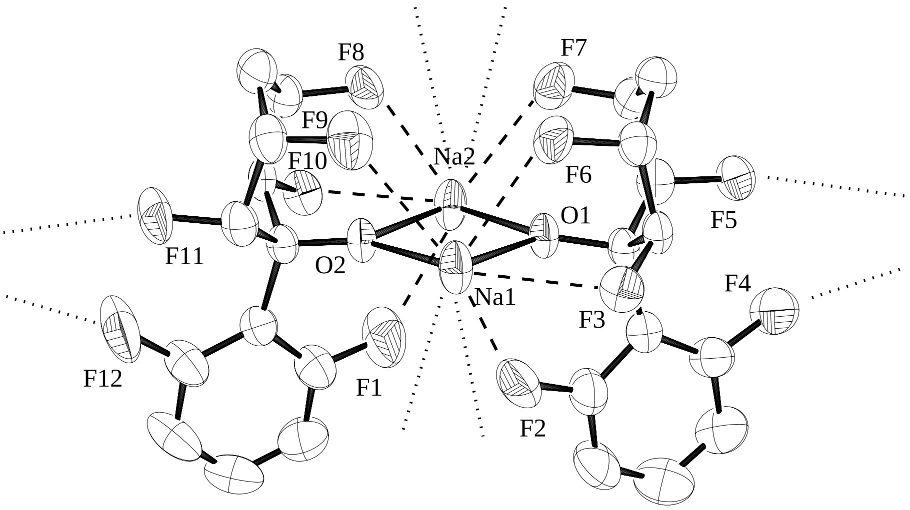

Fig. 51: Detail of the crystal structure of **6**, showing the sodium-fluorine coordination. Intramolecular contacts are indicated by dashed, intermolecular contacts by dotted lines. Some fluorine atoms omitted for clarity. Thermal ellipsoids drawn at 50% probability level. Distances in pm (intermolecular Na-F contacts marked with an asterisk): Na1-F3 273.7(1), Na1-F2 261.8(1), Na1-F9 297.7(1), Na1-F6 260.1(1), Na1-F4* 243.3(1), Na1-F5* 244.8(1), Na2-F7 271.0(1), Na2-F8 263.5(1), Na2-F10 273.7(1), Na2-F1 257.0(1), Na2-F11* 245.2(1), Na2-F12* 247.6(2), Na1-O1 225.8(1), Na1-O2 218.9(1), Na2-O1 218.9(1), Na2-O 225.9(1), O1-C 135.1(1), O2-C 134.5(1). Angles in °: Both Na-O-Na 93.0(1), both O-Na-O 86.9(1).

Fig. 52 shows a section of a two-dimensional polymeric layer of **6**, in which the sodium and oxygen atoms almost occupy a plane. There are no contacts between the layers with distances shorter than the sum of van-der-Waals radii (F-F: 294 pm, H-F: 267 pm).

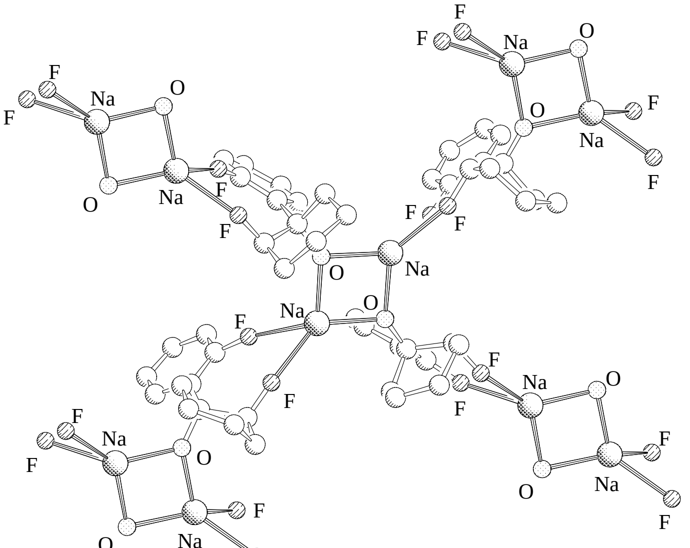

Fig. 52: Top-down view showing a section of a two-dimensional polymeric layer of **6**. Fluorine atoms not involved in intermolecular Na-F contacts and toluene molecules omitted for clarity.

Another crystal structure of the sodium alkoxide was obtained in the attempt to synthesize Na[Al(phex)$_4$] from **2** and sodium tetrahydridoaluminate in hexane. It was later found that the solvent was contaminated with water. $NaAlH_4$ instantly reacts with water under formation of $Al(OH)_3$ and NaOH, which in turn forms the sodium alkoxide with the available alcohol. However, even with complete transformation of sodium alanate, there is a 1:4 deficit of NaOH with respect to the alcohol **2** (Eq. 23).

$$\mathrm{NaAlH_4 + 4\,ROH} \xrightarrow[\substack{-\,4\,\mathrm{H_2}\\ -\,\mathrm{Al(OH)_3}}]{4\,\mathrm{H_2O}} \mathrm{NaOH + 4\,ROH} \longrightarrow \mathrm{NaOR + 3\,ROH + H_2O}$$

$$\mathrm{R = C_{12}F_{15}}$$

(Eq. 23)

Consequently, a new compound **6a** crystallizes from the solution, which can best be described as an adduct of **2** to the sodium alkoxide **6**. **6a** has the molecular formula $NaO(C_6F_{10})C_6F_5\cdot C_6F_5(C_6F_{10})OH\cdot 2H_2O$ and forms colorless, air- and moisture-stable block-shaped crystals. The space group was determined as triclinic $P\bar{1}$ with a = 9.81 Å, b = 10.84 Å, c = 15.35 Å, α = 72.7°, β = 79.2°, γ = 73.7° and Z = 2. For a detailed report of the structural parameters see section 6.11, Tab. 63. **6a** forms dimers containing planar four-membered Na-O rings with Na-O bond lengths of 238.6(1) and 235.7(1) pm (O-Na-O angle 84.5(2)°, Na-O-Na angle 95.5(1)°, Fig. 53). The center of inversion coincides with the center of these rings. In **6**, the Na-O distances are significantly shorter (218.9(1) and 225.8(1) pm) because the strongly electronegative phex ligand is involved in the ring formation.

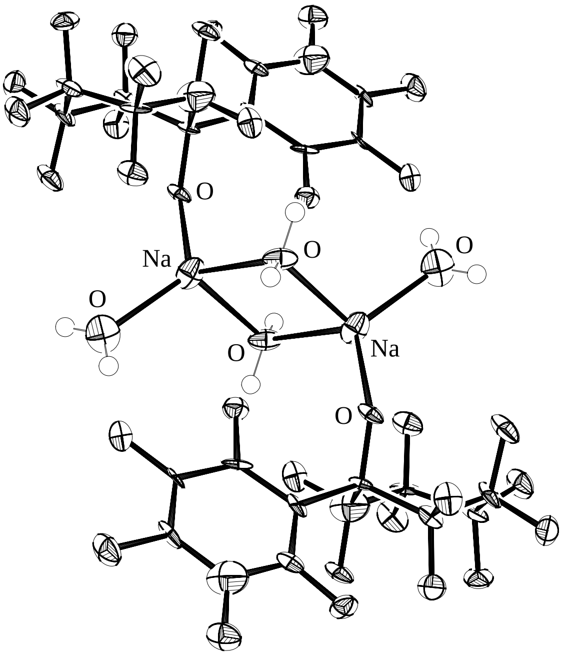

Fig. 53: Crystal structure of **6b**, thermal ellipsoids drawn at 70% probability. Two coordinating molecules of **2** omitted for clarity. Angles within the Na-O ring in °: O-Na-O 84.5(1), Na-O-Na 95.5(1).

Each sodium alkoxide is additionally coordinated by one molecule of the alcohol **2**, forming a contact between one fluorine atom in the ortho position of its C_6F_5 group and sodium (278.1(1) pm), as well as a hydrogen bridge with the oxygen atom of the alkoxide (OH: 107.5(1) pm, OH---O: 137.4(1) pm, O---O: 243.2(1) pm). The distances are significantly shorter than in the dimer of **2** (see Fig. 37 in chapter 3.1.3, OH: 79.6 pm, OH---O: 223.1 pm, O---O 301.2 pm) and within the range of a strong, almost symmetric hydrogen bridge comparable with $H_5O_2^+$ (OH---O: 134 pm, O---O 244 pm)[208]. Accordingly, the O-H-O angle approaches linearity with 166.6(3)°.

Fig. 54 shows the coordination around the sodium atom. Surprisingly, the Na-O bond connecting the alkoxy group (232.1(1) pm) is 6 pm longer than the shorter Na-O bond in **6**, in which the alkoxy groups are part of the four-membered ring. This is not a controversy, but rather another indication of the strength of the hydrogen bond resulting from the high electronegativity of $C_{12}F_{15}O^-$. Each Na atom is surrounded by four oxygen atoms in total, two of which belong to bridging water molecules. One belongs to the alkoxy group and one to a water molecule that exhibits no other contacts except with sodium. The latter one forms the shortest Na-O contact at 225.6(1) pm. Additionally there are two Na-F contacts, one with the coordinating alcohol molecule (described above) and one intramolecular contact with the CF_2 group in the 3-position of the aliphatic C_6F_{10} ring in the alkoxide (249.6(1) pm). Both Na-F distances are within the expected range for such interactions (d_{min} = 249 pm, d_{max} = 307 pm).[237, 238]

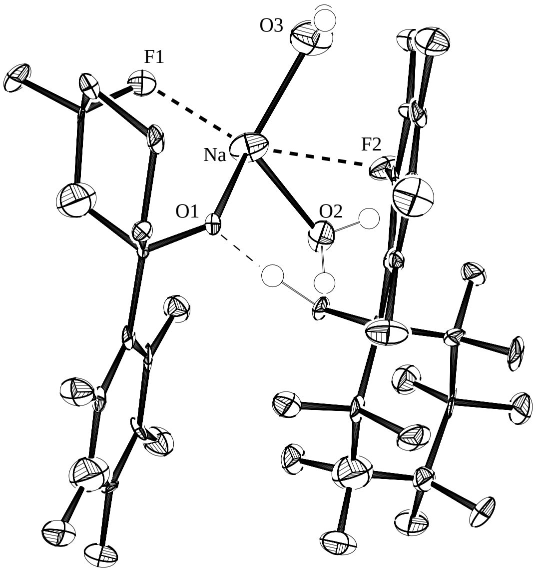

Fig. 54: Asymmetric unit of the crystal structure of **6b**, showing the coordination of sodium. Thermal ellipsoids drawn at 70% probability. The molecule on the right is the alcohol **2**, coordinated to the sodium alkoxide by a Na-F contact and a hydrogen bridge. O3 is the oxygen atom involved in the Na-O ring. Distances in pm: Na-F1 249.6(1), Na-O1 232.1(1), Na-F2 278.1(1), Na-O2 238.6(1), Na-O3 225.6(1), O1-H 137.4(1). Angles in °: Na-O1-C 136.3(1), Na-F1-C 131.6(2), Na-F2-C 125.6(2), O1-H-O 166.6(3).

3.2. New WCA salts based on perfluorinated alkoxyaluminates

3.2.1. Synthesis and characterization of $Li[Al(OC(CF_3)_2(C_6F_5))_4]$

Synthesis

$Li[Al(hfpp)_4]$ (hfpp = $OC(CF_3)_2(C_6F_5)$) **7** is prepared in analogy to $Li[Al(pftb)_4]$ (pftb = $OC(CF_3)_3$)[53] by reacting 4 equivalents of the parent alcohol **1** with lithium aluminum hydride in heptane. The product is then obtained in quantitative yield after removal of the solvent in vacuo.

IR spectroscopy

The IR spectrum of **7** shows good agreement with calculated bands and differs slightly from the parent alcohol **1** (section 6.6, Tab. 43). An OH band at 3610 cm^{-1} is not observed, indicating a quantitative reaction. When compared with $Li[Al(OC(CF_3)_3)_4]$,[53] differing bands can be assigned at 512, 558, 850, 951, 1138, 1206, 1259 and 1530 cm^{-1}. Of these, the simulation predicts only the last one to be a band clearly arising from the C_6F_5 group. The others are combined vibrations resulting from the coordination of lithium to two oxygen and four fluorine atoms in **7**, which is also observed in the crystal structure (see later in this chapter). In the region between 900 and 1300 cm^{-1} many bands are split with approximately equal intensities, which also hints at this mode of coordination.

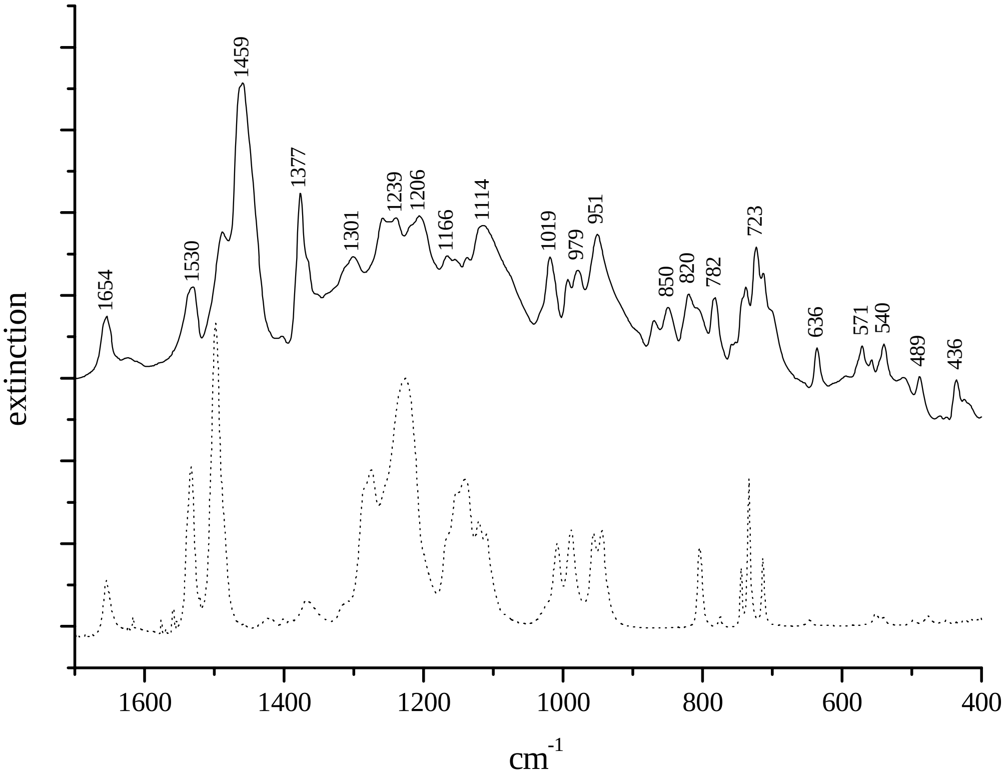

Fig. 55: IR spectrum of **7** (solid line). The dotted line shows the spectrum of the parent alcohol **1**. The band at 1377 cm^{-1} is assigned to nujol oil.

NMR spectroscopy

The ^{19}F and ^{13}C NMR spectra show the same signals and coupling patterns as the parent alcohol **1** (see 3.1.2 and Tab. 9). There is no residual signal of the hydroxyl group in the proton spectrum, indicating a quantitative reaction. The ^{27}Al spectrum shows a single broad peak at 27 ppm.

Tab. 9: Experimental and computed NMR shifts of **7**, compared with experimental chemical shifts of the parent alcohol **1**.

	shift (exp.) [ppm][a]	shift (calc.) [ppm][b]	1 exp. [ppm]	assignment[c]
$\delta^{13}C$	-	87.0	79.1	a
	111.7	108.4	105.4	c
	123.1	131.8	121.6	b
	136.3	139.1	138.3	f
	140.0	143.4	142.6	g
	146.8	146.1	146.3	d, e
$\delta^{19}F$	-75.8	-78.9	-76.2	b
	-132.8[d]	-126.5	-132.8	d
			-138.4	e
	-154.7	-148.6	-148.9	g
	-164.3	-158.1[d]	-160.2	f

[a] in $CDCl_3$/THF; [b] at BP86/SV(P) level, C_1 symmetry; [c] for assignment see Fig. 21, 3.1.2.; [d] due to the missing H-F interaction discussed in 3.1.2, the fluorine atoms in ortho positions of the C_6F_5 groups (d and e) become equivalent (but the peak is broadened, FWHM = 63 Hz).

Crystal structure determination

7 crystallizes as colorless platelets from concentrated pentafluorobenzene solutions in the triclinic space group $P\bar{1}$ with the cell parameters a = 9.60 Å, b = 12.21 Å, c = 19.74 Å, α = 83.0°, β = 78.5°, γ = 72.3° and Z = 2. The structure is best described as a molecular compound rather than a lithium salt (Fig. 56), with the lithium atom tightly coordinated by fluorine and oxygen atoms. All Al-O distances are comparable with those in typical structures containing the $[Al(OC(CF_3)_3)_4]^-$ anion (e.g. average Al-O distance in silver salts: 173.8 pm).[53] The lithium coordination leads to an asymmetry in Al-O bonding with two longer (179.4 and 178.3 pm) and two shorter distances (169.7 and 168.5 pm) due to a weakening of the coordinated Al-O bonds. Tab. 10 shows a comparison of key structural parameters of **7** with calculated parameters and the crystal structure of the closely related $Li[Al(OC(CF_3)_2(C_6H_5))_4]$ (Fig. 57).[55]

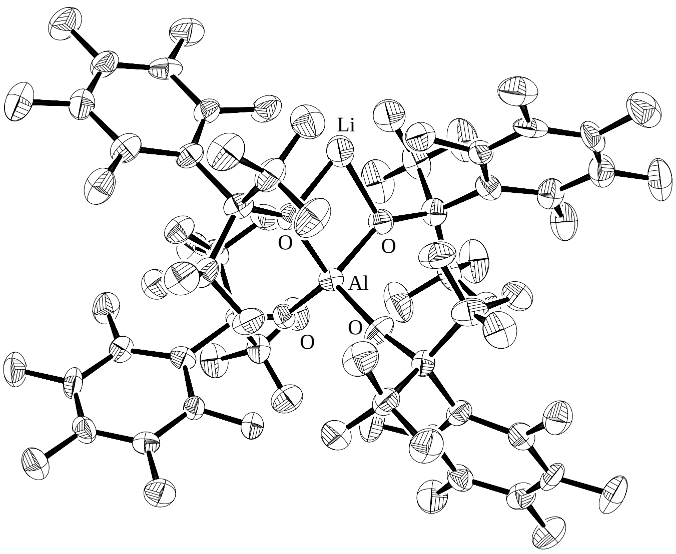

Fig. 56: Crystal structure of **7**, thermal ellipsoids drawn at 50% probability level.

It becomes apparent from the Al-O bond lengths, which are comparable between **7** and Li[Al(OC(CF_3)$_2$(C_6H_5))$_4$], that the stability of the new anion against ligand abstraction should be similar. The [Al(OC(CF_3)$_2$(C_6H_5))$_4$]$^-$ anion was reported to be stable against the NO^+ cation in the solid state and at least for a short time in solution.[246] While in the solid state structure of this salt, a weak donor-acceptor interaction links NO^+ and the anion, in solution an equilibrium between the associate and separated solvated ions exists. Upon decomposition, the fluoride-bridged species [((C_6H_5)(CF_3)$_2$CO)$_3$Al-F-Al(OC(CF_3)$_2$(C_6H_5))$_3$]$^-$ is formed in analogy to the mechanism shown in section 2.1 (Eq. 12). However, [NO][Al(OC(CF_3)$_3$)$_4$] is a stable ionic compound both in the solid state and in solution, owing to the slightly weaker coordinative ability and higher degree of fluorination of the anion.[54] Thus, it can be expected that with the slightly better acidity of the parent alcohol **1** (pK_a 7.9 vs. 8.8 in (CF_3)$_2$(C_6H_5)COH[54]) and its fluorinated C_6F_5 groups, the [Al(hfpp)$_4$]$^-$ anion approaches the stability of [Al(pftb)$_4$]$^-$.

Tab. 10: Selected bond distances and angles in the crystal structure and the calculated geometry of **7** and Li[Al(OC(CF_3)$_2$(C_6H_5))$_4$].[55]

	7 exp.	**7 calc.[a,b]**	**Li[Al(OC(CF_3)$_2$(C_6H_5))$_4$] exp.[b]**
Li-O [pm]	Li-O1 190.9(1)	192.3	197.8
	Li-O4 190.8(1)	190.8	196.6
av.	190.9	191.6	197.2
Li-F [pm]	Li-F1 192.1(1)	198.3	198.4
	Li-F2 264.0(1)	260.4	208.2
	Li-F3 186.8(1)	194.6	209.8
	Li-F4 231.6(1)	238.3	235.4
av.	218.6	222.9	213.0
O-Li-O [°]	81.5(2)	82.3	79.9
Li-O-Al [°]	95.0(2)	95.2	93.6
	95.3(2)	95.9	94.6
C-F [pm]	C-F1 137.0(1)	136.5	137.6
	C-F2 136.1(1)	136.3	136.1
	C-F3 135.6(1)	137.1	134.1
	C-F4 136.2(1)	136.2	138.4
	other C-F 132.2-135.3	132.9-135.6	other C-F 129.8-134.2
Al-O [pm]	Al-O2 179.4(1)	184.0	177.3
	Al-O1 178.3(1)	183.0	175.5
	Al-O3 169.7(1)	173.2	168.7
	Al-O4 168.5(1)	172.9	170.6
av.	174.0	178.3	173.0
Al-O-C [°]	Al-O1-C 145.2(2)	143.2	160.4
	Al-O2-C 140.9(3)	140.5	153.6
	Al-O3-C 169.0(3)	164.6	168.2
	Al-O4-C 153.9(2)	157.5	151.5
av.	152.3	151.5	158.4

[a] BP86/SV(P), C_1 symmetry; [b] where applicable, distances are equivalent to those of **7** in the same row.

Although the bond lengths in Tab. 10 are in good agreement the reference compound, there are major deviations in the Al-O-C angles. This is easily explained by the distorted geometry arising from the coordination of two fluorine atoms in ortho positions of C_6F_5 groups. In Li[Al(OC(CF_3)$_2$(C_6H_5))$_4$], the aromatic ligands point away from the lithium atom, which is only coordinated by CF_3 groups (Fig. 57).

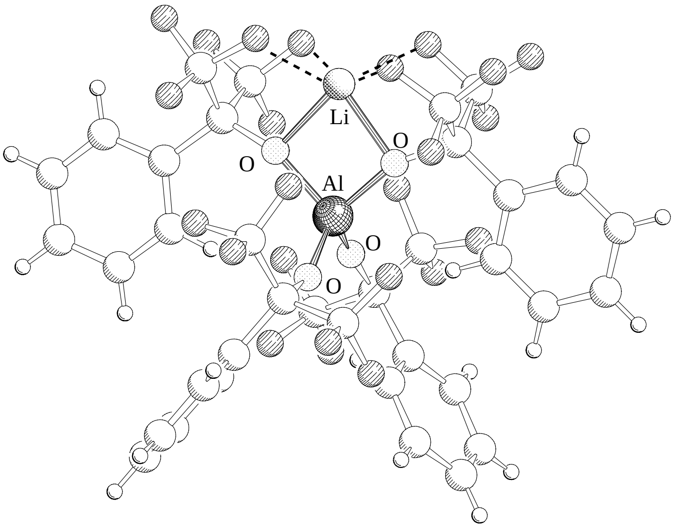

Fig. 57: Crystal structure of $Li[Al(OC(CF_3)_2(C_6H_5))_4]$,[55] thermal ellipsoids not deposited.

Fig. 58 shows the unusual, distorted trigonal prismatic coordination around the lithium atom in **7** in more detail. The Li-O distances are shorter than in $Li[Al(OC(CF_3)_2(C_6H_5))_4]$ by approximately 6 pm. However, it must be noted that the shortest contact is not with an oxygen, but with a fluorine atom (F3 in the aromatic ring: 186.8 pm, d_{min} = 206 pm, d_{max} = 247 pm,[234] lithium fluoride in the gas phase: 156.4 pm).[247] Both aromatic CF-Li contacts are significantly shorter than the shortest contact in $Li[Al(OC(CF_3)_2(C_6H_5))_4]$ (198.4 pm). Due to the hemilabile nature of these interactions and the associated availability of the lithium cation, $Li[Al(OC(CF_3)_2(C_6H_5))_4]$ was reported to be a highly active catalyst for carbon-carbon bond formations;[55] however **7** was not tested in that respect.

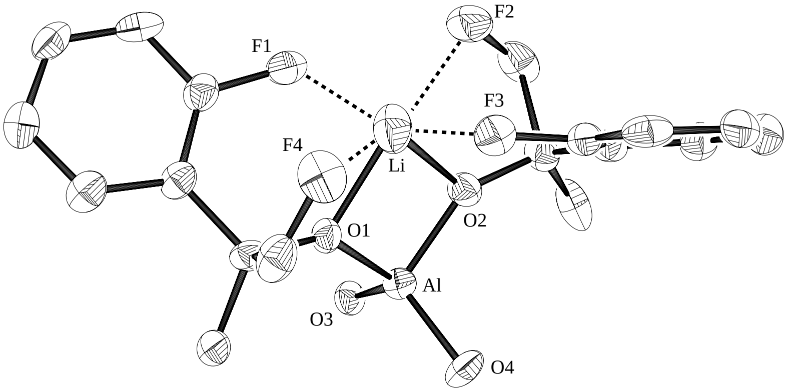

Fig. 58: Detail of the crystal structure of **7**, showing the coordination of the lithium atom. Fluorine atoms not involved in Li-F contacts are omitted for clarity. Thermal ellipsoids drawn at 50% probability level. Distances in pm: Li-O1 190.9(1), Li-O2 190.8(1), Li-F1 192.1(1), Li-F2 264.0(1), Li-F3 186.8(1), Li-F4 231.6(1), Al-O1 178.3(1), Al-O2 179.4(1), Al-O3 169.7(1), Al-O4 168.5(1).

3.2.2. Synthesis and characterization of $Ag[Al(OC(CF_3)_2(C_6F_5))_4]$

Synthesis

$Ag[Al(hfpp)_4]$ (hfpp = $OC(CF_3)_2(C_6F_5)$) **8** is prepared in analogy to $Ag[Al(pftb)_4]$[53] by a metathesis reaction of **7** with AgF (Eq. 24). The reaction is activated by short-time sonication.

$$\mathrm{Li[Al(hfpp)_4] + AgF} \xrightarrow[\text{- LiF}]{\mathrm{CH_2Cl_2}} \mathrm{Ag[Al(hfpp)_4]}$$

(Eq. 24)

After removal of the solvent, the product is first obtained as a yellowish resin, which slowly forms an off-white powder when kept in a vacuum. Very short Li-F contacts at 186.8(1) and 192.1(1) pm observed in the crystal structure of **7** hint at a decomposition pathway leading to oligomerization, which is initiated by elimination of a fluorine atom in ortho position under formation of LiF. The resulting arine could then attack the para position of a perfluorophenyl group of another anion in a nucleophilic aromatic substitution. Fluoride acts as a leaving group in such reactions and attacks generally occur in the para position of C_6F_5 (in the absence of a directing catalyst).[248-250] Resulting oligomeric by-products could explain why the product is first obtained as a resin. Although the fraction of by-products was determined to be small and the neat product can be obtained by recrystallization from 1,2-dichloroethane (85% total yield), in future syntheses the yield and purity could be improved by performing the reaction in a cooled ultrasonic bath and carefully monitoring the progress with NMR experiments.

IR spectroscopy

The IR bands of crystals with the composition $[Ag(1,2\text{-}C_2Cl_2H_4)_3][Al(OC(CF_3)_2(C_6F_5))_4]$ **8a** show good agreement with a simulation of non-coordinated anion, as well as with the recorded bands of the parent alcohol **1**. Additionally, the spectrum was compared with $[NEt_4][Al(pftb)_4]$[251] as a model compound with an anion that is not distorted by coordination (section 6.6, Tab. 44). Bands at 512, 558, 850, 951, 1138, 1206 and 1259 cm^{-1}, which are present in **7**, are no longer observed or significantly shifted due to the absence of coordinating lithium atoms (see 3.2.1).

NMR spectroscopy

The ^{13}C and ^{19}F NMR signal positions are identical with the spectrum of **7** (see Tab. 9 and section 6.4.10) and thus shall not be discussed here. Concentrations of by-products are too small to be observed in the ^{13}C spectrum. However, in the ^{19}F spectra, a four by-products with lower intensities (integration of main product vs. side products: 14:5:4:1:1) is also observed, possibly the result of the postulated oligomerization mechanism. Another possibility would be a ligand abstraction under formation of the Lewis acid Al(hfpp)$_3$ with ensuing formation of [FAl(hfpp)$_3$]$^-$. The latter is more likely, since the same by-products can be observed in spectra of the analogous sodium salt prepared at approximately the same reaction temperature, which is not synthesized by metathesis with **7**, but directly from NaAlH$_4$ (see chapter 3.2.3). The ^{27}Al spectrum shows two singlets at 24.6 and 36.4 ppm, the first being the main signal, the latter clearly resulting from a by-product (integration 7:1).

Crystal structure determination

8 crystallizes as yellow blocks **8a** from concentrated 1,2-dichloroethane solutions in the orthorhombic space group Fdd2 with the cell parameters a = 44.92 Å, b = 46.35 Å, c = 11.19 Å and Z = 16. The structure consists of isolated [Ag(1,2-C$_2$Cl$_2$H$_4$)$_3$]$^+$ cations and [Al(OC(CF$_3$)$_2$(C$_6$F$_5$))$_4$]$^-$ anions with one additional dichloroethane molecule in the unit cell (Fig. 59).

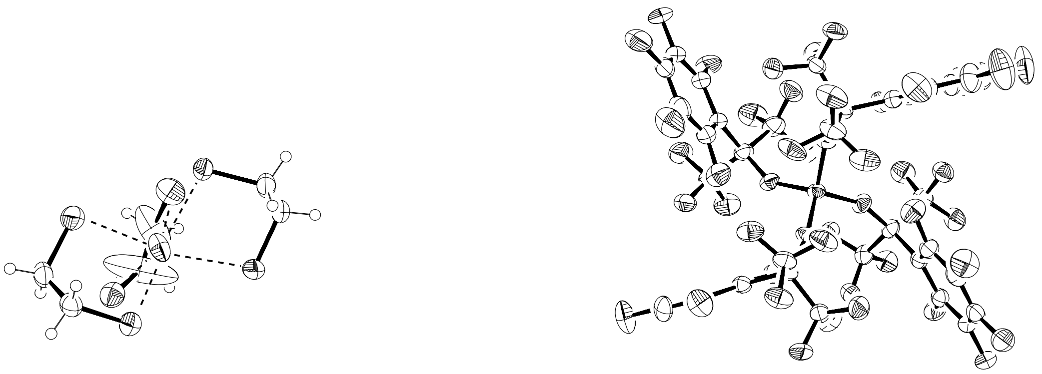

Fig. 59: Crystal structure of **8a**, thermal ellipsoids drawn at 50% probability level. One uncoordinated 1,2-$C_2Cl_2H_4$ molecule omitted for clarity.

All Al-O bond distances in the anion are approximately 4 pm shorter than in the calculated gas phase geometry (Tab. 11), but well within the normal range of stable alkoxyaluminate anions. Note that the calculations were performed in S$_4$ symmetry, while in the structure the anion is slightly distorted to C_1 as evident e.g. by the Al-O-C angles, which deviate from the average angle of 156.6° angle by up to 9° (cf. in $[Ag(1,2\text{-}C_2Cl_2H_4)_3]^+[Al(pftb)_4]$ the aluminum atom can be considered tetrahedrally coordinated with a deviation not exceeding 1.4°).[53] The O-Al-O bond angles range between 104.5(1) and 113.2(1)° (av. 109.5°). Al-O bond lengths which are not influenced by distorted Al-O-C angles, i.e. that are independent of orbital considerations, suggest a highly ionic bonding character. There is indeed no significant lengthening of the bonds with respect to the analogous silver salt of the $[Al(pftb)_4]^-$ anion, although this could have been expected due to the higher steric demand and lower electronegativity of the hfpp ligand. It can be reasoned that the ionic character of the Al-O bonds is comparable between **8** and $Ag[Al(pftb)_4]$ and thus, a comparable stability versus ligand abstraction can be expected. Additionally, all Al-O bonds are at least 5 pm shorter than the longest Al-O bonds in **7**, which denotes a stability gain upon introduction of the larger $[Ag(1,2\text{-}C_2Cl_2H_4)_3]^+$ counterion.

The silver cation exhibits no contacts except with the six chlorine atoms of three solvent molecules, which form a distorted octahedron (Fig. 60). The shortest interionic Ag-Cl distance is found at 395.8(2) pm. There is one weak Cl-F contact with a CF_3 group (305.1(1) pm, cf. sum of van-der-Waals radii of fluorine and chlorine: 330 pm). The cations form chains which are connected by weak Cl-Cl interactions (325.7(2) pm, cf. twice the sum of van-der-Waals radii of chlorine: 360 pm) of Cl1 and Cl2 with the equivalent chlorine atoms of neighboring ions.

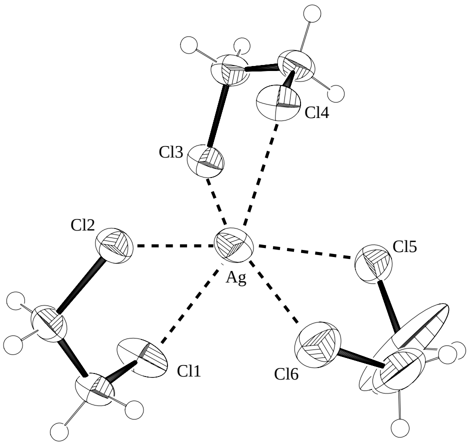

Fig. 60: Detail of the crystal structure of **8a**, showing the coordination of the silver atom in the cation. Thermal ellipsoids drawn at 50% probability level. The large ellipsoid in one of the solvent molecules hint at a slight disorder (not modeled). Distances in pm: Ag-Cl1 268.5(1), Ag-Cl2 280.0(1), Ag-Cl3 276.7(1), Ag-Cl4 266.7(1), Ag-Cl5 278.5(1), Ag-Cl6 280.2(1).

Tab. 11: Selected bond distances and angles in the crystal structure of **8a**, the calculated geometry of the isolated anion and the structure of $[Ag(1,2\text{-}C_2Cl_2H_4)_3]^+[Al(pftb)_4]^-$.[53]

	8a exp.	**$[Al(hfpp)_4]^-$ calc.[a]**	**$[Ag(Cl_2C_2H_4)_3]^+[Al(pftb)_4]^-$ exp.**
Ag-Cl [pm]	266.7(1)-280.2(1)	-	269.4-278.8
av.	275.1		274.2
Cl-C [pm]	173.4(1)-179.3(1)	-	170.3-181.5
av.	177.5		175.8
Al-O [pm]	Al-O1 173.0(1)		171.4-173.6
	Al-O2 173.8(1)		
	Al-O3 172.4(1)		
	Al-O4 173.2(1)		
av.	173.1	all 177.5	172.5
C-O [pm]	134.8(1)-136.5(1)		133.1-135.5
av.	135.6	all 135.1	134.3
Al-O-C [°]	Al-O1-C 161.8(1)		148.1-151.7
	Al-O2-C 159.1(2)		
	Al-O3-C 157.6(1)		
	Al-O4-C 147.5(1)		
av.	156.5	all 153.1	149.5
O-Al-O [°]	104.5(1)-113.2(1)		106.5-114.8
	109.5		

[a] BP86/SV(P), S_4 symmetry.

3.2.3. Synthesis and characterization of $Na[Al(OC(CF_3)_2(C_6F_5))_4]$

Synthesis

$Na[Al(OC(CF_3)_2(C_6F_5))_4]$ **9** is prepared similarly to $Li[Al(hfpp)_4]$ **7** from $NaAlH_4$ and the parent alcohol **2** in boiling toluene. The reaction proceeds slowly and produces a highly viscous brown oil, which must be washed with pentane to obtain a light grey powder. The NMR spectra show the existence of small amounts of by-products (see below). The pure product can be isolated by crystallization from a concentrated 1,2-dichloroethane solution.

IR spectroscopy

The IR bands of 9 show good agreement with the recorded bands of the parent alcohol **1**, as well as the lithium and silver salts **7** and **8** (section 6.6, Tab. 45). Differences in band positions and intensities between **9** and **8** are extremely small and thus a significantly different coordination of these two metal cations in the proximity of $[Al(hfpp)_4]^-$ is not apparent. The O-H band of the parent alcohol at 3610 cm-1 is not observed, indicating a quantitative reaction. However, even after drying the compound in vacuo, the region between 2800 and 3000 cm^{-1} exhibits characteristic C-H bands of toluene.

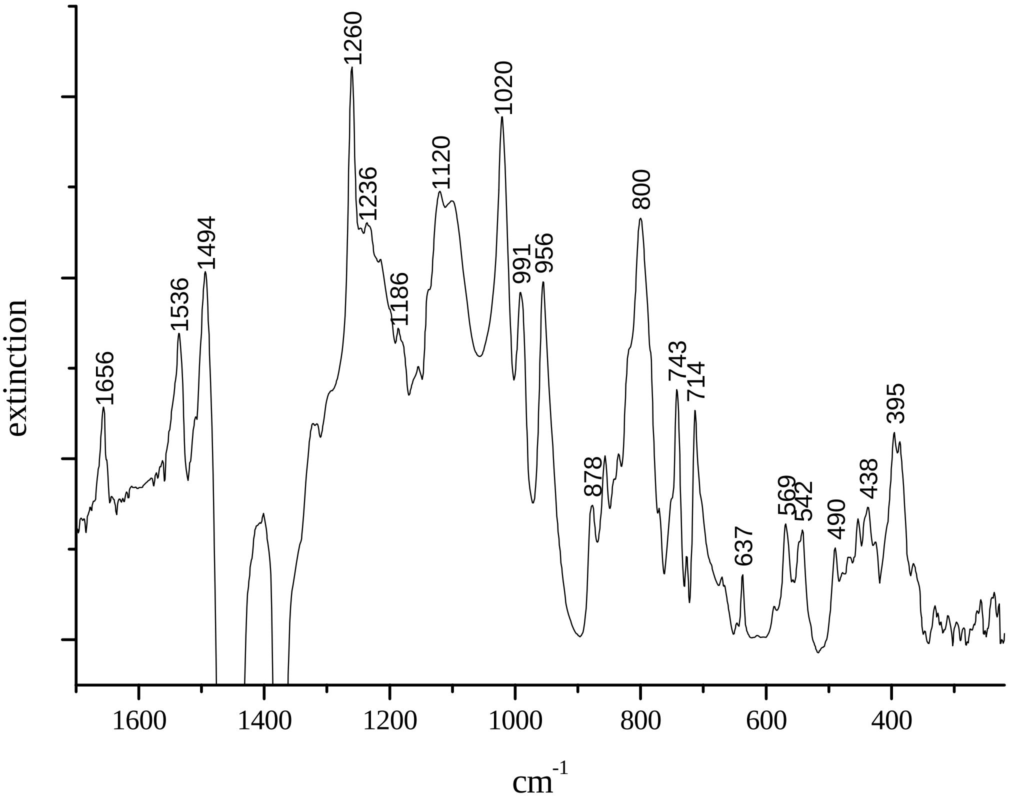

Fig. 61: IR spectrum of **9**. The region between 2800 and 3000 cm^{-1}, showing bands of residual toluene, was omitted for clarity.

NMR spectroscopy

A ^{13}C spectrum could not be recorded due to the poor solubility of **9**. The ^{19}F NMR shows two by-products that are identical with the by-products occurring in the synthesis of the silver salt **8** (see chapter 3.2.2). This is to be expected, because the same mechanisms of decomposition, namely ligand abstraction under formation of the Lewis acid Al(hfpp)$_3$ with ensuing formation of [FAl(hfpp)$_3$]$^-$ or oligomerization of the C_6F_5 groups are possible for **9**. The ^{19}F NMR shows two signal sets with almost equal intensity and a third set with very low intensity (integration 6:5:1). Signals of the two main products are identical to within 1 ppm with the spectrum of **8**. A splitting of the signal could be expected due to coordination of sodium with two oxygen atoms (see crystal structure below). However, the second species is also observed in the ^{27}Al spectrum, in which three peaks appear at 24.3, 37.1 (main signals, cf. **8**: 24.6 ppm) and 46.5 ppm (minor signal).

Crystal structure determination

9 crystallizes as colorless blocks **9a** from concentrated 1,2-dichloroethane solutions in the monoclinic space group C2/c with the cell parameters a = 14.98 Å, b = 16.18 Å, c = 41.04 Å, β = 93.7° and Z = 8. **9a** can be described as a molecular compound $Na[Al(OC(CF_3)_2(C_6F_5))_4]\cdot 1,2\text{-}Cl_2C_2H_4$ (Fig. 62), in which the sodium atom is coordinated by a single 1,2-dichloroethane molecule. The unit cell also contains an additional, uncoordinated solvent molecule.

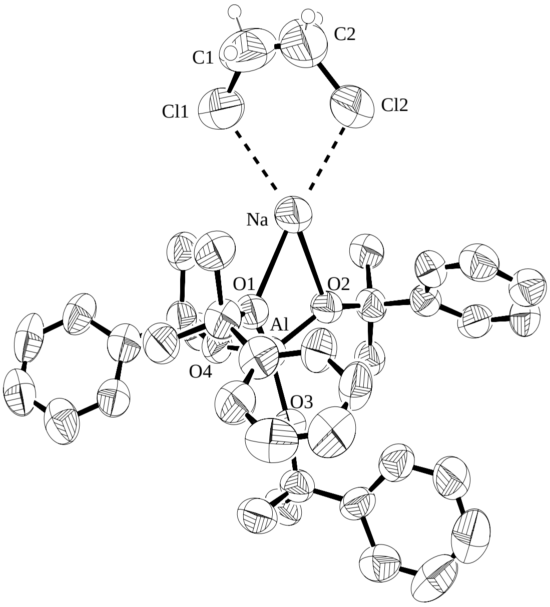

Fig. 62: Crystal structure of **9a**. Thermal ellipsoids drawn at 50% probability level. All fluorine atoms and one solvent molecule omitted for clarity. Distances in pm: Na-Cl1 291.2(1), Na-Cl2 290.3(1), Cl1-C1 178.1(1), Cl2-C2 171.2(1).

The sodium cation is coordinated by four fluorine atoms (Fig. 63), three of which belong to CF_3 groups. The last is a fluorine atom in the ortho position of a C_6F_5 group with a very short Na-F distance of only 232.1(1) pm (sum of van-der-Waals radii 374 pm, cf. shortest reported Na-F distance:[234, 252] 228.5 pm). The Na-O bond lengths are rather long with 246.6(1) and 246.7(1) pm and the Al-O bonds of the coordinated oxygen atoms are significantly weakened with bond lengths of 176.1(1) and 177.1(1) pm (171.1(1) and 171.2(1) pm for the two non-coordinated oxygens, av. in **8a**: 173.1 pm). Due to the Na-O coordination, the O-Al-O angles deviate significantly from the tetrahedral angle (e.g. O1-Al-O2: 95.1(1)°). In a recently published 2,6-Bis-(2,6-hydroxyphenyl)pyridine aluminum complex salt containing a similar, but slightly more asymmetric four-membered ring of two oxygen, one aluminum and one sodium atom, Na-O distances of 230.8 and 246.6 pm were reported.[253] However, in this compound, Na^+ is additionally coordinated by three ethanol molecules. The short Na-F contacts and Na-O bond lengths, comparable with a complex in which sodium is coordinated by three donors, are indications of a low coordinative strength of the anion. This would also explain the very unusual coordination of sodium by a 1,2-dichloroethane molecule (Na-Cl 291.2(1) and 290.3(1) pm, sum of van-der-Waals radii 374 pm). Some compounds, in which sodium is coordinated by chlorine atoms of transition metal- or lanthanide chloro complexes, are known. However, no crystal structures containing sodium coordinated by a chlorinated organic molecule have been published so far.[254]

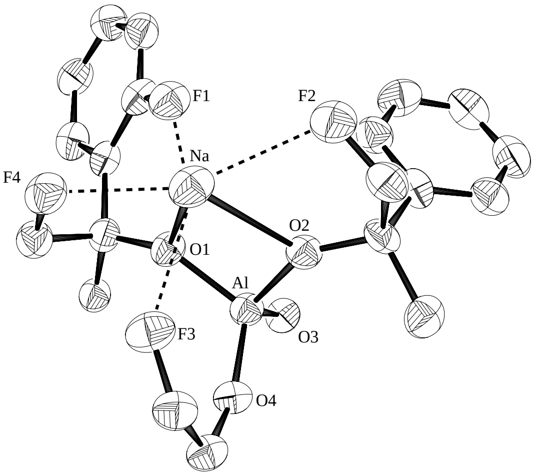

Fig. 63: Detail of the crystal structure of **9a**, showing the coordination of the sodium atom. Thermal ellipsoids drawn at 30% probability level. Distances in pm: Na-O1 246.7(1), Na-O2 246.681), Na-F1 232.1(1), Na-F2 259.0(1), Na-F3 250.0(1), Na-F4 261.2(1), Al-O1 176.1(1), Al-O2 177.1(1), Al-O3 171.2(1), Al-O4 171.1(1). Angles in °: Al-O1-C 141.1(1), Al-O2-C 142.3(1), Al-O3-C 166.2(1), Al-O4-C 157.1(2), O1-Al-O2 95.1(1), O3-Al-O4 113.8(1).

3.2.4. Synthesis and characterization of $Li[FAl(OC(C_6F_{10})C_6F_5)_3]$

Synthesis

$Li[FAl(phex)_3]$ (phex = $OC(C_6F_{10})C_6F_5$)) **10** is obtained as main product in attempted reactions to synthesize the lithium salt of the homoleptic alkoxyaluminate $Li[Al(OC(C_6F_{10})C_6F_5)_4]$. However, when four equivalents of the parent alcohol **2** are reacted with lithium alanate in analogy to the syntheses of Li[Al(hfpp)$_4$] **7**, **10** is obtained instead in near-quantitative yields (with respect to the postulated mechanism, see below). The product is a white powder which contains approximately 25% of the side product $C_{12}F_{14}O$ **11** (see below), a solid perfluorinated epoxide. The melting point of **10** was determined at 130°C, that of the main side product at 46°C (slightly lower than **2** with 52°C). **11** can not be completely sublimed out of the solid mixture, at temperatures above the melting point of **10** the epoxide stays dissolved in the melt. Attempts to wash out **11** with CH_2Cl_2, monofluorobenzene, 1,2-difluorobenzene and perfluorohexane failed because **10** is soluble in the same solvents. Reactions to directly obtain epoxide-free **10** were attempted (see 3.2.5).

Mechanism

10 can not be distinguished from the desired product $Li[Al(OC(C_6F_{10})C_6F_5)_4]$ by means of NMR or vibrational spectroscopy (see below). The formation of the $[FAl(phex)_3]^-$ anion instead of the homoleptic $[Al(phex)_4]^-$ was first discovered in a fragmentary crystal structure obtained by W. Scherer´s group in Augsburg, who tried to introduce $[Al(phex)_4]^-$ as counterion in a nickel phosphine complex salt.[255] Using starting material obtained as described above, the counterion was instead determined to be $[FAl(phex)_3]^-$. The possibility that $[FAl(phex)_3]^-$ is formed during subsequent metathesis reactions (e.g. to obtain the silver salt), which are often carried out under rather harsh conditions (ultrasonic activation), can thereby be ruled out. Instead, **10** must be directly formed from the reaction mixture of $LiAlH_4$ and the parent alcohol **2**. Fig. 64 shows two possible mechanisms along with an exploratory analysis of the energetics in the gas phase.

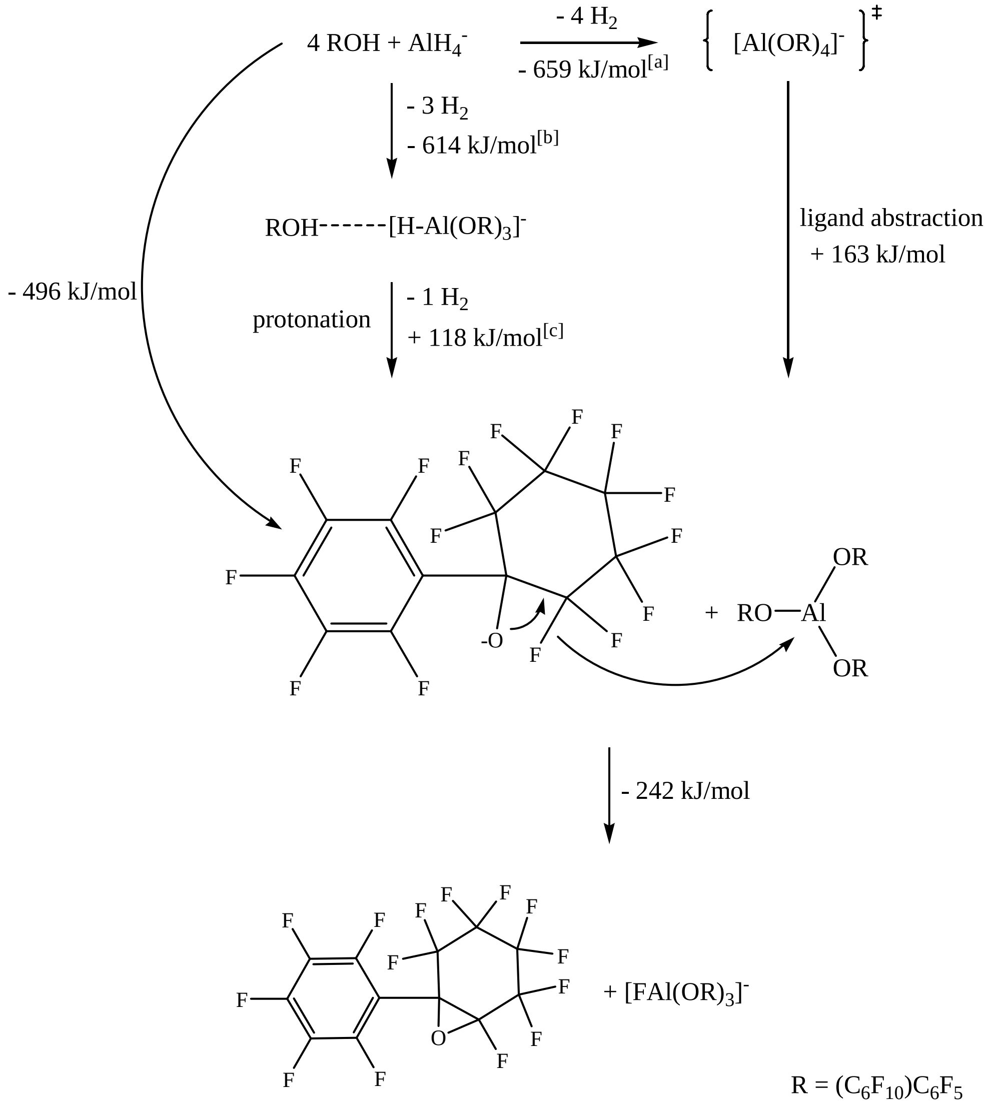

Fig. 64: Postulated mechanisms for the formation of $[FAl(phex)_3]^-$ (reaction enthalpies calculated at the BP86/SV(P) level at 0 K in the gas phase, corrected for zero-point vibrational energies). [a] Enthalpies of the first to fourth substitution steps: -212, -190, -212 and -45 kJ mol^{-1}; [b] sum of the enthalpies of the first to third substitution steps; [c] the transition state of the protonation step could not be modeled, therefore the enthalpy of the reaction of $[HAl(phex)_3]^-$ with a further equivalent of **2** was taken.

A comparison of the reaction enthalpies reveals an intermediate formation of the homoleptic anion to be unlikely, as the triple substitution followed by protonation is favored by 45 kJ mol^{-1} with respect to a ligand abstraction (in the ligand abstraction mechanism the highest energetic barrier is 163 kJ mol^{-1}, in the protonation mechanism it is only 118 kJ mol^{-1}, see Fig. 65).

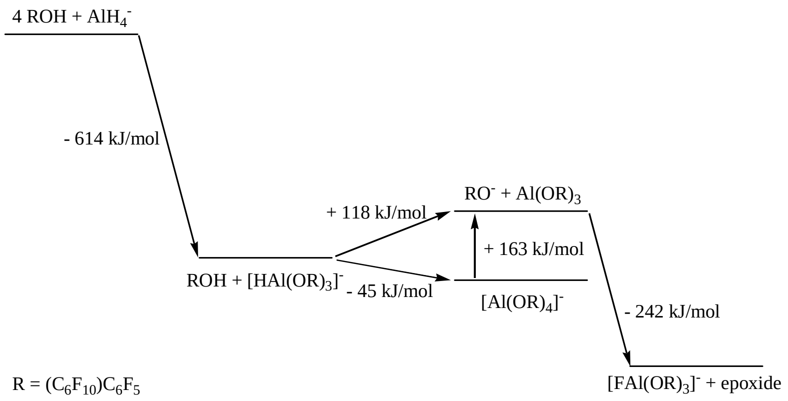

Fig. 65: Activation barriers in the formation of [FAl(phex)$_3$]$^-$ (reaction enthalpies calculated at the BP86/SV(P) level at 0 K in the gas phase, corrected for zero-point vibrational energies).

Additionally, while the first to third substitution steps are highly exothermic, steric strain seems to dominate in the last step (disfavored by 167 kJ mol^{-1} with respect to the third substitution). There is also experimental evidence for the protonation mechanism. In a reaction of trityl chloride with **10**, small amounts of crystalline CPh$_3$[ClAl(phex)$_3$] (see section 4.3.1) were obtained and characterized by X-ray diffraction. This means that trace amounts of Al(phex)$_3$ were still present in solid **10**. The epoxide C$_{12}$F$_{14}$O could never be isolated; however small colorless needle-shaped crystals were often found in reaction mixtures of **10**. The structure of these crystals could never be determined due to a characteristic diffuse scattering, which probably results from an overlay of the four possible stereoisomers. However, the cell constants (a = 6.0 Å, b = 21.8 Å, c = 10.5 Å, α = 90°, β = 104.9°, γ = 90°) and the volume of 617 Å^3 correspond well with C$_{12}$F$_{14}$O and Z = 2 (cf. **2**, which is monoclinic with β = 110.9° and Z = 8 has a cell volume of 2670.7 Å^3; 2670.7 Å^3 : 4 = 667.7 Å^3). This also raises the question if the intermediate [HAl(phex)$_3$]$^-$ could be isolated. In this anion, the hydride rests in a cage of three C$_6$F$_5$ groups (Fig. 66). Salts of this anion could be reducing agents with interesting properties, because the anion as a whole would be soluble in polar media while the hydride has a low-polar environment. A high selectivity can be expected due to steric shielding.

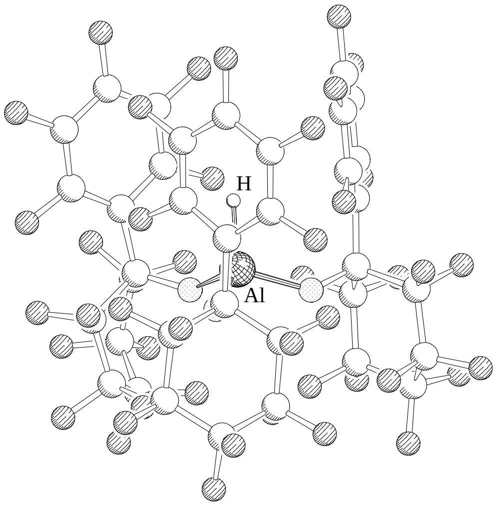

Fig. 66: Calculated geometry of $[HAl(phex)_3]^-$ (BP86/SV(P)), input coordinates based on a crystal structure containing the $[FAl(phex)_3]^-$ anion.

Vibrational spectroscopy

Because no crystal structure of **10** is available and thus the coordination of lithium in the compound is unknown, only vibrational bands of the uncoordinated $[FAl(phex)_3]^-$ anion (input geometry taken from a fragmentary crystal structure[255]) were calculated and compared with those of the parent alcohol and calculated bands of the epoxide **11** (see section 6.6, Tab. 46, Tab. 47). The experimental spectrum (Fig. 67) shows no residual O-H band of the parent alcohol **2** at 3623 cm^{-1}, indicating a quantitative reaction.

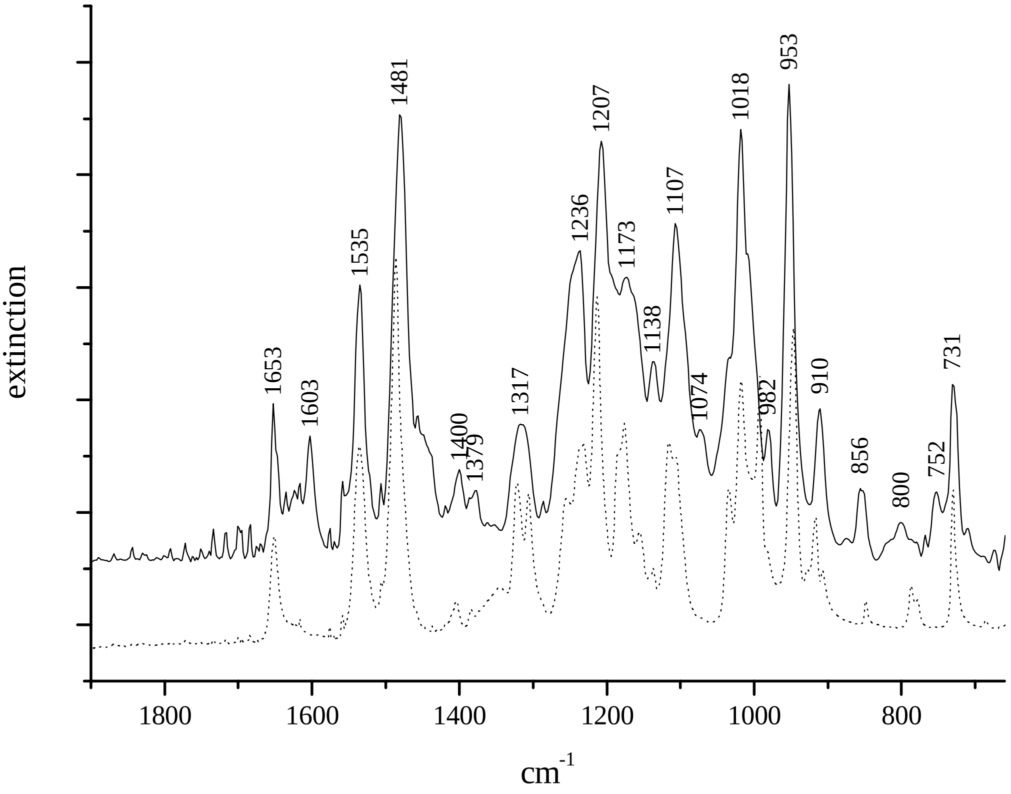

Fig. 67: IR spectrum of a reaction mixture of **10** (solid line). The dotted line shows the spectrum of the parent alcohol **2** for comparison.

Generally, while the intensities and wave numbers of most bands are similar to **2**, many bands appear broader than in the parent alcohol. Very weak bands in the range between 1558 and 1900 cm^{-1} stem from traces of water. There is one weak band in the typical range of epoxy group vibrations (800-1000 cm^{-1}) at 982 (calc. 962) cm^{-1} which can be assigned to the by-product **11**, because it neither appears in the spectrum of **2** nor in the calculated spectra of $[FAl(phex)_3]^-$, $Al(phex)_3$ or $C_{12}F_{15}O^-$ (Fig. 68). Visual examination of the calculated band showed that it indeed corresponds to a combination mode involving the epoxy function. This band could be used to spot impurities of **11** in reaction mixtures. All other bands are either predicted for other products and consequently may be overlapped, or already occur in the spectrum of **2**.

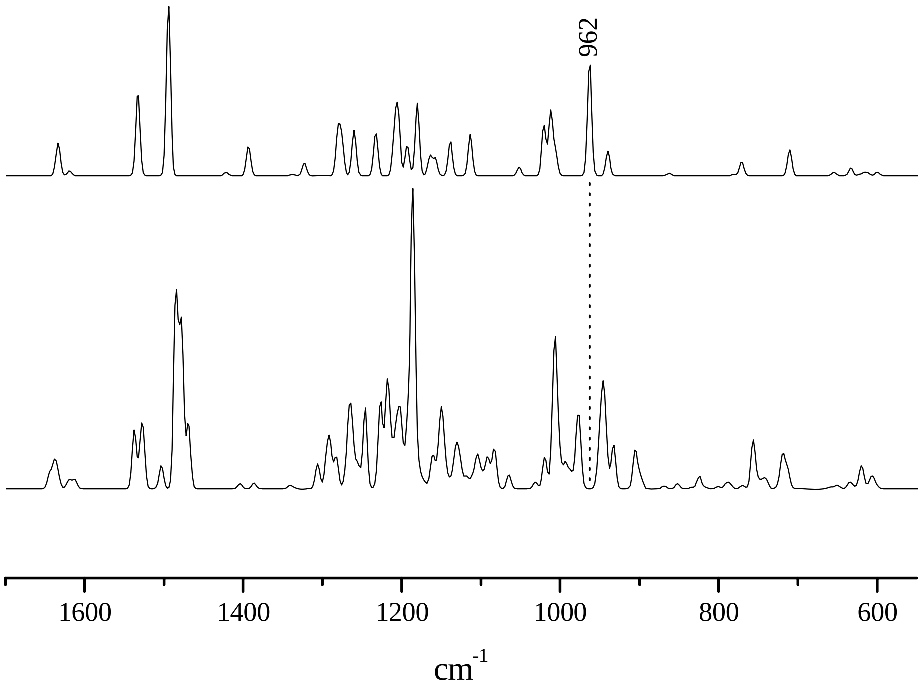

Fig. 68: Calculated IR spectrum of the epoxide **11** (upper graph) and the averaged calculated spectra of $[FAl(phex)_3]^-$, $C_{12}F_{15}O^-$ and $Al(phex)_3$ (lower graph), calculated on the BP86/SV(P) level of theory. The band which is characteristic for **11** is indicated by a dotted line.

The Raman spectrum of the reaction mixture is also very similar to the parent alcohol (Fig. 69). There is only one new band at 1010 cm^{-1} which, according to the simulations, could arise from $[FAl(phex)_3]^-$, $Al(phex)_3$ or the epoxide **11**.

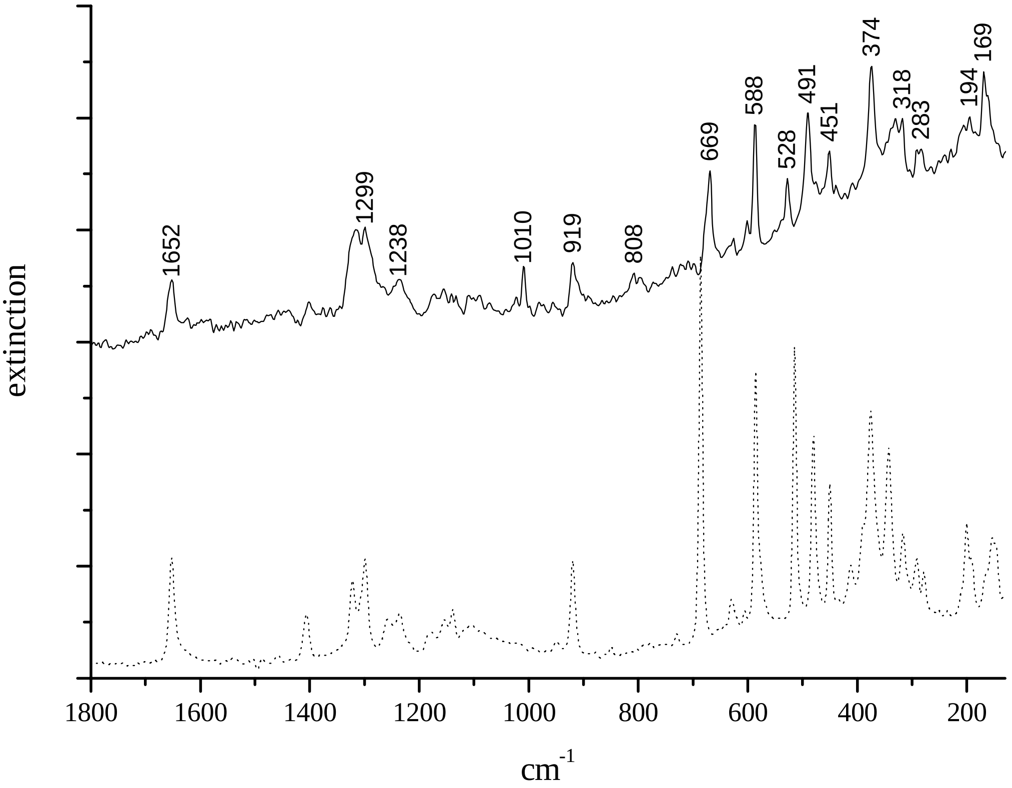

Fig. 69: Raman spectrum of a reaction mixture of **10** (solid line). The dotted line shows the spectrum of the parent alcohol **2** for comparison.

NMR spectroscopy

Proton spectra of **10** show no signals of residual OH functions. ^{13}C and ^{27}Al spectra could not be recorded due to poor solubility of the compound. However, ^{19}F spectra show a signal set for the main product which is in good agreement with spectra of the parent alcohol, as well as one major and several minor side products. The main side product is probably the lithium alkoxide **5** (see Tab. 12). The signal of the fluorine atom in the ortho position of the aromatic ring appears at -139.6 ppm, (cf. in neat **5**: -135.8 ppm), while the signal of the main product is is found at -133.5 ppm. All other signals do not deviate enough from signals of **2** to allow any conclusions. ^{19}F signals of the epoxide **11** were not found, but could well be hidden among the poorly resolved weaker signal sets.

Tab. 12: Experimental ^{19}F chemical shifts of a reaction mixture of **10**, compared with **2**, **5** and Al(phex)$_3$ (see chapter 3.3.2).

10 (main product) [ppm][a]	**10 (side product) [ppm]**[a]	**2 [ppm]**[a]	**5 [ppm]**[a]	**Al(phex)$_3$ [ppm]**[b]
-113.9	-113.3	-113.6	-112.6	-113.5
-117.9	-116.9	-117.6	-116.2	-117.5
-121.6	-121.6	-121.3	-120.7	-121.2
-131.6	-131.6	-131.1	-133.9	-131.0
-133.5[c]	-135.0	-132.8[c]	-135.4	-132.9[c]
-135.9	-139.6[c]	-135.8	-135.8[c]	-135.7
-140.7	-140.7	-140.6	-140.3	-140.6
-147.5[c]	-149.4[c]	-146.8[c]	-151.2[c]	-146.4[c]
-159.0[c]	-159.7[c]	-159.0[c]	-160.8[c]	-158.9[c]

[a] Recorded in CDCl$_3$; [b] recorded in toluene-D8; [c] signals of the aromatic C_6F_5 groups.

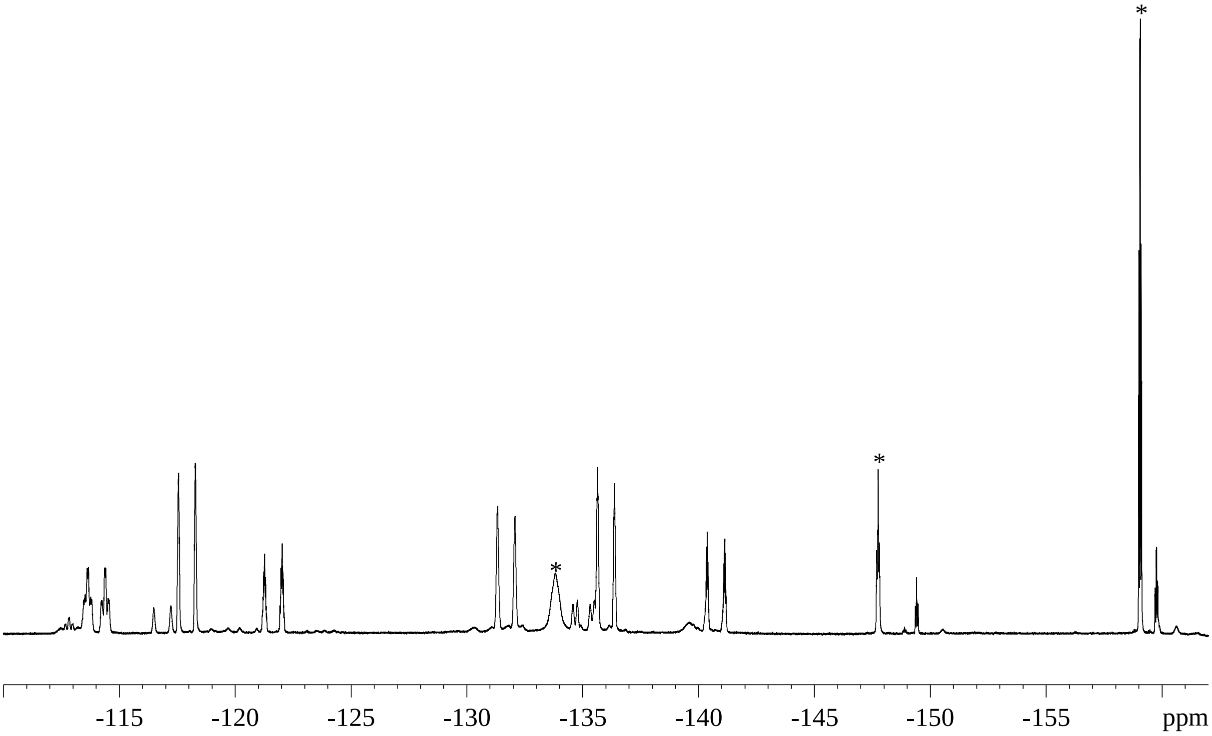

Fig. 70: ^{19}F NMR spectrum of a reaction mixture containing **10** and several side products. Aromatic signals of the main product are indicated by an asterisk.

However, crystals of dimeric lithium alkoxide **5b** are found when recrystallizing the reaction mixture from monofluorobenzene, in accordance with both mechanisms in Fig. 64. Indeed, a ^{19}F, ^{19}F NOESY spectrum shows exchange in the aromatic signals of the two stronger signal sets, which can only occur between [FAl(phex)$_3$]$^-$ and LiOC$_{12}$F$_{15}$ (Fig. 71). Accordingly, the ^{7}Li spectrum shows two signals at 0.19 and -0.15 ppm (Fig. 72).

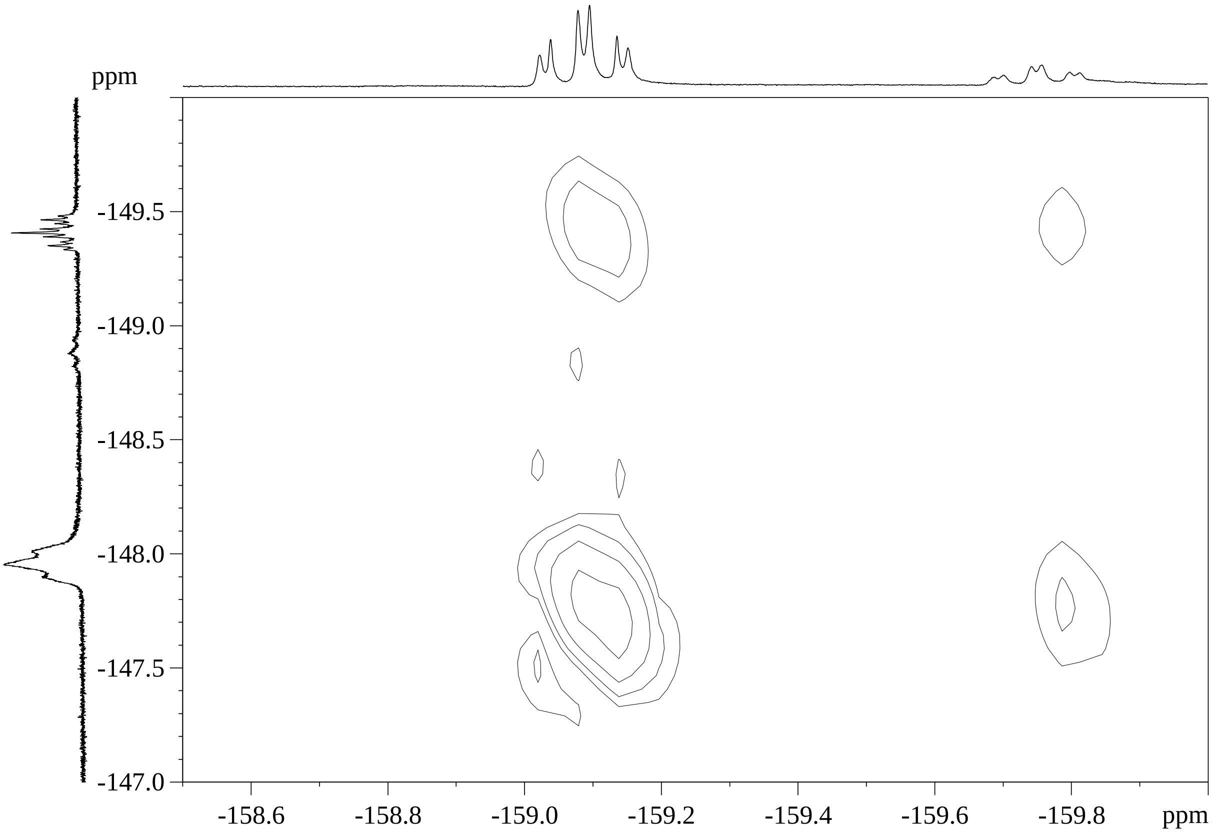

Fig. 71: Detail of the ^{19}F, ^{19}F NOESY spectrum of the reaction mixture of **10** and its side products, showing the interaction of the relevant aromatic signals (upper axis: meta positions, left axis: para positions, different scales have been chosen for the 1D projections for clarity). The existence of the upper left and lower right crosspeaks indicates exchange between the corresponding fluorine atoms in the main product and the major side product.

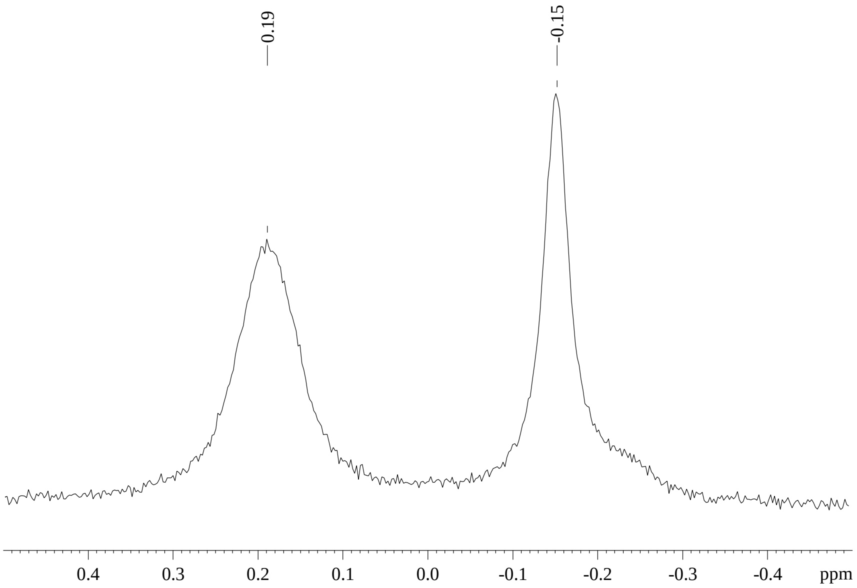

Fig. 72: ^{7}Li spectrum of the reaction mixture of **10**.

3.2.5. Attempts to synthesize neat Li[FAl(OC(C_6F_{10})C_6F_5)$_3$]

Synthesis

The postulated mechanism in Fig. 64 is supported by various experimental results. In a reaction of a product mixture of **10** with trityl chloride, an unexpected side product, $CPh_3[ClAl(phex)_3]^-$ (section 4.3.1) was formed, which can only result from the existence of $Al(phex)_3$. Furthermore, crystals of the lithium alkoxide **5** (cell constants determined by single crystal X-ray analysis) were found in the same mixtures and traces of the epoxide $C_{12}F_{14}O$ appear in the IR spectrum. **5** can also be observed in ^{19}F spectra. Additionally, a melting point of 46°C is observed, which is different from the melting point of **10** (130°C), the parent alcohol (52°C) and the alkoxide (139°C) and can possibly be assigned to $C_{12}F_{14}O$. Consequently, it should be possible to generate **10** directly starting from the Lewis acid $Al(phex)_3$ and a suitable fluoride donor.

Syntheses of pure $Li[FAl(phex)_3]$ **10** was attempted by generating the $Al(phex)_3$ in situ and reacting it with lithium tetrafluoroborate as a fluoride source (Eq. 25). Fluorobenzene was chosen as a solvent, because it generally dissolves compounds containing the phex ligand very well. Progress of the reaction was monitored by venting the formed methane through a bubble counter and metering the amount of gas. The second reaction step was monitored in intervals by ^{19}F NMR spectroscopy (BF_3 undergoes hydrolysis and thus the amount of formed gas can not be reliably counted).

$$3\,ROH + AlMe_3 \xrightarrow[-\,3\,CH_4]{} Al(OR)_3 \xrightarrow[-\,BF_3]{+\,LiBF_4} Li[FAl(OR)_3]$$

$$R = (C_6F_{10})C_6F_5$$

(Eq. 25)

The planned reaction pathway did not prove satisfactory. No reaction occurs at low temperatures (below 5°C), where $Al(phex)_3$ is stable in solution. At higher temperatures (20°C and above), a variety of side products is formed, while the desired reaction occurs very slowly.

NMR spectroscopy

The ^{19}F spectra of the reaction mixture show a variety of signal sets which proved too complicated to assign even with the help of COSY and NOESY experiments (Fig. 73).

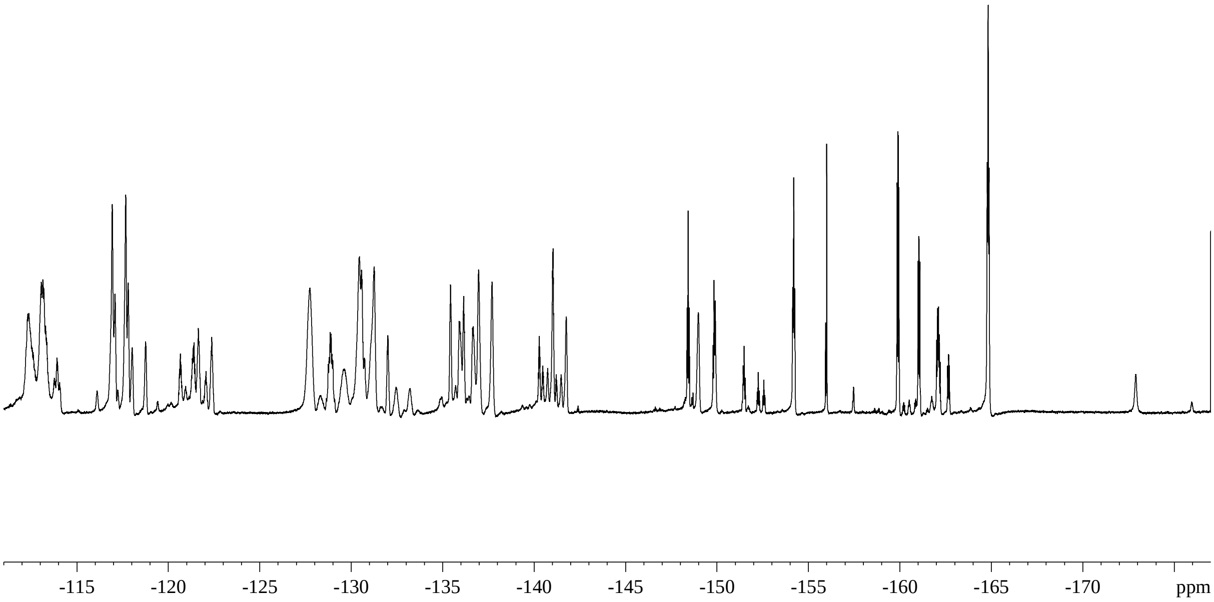

Fig. 73: ^{19}F NMR spectrum of a reaction mixture containing Al(phex)$_3$ and LiBF$_4$ after stirring at room temperature for 12 hours, recorded in CDCl$_3$ (THF was added because some of the components of the mixture were poorly soluble). Spectra at lower temperatures show only the signal set of Al(phex)$_3$. When heating the mixture to higher temperatures, only the relative intensities of the various signal sets change slightly.

^{7}Li spectra show a single peak at -0.82 ppm, which could arise from **10** or LiBF$_4$·THF, or indicate an exchange between the two species. At least two aluminum-containing species must exist (^{27}Al signals at 47.3 and 44.3 ppm, but some components of the reaction mixture are poorly soluble). The ^{11}B NMR (Fig. 74) shows one main signal at 0 ppm and three weaker peaks at -1.4, -0.8 and 0.6 ppm. The main signal probably arises from BF$_3$·THF (BF$_3$·Et$_2$O is the reference for ^{11}B NMR, hence the shift of 0 ppm). A strong ^{19}F signal is found at -127.7 ppm which would fit BF$_3$·THF (cf. δ^{19}F of BF$_3$: -126.8 ppm, but no B-F coupling is observed in the ^{19}F and ^{11}B spectra). This could mean that the reaction of tetrafluoroborate with Al(phex)$_3$ was not finished and continued in the NMR sample until the added THF formed complexes with Al(phex)$_3$, LiBF$_4$ and BF$_3$. Residual LiBF$_4$ must also be present (cf. δ^{11}B (CD$_3$CN) = -1.4 ppm[256]), but can only be clearly assigned in the ^{11}B spectrum because the relevant range in the ^{19}F (cf. δ^{19}F (CD$_3$CN) = -151.7 ppm[256]) is occupied by a large number of aromatic fluorine signals. The proton NMR shows traces of unreacted Al(CH$_3$) functions at -1.0 and -1.3 ppm (cf. 0.1 and -0.5 ppm for the bridged and terminal methyl groups in pure trimethyl aluminum[257]) and no residual OH signal of the alcohol **2**. Consequently, the ^{11}B signals at -0.8 and 0.6 ppm could arise from side reactions of BF$_3$ with excess acidic alcohol or its alkoxide, yielding new products such as BF$_3$·C$_{12}$F$_{15}$OH or [F$_3$B(phex)]$^-$. In summary, the multitude of possible side reactions and strong dependence on various parameters such as reaction time, exact temperature and stoichiometry, makes this synthetic strategy unsuitable for large-scale synthesis of pure **10**.

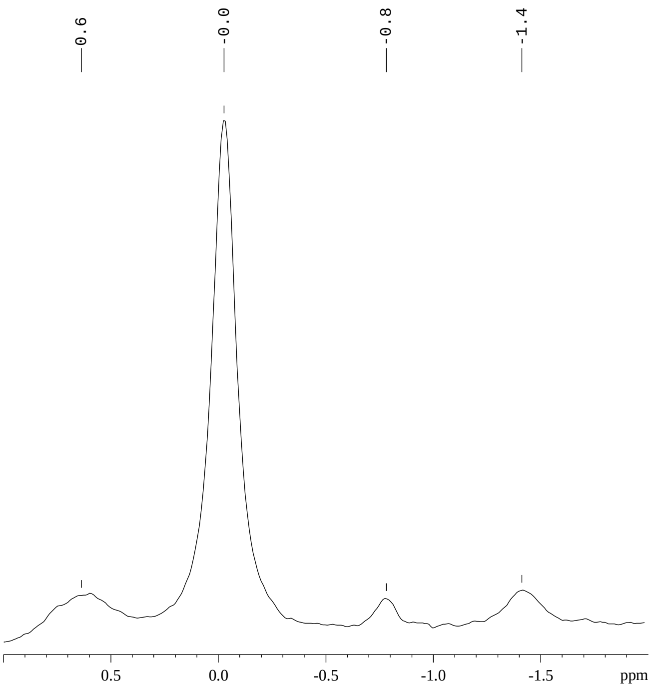

Fig. 74: ^{11}B NMR spectrum of a reaction mixture containing Al(phex)$_3$ and LiBF$_4$ after stirring at room temperature for 12 hours.

3.2.6. Synthesis and characterization of Ag[FAl(OC(C$_6$F$_{10}$)C$_6$F$_5$)$_3$]

Synthesis

Ag[FAl(phex)$_3$] (phex = OC(C$_6$F$_{10}$)C$_6$F$_5$) **12** is synthesized in a metathesis reaction from Li[FAl(OC(C$_6$F$_{10}$)C$_6$F$_5$)$_3$] **10** and AgBF$_4$ in CH$_2$Cl$_2$. The lithium salt was synthesized from LiAlH$_4$ and the parent alcohol **2** (see 3.2.4). After ultrasonic activation (3 h) and filtration of LiBF$_4$, a white powder with a melting point of 46°C (c.f. main side product in the synthesis of **10**: 46°C, lithium alkoxide **5**: 130°C) is obtained, from which neat **12** is obtained by crystallization. Judging from the melting points, it is likely that the epoxide **11** (see postulated mechanisms in Fig. 64) is still present in the mixture. However, apart from **12**, the only other product which crystallizes from dichloromethane or monofluorobenzene is the dimeric lithium alkoxide **5b** (cell constants determined by single crystal diffractometry, supporting both postulated mechanisms). The total yield of the pure product is unknown, but it is very likely that **12** can be obtained quantitatively when a pathway to pure starting material **10** is found. NMR experiments (see below) indicate that **12** can also be formed directly from Al(phex)$_3$ and AgBF$_4$.

IR spectroscopy

The IR spectrum of the product mixture containing **12** (Fig. 75) shows the same bands as in **10**, indicating that the same side products are still present. The relative intensities differ however, which can be expected because the solubilities of the various side products in CH$_2$Cl$_2$ should be different (**12** is generally more soluble than the lithium salt in solvents like toluene, CH$_2$Cl$_2$ or monofluorobenzene). IR spectra of single crystals could not be measured, because crystals of **12** can not be visually discriminated from crystals of the side product LiO(C$_6$F$_{10}$)C$_6$F$_5$ **5** and can only be identified by X-ray analyses.

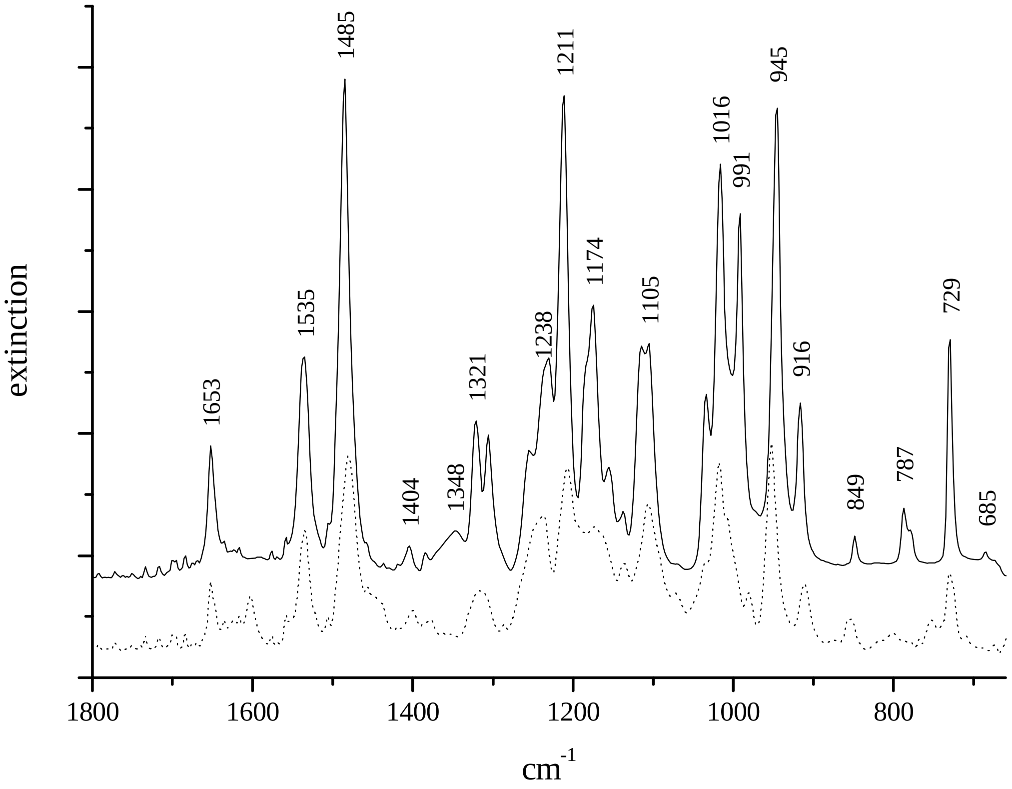

Fig. 75: IR spectrum of a reaction mixture of **12** (solid line). The dotted line shows the spectrum of a product mixture containing the lithium salt **10** for comparison (see 3.2.4).

NMR spectroscopy

The ^{27}Al spectrum shows a single peak at 47.6 ppm. According to the postulated mechanism, the second aluminum-containing species in reaction mixtures of **10** is Al(phex)$_3$, which would react with AgBF$_4$ under formation of **12** and BF$_3$, leaving only one ^{27}Al signal. A strong ^{19}F signal is found at -127.7 ppm which would fit BF$_3$ (cf. pure BF$_3$: δ^{19}F = -126.8 ppm) and is also observed when reacting Al(phex)$_3$ with LiBF$_4$ (3.2.5). However, further side products are present, as becomes obvious from the ^{19}F spectrum (Fig. 76). The two main species appear with comparable intensities. This can be explained simply by the wrong stoichiometry of AgBF$_4$, which partly reacts with Al(phex)$_3$ (forming directly Ag[FAl(phex)$_3$]), leaving excess Li[FAl(phex)$_3$] in the mixture (the aromatic signals at -147.5 and -159.1 ppm exhibit the exactly same chemical shift as in **10**). Signals of the aromatic C$_6$F$_5$ groups of lithium alkoxide are also observed at -151.6 and -161.4 ppm with relatively low intensities. Further side products are negligible.

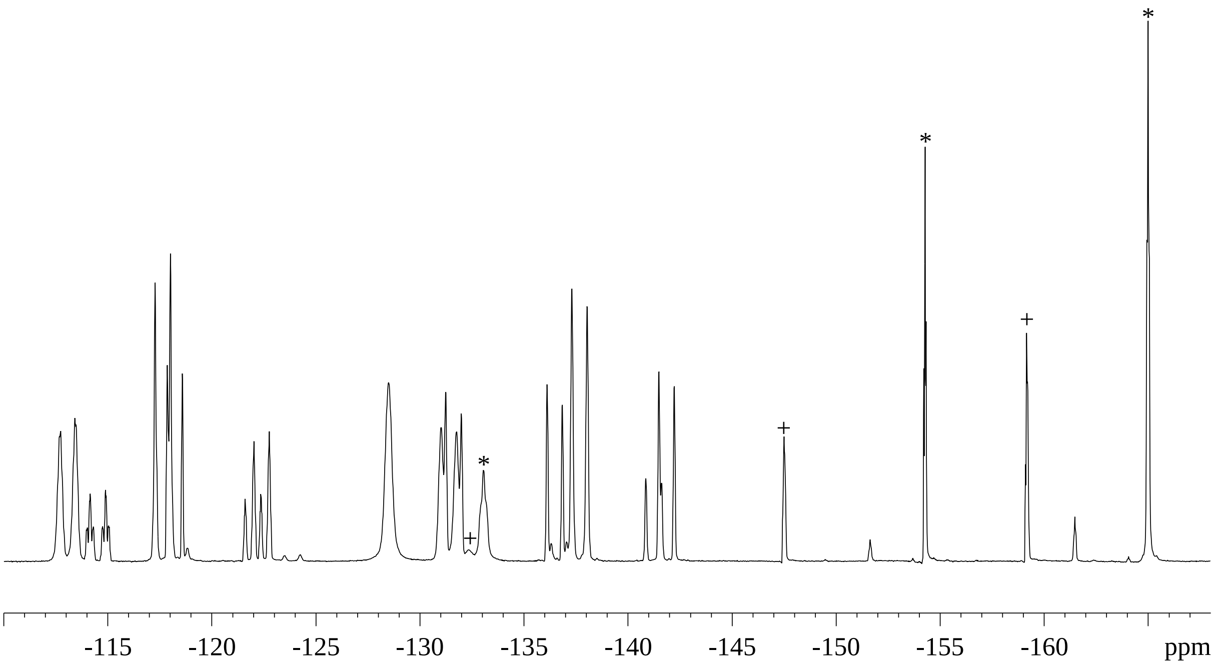

Fig. 76: ^{19}F NMR spectrum of reaction mixtures of **12**. Signals assigned to aromatic fluorine atoms in **12** are marked with an asterisk, those assigned to **10** are marked with a cross.

Crystal structure determination

12 crystallizes as colorless blocks **12a** from concentrated dichloromethane solutions in the monoclinic space group P2$_1$/c with the cell parameters a = 11.21 Å, b = 25.43 Å, c = 18.43 Å, β = 93.2° and Z = 4. The silver atom is coordinated by the fluorine atom connected to the aluminum center, as well as with five chlorine atoms of three CH$_2$Cl$_2$ solvent molecules (Fig. 77). Ag-Cl bond distances shall not be discussed because there is severe disorder, each solvent molecule being disordered across at least three positions. There is one further very weak Ag-F contact with an aliphatic CF$_2$ group at 310.1(2) pm (sum of van-der-Waals radii: 319 pm). All aliphatic C$_6$F$_{10}$ units point in the same direction as the Al-F bond, towards the silver atom.

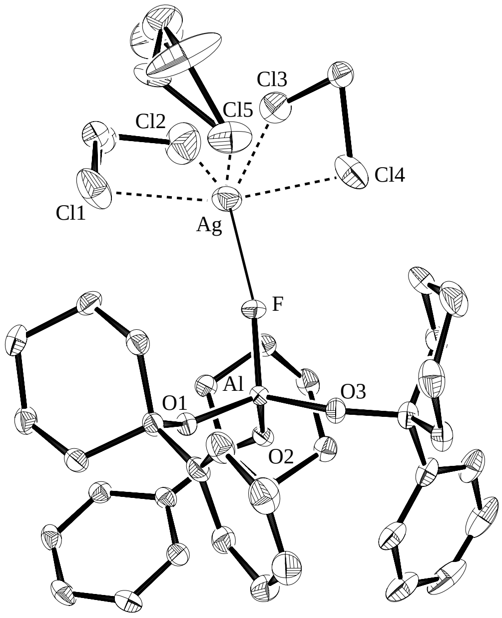

Fig. 77: Crystal structure of **12a**. Fluorine atoms bound to carbon atoms and hydrogen atoms were omitted for clarity. The coordinating CH_2Cl_2 molecules are severely disordered, only the main orientations are shown. Thermal ellipsoids are drawn at 50% probability level. Distances in pm: Ag-F 233.0(1), Al-O1 174.4(1), Al-O2 174.3(1), Al-O3 174.0(1), Al-F 168.9(1), Ag-Cl 255.3(1)-299.9(1). Angles in °: O-Al-F 107.7(1)-109.9(1), Al-O-C 142.0(1)-143.8(1), O-Al-O 109.1(1)-111.4(1), Al-F-Ag 169.0(1).

The known compound $Ag(C_6H_5F)_3[FAl(pftb)_3]$[190] exhibits average Al-O bond distances of 173.3 pm, which is only 0.6 pm shorter than in **12a**, indicating a comparable stability versus ligand abstraction, even though the phex ligand is sterically more demanding than the nonafluoro-^{t}butoxy ligand (cf. in $Ag(1,2\text{-}Cl_2C_2H_4)[Al(pftb)_4]$[53] with its very stable homoleptic anion, the average Al-O bond distance is 172.9 pm and thus only slightly shorter than in **12a**). The Al-F bond distance is 168.9(1) pm and the Ag-F bond distance is 233.0(1) pm (165.2 and 246.8 pm in $[Ag(C_6H_5F)_3]^+[FAl(pftb)]^-$), however the coordinative strength can only be directly compared in the same solvent, because it depends on the solvents´ donor strength (see below for a crystal structure with monofluorobenzene as donor). While silver is clearly coordinated by the anion, the O-Al-F and O-Al-O angles hardly deviate from the tetrahedral angle. An analysis of the coordinative strength of $[FAl(phex)_3]^-$ in this compound e.g. with I. D. Brown´s bond valence method[258] can not deliver reliable results due to the diffuse disorder of the coordinated methylene chloride molecules.

From monofluorobenzene, **12** crystallizes as colorless blocks with the composition $[Ag(C_6H_5F)_3][FAl(OC(C_6F_{10})C_6F_5)_3]$ **12b** in the monoclinic space group $P2_1/c$ with the cell parameters a = 11.77 Å, b = 25.57 Å, c = 19.54 Å, β = 92.2° and Z = 4. In **12b**, the silver atom is coordinated by three fluorobenzene molecules (FB1-3 in Fig. 78), two of which (FB2 and FB3) are η^2 coordinated and one is η^1 coordinated. The compound can be considered truly ionic with discrete cations and anions, and there is no Ag-F contact within the sum of van-der-Waals radii of 319 pm. The aluminum atom is tetrahedrally coordinated, with O-Al-O and O-Al-F angles very close to the tetrahedral angle. In FB1 the C-F bond is disordered about two positions, in FB3 about three positions. In FB2 the disorder of the fluorine atom can be described with slightly larger anisotropic displacement parameters.

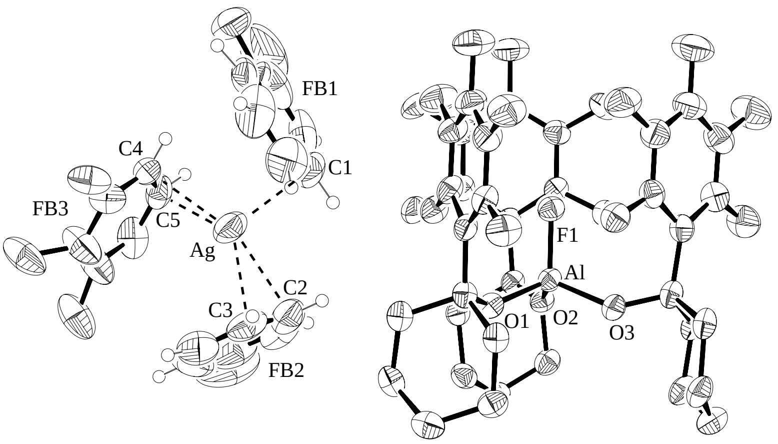

Fig. 78: Crystal structure of **12b**. Aliphatic fluorine atoms omitted for clarity. The coordinating monofluorobenzene molecules are disordered. Thermal ellipsoids are drawn at 50% probability level. Distances in pm: Al-F1 166.9(1), Al-O1 174.6(1), Al-O2 174.7(1), Al-O3 175.0(1), Ag-C1 249.2(1), Ag-C2 258.8(1), Ag-C3 245.7(1), Ag-C4 243.381), Ag-C5 250.1(1). Angles in °: O-Al-F 108.8(1)-110.7(1), Al-O-C 135.5(2)-137.8(2), O1-Al-O2 109.6(1), O1-Al-O3 108.4(1), O2-Al-O3 110.5(1).

Two analogous crystal structures with the $[FAl(pftb)_3]^-$ anion are known (Tab. 13).[190] A more electron-rich aromatic donor should lead to shorter Ag-C contacts. In the analogous $[FAl(pftb)_3]^-$ salt, all three monofluorobenzene molecules are η^2 coordinated. However, with the mixed η^2/η^1 coordination, **12b** is more similar to $[Ag(toluene)_3][FAl(pftb)_3]$, which seems quite contradictory at first sight and may well be due to packing effects. However, the same holds for the Ag-C distances, which are systematically shorter than in both $[FAl(pftb)_3]^-$ salts by an average 2.2, respectively 15.9 ppm (sum of bond valences of Ag-C bonds in **12b**: 0.977, cf. $[Ag(C_6H_5F)_3][FAl(pftb)_3]$: 0.873). The average Ag-C bond valence is 0.195 (cf. $[Ag(C_6H_5F)_3][FAl(pftb)_3]$: 0.130). In both reference compounds, albeit the contacts are weak, silver is clearly coordinated by the fluorine atom connected with the central aluminum atom (Al-F bond valence in $[Ag(C_6H_5F)_3][FAl(pftb)_3]$: 0.749, $[Ag(toluene)_3][FAl(pftb)_3]$: 0.692).

This is not the case in **12b** (Al-F bond valence 0.715, but the fluorine atom additionally exhibits three weak C-F contacts with the aromatic rings at 270.3(1), 273.6(1) and 274.3(1) pm, c.f. sum of van-der-Waals radii of C and F: 317 pm), where the silver atom has a much larger electron deficit, leading to the remarkable shortening in Ag-C bond lengths and a single η^1 coordinated fluorobenzene molecule (due to slightly higher steric demand).

Tab. 13: Comparison of selected bond parameters in **12b** with two compounds containing the $[FAl(pftb)_3]^-$ anion.[190]

	12b	**$[Ag(toluene)_3][FAl(pftb)_3]$**	**$[Ag(C_6H_5F)_3][FAl(pftb)_3]$**
Ag-F [pm]	-	254.4	246.8
Ag-C [pm]	Ag-C1 249.2(1)	250.2	253.3
	Ag-C2 258.8(1)	250.8	258.2
	Ag-C3 245.7(1)	251.3	259.9
	Ag-C4 243.3(1)	252.7	268.3
	Ag-C5 250.1(1)	252.9	271.8
	-	-	280.4
av.	249.4	251.6	265.3
Al-O av. [pm]	174.8	173.3	172.9
Al-F [pm]	166.9(1)	168.1	165.2

Consequently, the Al-F bond is shortened by 1.2 pm, the average Al-O bond lengthened by 1.5 pm with respect to $[Ag(toluene)_3][FAl(pftb)_3]$ ($[Ag(C_6H_5F)_3][FAl(pftb)_3]$ is not directly comparable because all atoms were refined isotropically due to poor crystal quality). While the effect on anion stability is probably negligible, $[FAl(phex)_3]$ is less coordinating than $[FAl(pftb)_3]$ in aromatic solvents.

The Al-O bond lengths are slightly longer than in **12a** (by an average 0.8 pm) which may result from the fact that silver is coordinated by fluorine in that compound. Remarkably, while in **12a** all aliphatic groups of the ligand point in the direction of the Al-F bond, the geometry is reversed in **12b**. The fluorine atom is encaged by three aromatic C_6F_5 rings, sterically shielding it from coordination. Whether this is a function of solvent polarity or concentration, resulting from a steering effect of the solvent during crystallization or of packing effects, remains unclear and appropriate experiments (e.g. low-temperature NMR) were not performed. In solution a coordinated species or an equilibrium between coordinated and uncoordinated species might exist.

3.2.7. Attempted syntheses of Li[Ga(O(C_6F_{10})C_6F_5)$_4$]

When comparing calculated geometries of the [Al(pftb)$_4$]$^-$, [Al(hfpp)$_4$]$^-$ and [Al(phex)$_4$]$^-$ anions (BP86/SV(P) level), it becomes apparent that the phex ligand is only slightly too bulky to allow the formation of a homoleptic anion. In the very stable [Al(pftb)$_4$]$^-$ anion, the Al-O distances are 176.4 pm (S_4 symmetry). [Al(hfpp)$_4$]$^-$ can still be synthesized, although the predicted Al-O bond lengths are 1.2 pm longer (177.6 pm, S_4 symmetry) than in [Al(pftb)$_4$]$^-$. However, in the calculated geometry of [Al(phex)$_4$]$^-$ the distances (C_1 symmetry) range from 177.2 to 179.4 pm, with an average distance of 178.6 pm. This elongation of 2.2 pm (1.0 pm with respect to [Al(hfpp)$_4$]$^-$) seems negligible, but [Al(pftb)$_4$]$^-$ can already be considered sterically crowded. Thus it is a good indication that the phex ligand is simply too bulky, which leads to the formation of [FAl(phex)$_3$]$^-$ instead of the homoleptic anion (see mechanisms in Fig. 64). Gallium is slightly larger than aluminum (covalent radii based on X-ray and neutron diffraction data for Al: 121 pm, Ga: 123 pm[259]) and accordingly it might be possible to synthesize a stable salt of a homoleptic [Ga(phex)$_4$]$^-$ anion.

The choice of suitable starting materials to introduce gallium is limited to Ga(III) halides and lithium gallanate. $LiGaH_4$ was prepared[260, 261] and reactions with the alcohol **2** were attempted. However, this route proved unsuccessful due to the low reactivity and poor solubility of both reagents at low temperatures (reactions were attempted in hexane and monofluorobenzene). At temperatures above 10°C, formation of hydrogen gas and simultaneous precipitation of elemental gallium is observed due to decomposition of the unstable gallanate. IR and ^{19}F NMR spectra show residual alcohol as main component and several side-products containing the phex ligand in very low concentrations.

An alternative route, staring from Ga(III) halides and the Li alkoxide **5** seems more promising, especially because the reagents are stable at higher temperatures.

Synthesis

As shown in (Eq. 26, 4 equivalents of the lithium alkoxide **5** are reacted with the gallium halide in monofluorobenzene (ultrasonic activation). Precipitation of LiX is observed. After filtration and removal of the solvent in vacuo, a white powder is obtained. The melting points (reaction with GaCl3: 141°C, reaction with GaBr3: 142°) are approximately identical to the m.p. of donor-free **5**. Lower-melting components, such as unreacted $GaCl_3$ (m.p. 78°C) or $GaBr_3$ (121°C), are not observed.

$$4\ \mathrm{LiOR} + \mathrm{GaX_3} \xrightarrow[-\ 3\ \mathrm{LiX}]{} \mathrm{Li[Ga(OR)_4]}$$

$$\mathrm{R} = \mathrm{(C_6F_{10})C_6F_5},\ \mathrm{X} = \mathrm{Cl, Br}$$

(Eq. 26)

Already from a comparison of the melting points, it becomes apparent that the reactions do not proceed as planned. Instead, an incomplete substitution seems more likely (Eq. 27). IR and NMR spectroscopy consequently confirm that the main component in the solvent-free product mixture is indeed the lithium alkoxide **5**.

$$4\ \mathrm{LiOR} + \mathrm{GaX_3} \xrightarrow[-\ \mathrm{LiX}]{} 2\ \mathrm{LiOR} + \mathrm{Li(OR)_2GaX_2}$$

$$\mathrm{R} = \mathrm{(C_6F_{10})C_6F_5},\ \mathrm{X} = \mathrm{Cl, Br}$$

(Eq. 27)

IR spectroscopy

The IR spectra of the reaction products of **5** with $GaCl_3$ and $GaBr_3$ are identical. Both spectra can not be distinguished from the spectrum of **5** (section 6.6, Tab. 48). It can be deducted that the obtained product mixture predominantly consists of the lithium alkoxide. A second product is only observed in ^{19}F NMR spectra and by X-ray structure analyses (see below).

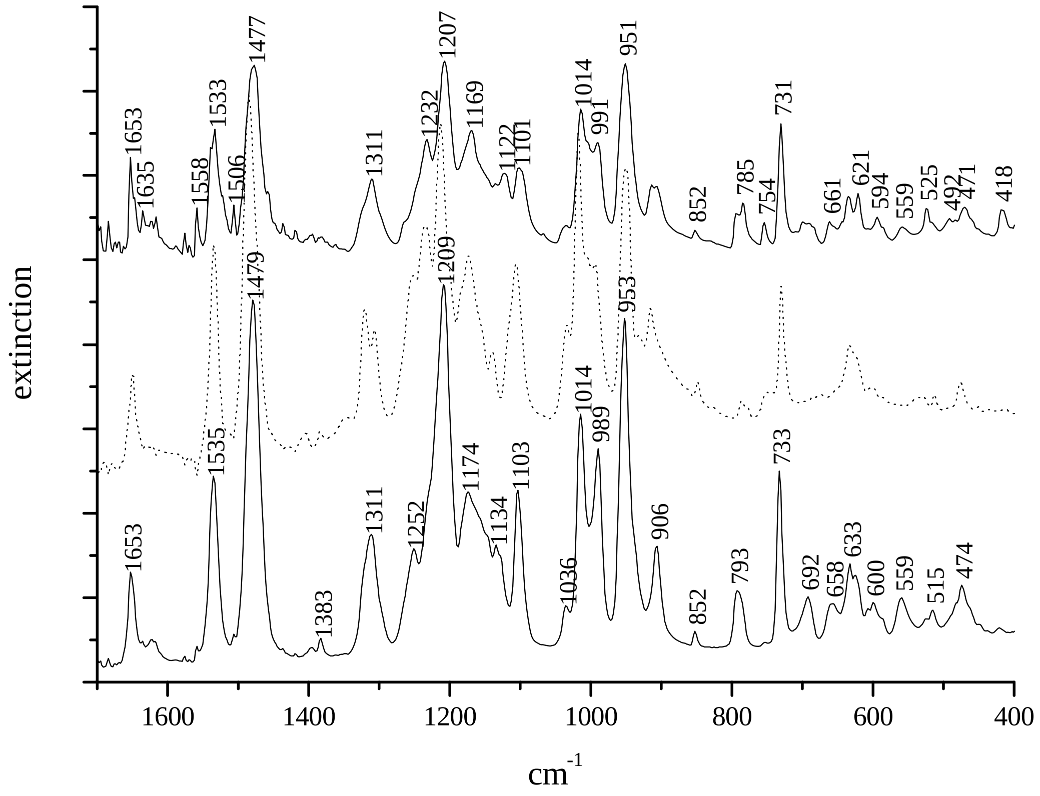

Fig. 79: Infrared spectra of solid **13** (upper graph, crystals grown in fluorobenzene, signals of fluorobenzene around 3000 cm^{-1} omitted) and **14** (lower graph, powder obtained after filtration and removal of the solvent in vacuo) in comparison with the alkoxide **5** (dotted line).

NMR spectroscopy

^{19}F NMR spectra of **13** and **14** are identical, each showing two signal sets (not shown due too poor signal-to-noise ratio). The main signal set is within 0.2 ppm identical with that of the alkoxide **5**, while the second signal is only slightly shifted with respect to the first (by less than 1 ppm). The only exception is the signal of the para C_6F_5 fluorine atom, which appears at -138.9 ppm (cf. **5**: -136.6 ppm). Spectra were recorded in toluene-D_8; no signals of fluorobenzene were found (after drying the product in vacuo). Considering the IR spectra, it can be deducted that one of the two products must be the lithium alkoxide **5**.

Crystal structure determination

In both reactions, when crystallized from fluorobenzene, most of the crystals are colorless blocks of dimeric lithium alkoxide **5b**. However, a few crystals are visually different (see below) and their structures could be elucidated. Product mixtures from reactions with $GaCl_3$ form crystals of $Li(OC(C_6F_{10})C_6F_5))_2GaCl_2{\cdot}C_6H_5F$ **13**, while those with $GaBr_3$ form the analogous $Li(OC(C_6F_{10})C_6F_5))_2GaBr_2{\cdot}C_6H_5F$ **14**. Both structures are closely related to the structure of the parent lithium alkoxide **5**, which also crystallizes as a dimer **5b** from monofluorobenzene (see 3.1.7). In **13** and **14**, the GaX_2 fragment occupies the place of one Li-FC_6H_5 unit in **5b**.

13 crystallizes as colorless cubes from concentrated monofluorobenzene solutions in the orthorhombic space group Fdd2 with the cell parameters a = 28.37 Å, b = 10.83 Å, c = 23.40 Å and Z = 8 (for a detailed report of structural parameters see section 6.11, Tab. 65).

14 crystallizes as colorless antiprismatic blocks from concentrated monofluorobenzene solutions in the monoclinic space group Cc with the cell parameters a = 23.50 Å, b = 10.86 Å, c = 18.06 Å, β = 128.4° and Z = 4. The crystal quality is very poor, with crystals being very small, weakly scattering and twinned. Thus, the structure must be considered preliminary and not all atoms could be assigned anisotropic displacement parameters. A more detailed report of structural parameters is given in section 6.11, Tab. 66.

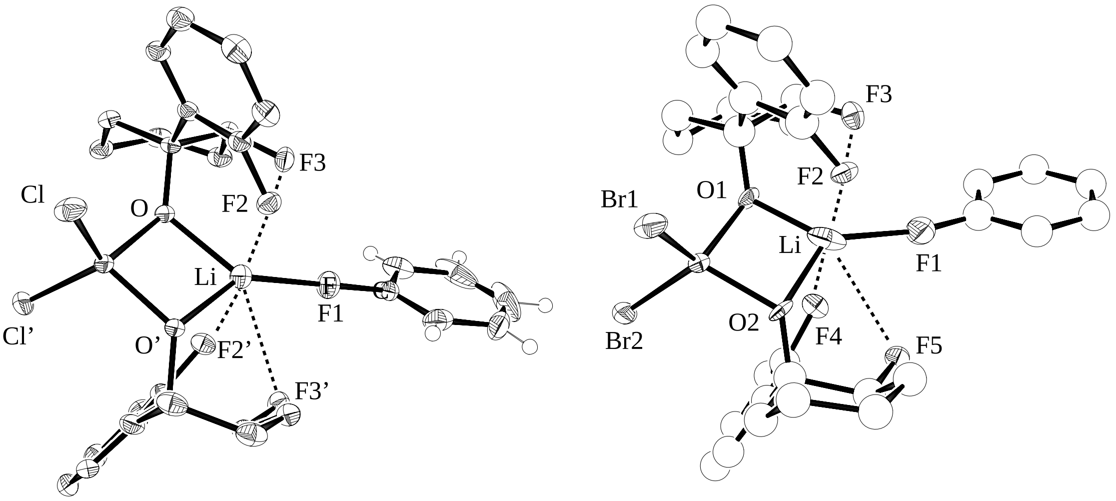

Fig. 80: Crystal structure of **13** (left) and fragmentary crystal structure of **14** (right, carbon atoms refined isotropically). Symmetry equivalents are marked with an inverted comma. Fluorine atoms of the ligands omitted for clarity, thermal ellipsoids drawn at 50% probability level.

In **13**, the Ga and Li atoms, the F-C bond and C-H bond in para position of the coordinated fluorobenzene rest on a C_2 rotation axis (Li-F1-C angle 180(0)°). Lithium is additionally coordinated by four fluorine atoms of the phex ligand (see Tab. 14, two in ortho position of C_6F_5 and two in 2-position of C_6F_{10}). There are no significant intermolecular contacts. **14** exhibits no symmetry elements within the dimer, but the coordination of the lithium atom by fluorobenzene and four fluorine atoms of the ligand is similar, albeit with slightly differing contact distances. **14** has a nonlinear Li-F1-C angle of 172.2(1)° and also shows no intermolecular contacts. Apart from minor differences resulting from the different sizes of chlorine and bromine, the two crystal structures can be considered equivalent. Tab. 14 shows a comparison of selected structural parameters of **13** and **14** compared with the dimeric lithium alkoxide **5b**.

Tab. 14: Comparison of selected structural parameters of **13**, **14** and the dimeric lithium alkoxide **5b**.

	13	**14**[a]	**5b**[b]
Li-O [pm]	200.1(1)	Li-O1 193.5	Li1-O1 186.4(1)
		Li-O2 193.6	Li1-O2 188.6(1)
Ga-O [pm]	188.9(1)	Ga-O1 189.4	
		Ga-O2 189.7	
Ga-X [pm][c]	214.4(1)	Ga-Br1 228.6	
		Ga-Br2 229.5	
Li-F [pm]	Li-F1 191.1(1)	Li-F1 194.4	Li-F1 201.4(1)
	Li-F2 214.8(1)	Li-F2 209.3	Li-F2 208.1(1)
	Li-F3 267.4(1)	Li-F3 268.1	Li-F3 279.9(1)
		Li-F4 219.0	
		Li-F5 274.2	
F-C [pm]	F1-C 137.1(1)	F1-C 133.9	137.9(1)
O-C [pm]	139.5(1)	O1-C 138.2	135.2(1)
		O2-C 139.0	
O-Li-O [°]	81.7(1)	83.7	94.4(1)
O-Ga-O [°]	87.7(1)	85.9	
Ga-O-Li [°]	95.3(1)	Ga-O1-Li 95.2	
		Ga-O2-Li 95.1	
X-Ga-X [°][b]	113.4(1)	112.3	
Li-F1-C [°][c]	180.0(0)	172.2	164.4(2)
Li-O-Li [°]			85.6(1)

[a] No standard deviations given (preliminary structure); [b] see Fig. 45; [c] X = Cl (**13**), Br (**14**).

All three compounds share the motif of coordination around lithium. Remarkable is the shortening of the Li-F1 bond by more than 10 pm in **13** (and 6 pm in **14**) with respect to the already extremely short distance in **5b**, approaching the shortest reported Li-FC_6H_5 contact of 186.6 pm (it should again be emphasized that so far only one publication describes the coordination of mono- or difluorobenzene to lithium).[242]

3.2.8. Evaluation of WCA stabilities

Apart from the acidity of the ligand´s parent alcohol (see chapter 3.1.1), other criteria can be utilized to appraise the stability of a given weakly coordinating anion.[262] Among these, the *f*luoride *i*on *a*ffinity (FIA) is most widely used. All WCAs $[E^n(L)_{n+1}]^-$ (E = B, Al, Ga, Sb, Nb etc., L = singly-charged ligand) with Lewis acidic central atoms are prone to ligand abstraction. The FIA is a measure of the strength of the parent Lewis acid $E^n(L)_n$ and thus of the stability of the WCA itself. It is defined as the negative reaction enthalpy of a fluoride addition to this Lewis acid (Eq. 28).

$$E(L)_n + F^- \xrightarrow{\Delta H = -FIA} [F\text{-}E(L)_n]^-$$

(Eq. 28)

Accordingly, a strong Lewis acid has a high FIA, resulting in a higher thermodynamic stability of the respective WCAs $[E^n(L)_n(L')]^-$ (L and L' not necessarily identical). To obtain more reliable data, the FIA is calculated with the help of an isodesmic reaction incorporating the experimentally determined FIA of OCF_2 (209 kJ mol^{-1}).[262, 263]

The *l*igand *a*ffinity (LA) is defined as the enthalpy of reaction necessary to remove a ligand L^- from the ion $[E^n(L)_{n+1}]^-$ (Eq. 29). It is always endothermic and a higher LA value denotes a higher stability of the WCA against ligand abstraction.[264] However, the LA also reflects the intrinsic stability of the generated L^- anion. E.g. for $C_6F_5(C_6F_{10})O^-$, in which the basic O^- is well-shielded by fluorine atoms, the LA can be expected to be comparatively lower than in anions with less stable ionic ligands such as $C_6H_3(CF_3)_2^-$.

$$[E(L)_{n+1}]^- \xrightarrow{\Delta H = LA} E(L)_n + L^-$$

(Eq. 29)

To obtain more reliable results, the LA is calculated by an isodesmic reaction, combining relatively low-level DFT with Møller-Plesset perturbation calculations. (Eq. 30) depicts such a reaction for the case of alkoxyaluminate anions.

$$[\mathrm{Al(OR)_4}]^- + \mathrm{AlF_3} \xrightarrow[\text{DFT}]{\text{isodesmic}} \mathrm{Al(OR)_3} + [\mathrm{F_3AlOR}]^-$$

$$[\mathrm{F_3AlOR}]^- \xrightarrow[\text{MP2}]{\text{non-isodesmic}} \mathrm{AlF_3} + \mathrm{RO}^-$$

$$[\mathrm{Al(OR)_4}]^- \xrightarrow{\Delta H = \mathrm{LA}} \mathrm{Al(OR)_3} + \mathrm{RO}^-$$

(Eq. 30)

Other authors showed by systematic analyses of a variety of compounds that the combination of BP86/SV(P) and MP2/TZVPP can be applied to WCA with fluorinated ligands and is generally reliable to within 25 kJ mol^{-1},[262] thus only these methods were used to evaluate the anions presented in this thesis.

The thermodynamic stability of a given WCA against attacks of hard or soft electrophiles can be assessed by the isodesmic decomposition reactions of $[\mathrm{E}^n(\mathrm{L})_{n+1}]^-$ with H^+ (hard, *p*roton-induced *d*ecomposition PD) or Cu^+ (soft, *Cu*-induced *d*ecomposition CuD) (Eq. 31).

$$[\mathrm{E(L)}_{n+1}]^- + \mathrm{H}^+ \xrightarrow{\Delta H = \mathrm{PD}} \mathrm{E(L)}_n + \mathrm{HL}$$

$$[\mathrm{E(L)}_{n+1}]^- + \mathrm{Cu}^+ \xrightarrow{\Delta H = \mathrm{CuD}} \mathrm{E(L)}_n + \mathrm{CuL}$$

(Eq. 31)

Both PD and CuD are exothermic because two ions react in the gas phase forming two neutral species. Less negative values indicate a higher stability of the WCA versus hard and soft electrophilic attack. Additionally, both values are independent of the intrinsic stability of the L^- anion.

Other considerations involve the orbital energies. The HOMO energy of a WCA correlates with its sensitivity towards oxidation because it is harder to remove an electron from low-energetic orbitals. Low HOMO energies are thus desirable for better stability. In turn, the HOMO-LUMO gap can be associated with the resilience of a WCA against reduction. Comparably small gaps, such as in $[\mathrm{Sb_4F_{21}}]^-$ (3.256 eV)[262] indicate an oxidizing character of the anion, which may interfere with easily oxidized cations. As the HOMO energy and HOMO-LUMO gap are calculated in DFT calculations, they should be considered indirect measures of anion stability because the absolute values are inaccurate.

Tab. 15: Key properties of selected WCAs, calculated on the BP86/SV(P) level of theory[264] (0 K in the gas phase, energies not corrected for ZPE).

	FIA	**LA**	**PD**	**CuD**	**HOMO**	**gap[a]**
	[kJ mol^{-1}]	**[kJ mol^{-1}]**	**[kJ mol^{-1}]**	**[kJ mol^{-1}]**	**[eV]**	**[eV]**
$[BF_4]^-$	338	[b]	-1212	-521	-1.799	10.820
$[PF_6]^-$	394	[b]	-1156	-465	-2.672	8.802
$[AsF_6]^-$	426	[b]	-1124	-433	-3.149	6.284
$[SbF_6]^-$	489	[b]	-1061	-371	-3.911	5.135
$[Sb_2F_{11}]^-$ (vs. Sb_2F_{10})	549	[b]	-1026	-336	-5.540	4.336
$[Sb_3F_{16}]^-$ vs. (Sb_3F_{15})	582	[b]	-994	-303	-6.342	3.886
$[Sb_4F_{21}]^-$ vs. (Sb_4F_{20})	584	[b]	-991	-301	-6.579	3.256
$[B(OTeF_5)_4]^-$	550	274	-1040	-420	-5.811	2.593
$[As(OTeF_5)_6]^-$	593	290	-1023	-403	-6.335	2.204
$[Sb(OTeF_5)_6]^-$	633	341	-973	-353	-6.610	2.326
$[Al(hfpp)_4]^-$	**515**	**405**	**-1134**	**-439**	**-4.087**	**4.229**
$[FAl(phex)_3]^-$	**530**	**333**	**-1053**	**-361**	**-3.987**	**4.111**
$[Al(pftb)_4]^-$	537	342	-1081	-395	-4.100	6.747
$[(pftb)_3Al\text{-}F\text{-}Al(pftb)_3]^-$	685[c]	441	-983	-297	-4.987	6.500
$[B(C_6H_5)_4]^-$	342	324	-1402	-649	-2.150	4.087
$[B(C_6H_3(CF_3)_2)_4]^-$	471	382	-1251	-506	-3.789	3.816
$[B(C_6F_5)_4]^-$	444	296	-1256	-538	-3.130	4.196
$[B(CF_3)_4]^-$	552	490	-1136	-379	-3.530	9.158

[a] Difference between HOMO and LUMO orbital energies; [b] FIA and LA are identical in this case; [c] FIA calculated with respect to 2 equivalents of $Al(pftb)_3$.

Tab. 15 shows a comparison of the key values of some regularly used or exceptionally stable WCAs. In DFT calculations, error limits of 10 kJ mol^{-1} are common. With this in mind, $[Al(hfpp)_4]^-$ and $[FAl(phex)_3]^-$ rank among the most stable currently known WCAs. The FIA of $Al(phex)_3$ is only 7 kJ mol^{-1} worse than the FIA of $Al(pftb)_3$. PD and CuD values of $[FAl(phex)_3]^-$ are even slightly better than those of the homoleptic anion. The HOMO energies of the two new anions are comparable and within the normal range for alkoxyaluminates. Considering their advantages in crystallography and still quite practicable synthesis, $[Al(hfpp)_4]^-$ and $[FAl(phex)_3]^-$ might be good alternatives to the $[Al(pftb)_4]^-$ anion.

3.3. $Al(O(C_6F_{10})C_6F_5)_3$, a new, isolable Lewis superacid

3.3.1. Introduction

Very strong molecular Lewis are commonly used in rearrangement reactions, catalysis, ionization and bond heterolysis reactions.[31, 265] A reliable measure to assess the strength of a given Lewis acid is the *f*luoride *i*on *a*ffinity FIA (Eq. 28), already described in the previous chapter. It has been suggested to use the FIA as a quantitative measure for Lewis acidity and a large number of values have been tabulated.[263, 266] SbF_5 is the strongest conventional Lewis acid and familiar to many chemists. However, from recent work[262] it became evident that stronger acids are now synthetically available, e.g. $As(OTeF_5)_5$,[267, 268] $B(OTeF_5)_3$,[269] 1,2-$((C_6F_5)_2B)_2C_6F_4$[270] and others. The simplest and most general access to reliable FIA values now comprises the use of quantum chemical calculations in isodesmic reactions.[263]
Many strong Lewis acids like $Sb(OTeF_5)_5$,[85] $CB_{11}F_{11}$ or $B(CF_3)_3$[271] are only available on computational grounds or are not suitable for large-scale application due to high price, tedious syntheses or complicated handling (e.g. $As(OTeF_5)_5$,[267] $Al(C_6F_5)_3$ even has a reputation of being explosive).[272] Some of the very strong Lewis acids are either highly oxidizing (AsF_5, SbF_5, $M(OTeF_5)_5$, etc.) or easily hydrolyzed with formation of anhydrous HF. This does not hold for the organometallic boron-centered acids $B(Ar^F)_3$ (Ar^F = C_6F_5 etc.).[28, 273, 274] However, apart from the chelating 1,2-$((C_6F_5)_2B)_2C_6F_4$[270] they are less acidic. Thus, a simple access to a non-oxidizing, very strong Lewis acid that does not hydrolyze under formation of hazardous chemicals like anhydrous HF would be desirable. The FIAs of small gaseous aluminum-centered Lewis acids like monomeric AlX_3 (X = F, Cl, Br, I; FIA = 457 - 499 kJ mol^{-1}) were reported to be close to or even higher than that of monomeric SbF_5 (489 kJ mol^{-1}).[266] Generally, replacement of monoatomic ligands like fluoride by electronegative polyatomic ligands like $OTeF_5$, CF_3 or C_6F_5 leads to a large increase in Lewis acidity. Bulky ligands should also prevent dimerization. Thus it appears reasonable to prepare an aluminum-centered Lewis acid bearing a perfluorinated alkoxy ligand such as pftb (pftb = $OC(CF_3)_3$). Indeed, the synthesis and characterization of $Al(pftb)_3$ and its more stable donor adduct $C_6H_5F{\rightarrow}Al(pftb)_3$ was recently reported.[266] Quantum chemical calculations predict the FIA of $Al(pftb)_3$ at 537 kJ mol^{-1}, and the authors refer to it as a “Lewis superacid” (because it is stronger than SbF_5, in analogy to Brønsted superacids which are more acidic than the strongest conventional Brønsted acid 100% H_2SO_4). However, while the compound is metastable in solution at temperatures below 0 °C, isolation of solid $Al(pftb)_3$ from toluene, dichloromethane, pentane or hexane at ambient conditions proved difficult due to self-

decomposition by C-F activation and formation of aluminum fluorides. The DFT optimized structure illustrates the reason for the C-F activation. Due to the high Lewis acidity of the tricoordinate aluminum atom, it binds two fluorine atoms of the CF_3 groups at 213 pm (av., Fig. 81).

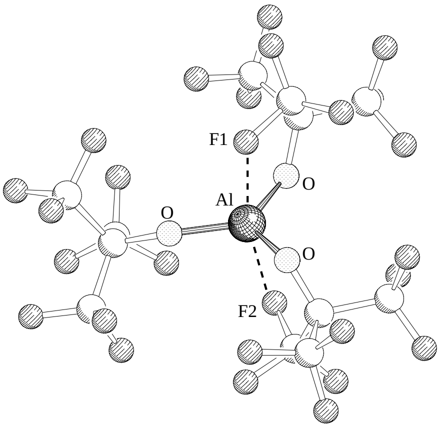

Fig. 81: Calculated geometry of $Al(pftb)_3$ (BP86/SV(P)). Distances in pm: Al-F1 211.5, Al-F2 214.3.

This was interpreted as the first step towards C-F bond cleavage and decomposition. In monofluorobenzene, the Lewis acid forms the adduct $Ph\text{-}F \rightarrow Al(pftb)_3$, which is highly soluble and stable in solution at room-temperature. The compound could be crystallized and fully characterized by the authors. Calculations of the $Al(phex)_3$ (**15**) Lewis acid on the same level of theory are very promising (Fig. 82). Through steric crowding of the larger ligand, the central aluminum atom becomes less accessible for coordination, thus it may be possible to access the donor-free Lewis acid even from monofluorobenzene solution. Furthermore, aluminum is coordinated by two fluorine atoms of pentafluorophenyl rings. While the coordination is slightly stronger (av. 207 pm, i.e. 6 pm shorter than in $Al(pftb)_3$), C-F bond cleavage is less likely due to aromaticity. Accordingly, the coordinating C-F bonds are elongated by only 3% (5 pm) with respect to the other aromatic C-F bonds.

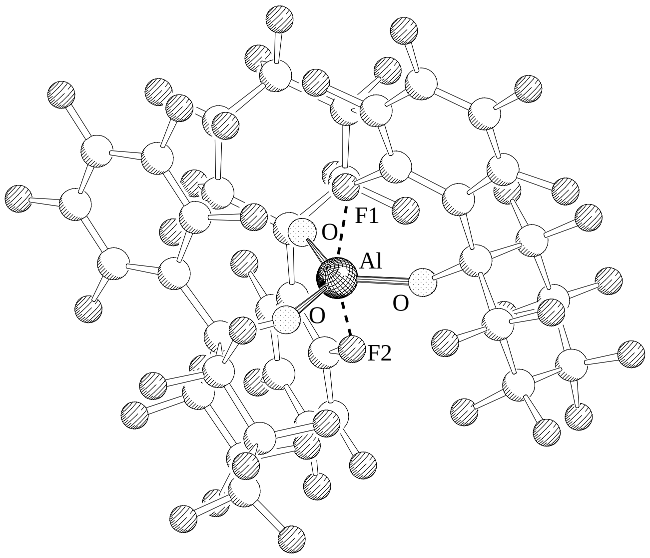

Fig. 82: Calculated geometry of Al(phex)$_3$ **15** (BP86/SV(P)), input geometry based on a crystal structure. Distances in pm: Al-F1 206.9, Al-F2 207.5.

The FIA of Al(phex)$_3$ was calculated as 530 kJ mol^{-1}, ranking the Lewis acid slightly weaker than Al(pftb)$_3$ (537 kJ mol^{-1}), which could be explained by the shorter Al-F contacts. However, the error limits of this type of calculations are in the range of 10-20 kJ mol^{-1} and the predictions are carried out for single molecules in the gas phase at 0 K.

3.3.2. Synthesis and characterization of Al(O(C$_6$F$_{10}$)C$_6$F$_5$)$_3$

Synthesis

Al(phex)$_3$ (phex = O(C$_6$F$_{10}$)C$_6$F$_5$) **15** is synthesized from trimethylaluminum (2M solution in hexane) and three equivalents of the alcohol **2** in fluorobenzene. The product is stable at 5°C in solution, thus the synthesis of **15** and all ensuing reactions should be carried out at that temperature (at temperatures above 10°C, the reaction solution turn first yellow, then dark brown and various decomposition products appear in the ^{19}F NMR spectra). After no further methane development is detected, the solvent is slowly removed in vacuo at 5°C or below and the product is obtained as a white powder (quantitative yield). Solid **15** decomposes very slowly at room temperature (at least a residue of **15** was still present in a storage flask after three months at slightly elevated temperatures in a glove box), but is extremely sensitive to moisture (contact with atmosphere instantly decomposes the product). The solvent-free substance is stable when stored at 10°C or lower temperatures.

IR spectroscopy

Fig. 83 shows the IR bands of solid **15**. There is an almost perfect fit with the simulated spectrum (section 6.6, Tab. 49), which is based on the geometry of the crystal structure (see below). Faint bands between 1400 and 1800 cm^{-1} are in the typical range for bands of residual fluorobenzene (and thus no weak bands from the calculated spectrum are assigned to **15** in this region). Strong C-H bands of the solvent in the range of 3000-3200 cm^{-1} are also observed.

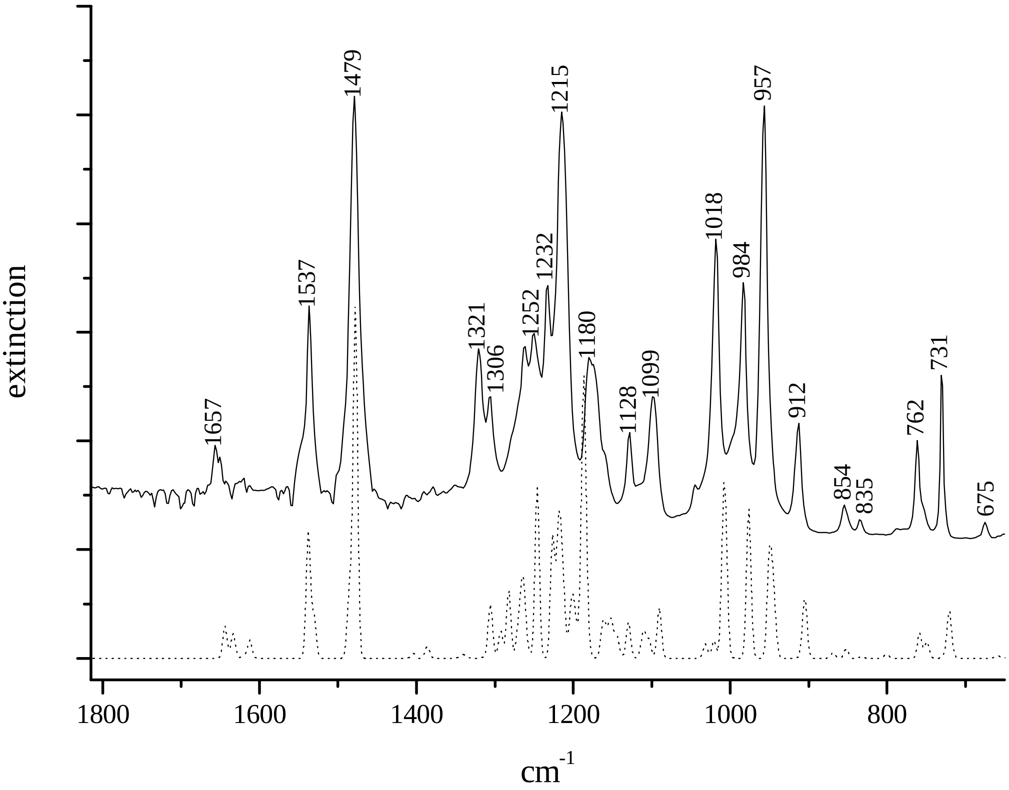

Fig. 83: IR spectrum of solid **15** (solid line) and simulated spectrum of Al(phex)$_3$ (dotted line, BP86/SV(P) level, input geometry based on crystal structure). Bands of residual monofluorobenzene in the range of 3000-3200 cm^{-1} omitted for clarity.

The O-H band at 3623 cm^{-1} is not detected, indicating a quantitative reaction.

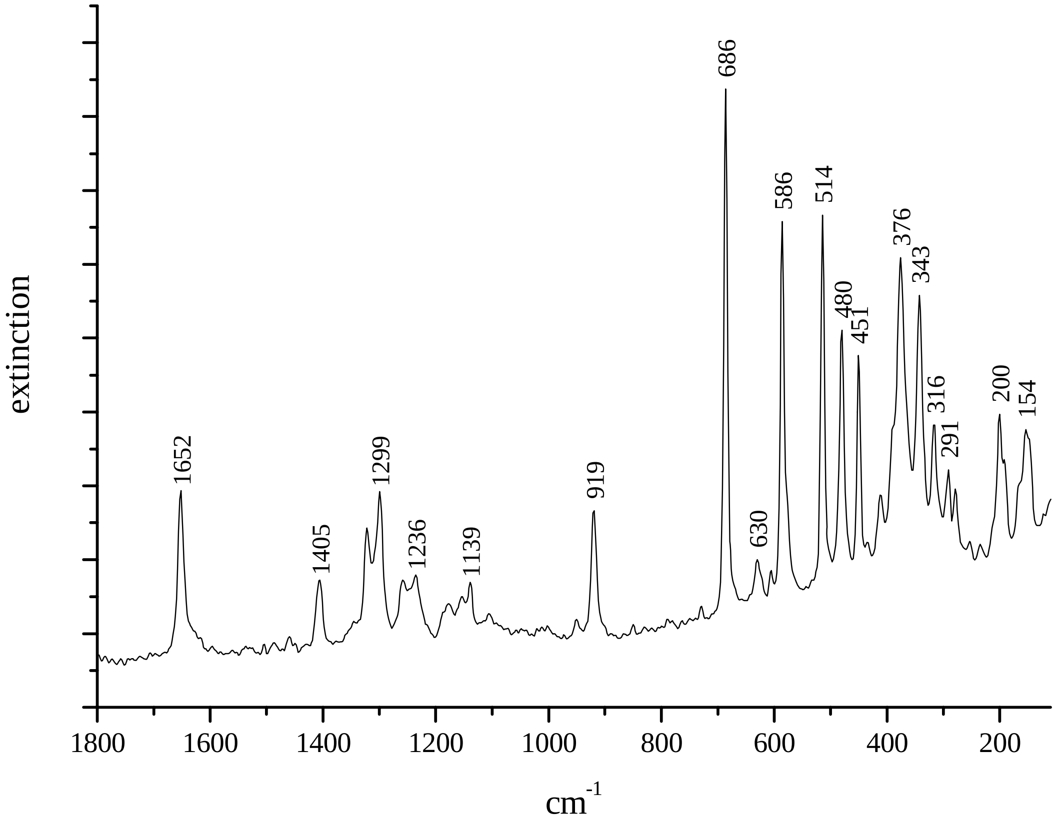

Fig. 84: Raman spectrum of solid **15**. An overlay with the simulated spectrum is not shown because the Raman bands are too weak compared to the IR bands (eg. the strongest Raman band at 686 cm^{-1} is very weak in the simulation). Bands of residual monofluorobenzene in the range of 2700-2900 cm^{-1} omitted for clarity.

NMR spectroscopy

Proton NMR spectra in toluene-D$_8$ show only traces of residual hexane at 0.97 and 1.38 ppm and a negligible signal of the hydroxyl group of the alcohol **2** at 3.27 ppm (probably due to a slightly incorrect stoichiometry, cf. δ^1H = 4.21 ppm in $CDCl_3$). The ^{19}F NMR spectrum is almost identical with spectra of the parent alcohol **2** (Fig. 85). Only the signal of the fluorine atoms in meta position of the C_6F_5 unit is shifted by 0.9 ppm with respect to **2**. The ^{19}F spectrum shows no signs of decomposition or by-products.

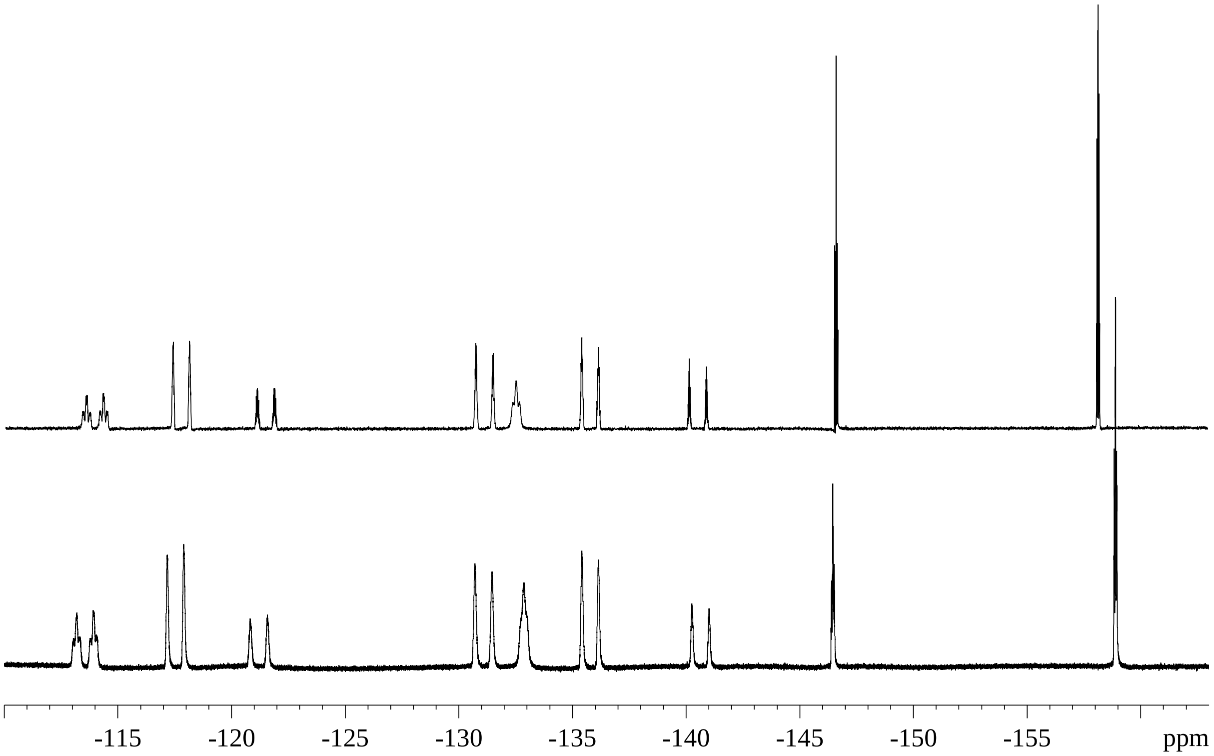

Fig. 85: ^{19}F NMR spectra of **2** (upper spectrum, RT) and **15** (lower spectrum, 5°C), recorded in toluene-D8.

No second signal set is detected, which might arise from the coordination of aluminum by two aromatic fluorine atoms of two phex ligands, as predicted in the calculated geometry (Fig. 82, Al-F1 206.9, Al-F2 207.5 pm). Thus, in solution at 5°C and above, the ligands are freely rotating on the NMR timescale and the Lewis acidic aluminum atom is accessible. Additionally, no signals of residual fluorobenzene are found (^{1}H and ^{19}F). It can be deduced that no stable adduct with monofluorobenzene is formed, as in PhF→Al(pftb)$_3$, in accordance with the observation that solutions of **15** in monofluorobenzene decompose above 10°C. Thus internal coordination of aluminum seems to be preferred.

Tab. 16: Experimental ^{19}F chemical shifts of Al(phex)$_3$ **15** and the parent alcohol **2**.

	15 (exp.) [ppm][a]	**2 (exp.) [ppm][a]**	**assignment[b]**
δ^{19}F	-113.5	-113.6	1a
	-117.5	-117.6	2a
	-121.2	-121.3	3a
	-131.0	-131.1	1e
	-132.8	-132.8	b
	-135.7	-135.8	2e
	-140.6	-140.6	3e
	-146.4	-146.6	d
	-158.9	-158.0	c

[a] Recorded in toluene-D8; [b] see Fig. 29 in section 3.1.3.

Crystal structure determination

15 crystallizes in the form of colorless platelets (stable at room temperature) from concentrated monofluorobenzene solutions in the monoclinic space group P2$_1$/n, with the cell parameters a = 11.76 Å, b = 21.81 Å, c = 16.24 Å, β = 103.3° and Z = 4. The crystal structure is in good agreement with the calculated geometry (Fig. 86), although the Al-F bond distances of the penta-coordinated central aluminum atom are slightly longer than predicted (208.5(1) and 211.3(1) pm vs. 206.9 and 207.5 pm in the BP86/SV(P) geometry). The Lewis acid is not coordinated by monofluorobenzene.

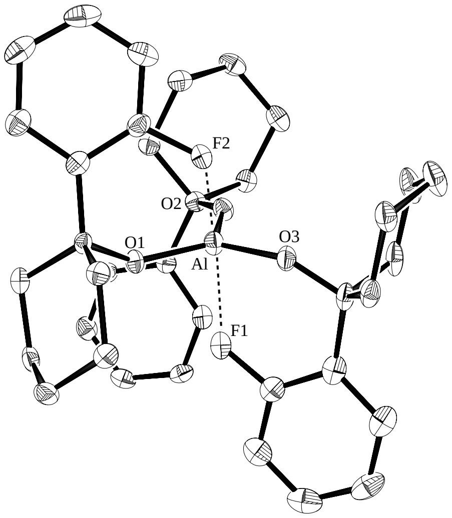

Fig. 86: Crystal structure of **15**. Thermal ellipsoids are drawn at 50% probability level. Fluorine atoms not involved in coordination are omitted for clarity. Distances in pm: Al-F1 208.5(1), Al-F2 211.3(1), Al-O1 169.0(1), Al-O2 169.5(1), Al-O3 170.5(1) pm. Angles in °: F1-Al-F2 154.4(1), O1-Al-O2 114.9(1), O1-Al-O3 126.4(1), O2-Al-O3 118.6(1).

Aluminum is coordinated in a distorted trigonal bipyramid by two fluorine and three oxygen atoms (F1-Al-F2 154.4(1)°). In agreement with calculations, the fluorine atoms are not part of the aliphatic, but of the aromatic part of the ligand with more stable C-F bonds (C-F bonds of the coordinated fluorine atoms elongated by 5 pm av., compared to the other aromatic C-F bonds). All three oxygen atoms and the aluminum atom occupy the same plane (the sum of O-Al-O angles is exactly 360(1)°). There are no significant intermolecular contacts (the strongest is a weak repulsive F-F interaction at 271.3(1) pm, cf. double van-der-Waals radius of fluorine: 294 pm).

Tab. 17: Comparison of selected bond parameters of the crystal structure of **15**, structural data from $C_6H_5F \rightarrow Al(pftb)_3$[266] and the calculated geometry (BP86/SV(P), C_1 symmetry, input geometry based on crystal data).

	15 exp.	**15 calc.**	**$C_6H_5F \rightarrow Al(pftb)_3$**
Al-O [pm]	Al-O1 169.0(1)	Al-O1 172.8	170.6(2)
	Al-O2 169.5(1)	Al-O2 173.4	169.3(2)
	Al-O3 170.5(1)	Al-O3 173.7	168.5(2)
Al-F [pm]	Al-F1 208.5(1)	Al-F1 206.9	186.4(2)[a]
	Al-F2 211.3(1)	Al-F2 207.5	
Σ(Al-O bond valences)	2.440		2.453
Σ(Al-F bond valences)	0.447		0.422
Σ(all Al bond valences)	2.887		2.875
Σ(O-Al-O) [°]	360.0	359.9	350.4
Al-O-C [°]	Al-O1-C 146.5(1)	Al-O1-C 147.1	[b]
	Al-O2-C 144.5(1)	Al-O2-C 147.2	
	Al-O3-C 143.1(1)	Al-O3-C 144.1	
O-Al-F [°]	O1-Al-F1 81.4(1)	O1-Al-F1 83.0	95.3(1)[a]
	O2-Al-F1 84.5(1)	O2-Al-F1 86.4	103.0(1)[a]
	O3-Al-F1 104.2(1)	O3-Al-F1 98.6	102.8(1)[a]
	O1-Al-F2 87.5(1)	O1-Al-F2 87.4	
	O1-Al-F2 83.6(1)	O1-Al-F2 83.2	
	O1-Al-F2 101.4(1)	O1-Al-F2 102.7	

[a] Fluorine contact with the coordinated fluorobenzene molecule; [b] not deposited.

Tab. 17 shows a comparison of structural parameters of **15** with $PhF \rightarrow Al(pftb)_3$. The sum of bond valences of Al-O and Al-F bonds is comparable in both compounds. However, in the $Al(pftb)_3$ adduct the contribution from Al-F coordination arises only from the coordinated fluorobenzene molecule, whereas in **15** two significantly weaker intramolecular Al-F contacts contribute. Because these contacts fluctuate in solution (see NMR results above), a high reactivity can be expected. Consequently, while the Al(pftb)$_3$ adduct is only in fluorobenzene stable at temperatures above -10°C, solid **15** can additionally serve as a stable storage compound and is compatible with other solvents (toluene, CH_2Cl_2, 1,2-difluorobenzene) at temperatures up to 5°C.

3.4. Conclusions to chapter 3

Two new alcohols, $C_6F_5(CF_3)_2COH$ (hfpp-H) **1** and $C_6F_5(C_6F_{10})OH$ (phex-H) **2** could be synthesized and fully characterized. Both compounds are good starting materials for the syntheses of new WCAs and **2** is additionally available in near-quantitative yields in 100 g scale. **1** and **2** exhibit short H-F contacts, in the range of typical asymmetric hydrogen bridges (Tab. 18).

Tab. 18: Comparison of hydrogen-fluorine bridges.

	1 calc./GED	**2 calc./X-ray**	**$(HF)_6$[208]**	**$(H_2O)_n$[208]**
H-F [pm]	$H\text{-}F_{CF3}$ 246/235	$H\text{-}F_{C6F10}$ 234/ 232		
	$H\text{-}F_{C6F5}$ 184/198	$H\text{-}F_{C6F5}$ 203/220		
O-F / F-F / O-O [pm]	$O\text{-}F_{CF3}$ 271/270	$O\text{-}F_{C6F10}$ 269/273	F-F 253	O-O 275
	$O\text{-}F_{C6F5}$ 260/264	$O\text{-}F_{C6F5}$ 250/250		

A variety of new perfluorinated metal alkoxides was presented, all of which are available in simple, quantitative reactions. The sodium salt $NaO(C_6F_{10})C_6F_5$ **6** can even be prepared in aqueous NaOH and extracted with boiling toluene, without the need for inert conditions. One modification of the alkoxide (**6b**) exhibits strong hydrogen bonding to a molecule of the parent alcohol **2**, with an O--O distance of 244 pm and an OH--O distance of 134 pm. For comparison, an O--O distance of 229 pm is found in $H_3O_2^-$ (which is formally a H-bridged adduct of OH^- to water).[208] In HF_2^- the F--F distances are 226 pm.[208] It can be concluded that the strong hydrogen bonding in **6b**, approaching the strongest hydrogen bridges, is the direct result of the high electron withdrawing effect of the phex ligand (see discussion in section 3.1.1). Lithium alkoxides $LiO(C_6F_{10})C_6F_5$ exhibit very short Li-F contacts, both in the trimeric, donor-free form **5a** and the dimeric, fluorobenzene-stabilized form **5b**. These contacts approach the shortest reported intramolecular Li-F interactions (Tab. 19). In **5b**, Li^+ is additionally coordinated by a fluorobenzene molecule, i.e. the cation is very Lewis acidic in this compound. Only one other compound with this motif has been reported so far (Li-F 186.6 pm).[242]

Tab. 19: Shortest Li-F contacts in **5** and **7**, compared to the shortest Li-F contact reported in the literature.

5a	**5b**	**7**	**$Li[Al(OC(C_6H_5)(CF_3)_2)_4]$[55]**
209.6 pm	201.4 pm[a]	192.1 pm	198.4 pm
211.2 pm	208.1 pm	264.0 pm	208.2 pm

[a] Intermolecular contact with fluorobenzene.

An even shorter Li-F contact exists in the WCA salt Li[Al(OC(CF_3)$_2$(C_6F_5))$_4$] (Li[Al(hfpp)$_4$]) **7**. Apart from [Al(hfpp)$_4$]$^-$, the new WCA [FAl(phex)$_4$]$^-$ could be synthesized in the form of its lithium and silver salts (**10** and **12**) and was fully characterized. Two of the core concepts of chemistry with WCAs are the reduction of coulombic interactions by an increase in anion size and the replacement of few strong cation-anion interactions with many weak ones, such as fluorine contacts (see chapter 1). Both new alkoxyaluminates contain more fluorine atoms ([Al(hfpp)$_4$]$^-$: 44 F, [FAl(phex)$_4$]$^-$: 46 F) than [Al(OC(CF_3)$_3$)$_4$]$^-$, which is one of the least coordinating anions.[53] Volumes of ions can be estimated from structural data by simple considerations: The thermochemical volume of [Ag(1,2-$C_2H_4Cl_2$)$_3$]$^+$ is approximately 318 Å^3, as can be calculated from the crystal structure of [Ag(1,2-$C_2H_4Cl_2$)$_3$][Al(pftb)$_4$] (V = 4302 Å^3, Z = 4)[53] and the thermochemical volume of the [Al(pftb)$_4$]$^-$ anion (758 Å^3).[52] With this value, the thermochemical volume of the new [Al(hfpp)$_4$]$^-$ anion can be estimated from the crystal structure of **8a** as 1176 Å^3 (V = 23900 Å^3, Z = 16, the real value must be smaller due to an additional ½ 1,2-$C_2H_4Cl_2$ molecule in the asymmetric unit). A slightly underestimated volume of 1076 Å^3 is obtained when subtracting the volume of the Li$^+$ cation (1.99 Å^3)[122] from the volume of the asymmetric unit of the lithium salt **7** (V = 2156 Å^3, Z = 2), because Li is coordinated in **7**. From the crystal structures of [Ag(C_6H_5F)$_3$][FAl(pftb)$_3$] (V = 1923 Å^3, Z = 4),[275] CPh$_3$[FAl(pftb)$_3$] (V = 3703 Å^3, Z = 4)[190] and [Ag(C_6H_5F)$_3$][FAl(phex)$_3$] **12b**, the volume of the new [FAl(phex)$_3$]$^-$ anion can also be extrapolated: Subtraction of the thermochemical volume of the BF_4^- anion (73 Å^3)[122] from the crystallographic molecular volume of trityl tetrafluoroborate (V = 1680 Å^3, Z = 4)[276] gives an estimate for the thermochemical volume of the trityl cation (346 ± 9 Å^3). This allows an estimate of the size of [FAl(pftb)$_3$] (609 Å^3) and finally the [Ag(C_6H_5F)$_3$]$^+$ cation (353 ± 9 Å^3). By subtraction of this value from the volume of [Ag(C_6H_5F)$_3$][FAl(phex)$_3$] **12b** (V = 5863 Å^3, Z = 4), the volume of [FAl(phex)$_3$]$^-$ can be evaluated as 1113 Å^3.

The attempt to replace the central aluminum atom by gallium, to obtain homoleptic anions with four phex ligands, failed and only two ligands could be introduced. Due to various problems, including the stability of Ga-X (X = Br, Cl) bonds, low solubilities and the bulkiness of the ligand, a better strategy would probably be the introduction of a fourth, smaller ligand at the aluminum core, instead of changing the central atom. This would allow the use of already available, well-documented starting materials and established synthetic procedures. However, [FAl(phex)$_4$]$^-$, while formally containing a basic fluorine atom, was shown to be weakly coordinating. There are two modifications of this WCA with different coordinative strengths, depending on the orientation of the C_6F_5 groups. If the C_6F_5 groups point in the direction of the Al-F bond, the anion is clearly non-coordinating (due to steric shielding of the basic site), as seen in the crystal structure of its silver salt **12b**.

The new Lewis acid $Al(O(C_6F_{10})C_6F_5)_3$ **15** could be synthesized in a rational synthesis and was fully characterized. 10 g of the compound can be obtained in 2 days (quantitative yield) and the substance is stable at room temperature in the solid state. According to calculations, $Al(O(C_6F_{10})C_6F_5)_3$ is among the strongest Lewis acids with a FIA of 530 kJ mol^{-1}, which is only slightly smaller than the FIA of $Al(OC(CF_3))_3)_3$ (which is only stable at room temperature in the form of its fluorobenzene adduct).

4. Applications of WCAs and Lewis acids

“There is no use trying,” said Alice; “one can´t believe impossible things.”
“I dare say you haven´t had much practice,” said the Queen. “When I was your age, I always did it for half an hour a day. Why, sometimes I´ve believed as many as six impossible things before breakfast.”

4.1. Highly electrophilic carbocations

4.1.1. Introduction

Carbocations are discussed as intermediates in plasma etching processes and organic reactions, e.g. Friedel-Crafts acylations.[277-279] Weakly coordinating anions have traditionally been used to stabilize these highly reactive electrophiles. A few carbocations, such as the trityl (triphenylcarbenium) ion, stabilized by the strong +M effect of three phenyl ligands, are sufficiently stable to form isolable salts with “classic” (but still basic) WCAs, such as $[BF_4]^-$, $[PF_6]^-$ or $[SbF_6]^-$.[280] More reactive cations can normally only be observed in the gas phase by mass spectrometry[281-283] or in superacidic media at low temperatures.[277] Prominent examples include the trihalomethyl cations CX_3^+ (X = Cl-I),[7] which have been characterized at -80°C in SbF_5/SO_2ClF by ^{13}C NMR spectroscopy (Eq. 32).[284-288]

$$CX_4 + \text{excess } SbF_5 \xrightarrow[\text{- 78 °C}]{SO_2ClF} CX_3^+[Sb_nF_{5n+1}]^- + ...$$

(Eq. 32)

In recent years, solid state structures of several salts of CX_3^+(X = Cl, Br,[90] I[4, 20]) and related cations, such as CFX_2^+ (X = Cl, Br,[90, 189] p-FC_6H_4[289]), Me_2CF^+,[16] $C(OH)_3^+$[290] and $(H_3CO)C(H)X^+$ (X = F, Cl),[291] were published. All of these cations were stabilized by robust weakly coordinating anions with low basicities. CF_3^+ remains unknown in the condensed phase, but has been observed in electron impact studies in the gas phase.[281] This can be explained by a delocalization of the formal positive charge from carbon to the ligand (Eq. 37), which is disfavored in CF_3^+ due to the high electronegativity of the fluorine atoms.

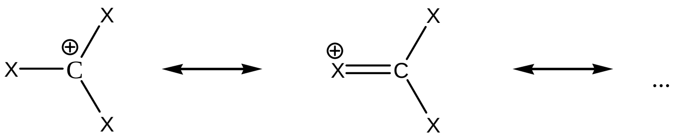

(Eq. 33)

In the closely related FCO^+ cation (isoelectronic with XCN,[292] N_2F^+ and CO_2), two fluorine atoms are replaced by one oxygen atom, which should be a slightly better p(π) back-donor. FCO^+ has been characterized in the gas phase (electron affinity,[293] rotational spectra,[294] photoelectron spectra).[295] Other cationic species of the general type XCO^+ (X = Cl-I) could be characterized by NMR spectroscopy in solution.[23, 24] $ClCO^+$ was additionally characterized by IR spectroscopy and was found to be the only XCO^+ cation which is stable at room temperature for a short time when paired with a $[Sb_nF_{5n+1}]^-$ anion (n ≈ 3).[296] (Eq. 34) shows the hitherto reported synthetic routes to halocarbonyl cations.

$$Cl_2CO + \text{excess } SbF_5 \xrightarrow[\text{- 78 °C}]{SO_2ClF} ClCO^+[Sb_nF_{5n+1}]^- + ...$$

$$Cl_2C_2O_2 + \text{excess } SbF_5 \xrightarrow[\substack{\text{- 78 °C} \\ \text{- CO}}]{SO_2ClF} ClCO^+[Sb_nF_{5n+1}]^- + ...$$

$$X_2 + \text{excess } SbF_5 \xrightarrow[\text{- 78 °C}]{\substack{SO_2ClF \\ + CO}} XCO^+[Sb_nF_{5n+1}]^- + ...$$

(X = Cl, Br, I)

(Eq. 34)

No experimental data has been reported about the homologous cations ECX^+ (E = S, Se, Te, X = F-I), however the chlorothioformyl radical ClCS was characterized in noble gas matrix and gas phase experiments.[26-29] As already described in section 3.2.8, the FIA is often used as a measure for the stability of Lewis acids or electrophiles. Tab. 20 shows a comparison of various calculated FIAs of XCO^+, XCS^+ and CX_3^+ (X = F-I) cations.

Tab. 20: Fluoride ion affinities (FIAs) of halocarbonyl and halothiocarbonyl cations in comparison with CX_3^+ (X = halogen; calculated at the MP2/TZVPP level at 0 K in the gas phase). Species printed in italics have not yet been observed in the condensed phase.

X	XCO^+ [kJ mol^{-1}]	XCS^+ [kJ mol^{-1}]	CX_3^+ [kJ mol^{-1}][15]
F	*1053*	*921*	*1099*
Cl	923[25-27]	*826*	904[90, 189]
Br	896[23, 24]	*810*	871[90, 189]
I	849[23, 24]	*778*	813[4]

According to the prediction, the halothiocarbonyl cations should be significantly more stable than e.g. CCl_3^+, which has already been characterized by crystal structure determination. The current benchmark is set by $ClCO^+$ with a FIA of 923 kJ mol^{-1}. It should be possible to stabilize all other cations shown in Tab. 20, except for CF_3^+ and FCO^+, at least for a short time, by pairing them with a suitable WCA.

4.1.2. Synthesis and characterization of ICS[Al(OC(CF_3)$_3$)$_4$]

Synthesis and mechanism

In attempts to crystallize CI_3^+[Al(OC(CF_3)$_3$)$_4$] (obtained by reactions of CI_4 with Ag[Al(pftb)$_4$], pftb = OC(CF_3)$_3$)[15] from carbon disulfide, formation of elemental iodine was observed. Additionally, orange block-shaped crystals of ICS[Al(pftb)$_4$] **16** were found and could be fully characterized (see below and section 6.5.1). **16** is stable at room temperature, which is in agreement with Tab. 20 (according to the FIA, **16** should be stabilized by 35 kJ mol^{-1} with respect to CI_3^+[Al(pftb)$_4$], which is also stable at RT).

The exact mechanism of the reaction is unknown. However, according to a recent publication, which describes the photolytic reactions of CS_2 with Cl_2, Br_2 and BrCl in an argon matrix at 15 K,[297] the authors found and characterized a wide range of intermediates by IR spectroscopy. Among these species were thiophosgene Cl_2CS, the carbene CCl_2 and elemental sulfur. It is also known that CI_4 decomposes to CI_2 and I_2 in the presence of light, respectively I_2CO, CO and CO_2 in the presence of oxygen and light.[298] Accordingly, a catalytic mechanism can be postulated, in which CS_2 and iodine are constantly regenerated, in agreement with the observed formation of iodine during the reaction (Fig. 87).

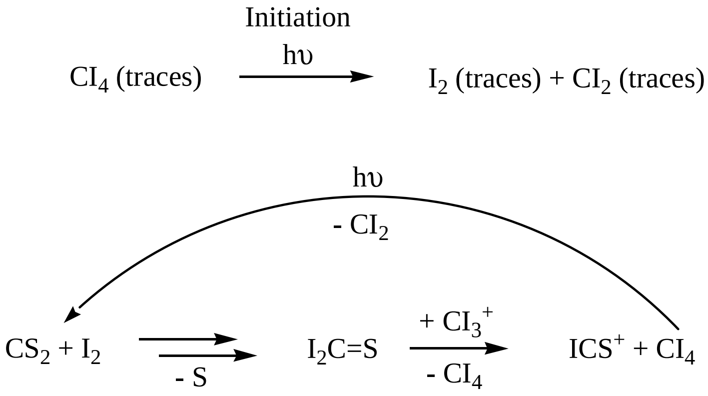

Fig. 87: Possible mechanism for the formation of ICS^+ from CI_3^+ and CS_2, initiated by the well-known decomposition of CI_4. A reaction enthalpy for the formation of I_2CS was not calculated, because the intermediate reaction steps are unknown. The reaction enthalpy for iodide abstraction by CI_3^+ was calculated as -29 kJ mol^{-1} (MP2/TZVPP, gas phase, 0 K).

It must be noted that CI_3^+ is not needed as a reagent in this reaction pathway, another electrophile could be used for iodine abstraction. The mechanism remains to be verified by reacting CS_2 with iodine and adding Ag[Al(pftb)$_4$] as a metathesis agent. Reactions of CI_3[Al(pftb)$_4$] with S_8 were also attempted, but always led only to the formation of CS_2 (observed $\delta^{13}C = 193.5$ ppm).

Another possible mechanism is shown in Fig. 88. The intermediate $C_2S_2I_3^+$ can be understood as a cationic adduct of ICS^+ with I_2CS. The observed formation of iodine would result from decomposition of I_2CS in this case.

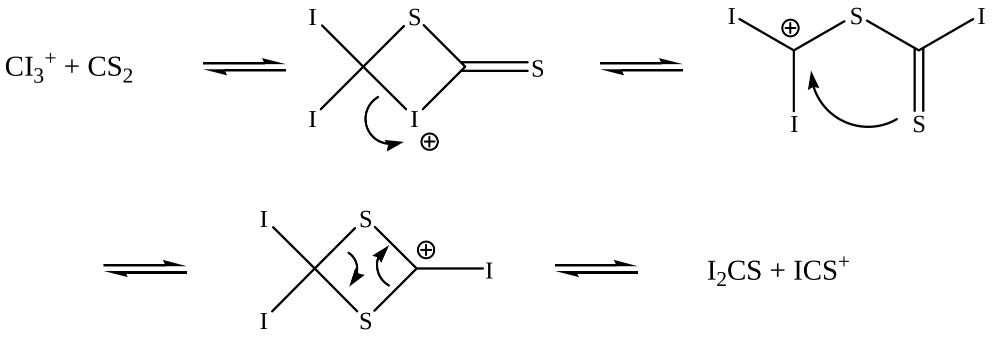

Fig. 88: Possible mechanism for the formation of ICS^+ from intermediate adducts of CI_3^+ and CS_2.

By analogy (see section 4.1.3), it was shown that $ClCS^+$ forms dimeric $Cl_3C_2S_2^+$ cations with thiophosgene during attempts to synthesize the homologous salt ClCS[Al(pftb)$_4$].

IR spectroscopy

Apart from bands of the anion, infrared spectra of **16** (see section 6.7, Tab. 50) exhibit bands at 1465, 1174, 1017, 859 and 805 cm^{-1} (Fig. 89). The first clearly corresponds to the C=S stretching mode of ICS^{+}, which has been calculated at 1468 cm^{-1} (MP2/TZVPP, cf. the isoelectronic CS_2: 1533 cm^{-1}[121] and SCTe: 1347 cm^{-1}).[299] The other bands are not detected in spectra of $[NEt_4][Al(pftb)_4]$, in which the anion is almost undistorted.[251, 300] However, similar bands are observed in spectra of $Li[Al(pftb)_4]$, in which the cation coordinates the anion, which leads to a splitting of Al-O bands (cf. bands observed in $Li[Al(pftb)_4]$, but not in $[NEt_4][Al(pftb)_4]$: 1184, 1017, 863, 863 and 798 cm^{-1}).[300] Thus, ICS^{+} is coordinated by the anion in **16** (see also crystal structure below).

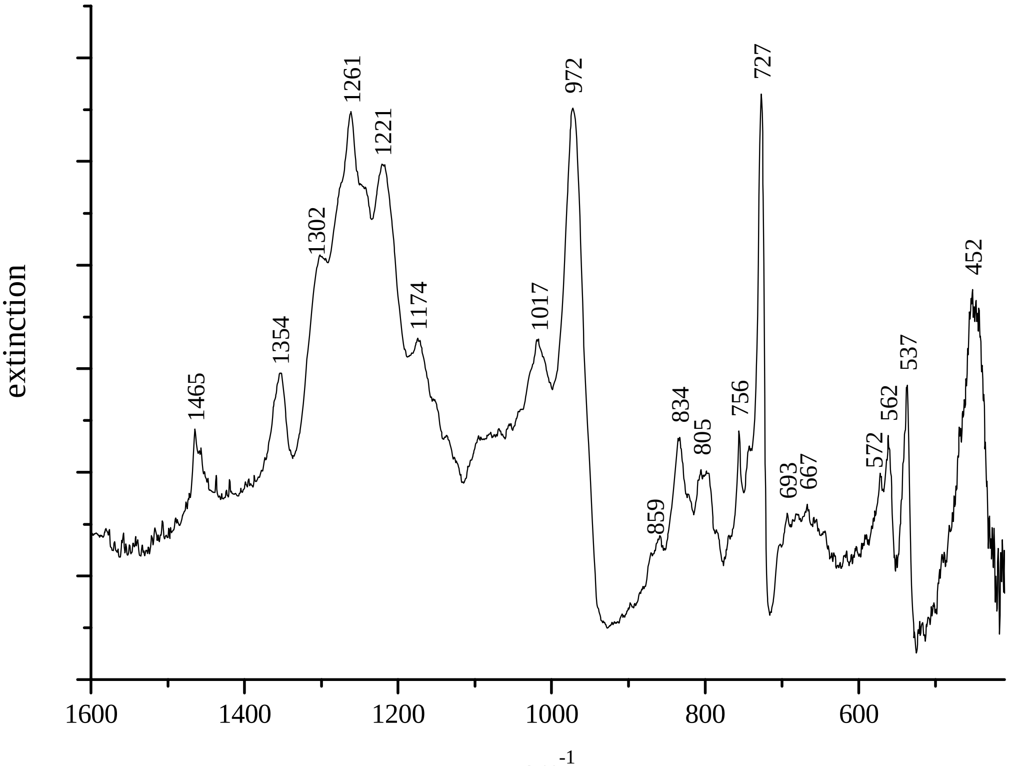

Fig. 89: IR spectrum of **16**, the band at 1465 cm^{-1} is assigned to ICS^{+}.

NMR spectroscopy

^{13}C NMR spectra show partial decomposition of the anion (two signals for the CF_3 groups at 121.3 and 120.8 ppm). The minor signal at 120.8 ppm is assigned to the $[(pftb)_3AlFAl(pftb)_3]^-$ anion.[64] ^{27}Al NMR spectra exhibit only one signal at 36.0 ppm.

The signal of ICS^{+} appears in ^{13}C NMR spectra of isolated crystals at 149.7 ppm. For comparison, the chemical shift of ClCS^{+} can be calculated without relativistic corrections as

199.4 ppm (MP2/6-311+G(2df)) and is in good agreement with experimental data (191.2 ppm, see 4.1.3). The signal of the ICS^+ cation is shifted towards high field with respect to $ClCS^+$ by 41-46 ppm, which is within the expected range of a shift induced by introduction of the heavier halogen[38, 39] (cf. $\delta^{13}C$ of CH_3Cl: 24.9 ppm, CH_3I: -20.8 ppm, $\Delta\delta^{13}C$: 45.7 ppm).[301] Additionally, the chemical shift can be compared with the couple CO_2/ICO^+[193] ($\delta^{13}C$ of CO_2: 123 ppm, ICO^+: 100 ppm, $\Delta\delta^{13}C$: 23 ppm): CS_2 exhibits a chemical shift of 193 ppm and thus the signal of ICS^+ would be expected in the range between 160 and 170 ppm (neglecting any influence of sulfur).

^{13}C NMR spectra (in CD_2Cl_2) of powder taken directly from the reaction vessel show two additional signals at 185.9 ppm and 46.1 ppm. The signal at 185.9 ppm could stem from $CS_2I_3^+$ (Eq. 35, Fig. 90, cf. $\delta^{13}C$ of $CS_2Br_3^+$: 209.7 ppm,[302] $\Delta\delta^{13}C$ ($CS_2Br_3^+$ vs. $CS_2I_3^+$): 23.8 ppm, CH_3Br: 9.8 ppm, CH_3I: -20.8 ppm, $\Delta\delta^{13}C$ (CH_3Br vs. CH_3I): 30.6 ppm).[301]

$$CI_3^+ + 2\,I_2 + CS_2 \longrightarrow CS_2I_3^+ + CI_4$$

(Eq. 35)

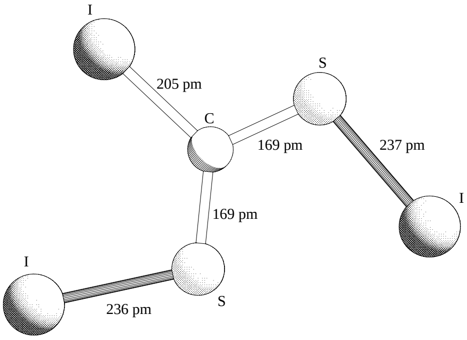

Fig. 90: Calculated structure of the $CS_2I_3^+$ ion (C_s symmetry, MP2/TZVPP level).

Another possible explanation for both peaks could be the formation of $C_2S_2I_3^+$ (see Fig. 88). As discussed above, the difference in chemical shift between CH_3Cl and CH_3I is 45.7 ppm. $Cl_3C_2S_2^+$ is observed at 232.5 (C-Cl) and 79.8 ppm (C-Cl_2) (see 4.1.3). The shift of the mono-iodo substituted carbon atom in $I_3C_2S_2^+$ is observed at almost exactly the expected position (232.5 ppm - 45.7 ppm = 186.8 ppm) at 185.9 ppm. However, $\Delta\delta^{13}C$ should be larger for the di-iodo substituted carbon atom (observed at 46.1 ppm, cf. $\delta^{13}C$ of CH_2Cl_2: 54.0 ppm, CH_2I_2: -54 ppm, $\Delta\delta^{13}C$: 108 ppm), and its signal should be shifted to a negative ppm range. Intermolecular exchange between $I_3C_2S_2^+$ cations could possibly negate this effect.

In summary, the second species in NMR spectra of **16** can not be clearly identified, but $I_3C_2S_2^+$ or $CS_2I_3^+$ (paired with another species) are possible candidates.

Crystal structure determination

16 crystallizes in the form of orange, block-shaped crystals from mixtures of CH_2Cl_2 and CS_2. The structure was solved in the cubic space group $P2_13$ with a = 14.72 Å and Z = 4 (see section 6.12, Tab. 84). ICS[Al(pftb)$_4$] is best described as an ionic compound with separated ICS^+ cations and $[Al(pftb)_4]^-$ anions (Fig. 91).

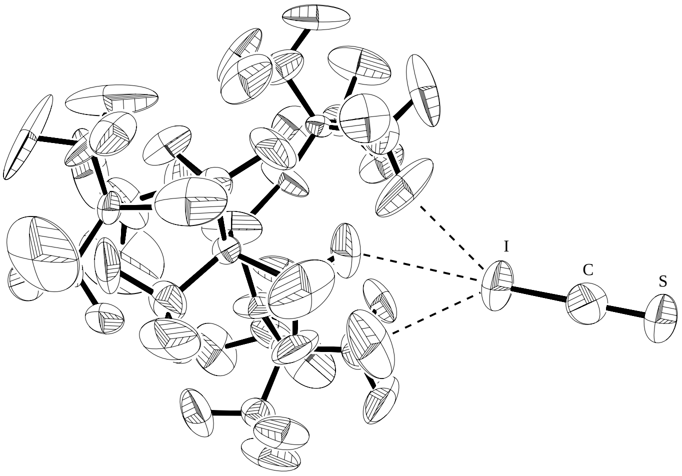

Fig. 91: Crystal structure of **16**, the part of the disorder which contributes less to the model was omitted for clarity. Thermal ellipsoids drawn at 50 % probability level. The carbon atom in the ICS^+ cation was refined isotropically due to positional disorder of the sulfur and iodine atoms. Distances (rounded to full pm): C-I 185, C-S 149, I-S 335. Contacts with fluorine (F-I 329 pm) are indicated by a dotted line. R_1: 6.3 %, wR_2: 16.4 %.

The ICS^+ cation is linear (I-C-S 180.0(1)°) and contains an orientational disorder (position exchange of the I and S atoms, ratio approximately 4:1), thus the C-I and C-S bond lengths can not be discussed. However, the I-S distance of 334.6 pm is only slightly shorter than in the calculated geometry (344.9 pm, MP2/TZVPP in C_{6v} symmetry). There are three weak contacts (329 pm) between the cation and CF_3 groups of the anion. These are probably I-F contacts (cf. sum of van-der Waals radii of iodine and fluorine: 345 pm, sulfur and fluorine: 327 pm).

While the anion exhibits disorder in all four ligands (two orientations with a ratio of approximately 6:1), all key structural parameters of $[Al(pftb)_4]^-$ in **16** are within the expected ranges known from other crystal structures (Tab. 21) and the anion can be considered almost undistorted.

Tab. 21: Comparison of structural parameters of the $[Al(pftb)_4]^-$ anion in **16** and $[Ag(1,2\text{-}C_2H_4Cl_2)_3][Al(pftb)_4]$.[41]

	16	**$[Ag(1,2\text{-}C_2H_4Cl_2)_3][Al(pftb)_4]$**
Al-O [pm]	168.6(1)-170.7(1)	171.4-173.6
av.	169.7	172.5
C-O [pm]	134.2(1)-134.3(1)	133.1-135.5
av.	134.3	134.3
Al-O-C [°]	151.5(1)-158.4(1)	148.1-151.7
av.	155.0	149.5

4.1.3. Synthesis and characterization of $Cl_3C_2S_2[Al(OC(CF_3)_3)_4]$

As described in section 4.1.2, I_2CS is probably an intermediate in the formation of ICS^+ cations. According to a comparison of the FIAs (Tab. 20), again using the assumption that cations with a lower FIA than CCl_3^+ (904 kJ mol^{-1}) can be stabilized in the condensed phase, it should be possible to obtain salts of other XCS^+ (X = Cl-I) cations by halide abstraction from X_2CS with Ag^+. Tab. 22 shows the calculated reaction enthalpies for the formation of these cations.

Tab. 22: ΔH (at 0 K) and ΔG^o (at 298 K) in kJ mol^{-1} of the reaction $X_2CS + Ag^+ \rightarrow XCS^+ + AgX$. The values are corrected for the sublimation enthalpy of AgX (AgF = 227.0, AgCl = 231.5, AgBr = 214.8, AgI = 196.9 kJ mol^{-1}).[131] Values which would be positive without this contribution are printed in italics. Contributions of solvation enthalpy to ΔG^o were calculated with the COSMO model (CH_2Cl_2, $\varepsilon = 8.9$).

	X =	**ΔH BP86/SV(P)**	**ΔG^o (CH_2Cl_2) BP86/SV(P)**	**ΔH MP2/TZVPP**	**ΔG^o (CH_2Cl_2) MP2/TZVPP**
$X_2CS + Ag^+ \rightarrow XCS^+ + AgX$	F	-52	*-88*	-2	*-38*
	Cl	-269	-281	-218	*-230*
	Br	-293	-294	-240	-241
	I	-325	-314	-257	-246

FCO^+ (FIA: 1053 kJ mol^{-1}) can only be observed in the gas phase (see discussion in 4.1.1). Although the Gibbs free energy of its formation is negative, the FCS^+ is simply too Lewis-acidic to be stabilized in the condensed phase (FIA: 1099 kJ mol^{-1}). $BrCS^+$ and $ClCS^+$ should be stable in salts with alkoxyaluminate WCAs, as their FIAs are comparable with the FIA of CI_3^+ ($BrCS^+$: 810 kJ mol^{-1}, $ClCS^+$: 826 kJ mol^{-1}, CI_3^+: 813 kJ mol^{-1}) and $CI_3[Al(pftb)_4]$ is stable at room temperature.

Synthesis

While syntheses of other X_2CE (E = S, O) analogs have been reported,[303] thiophosgene Cl_2CS is the only commercially available, stable compound in this series. Accordingly, $ClCS^+$ was chosen as a target cation. However, instead of ClCS[Al(pftb)$_4$], $Cl_3C_2S_2$[Al(pftb)$_4$] **17** is formed in 1:1 reactions of Ag[Al(pftb)$_4$][53] (in CH_2Cl_2) with freshly distilled thiophosgene (kept in the dark to prevent light-induced dimerisation).[304, 305] Precipitation of AgCl is instantly observed. The primary product **17** is obtained as an orange powder, which is stable at room temperature.

Crystal structure determination

17 crystallizes from highly concentrated CH_2Cl_2 solutions at -30°C in the form of yellow platelets. The space group was determined as orthorhombic $P2_12_12_1$ with a = 12.09 Å, b = 16.42 Å, c = 19.31 Å and Z = 4. However, the structure could not be refined to reasonable R values (best R_1: 13.2 %, see section 6.12, Tab. 84) due to unresolved crystallographic problems (possibly pseudo-merohedral twinning). The anion shows unusually large anisotropic displacement parameters (which could not be treated satisfactorily by modelling disorder of the CF_3 groups) and thus the structure must be considered fragmentary. However, all displacement parameters, bond lengths and angles of the cation are reasonable. Variation of the crystal growth conditions (temperature and concentration) and repetition of the measurements (4 independent data sets) did not lead to a better solution, but the model could always be reproduced with approximately the same R values.

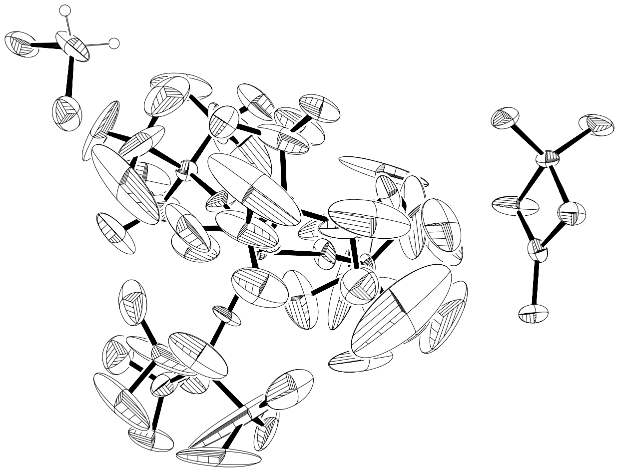

Fig. 92: Crystal structure of **17**. Thermal ellipsoids drawn at the 50 % probability level.

The crystal structure can be described as ionic, with separated $Cl_3C_2S_2^+$ cations (Fig. 93) and $[Al(pftb)_4]^-$ anions, as well as one CH_2Cl_2 molecule in the asymmetric unit. There are three weak Cl-F contacts (302-318 pm, cf. sum of van-der-Waals radii: 322 pm) and one S-F contact (285 pm, cf. sum of van-der-Waals radii: 327 pm) between the cation and anion.

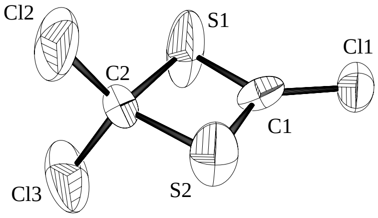

Fig. 93: Detail of the crystal structure of **17**, showing only the $Cl_3C_2S_2^+$ cation. Thermal ellipsoids drawn at the 50 % probability level. C1 has a planar environment (sum of S-C-Cl1 and S1-C-S2 angles 360.0(1)°).

One crystal structure of an isostructural salt, $[F_3C_2S_2][AsF_6]$,[306] has been reported, in which the cation is C_{2v} symmetric. The compound was synthesized by halide abstraction from $(F_2CS)_2$ with AsF_5 in SO_2. NMR spectra of $F_3C_2S_2^+$ and $F_2C_2S_2Cl^+$ have also been recorded.[307] Structural parameters of the cation in **17** are in good agreement with $[F_3C_2S_2][AsF_6]$, the calculated geometry and experimental data of dithiophosgene (Tab. 23).[305] The coordination around C1 in Fig. 93 is planar, as can be expected for a sp^2-hybridized carbon atom. Angular distortions in the C-S-C-S ring with respect to $(Cl_2CS)_2$ are minor and might result from packing effects. The same holds for all S-C-Cl angles involving the tetrahedrally coordinated carbon atom C2. As expected, $Cl_3C_2S_2^+$ exhibits shorter bond lengths than the thiophosgene dimer, especially around the sp^2-hybridized carbon atom. The shortening in the C1-Cl1 bond length is 17 pm with respect to $(Cl_2CS)_2$, (cf. sum of covalent radii of C and Cl: 176 pm). A shortening of C2-Cl bond lengths (by 9 pm) is also observed, but not as pronounced.

Tab. 23: Comparison of experimental and calculated structural parameters of the $Cl_3C_2S_2^+$ cation, experimental data of the $F_3C_2S_2^+$ cation[306] and the thiophosgene dimer.[305]

	17 exp.	**$Cl_3C_2S_2^+$ calc.[a]**	**$Cl_3C_2S_2[AsF_6]$ exp.[b]**	**$(Cl_2CS)_2$ exp.**
C-X [pm]	C1-Cl1 160.9(3)	C1-Cl1 165.8	C1-F1 124.8	
	other C-Cl 168.3(3)	other C-Cl 173.4	other C-F 129.4	all C-Cl 177.4
C-S [pm]	C1-S1 170.0(3)	C1-S 168.7	C1-S 168.1	C1-S1, C2-S2 181.4
	C1-S2 164.5(3)			C1-S2, C2-S1 180.7
	C2-S1 183.3(3)	C2-S 187.4	C2-S 184.8	
	C2-S2 183.3(3)			
av.	175.3	178.1	176.3	181.1
S--S [pm]	261.2(2)	271.2	272.5	268.7
S-C-S [°]	S1-C2-S2 90.8(1)	S1-C2-S2 92.9	95.0	all 95.8
	S1-C1-S2 102.6(1)	S1-C1-S2 107.2	108.3	
C-S-C [°]	C1-S1-C2 82.5(1)	all 80.0	both 78.4	all 84.2
	C1-S2-C2 84.0(1)			
S-C-Cl [°]	S1-C1-Cl1 125.7(2)	S-C-Cl1 126.4		
	S2-C1-Cl1 131.7(2)			
	other S-C-Cl 111.3(2)-113.8(2)	other S-C-Cl 112.1		112.7-113.6

[a] MP2/TZVPP, C_{2v} symmetry; [b] S-C-F angles not deposited.

S--S contact distances in $(Cl_2CS)_2$ as well as in $Cl_3C_2S_2^+$ are almost 100 ppm shorter than twice the van-der-Waals radius of sulfur (360 pm, cf. S--S in S_4N_4: 259.7 pm).[308] However, an analysis with the AIM (*a*toms *i*n *m*olecules) method[309] (MP2/TZVPP) reveals no S--S bond critical point. Although the CF_3 groups of the anion in **17** are disordered and show large anisotropic displacement parameters, the structural parameters of the Al-O-C backbone are in good agreement with reported crystal structures containing $[Al(pftb)_4]^-$ and the anion can be considered almost undistorted.

Tab. 24: Comparison of structural parameters of the $[Al(pftb)_4]^-$ anion in **17** and $[Ag(1,2\text{-}C_2H_4Cl_2)_3][Al(pftb)_4]$.[53]

	17 exp.[a]	**$[Ag(1,2\text{-}C_2H_4Cl_2)_3][Al(pftb)_4]$**
Al-O [pm]	166.6-170.4	171.4-173.6
av.	169.1	172.5
C-O [pm]	132.0-135.1	133.1-135.5
av.	133.7	134.3
Al-O-C [°]	155.4-167.1	148.1-151.7
av.	161.3	149.5

[a] No standard deviations are given due to poor quality of the anionic part of the crystal structure.

IR spectroscopy

The spectrum of **17** was simulated by calculating the modes of $Cl_3C_2S_2^+$ and the $[Al(pftb)_4]^-$ anion separately and subsequently overlaying both simulations (Fig. 106). Real spectra are in good agreement with the simulation. Additionally, no decomposition of the anion can be detected by comparison with other compounds containing $[Al(pftb)_4]^-$ (see section 6.7, Tab. 51). Five bands are predicted for $Cl_3C_2S_2^+$ (BP86/TZVPP, C_{2v} symmetry) at 550, 751, 821, 978 and 1089 cm^{-1}. Of those, two are obscured by the anion (756 and 973 cm^{-1}). One band normally associated with $[Al(pftb)_4]^-$ is split into 561 and 559 cm^{-1} and one of the two peaks might correspond to the calculated band of the cation at 550 cm^{-1}. Two bands of the cation can be clearly identified at 804 and 1111 cm^{-1}, where no signals of the anion are expected. Bands of thiophosgene are not detected.

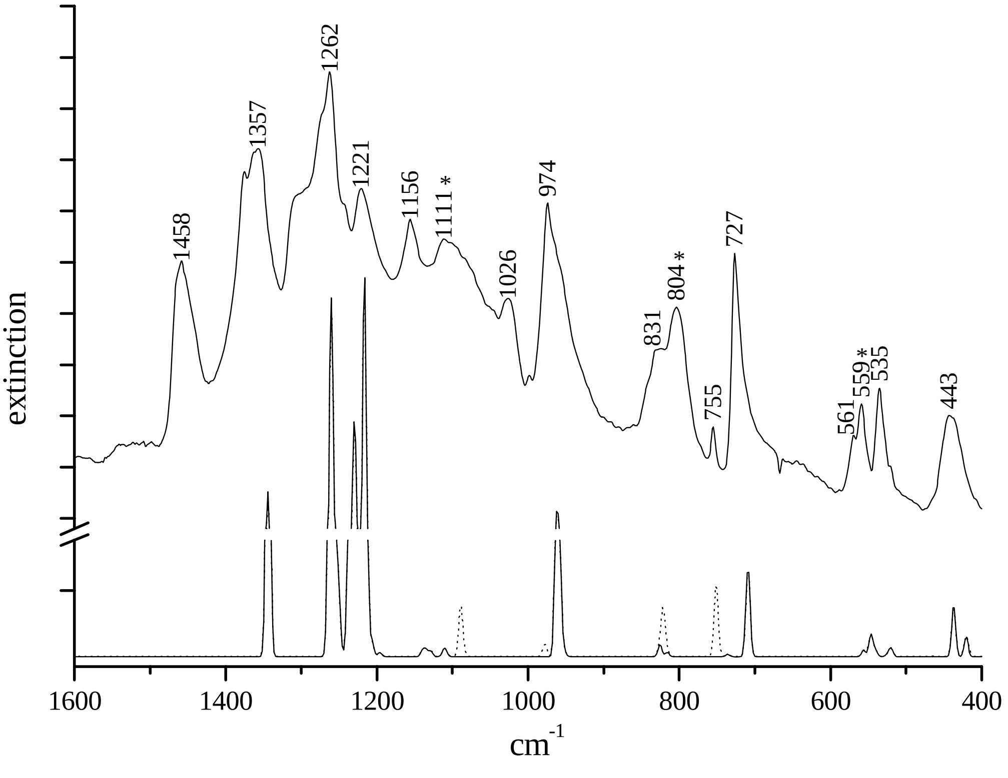

Fig. 94: IR spectrum of solid **17** (upper solid line) and simulated of the spectrum (lower solid line: calculated bands of the $[Al(pftb)_4]^-$ anion, lower dotted line: calculated bands of $Cl_3C_2S_2^+$, BP86/SV(P) level). The bands at 1377 and 1458 cm^{-1} are assigned to nujol oil. Bands of the $Cl_3C_2S_2^+$ cation are marked with an asterisk.

NMR spectroscopy, mechanism and attempts to isolate the $ClCS^+$ cation

Only $Cl_3C_2S_2^+$ (232.5 and 79.5 ppm, cf. $F_2C_2S_2Cl^+$: 241.3 and 107.8 ppm),[307] trace amounts of thiophosgene (171.2 ppm) and the $[Al(pftb)_4]^-$ anion are detected in ^{13}C NMR spectra in CD_2Cl_2. ^{19}F and ^{27}Al spectra show only one signal for the anion. The anion stays intact for weeks at room temperature. It is likely that an equilibrium exists between $Cl_3C_2S_2^+$, $ClCS^+$ and thiophosgene and that the $ClCS^+$ cation can be observed under different reaction conditions. Small cationic species should be stabilized by a more polar environment, thus to obtain proof for the existence of $ClCS^+$, the same reaction was carried out in 1,2-$C_2D_4Cl_2$ (ε = 12, cf. CD_2Cl_2: ε = 8.9) with different stoichiometries (thiophosgene:Ag^+ 1:1 and 1:3). Additionally, to further raise the polarity (see chapter 1) and prevent possible decomposition of the anion by the more electrophilic $ClCS^+$, the reactions were performed at lower temperatures. Fig. 95 shows the resulting ^{13}C NMR spectra.

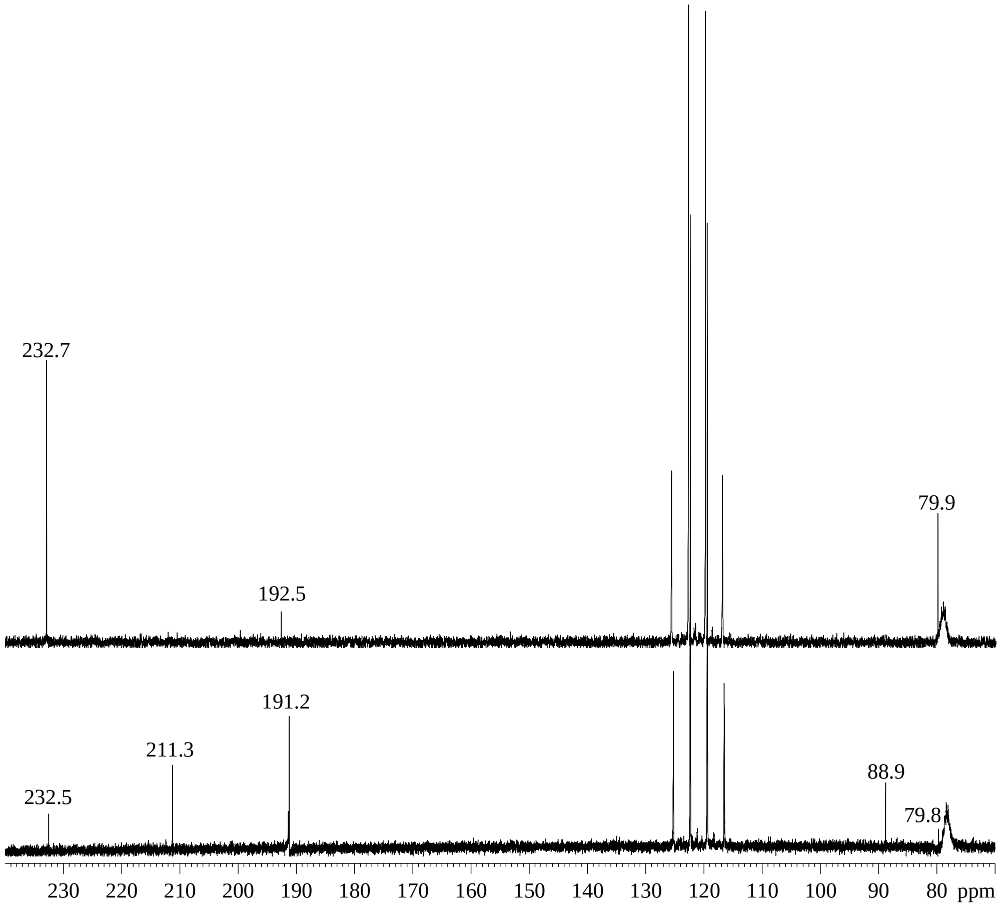

Fig. 95: ^{13}C NMR spectra of 1:1 reaction mixtures of Ag[Al(pftb)$_4$] and thiophosgene in 1,2-$C_2D_4Cl_2$ (upper spectrum recorded at 5°C, lower spectrum recorded at -25°C).

Independent of the stoichiometry, at 5 °C a new signal at 192.5 ppm appears and instantly, some decomposition of the anion is observed (the CF_3 signal splits in the ^{19}F and ^{13}C spectra). While $Cl_3C_2S_2^+$ is still the main cationic species observed, this is a clear indication of the existence of $ClCS^+$ (and not CS_2, cf. $\delta^{13}C$: 192 ppm in $CDCl_3$). The ^{13}C NMR shift of the isoelectronic $ClCO^+$ was reported at 133.7 ppm[193] (cf. CO_2: 123 ppm, $\Delta\delta^{13}C$: 10.7 ppm). Accordingly, a signal of $ClCS^+$ can be expected between 190 and 200 ppm, which is confirmed by MP2 calculations with a flexible basis set (Tab. 25). At lower temperatures, the formation of $ClCS^+$ should be more favored due to the slightly higher polarity of the reaction medium (but this may be counterbalanced by the loss of entropy). The decomposition of the anion should be disfavored due to the activation barrier. Indeed, at -25°C an increase of the signal at 192.5 ppm is detected. At the same time, a third species is formed, with new signals appearing at 211.3 and 88.9 ppm. The neutral species X_2CS are known to form dimers $X_4C_2S_2$ and trimers $X_6C_3S_3$ (Eq. 36).[304]

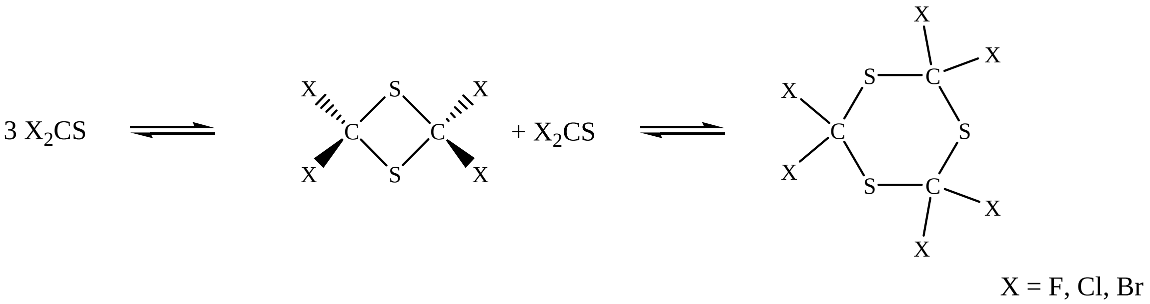

(Eq. 36)

It seems likely that a similar reaction is observed in the Ag^+ / Cl_2CS system and simulations of NMR shifts of the trimeric cation $Cl_5C_3S_3^+$ are in excellent agreement with the experiments (Tab. 25). A measurement of the sample at room temperature showed the whole reaction to be reversible. The signal of the trimeric cation vanishes, while the original intensity distribution of $Cl_3C_2S_2^+$ and $ClCS^+$ reappears.

Tab. 25: Comparison of observed and calculated ^{13}C NMR shifts in 1,2-$C_2D_4Cl_2$ solutions of **17** (see Fig. 95).

$\delta^{13}C$ exp. (5°C) [ppm]	$\delta^{13}C$ exp. (-25°C) [ppm]	$\delta^{13}C$ calc. [ppm]	assignment
192.5	191.2	199.4[a]	$ClCS^+$
232.7	232.5	233.0[b][c]	$Cl_3C_2S_2^+$
79.9	79.8	76.9[b][d]	
	211.3	211.4[b][c]	$Cl_5C_3S_3^+$
	88.9	92.3[b][d]	

[a] MP2/6-311+G(2df) level, referenced on CS_2; [b] BP86/SV(P) level; [c] sp^2 carbon atom, referenced on $F_2ClC_2S_2^+$;[307] [d] sp^3 carbon atom, referenced on $(Cl_2CS)_2$.[307]

Various reaction pathways have been calculated for the formation of $Cl_5C_3S_3^+$ (Tab. 26). The most favored route is, in agreement with the NMR results, the direct formation of $ClCS^+$ (#3 in Tab. 26), which immediately forms the $Cl_3C_2S_2^+$ or $Cl_5C_3S_3^+$ adduct with thiophosgene (#4 and #5 in Tab. 26). $Cl_3C_2S_2^+$ then reacts with a further Cl_2CS molecule to form $Cl_5C_3S_3^+$ (#7a in Tab. 26). Fig. 96 shows a possible transition state and associated activation barrier for such a reaction.

Tab. 26: ΔG^{o} (at 298 K) in kJ mol^{-1} of the reaction pathways leading to the formation of $Cl_{2n-1}C_nS_n^+$ cations (n = 1-3), calculated with different dielectric constants (MP2/TZVPP level, corrected for solvation effects with COSMO). Reversible reactions are indicated by double arrows for clarity.

Reaction paths leading to $Cl_{2n-1}C_nS_n^+$ (n = 1-3)	**Path[a]**	**ε = 8.9[a]**	**ε = 12[b]**	**ε = 54[c]**
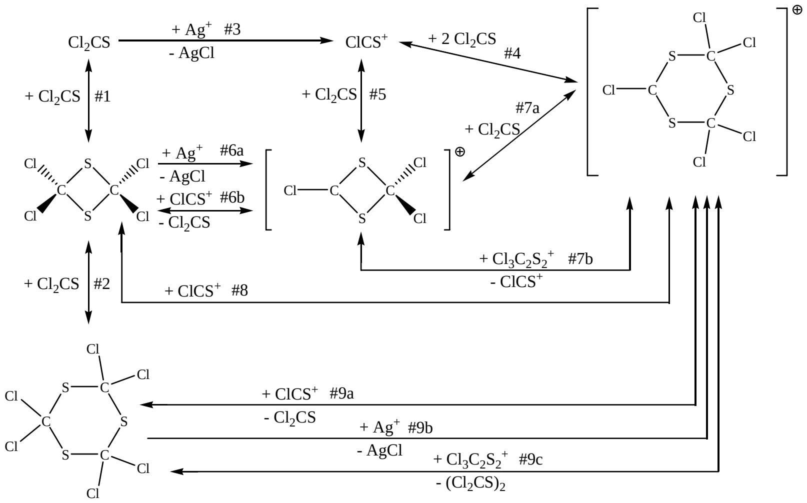	#1	2	2	3
	#2	-11	-11	-10
	#3[d]	-269	-270	-272
	#4[e]	-31	-28	-21
	#5	-27	-25	-20
	#6a[d]	-299	-298	-296
	#6b	-29	-27	-23
	#7a	-4	-3	0
	#7b	23	22	20
	#8	-33	-30	-23
	#9a	-22	-19	-13
	#9b[d]	-292	-290	-286
	#9c	7	8	10

[a] e.g. CH_2Cl_2; [b] e.g. 1,2-$C_2H_4Cl_2$; [c] e.g. CH_2F_2; [d] corrected by the sublimation enthalpy of AgCl (-231.5 kJ mol^{-1});[131] [e] kinetically hindered (3-particle reaction).

Although thermodynamically less favored, intermediate formation of neutral dimeric and trimeric species also seems feasible, but no NMR evidence for the presence of these was found. In the absence of Ag^+, reactions #3, #4, #5 and #7a are the only possible ways to obtain $Cl_5C_3S_3^+$.

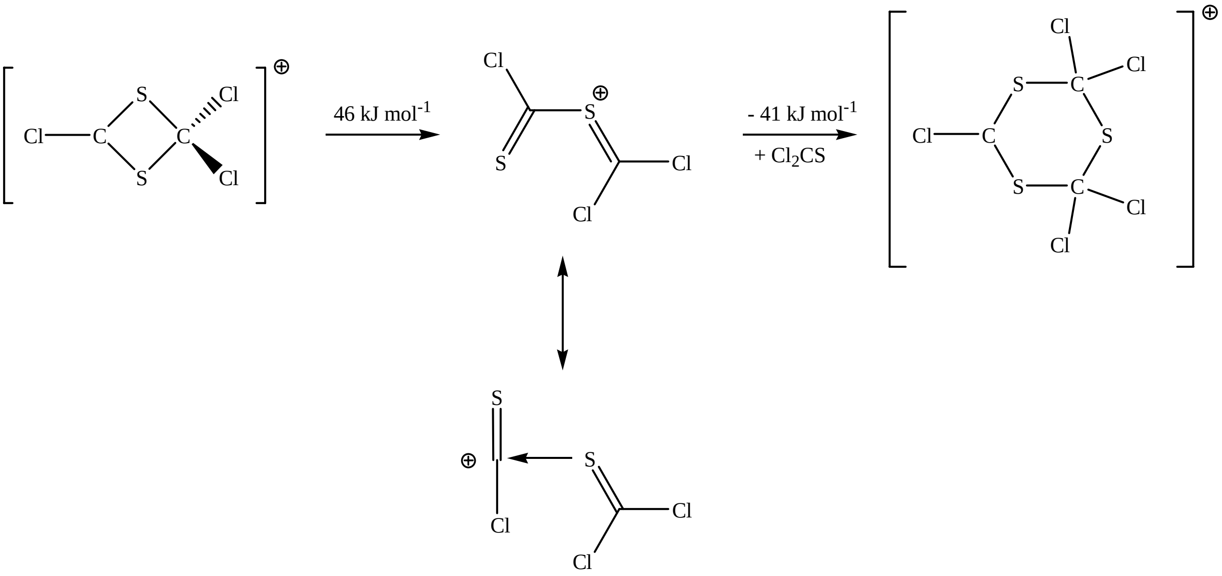

Fig. 96: Possible intermediate (see also Fig. 97) for the formation of $Cl_5C_3S_3^+$ from $Cl_3C_2S_2^+$ and thiophosgene. ΔG^o (at 298 K) calculated with at MP2/TZVPP level, corrected for solvation effects in 1,2-$C_2H_4Cl_2$ ($\varepsilon = 12$) with COSMO.

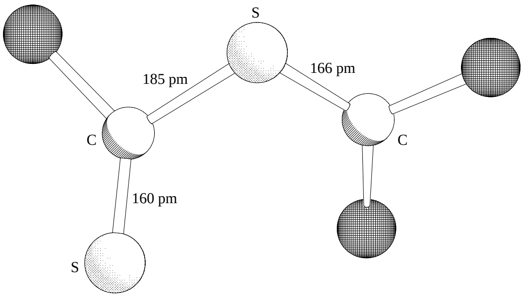

Fig. 97: Calculated geometry (C_1 symmetry, MP2/TZVPP) for the possible intermediate of the formation of $Cl_5C_3S_3^+$ from $Cl_3C_2S_2^+$ and thiophosgene.

In all cases, the effect of solvent polarity is comparably small, with enthalpy differences ranging between 2 and 10 kJ mol^{-1}. In summary, while crystals of ClCS[Al(pftb)$_4$] could not be obtained, the cation was clearly identified in NMR experiments at 5 and -25° C. It might be possible to isolate the salt with another anion with different crystallographic properties. However, the right reaction conditions (temperature, anion type, polarity of the solvent) to obtain $ClCS^+$ as the main cationic species were not found. In future experiments, the reaction could be carried out in SO_2, for example.

4.1.4. Attempts to synthesize $CCl_3[FAl(O(C_6F_{10})C_6F_5)_3]$

For first attempts to synthesize the salt of a highly electrophilic cation and the $[FAl(phex)_3]^-$ anion, CCl_4 was chosen as a reagent. As described in section 4.1.1 (Tab. 20), CCl_3^+ is a benchmark for anion stability[90, 189] and ranks among the most electrophilic cations that could be characterized in the solid state, with a FIA of 904 kJ mol^{-1}. It should be possible to stabilize $CCl_3[FAl(O(C_6F_{10})C_6F_5)_3]$ **18**, at least at low temperatures.

Synthesis

When $Ag[FAl(phex)_3]$ **12** is reacted with an excess of carbon tetrachloride at -20°C, slow formation of AgCl is observed. At lower temperatures, precipitation is not observed. NMR measurements could be carried out at room temperature, but the solutions turn brown within 6 hours.

NMR spectroscopy

^{19}F NMR spectra show the known side products of the synthesis of **12** (see section 3.2.6), but no further signal sets appear. This indicates that the anion stays intact. Apart from the CCl_4 signal at 96.6 ppm,[301] a signal at 211.6 ppm is observed in the ^{13}C NMR spectrum (cf. $CCl_3[Sb(OTeF_5)_6]$ at -80°C in SO_2ClF: $\delta^{13}C = 237.1$ ppm[90], calculated $\delta^{13}C$ of CCl_3^+ with relativistic corrections: 218.2 ppm).[303] CCl_3^+ has been reported by other authors to be stable in the presence of excess CCl_4 (cf. CCl_3^+ in $SbF_5/SO_2ClF/CCl_4$ at -50°C: $\delta^{13}C = 236.3$ ppm).[7]

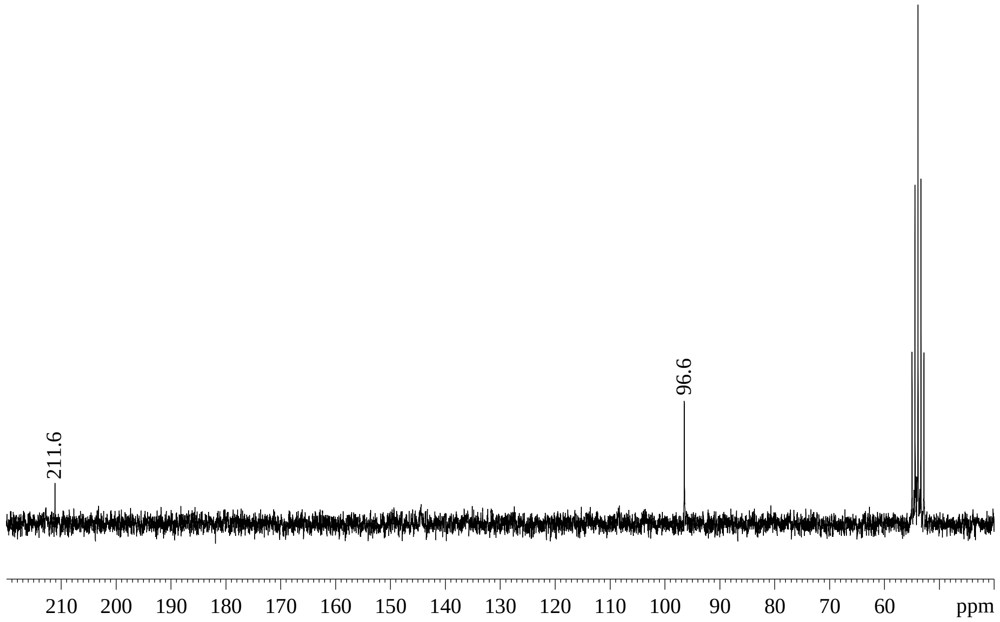

Fig. 98: ^{13}C NMR spectrum (298 K, CD_2Cl_2) showing a signal at 211.6 ppm, which might be assigned to the $[FAl(phex)_3]^-$ coordinated CCl_3^+ cation.

The observed signal is in good agreement with the calculated value. For comparison: With the same method (with relativistic spin-orbit corrections), the calculated chemical shift of CI_3^+ is 123.8 ppm (exp. $\delta^{13}C$ = 97.0 ppm). Accordingly, although relativistic effects are much less pronounced, the signal of CCl_3^+ should appear at a slightly higher field than predicted. The high-field shift with respect to the reported measurements in SO_2ClF of 25 ppm might be resulting from temperature and solvent effects. In conclusion, the formation of **18**, which can be understood as an adduct of the CCl_3^+ cation with $[FAl(O(C_6F_{10})C_6F_5)_3]$, seems likely, but no proof apart from ^{13}C NMR spectra exists. All attempts to crystallize the product failed.

4.2. Weakly bound complex cations

4.2.1. Introduction

Generally, to obtain a cationic complex $M(L)_n^{m+}$ of a metal ion with a weak base such as S_8 or P_4, the anion must be significantly less basic than the ligand to prevent coordination of the cation by the anion. Additionally, large anion size and the associated loss of lattice energy lead to a higher stabilization of the complex cation against dissociation into M^{m+} and the free base, as illustrated for the example of $Ag(S_8)_2^+$ by a simple Born-Fajans-Haber cycle (Fig. 99).

$$\begin{tikzcd}[column sep=large, row sep=large]
Ag(S_8)_2^+\ (g) + [A]^-\ (g) \arrow[r, "+\ \Delta H_r\ (g)"] & Ag^+\ (g) + [A]^-\ (g) \arrow[d, "-\ \Delta H_{latt}", "{\begin{array}{c}[AsF_6]^-\text{: - 586 kJ mol}^{-1}\\ {[Al(pftb)_4]^-}\text{: - 361 kJ mol}^{-1}\end{array}}"'] & +\ 2\ S_8\ (g) \arrow[d, "-\ 2\ \Delta H_{subl}"] \\
Ag(S_8)_2^+[A]^-\ (s) \arrow[u, "+\ \Delta H_{latt}", "{\begin{array}{c}[AsF_6]^-\text{: + 393 kJ mol}^{-1}\\ {[Al(pftb)_4]^-}\text{: + 327 kJ mol}^{-1}\end{array}}"'] \arrow[r, "+\ \Delta H_r\ (s)"] & Ag^+[A]^-\ (s)\ + & 2\ S_8\ (s)
\end{tikzcd}$$

Fig. 99: Born-Fajans-Haber cycle for the dissociation of solid $Ag(S_8)_2^+[A]^-$ into S_8 and $Ag^+[A]^-$.

In this example, the stability can be judged by the lattice energy difference between the silver salt and the complex cation salt, as the sublimation enthalpy of S_8 is the same in both cases. The lattice potential enthalpies for $Ag(S_8)_2^+[AsF_6]^-$[310] and $Ag(S_8)_2^+[Al(pftb)_4]^-$[49] were calculated at 393 and 327 kJ mol^{-1}, respectively ($Ag^+[AsF_6]^-$: 586 kJ mol^{-1}, $Ag^+[Al(pftb)_4]^-$: 361 kJ mol^{-1}).[122, 129] This yields a gain in lattice enthalpy upon dissociation of 193 kJ mol^{-1} for the small $[AsF_6]^-$ anion, but only 34 kJ mol^{-1} for the significantly larger alkoxyaluminate anion. In other words, by changing the anion from $[AsF_6]^-$ to $[Al(pftb)_4]^-$, a 159 kJ mol^{-1} higher stabilization vs. ligand dissociation is achieved.

The new alkoxyaluminate WCAs presented in this thesis should fulfill both the criteria of large size and low basicity. Several reactions were attempted to assess their suitability for the stabilization of weakly bound Lewis-base adducts and first, results will be discussed in the following.

4.2.2. Synthesis and characterization of $[Ag(P_4)_2][Al(OC(CF_3)_2(C_6F_5))_4]$

Introduction

Complexes of the tetrahedral P_4 molecule with Li^+,[311] H^+[312] and Ag^+[11] have been examined by mass spectrometry in the gas phase. Few structures containing a tetrahedral P_4 coordinated to a transition metal are known,[313-316] in which P_4 moiety is bound end-on to the metal. Several compounds of the type $[Ag(P_4)_n][A]$ (n = 1, 2; A = weakly coordinating alkoxyaluminate anion) have been reported as the first species containing an η^2-coordinated tetrahedral P_4, which could be isolated in the solid state.[53, 54] This is contradicts earlier theoretical findings, which also predicted η^1-coordinated Ag^+.[11] $[AgP_4][Al(hftb)_4]$ and $\{[AgP_4][Al(hfip)_4]\}_2$ are molecular compounds, in which the silver atom is additionally coordinated by two oxygen atoms of the more basic anion. With the considerably less basic $[Al(pftb)_4]$ anion, $Ag(P_4)_2^+$ can be stabilized. White phosphorous is a very weak Lewis base, and only a WCA that is sufficiently less basic than P_4 induces Ag^+-P_4 complex formation. $[Ag(P_4)_2][Al(pftb)_4]$ exhibits an almost planar coordination around the silver atom, which was interpreted as the result of additional $d_{x2-y2}(Ag)\rightarrow\sigma^*(P\text{-}P)$ backdonation.[13] However, the authors found the stabilizing effect to be small, with only 5.2 kJ mol^{-1} difference between the planar and tetrahedral coordination (calculated at MPW1PW91/TZV(df) level).

Synthesis

White phosphorous was reacted with $Ag[Al(OC(CF_3)_2(C_6F_5))_4]$ ($Ag[Al(hfpp)_4]$ **8**) at room temperature in CH_2Cl_2. From highly concentrated (viscous) solutions, the $[Ag(P_4)_2][Al(OC(CF_3)_2(C_6F_5))_4]$ **19** was obtained by crystallization at -80 °C in the form of orange, needle-shaped crystals in nearly quantitative yield.

Vibrational Spectroscopy

IR spectra of isolated crystals are identical with the spectra of the silver salt **8a** (see section 6.7, Tab. 52), and no bands which could be assigned to the cation are observed. Thus the geometry of the anion is not significantly distorted by coordination (this is confirmed by an analysis of the crystal structure, see below). In the Raman spectra, a splitting of the three A_1, E and T_2 Raman bands of free P_4 (607, 374 and 468 cm^{-1}[317]) can be expected due to the lowering of the local symmetry. The cation in the comparable $Ag(P_4)_2[Al(pftb)_4]$[58] has an overall D_{2h} symmetry (i.e. the Ag-P_4 subunits are almost C_{2v} symmetric), which leads to six Raman active modes. In **19**, one of the Ag-P_4 moieties in the cation is C_{2v} symmetric, while the other only has C_s symmetry (see below). However, a further splitting of the signals is not observed. Most signals are obscured by fluorescence and only five bands are visible, which are in agreement with the reported spectra of $Ag(P_4)_2[Al(pftb)_4]$. Tab. 27 shows a comparison of Raman frequencies of **19**, P_4 and $Ag(P_4)_2[Al(pftb)_4]$.

Tab. 27: Experimental Raman spectrum of **19**, compared with calculated frequencies and the experimental and calculated spectra of $Ag(P_4)_2[Al(pftb)_4]$[58] and P_4.[317] All experimental data recorded at RT.

19 exp.[a]	**$Ag(P_4)_2[Al(pftb)_4]$ exp.**	**$Ag(P_4)_2$ calc.**[b]	**P_4 exp.**
362 (w)	374 (vw)	361	374
383 (vw)	381 (sh)	366	
420 (vw)	413 (vw)	413	
458 (m)	458 (w)	465	
	473 (w)	468	468
599 (vs)	601 (vs)	595	607

[a] From single crystal; [b] D_{2h} symmetry.

NMR spectroscopy

^{19}F NMR and ^{27}Al NMR spectra of isolated crystals (in CD_2Cl_2) exhibit the typical signals of $[Al(hfpp)_4]^-$ (see sections 6.5.4 and 3.2.2). Signals of decomposition products of the anion are observed, but negligible. ^{31}P NMR spectra show a single sharp signal at -500.5 ppm (FWHM = 7 Hz, free P_4 is not observed), which is in good agreement with the reported shift of $[Ag(P_4)_2][Al(pftb)_4]$ (-497 ppm).[58] For this compound, the authors have reported temperature-dependent NMR experiments, which clearly show that all phosphorous atoms are equivalent at ambient temperature due a fast equilibrium of several η^1- and η^2-coordinated species on the NMR timescale.

Crystal structure determination

From highly concentrated CH_2Cl_2 solutions, **19** crystallizes as orange needles. The crystals are extremely pyrophoric and samples must be prepared under inert conditions in a dried argon stream at -50°C. The space group was determined as triclinic $P\bar{1}$ with a = 11.67 Å, b = 16.54 Å, c = 16.54 Å, α = 84.7°, β = 71.8°, γ = 71.8° and Z = 2. As already indicated by the cell constants, the structure is twinned (exchange of the b and c axes, twin law 100 001 010). For a detailed report of the structural parameters see section 6.12, Tab. 84. The structure can be described as ionic with isolated $Ag(P_4)_2^+$ cations and $[Al(hfpp)_4]^-$ anions and two CH_2Cl_2 molecules in the asymmetric unit.

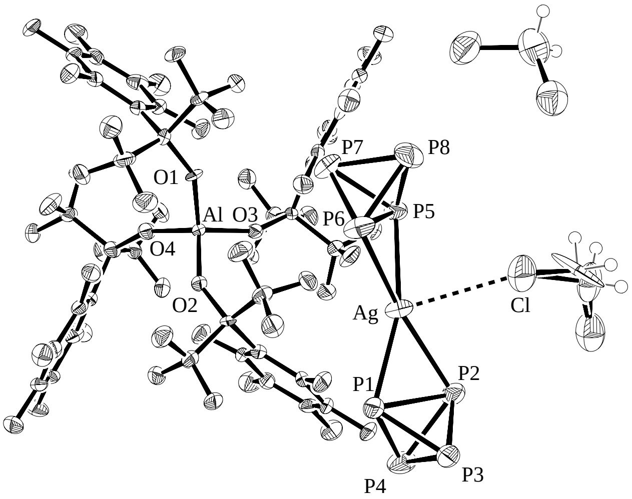

Fig. 100: Crystal structure of **19**. One of the CH_2Cl_2 solvent molecules is disordered. Thermal ellipsoids drawn at 50 % probability level. Distances in pm: Ag-P1 255.2(1), Ag-P2 256.9(1), Ag-P5 254.5(1), Ag-P6 258.7(1), P1-P2 231.2(1), P5-P6 231.2(1), P3-P4 219.8(1), P7-P8 219.6(1), Ag-Cl 331.7(1). Angles in °: P1-Ag-P2 53.7(1), P5-Ag-P6 53.5(1).

Structural parameters of the anion are in good agreement with the structure of the silver salt **8a** (Tab. 28).

Tab. 28: Comparison of structural parameters of the $[Al(hfpp)_4]^-$ anion in **19** and **8a**.

	19 exp.	**8a exp.**
Al-O [pm]	Al-O1 172.3(1)	Al-O1 173.0(1)
	Al-O2 173.0(1)	Al-O2 173.8(1)
	Al-O3 172.8(1)	Al-O3 172.4(1)
	Al-O4 172.5(1)	Al-O4 173.2(1)
av.	172.7	173.1
C-O [pm]	135.9(1)-137.6(1)	134.8(1)-136.5(1)
av.	136.5	135.6
Al-O-C [°]	Al-O1-C 148.5(1)	Al-O1-C 161.8(1)
	Al-O2-C 146.8(1)	Al-O2-C 159.1(2)
	Al-O3-C 156.8(1)	Al-O3-C 157.6(1)
	Al-O4-C 158.7(1)	Al-O4-C 147.5(1)
av.	152.7	156.5
O-Al-O [°]	104.4(1)-117.8(1)	104.5(1)-113.2(1)
	109.5	109.5

While the $Ag(P_4)_2^+$ ion in the analogous complex salts with the $[Al(pftb)_4]^-$ anion exhibits a planar coordination of the silver atom,[58] in **19** the two P_4 cages are twisted with an angle of

34.6° between the two P-Ag-P planes. This geometry is similar to $Ag(P_4)_2^+$ in the salt of the larger $[(pftb)_3AlFAl(pftb)_3]^-$ anion (44.2°).[64] As mentioned above, the calculated energetic difference between the planar (P-Ag-P 180°) and tetrahedral (P-Ag-P 90°) coordination is only 5.2 kJ mol^{-1} and consequently the twist may be explained by packing effects or weak P-F contacts.[64] There are in total 8 P-F contacts within the sum of van-der-Waals radii of P and F (327 pm), ranging from 311.1(1) to 326.6(1) pm and one weak contact between silver and a CH_2Cl_2 molecule (Ag-Cl 331.7(1) pm, cf. sum of van-der-Waals radii: 347 pm).

Tab. 29 shows a comparison of bond parameters of the cation between **19**, $Ag(P_4)_2[(pftb)_3AlFAl(pftb)_3]$ and $Ag(P_4)_2[Al(pftb)_4]$.

Tab. 29: Structural parameters of the $Ag(P_4)_2^+$ cations in **19**, $Ag(P_4)_2[(pftb)_3Al\text{-}F\text{-}Al(pftb)_3]$ and $Ag(P_4)_2[Al(pftb)_4]$ (see Fig. 101 for assignment of atom labels).[58]

	19	**$Ag(P_4)_2[(pftb)_3AlFAl(pftb)_3]$**	**$Ag(P_4)_2[Al(pftb)_4]$**
Ag-P [pm]	254.5(1)-258.7(1)	253.8(1)-254.0(1)	253.6(1)-254.8(1)
av.	256.3	253.9	254.1
P1-P2 / P5-P6 [pm]	both 231.2(1)	both 233.0	232.8(2)-233.0(2)
av.			232.9
P3-P4 / P7-P8 [pm]	219.6(1)-219.8(1)	both 219.5(1)	217.2(2)-217.4(2)
av.	219.7		217.3
other P-P [pm]	214.6(1)-216.6(1)	215.6(1)-216.1(1)	214.5(2)-216.3(2)
av.	215.5	215.9	215.4
P-P-P [°]	57.3(1)-65.0(1)	57.3(1)-65.4(1)	56.9(1)-65.5(1)
P_4-Ag-P_4 twist angle [°]	34.6	44.2	10.6/0.0[a]

[a] at 150 K, at 200 K the cation becomes D_{2h} symmetric with an angle of 0°.

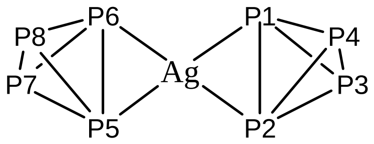

Fig. 101: Assignment of atom labels in the $Ag(P_4)_2^+$ cation.

While $Ag(P_4)_2[Al(pftb)_4]$ exhibits a local C_{2v} symmetry of the Ag-P_4 moieties (Ag-P distances differ less than 1 pm), in **19** only one Ag-P_4 subunit has a C_{2v} symmetry within reasonably limits (2 pm difference in Ag-P distances). The other is C_s symmetric, with a difference in Ag-P bond lengths of more than 4 pm. The angle between the centers of the P_4 cages and the silver atom deviates significantly from linearity with 169.8(1)°. The coordinated edges of the P_4 molecules are elongated by 10 pm compared with free P_4 (221 pm). All other P-P distances are shortened by 1-6 pm. However, the overall tetrahedral geometry is only slightly distorted, as seen by the small deviations in P-P-P angles (57.3(1)-65.0(1)°, av. 60.1°).

4.2.3. Synthesis and characterization of $[Ag(S_8)(1,2\text{-}C_6H_4F_2)][FAl(O(C_6F_{10})C_6F_5)_3]$

Introduction

Several binary silver-sulfur complexes have been examined in the gas phase, such as AgS_4^+, AgS_8^+ and AgS_{16}^+.[318, 319] Albeit sulfur is a weak ligand, some crystal structures of complex salts of $Ag(S_8)_n^+$ (n = 1, 2) cations with weakly coordinating anions have already been reported.[129, 310, 320] Suitable anions include $[AsF_6]^-$, $[SbF_6]^-$, $[Sb(OTeF_5)_6]^-$, $[Al(hfip)_4]^-$ and $[Al(pftb)_4]^-$. In the solid state structure of $Ag(S_8)_2[AsF_6]$, two Ag-F contacts significantly distort the geometry of the cation.[310, 320] The $[Al(hfip)_4]^-$ cation coordinates to Ag^+, which in turn leads to coordination of only one S_8 moiety with silver and results in the complex $AgS_8[Al(hfip)_4]$.[129] In contrast, the cation in $Ag(S_8)_2[Al(pftb)_4]$ can be considered almost uncoordinated due to the weakly basic perfluorinated alkoxyaluminate anion, with a geometry that is close to D_{4d} symmetry. Consequently, $Ag(S_8)_2^+$ cations are ideal test cases to assess the basicity of a given anion.

Synthesis

In attempts to synthesize mixed cationic silver-sulfur-selenium species from $Ag[FAl(phex)_3]$ **12**, sulfur and red selenium in 1,2-difluorobenzene, it is found that selenium does not take part in the reaction. Instead, after activating the reaction by sonication and removing selenium by filtration, crystals of $[Ag(S_8)(C_6H_4F_2)][FAl(O(C_6F_{10})C_6F_5)_3]$ **20** could be obtained. The compound is stable at room temperature.

Crystal structure determination

20 crystallizes as yellow crystals from $1,2\text{-}C_6H_4F_2$. The space group was determined as triclinic $P\bar{1}$ with a = 10.99 Å, b = 15.60 Å, c = 17.80 Å, α = 82.0°, β = 72.5°, γ = 82.1° and Z = 2. For a detailed report of the structural parameters see section 6.12, Tab. 85. The structure is clearly ionic, consisting of separated $[Ag(S_8)(1,2\text{-}C_6H_4F_2)]^+$ cations and $[FAl(phex)_3]^-$ anions (Fig. 102). Seven very weak S-F contacts exist between the ions, which are shorter than the sum of van-der-Waals radii of sulfur and fluorine (327 pm), ranging between 307.3(1) and 326.1(1) pm. Ag^+ is η^4-coordinated by a S_8 molecule and η^1-coordinated by one disordered 1,2-difluorobenzene solvent molecule. The three shortest Ag-C distances are

240.5(1), 281.9(1) and 276.5(1) pm (angle between C_6 plane and Ag-C bond 87.3(1)°). There are no other contacts to the Ag^+ cation shorter than the sum of van-der-Waals radii.

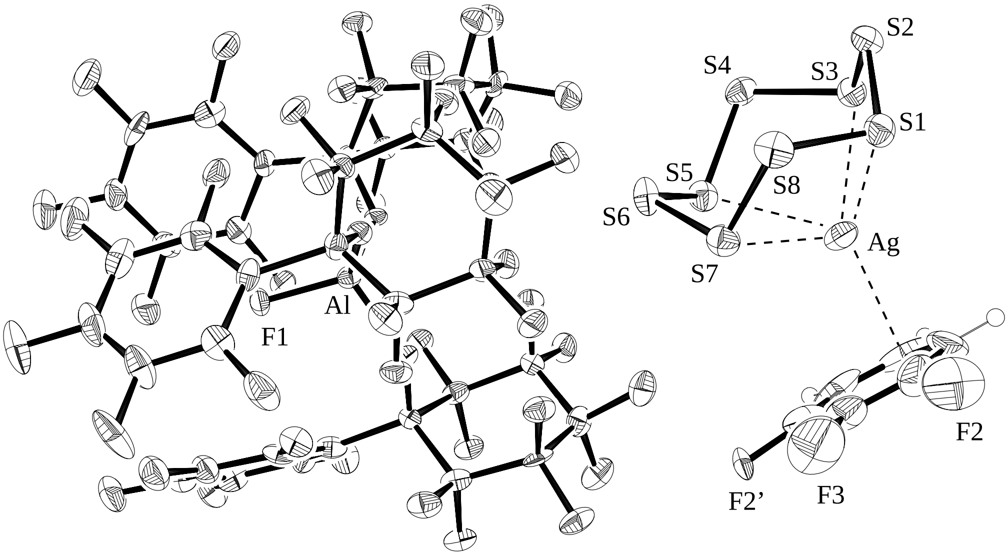

Fig. 102: Crystal structure of **20**. The 1,2-difluorobenzene molecule is disordered (positions F2 and F2’ are only half-occupied by fluorine). Thermal ellipsoids drawn at 50 % probability level.

The geometry of the $Ag(S_8)(1,2\text{-}C_6H_4F_2)^+$ unit is compared with known $Ag(S_8)^+$ and $Ag(S_8)_2^+$ salts in Tab. 30. Ag^+ forms a distorted pyramid with the surrounding sulfur atoms (4 Ag-S contacts). Compared to AgS_8[Al(hfip)$_4$] and $Ag(S_8)_2$[Al(pftb)$_4$], in which the Ag-S distances show a variation of 17 pm and 43 pm respectively, the AgS_8 subunit is less distorted (Ag-S distance variation: 11 pm), closely approaching C_{4v} symmetry. Consequently, all S-Ag-S angles are almost identical (69.1(1)-71.6(1)°) and the average S-S bond distances and S-S-S angles are very similar to orthorhombic sulfur (S-S: 205.6 pm in **20** vs. 205.1 pm in S_8, S-S-S: 107.3° in **20** vs. 107.4° in S_8). Overall, the Ag-S distances in **20** (av. 283.6 ppm) are significantly shorter than in AgS_8[Al(hfip)$_4$] (av. 292.4 ppm) and comparable to $Ag(S_8)_2$[Al(pftb)$_4$] (av. 282.7 ppm).

Tab. 30: Comparison of structural parameters of **20** with other AgS_8 complexes,[129] the calculated structure of free S_8 in the gas phase and experimental X-ray data.[321]

	20	**$AgS_8[Al(hfip)_4]$**	**$Ag(S_8)_2[Al(pftb)_4]$**	**S_8 calc.[a]**	**S_8 exp.[b]**
Ag-S [pm]	Ag-S3 277.8(1)	283.5	262.2		
	Ag-S1 287.3(1)	291.2	279.4		
	Ag-S5 280.4(1)	294.5	283.8		
	Ag-S7 288.9(1)	300.2	305.3		
av.	283.6	292.4	282.7		
Ag-O [pm]		234.5	317.3		
	331.8(1)	273.7	318.2		
Ag-F [pm]	343.8(1)	323.0	327.1		
	240.5(1)	325.7	352.4		
Ag-C [pm]	276.5(1)				
	281.9(1)				
S-S [pm]	204.6(1)-207.0(1)	204.3-205.2	203.8-206.7	all 205.8	all 205.1
av.	205.6	204.8	205.0		
$S-S_{Ag}-S$ [°]	109.1(1)-109.9(1)	109.0-109.3	108.1-110.0	all S-S-S 107.4	all S-S-S 108.2
$S_{Ag}-S-S_{Ag}$ [°]	104.8(1)-105.9(1)	104.9-105.8	105.5-107.1		
# S-F contacts	11	10	18		
S-F [pm]	303.4(1)-328.8(1)	314.7-334.8	301.1-331.5		

[a] MP2/TZVPP, D_{4d} symmetry; [b] orthorhombic S_8.[321]

Tab. 31 shows a comparison of structural parameters of the $[FAl(phex)_3]^-$ anion in **20** and the silver salt **12b** (section 3.2.6). In both compounds the anion is not coordinated by the cation and has a conformation in which all C_6F_5 groups point in the direction of the Al-F bond, effectively shielding the basic fluoride. As already observed in the crystal structure of the silver salt **12b**, the presence of a weak donor ligand such as 1,2-difluorobenzene is sufficient to prevent coordination of the Al-F bond in $[FAl(phex)_3]^-$.

Tab. 31: Structural parameters of the anions in **20** and **12b** ($[FAl(phex)_3]^-$).

	20	**12b**
Al-O [pm]	174.4(1)-175.5(1)	174.6(1)-175.0(1)
Al-F [pm]	167.8(1)	166.9(1)
O-Al-O [°]	107.8(1)-110.5(1)	109.6(1)-110.5(1)
O-Al-F [°]	109.0(1)-110.1(1)	108.8(1)-110.7(1)
Al-O-C [°]	136.4(1)-137.6(1)	135.5(2)-137.8(2)

4.3. Applications of the Lewis acid $Al(O(C_6F_{10})C_6F_5)_3$

4.3.1. Synthesis and characterization of $CPh_3[ClAl(O(C_6F_{10})C_6F_5)_3]$

Introduction

Trityl cations CPh_3^+ act as catalysts or co-catalysts in a wide range of reactions.[56-62] A prominent example is the generation of $[cp_2ZrMe]^+[A]^-$ ($[A]^-$ = weakly coordinating anion)[59, 60] from cp_2ZrMe_2 (cp = η^5-C_5H_5) and $CPh_3^+[A]^-$ by methanide abstraction. $[cp_2ZrMe]^+$ is a typical catalyst for Ziegler-Natta olefin polymerization. Generally, trityl cations can be used for hydride or alkanide abstraction, e.g. in the synthesis of silylium cation salts R_3Si^+ from R_3SiH.[322] Thus, trityl salts are valuable starting materials to introduce WCAs and to generate the desired counterion at the same time. There are two synthetic routes towards trityl salts of WCAs, metathesis and halide abstraction by a Lewis acid under formation of a heteroleptic anion (Eq. 37):

$$Ph_3CX + Li[A] \xrightarrow{-\ LiX} CPh_3^+[A]^-$$

$$Ph_3CX + L \xrightarrow{\quad} CPh_3^+[LX]^-$$

X = Br, Cl; $[A]^-$ = WCA; L = Lewis acid

(Eq. 37)

Synthesis

A reaction mixture of **10** (see section 3.2.4), containing $Li[FAl(O(C_6F_{10})C_6F_5)_3]$ and side products, was reacted with trityl chloride in CH_2Cl_2. Formation of LiCl was observed, but after filtration and crystallization, $CPh_3[ClAl(O(C_6F_{10})C_6F_5)_3]$ **21** was instead identified by X-ray analysis. This can be explained by the existence of residual Lewis acid $Al(O(C_6F_{10})C_6F_5)_3$, which forms the $[ClAl(phex)_3]^-$ anion by chloride abstraction. The main reaction product is probably $CPh_3[FAl(O(C_6F_{10})C_6F_5)_3]$, formed in the expected metathesis reaction, but other crystals from the reaction mixture could not be analyzed due to poor crystal quality.

NMR spectroscopy

Proton NMR spectra show the normal signals of the trityl cation. Other species are not observed. ^{19}F spectra show a range of side products of the synthesis of **10**, and single signals could not be resolved.

Crystal structure determination

21 crystallizes from CH$_2$Cl$_2$ in slim, rod-shaped yellow crystals. The space group was determined as trigonal R3$_2$ with a, b = 16.25 Å, c = 89.73 Å and Z = 12. The crystals were racemic twins. For a detailed report of the structural parameters see section 6.12, Tab. 85. The structure is ionic with two symmetry independent ion pairs in the asymmetric unit (structural parameters of the anions in both pairs are identical within reasonable limits, see Tab. 32). The Al-Cl bonds and central carbon atoms of the planar trityl cations reside on C$_3$ rotation axes. Thus, the central plane of the cation is normal to the Al-Cl bond, yet coordination with chlorine can be excluded (closest C-Cl contacts 542, respectively 559 pm).

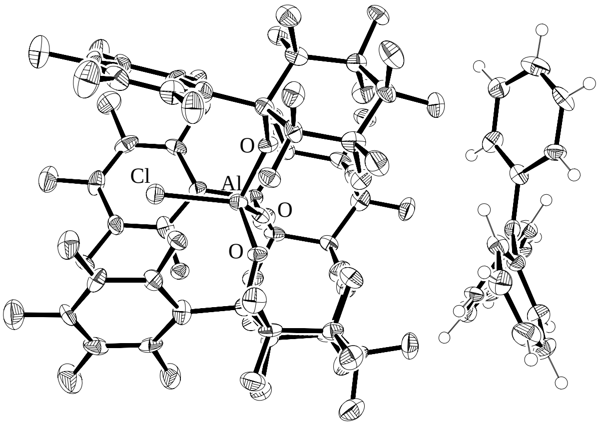

Fig. 103: Crystal structure of **21**. The asymmetric unit contains two independent CPh$_3$[ClAl(phex)$_3$] moieties, only one of which is shown. Thermal ellipsoids drawn at 50 % probability level.

Tab. 32: Structural parameters of the anions in **21** and **12b** ([FAl(phex)$_3$]$^-$).

	21[a]	**21**[a]	**12b**
Al-O [pm]	176.5(1)	174.7(1)	174.6(1)-175.0(1)
Al-X [pm][b]	215.1(1)	215.2(1)	166.9(1)
O-Al-O [°]	108.6(1)	108.6(1)	109.6(1)-110.5(1)
O-Al-X [°][b]	110.3(1)	110.3(1)	108.8(1)-110.7(1)
Al-O-C [°]	139.1(2)	139.8(1)	135.5(2)-137.8(2)

[a] 2 symmetry-independent moieties. [b] X = Cl in **21**, F in **12b**.

The geometry of the cation is typical for CPh$_3^+$, with C-C distances between the central carbon atom and the phenyl group of 144.9(1) and 143.7(1) pm, and out-of-plane angles of the phenyl groups of 33.6 and 34.7°.

4.4. A new starting material for Ga(I) chemistry ?

4.4.1. Introduction

Cationic organoaluminum compounds have been examined by many groups with the aim of developing transition metal free polymerization catalysts.[64-67] Very reactive cations, such as the alumenium cations R_2Al^+ (R = alkyl), must be partnered with extremely stable anions like halogen-substituted carboranates to prevent electrophilic attack and anion decomposition.[323] Few experimental data has been reported on the less Lewis-acidic and thus slightly more stable gallium analogs. For example, the compound $[(2,6\text{-}Mes_2C_6H_3)_2Ga][Li\{Al(hfip)_4\}_2]$, in which the gallium cation is coordinated by two bulky m-terphenyl substituents, shows some catalytic reactivity.[324] Ga(I) can also form stable complexes with arenes, in which it is often strongly coordinated and paired with $[GaX_4]^-$ (X = Cl, Br) anions.[70, 71] One strategy to prevent coordination of the cation involves embedding Ga^+ into a bulky cage ligand containing arene groups.[76, 77] While in $[(2,6\text{-}Mes_2C_6H_3)_2Ga][Li\{Al(hfip)_4\}_2]$ (see above), a bulky ligand (shielding the cation) is combined with the introduction of a weakly coordinating anion, WCA salts of uncoordinated Ga^+ have not been published. Recently, Ga(I) complex cation salts with two weakly bound 1,2-difluorobenzene ligands could be stabilized with the $[Al(pftb)_4]^-$ and $[(pftb)_3AlFAl(pftb)_3]^-$ anions.[325]

The fluorine atom bound to the aluminum center in $[FAl(phex)_3]^-$ is coordinated in some compounds (e.g. the $[Ag(CH_2Cl_2)_3]^+$ salt **12a**) and uncoordinated in others (e.g. the $[Ag(C_6H_5F)_3]^+$ salt **12b**). If an univalent gallium cation should coordinate the $[FAl(phex)_3]^-$ anion, the resulting compound could be mainly ionic in nature (“$Ga^+[FAl(phex)_3]^-$“) or exhibit covalent character like molecular gallium(I)fluoride (“GaF-$Al(phex)_3$“). Many low-valent gallium compounds are known in the condensed phase,[326-329] including prominent examples such as the univalent cyclopentadienylgallium, pentamethylcyclopentadienylgallium[83-85] and several gallium subhalides.[86-88] Molecular GaBr, which is only stable at high temperatures in its uncoordinated form, can be obtained by co-condensation with organic donor molecules.[89, 90] Amorphous “GaI”, which behaves like a monovalent gallium system, can be synthesized from iodine and elemental gallium.[330] Gallium(I) fluoride, which is isolelectronic with carbon monoxide, has so far only been characterized in the gas phase[331] and in noble gas matrices.[332]

4.4.2. Synthesis and characterization of (1,2-$C_6H_4F_2$)GaFAl(O(C_6F_{10})C_6F_5)$_3$

Synthesis

(1,2-$C_6H_4F_2$)GaFAl(O(C_6F_{10})C_6F_5)$_3$ **22** is prepared by oxidation of elemental gallium with the silver salt Ag[FAl(O(C_6F_{10})C_6F_5)$_3$] **12** in 1,2-difluorobenzene. Slow formation of a silver mirror is observed and the product forms yellow crystals when concentrating the solution in vacuo. No decomposition of the compound is observed at room temperature.

Vibrational spectroscopy

Fig. 104 and Fig. 105 show the IR and Raman spectra of isolated crystals of **22**, which exhibit good agreement with Li[FAl(phex)$_3$] **10** and the simulated spectrum of a model compound (GaFAl(phex)$_3$, 1,2-difluorobenzene molecule removed, input geometry taken from crystal structure and optimized on BP86/SV(P) level, see section 6.7, Tab. 53). In the simulation, combination modes involving an Al-F and Ga-F contributions are predicted at 578 and 588 cm^{-1}. The IR spectrum shows very weak signals at 546 and 567 cm^{-1} and the Raman spectrum exhibits a strong signal at 588 cm^{-1} which could be assigned to these modes. The stretching frequency of molecular gallium(I)fluoride in the gas phase was calculated at 637 cm^{-1} (IR and Raman, BP86/SV(P)). Experimental IR bands of GaF were detected by other authors in noble gas matrix experiments at 590/592 cm^{-1} (^{71}GaF/^{69}GaF, Ar matrix) and 607/609 cm^{-1} (^{71}GaF/^{69}GaF, Ne matrix).[332] The slight redshift of the signals in **22** by approximately 20-50 cm^{-1} is in agreement with a Ga-F bond weakening (with respect to free GaF) and the contribution of Al-F vibration. The good agreement between the IR spectra of the lithium salt **10** and **22** indicates similar solid state structures and modes of coordination. Additionally, the IR spectrum, which was recorded after removal of the solvent in vacuo, shows no bands of 1,2-difluorobenzene, indicating that the solvent can be removed from **22**.

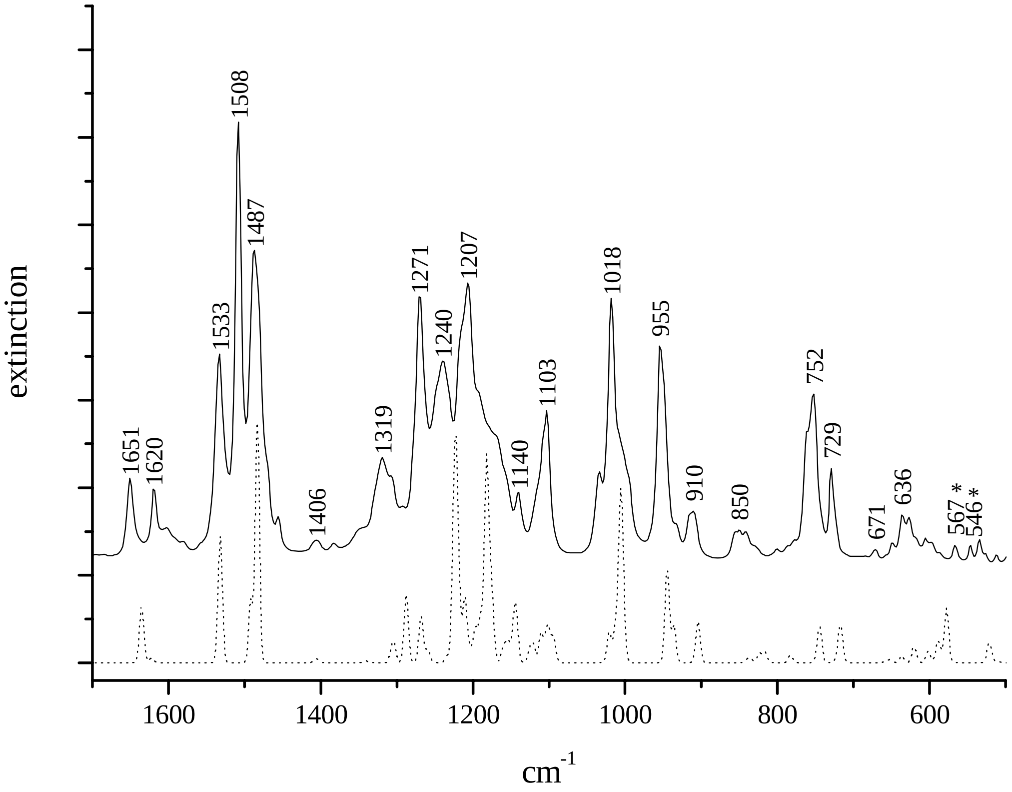

Fig. 104: IR spectrum of crystals of **22** (solid line) and simulated spectrum of the model compound GaFAl(phex)$_3$ (dotted line, BP86/SV(P)). Bands assigned to Ga-F-Al combination modes are indicated by an asterisk.

The Raman spectrum of crystalline **22** shows bands in the characteristic ranges of aromatic C-H (2937, 2908 and 2757 cm^{-1}, omitted in Fig. 105) and C=C valence vibrations (1557 cm^{-1}). This is in agreement with the crystal structure (see below), which shows that gallium is not only coordinated by the anion, but also by one 1,2-difluorobenzene molecule.

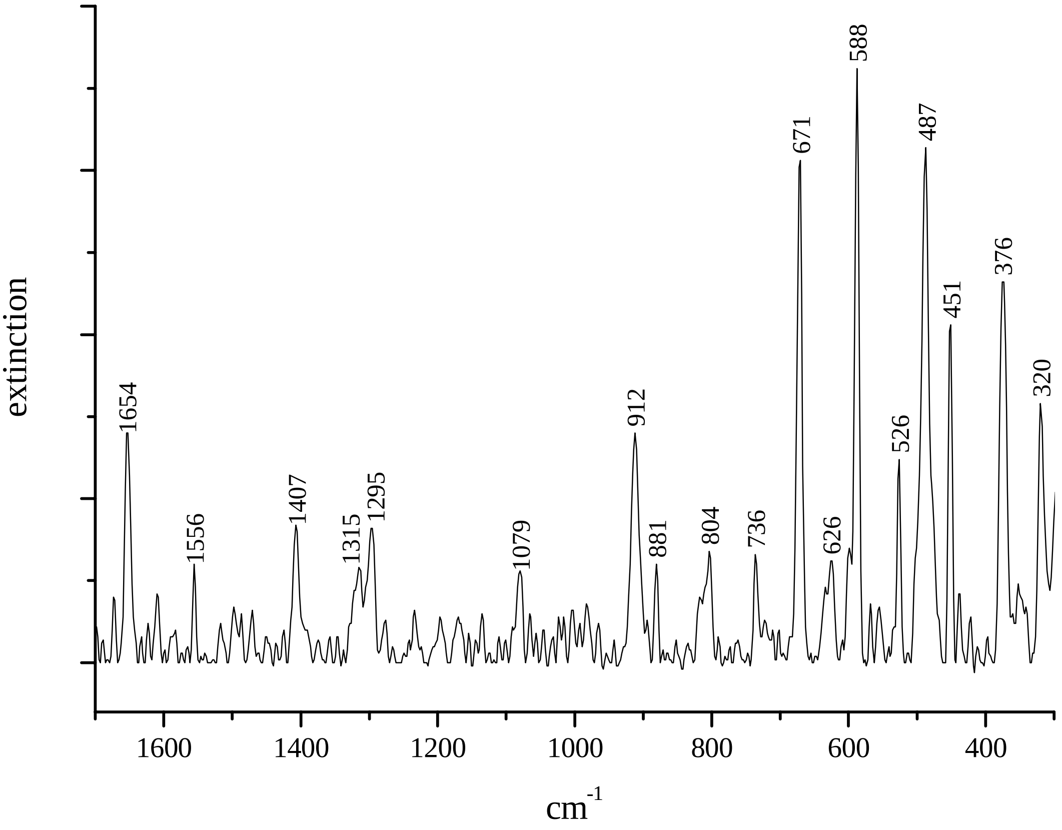

Fig. 105: Raman spectrum of crystals of **22**. Bands below 320 cm^{-1} are obscured by strong fluorescence. The crystals are weak Raman scatterers, hence the noisy background. Bands at 2937, 2908 and 2757 cm^{-1} (solvent) omitted for clarity.

Crystal structure determination

22 crystallizes from 1,2-difluorobenzene in yellow, block-shaped crystals. The space group was determined as orthorhombic $P2_12_12_1$ with a = 14.11 Å, b = 17.96 Å, c = 19.11 Å and Z = 4. For a detailed report of the structural parameters see section 6.12, Tab. 85. In the crystal structure, the Ga^+ cation and the anion are not separated. Gallium is coordinated by the fluorine atom attached directly to aluminum (Fig. 106). In analogy to the silver salt $[Ag(CH_2Cl_2)_3][FAl(O(C_6F_{10})C_6F_5)_3]$ **12a**, in which the silver atom is also coordinated by a fluorine atom, all aromatic C_6F_5 groups point in the opposite direction of the Al-F bond.

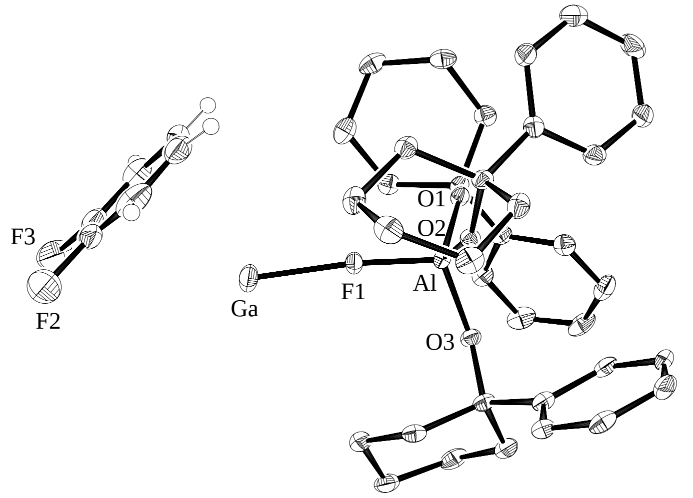

Fig. 106: Crystal structure of **22**. Most fluorine atoms omitted for clarity. Thermal ellipsoids drawn at 50 % probability level. Distances in pm: Ga-F1 208.8(1), Al-F1 172.5(1), Al-O1 173.2(1), Al-O2 172.7(1), Al-O3 173.8(1). Angles in °: O1-Al-F1 105.7(1), O2-Al-F1 105.9(1), O3-Al-F1 107.9(1), O1-Al-O2 111.8(1), O1-Al-O3 113.7(1), O2-Al-O3 111.4(1), Al-F1-Ga 173.1(1), Al-O1-C 138.5(1), Al-O2-C 141.2(1), Al-O3-C 141.1(1).

Most structural parameters of the anion are within the expected range known from other compounds (Tab. 33). The Al-O-C angles deviate slightly from **12b** due to the inverted orientation of the three phex ligands.

Tab. 33: Structural parameters of the $[FAl(phex)_3]^-$ anion in **22** and the silver salt **12**.

	22	**12a**[a]	**12b**[b]
Al-F [pm]	172.5(1)	168.9(1)	166.9(1)
F-M	208.8(1)	233.0(1)	
Al-O av. [pm]	173.2	174.2	174.8
O-Al-F [°]	105.7(1)-107.9(1)	107.7(1)-109.9(1)	108.8(1)-110.7(1)
Al-O-C [°]	138.5(1)-141.2(1)	142.0(1)-143.8(1)	135.5(2)-137.8(2)
O-Al-O [°]	111.4(1)-113.7(1)	109.1(1)-111.4(1)	108.4(1)-110.5(1)
Al-F-M	173.1(1)	169.0(1)	

[a] $[FAl(phex)_3]^-$ anion coordinated; [b] $[FAl(phex)_3]^-$ anion not coordinated; [c] M = Ga in **22**, Ag in **12a**.

As expected, the Al-F bond is significantly elongated (by 5.6 pm with respect to the uncoordinated anion) due to the coordination with the gallium atom. In **12a**, the anion is coordinated by Ag^+. However, the Ag^+ cation in this compound also forms 5 Ag-Cl contacts with 3 CH_2Cl_2 molecules (see section 3.2.6). In **22**, the coordination of gallium by the solvent is weaker and thus the Ga-F coordination stronger, hence the Al-F bond distance is slightly elongated with respect to **12a** (by 3.6 pm). This can be demonstrated by a comparison of bond lengths with sums of van-der-Waals radii. The Ga-F distance is 208.8(1) pm, amounting to 63% of the sum of van-der-Waals radii of Ga and F (334 pm). In **12a**, this ratio is 73% (sum of van-der-Waals radii of Ag and F: 319 pm, Ag-F bond length: 233 pm). Compared with free GaF in the gas phase (MP2/TZVPP: 178.1 pm, exp. 177.4 pm[331]), the bond is elongated by more than 30 pm, indicating a strongly ionic character. This is consistent with the Al-F-Ga angle, which approaches linearity (173°). This was examined in detail with several theoretical methods (see below), to gain deeper insight into the coordinative strength of the $[FAl(phex)_3]^-$ anion.

Fig. 107 shows the coordination around the Ga atom, which rests on a central position above the $C_6H_4F_2$ ring. All Ga-C contacts are weak, with distances between 305.8 and 326.4 pm (sum of van-der-Waals radii of Ga and C: 357 pm). The shortest contacts are with the most electron-rich carbon atoms in the 4 and 5 positions and are 18, respectively 22 pm longer than the shortest Ga-C distance in $[(1,2\text{-}C_6H_4F_2)_2Ga][Al(pftb)_4]$ (288.1 pm).[325] Due to the lone electron pair on gallium, the angle defined by the Ga-F bond and the C_6 plane is 54.1(1)°.

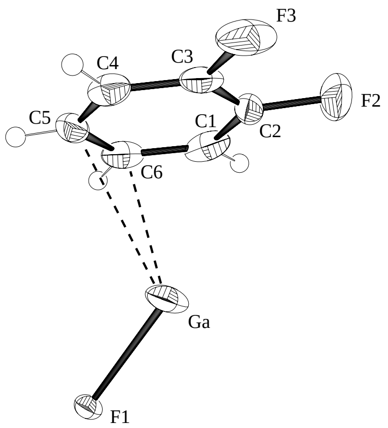

Fig. 107: Detail of the crystal structure of **22**, showing the coordination of the gallium atom. Only the two shortest Ga-C contacts are indicated. Thermal ellipsoids drawn at 50 % probability level. Distances in pm: Ga-F1 208.8(1), Ga-C1 319.3(1), Ga-C2 326.4(1), Ga-C3 323.6(1), Ga-C4 313.6(1), Ga-C5 305.8(1), Ga-C6 309.6(1). Plane between C_6 ring plane and Ga-F bond: 54.1(1)°. Distance from Ga to the centroid of the C_6 ring: 285.1(1).

Tab. 34 shows a comparison of the structural parameters of the cation in **22** with two salts containing $[Ga(1,2\text{-}C_6H_4F_2)_2]^+$ complex cations. In **22**, the coordination with ortho-difluorobenzene is significantly weaker due to coordination of Ga by the anion. Additionally, two weaker Ga-F contacts (322.6(1) and 330.8(1) pm) exist.

$[Ga(1,2\text{-}C_6H_4F_2)_2][Al(pftb)_4]$ and $[Ga(1,2\text{-}C_6H_4F_2)_2][(pftb)_3AlFAl(pftb)_3]$ fully expel the coordinated solvent in vacuo (10^{-3} mbar, 24 hours).[325] Already after removal of the solvent for one hour at the same pressure, no traces of difluorobenzene were detected in IR measurements of **22** (see above).

Tab. 34: Comparison of structural parameters of the cations in **22**, $[Ga(1,2\text{-}C_6H_4F_2)_2][Al(pftb)_4]$ and $[Ga(1,2\text{-}C_6H_4F_2)_2][(pftb)_3AlFAl(pftb)_3]$.[325]

	22	$[Ga(1,2\text{-}C_6H_4F_2)_2]$ $[Al(pftb)_4]$	$[Ga(1,2\text{-}C_6H_4F_2)_2]$ $[(pftb)_3AlFAl(pftb)_3]$
Ga-C [pm]	**305.8-326.4**	**287.3-311.9**	**294.2-313.9**
Ga-centroid	**285.1**	**av. 268.4**	**av. 269.6**
shortest Ga-F	**208.8**	**311.9**	**317.1**
# Ga-F contacts[a]	**3**	**2**	**1**

[a] Contacts shorter than the sum of van-der-Waals radii of Ga and F (334 pm).

Computational analysis

Atomic charges from population analyses were calculated to assess the nature of the Ga-F bond in **22** (Tab. 35). An optimization of the full geometry of **22** was not possible due to oscillation (rotation of the very weakly bound 1,2-difluorobenzene molecule). Therefore, Ga-F-AlF_3 was first chosen as a model system. However, depending on the input geometry (C_1 or C_s symmetric), the model system collapsed to $Ga[AlF_4]$, either in C_{2v} (global minimum) or C_{3v} (local minimum at 15 kJ mol^{-1} higher energy) symmetry. Another tested model system, Ga-F-$Al(OCF_3)_3$ also collapsed, resulting in a geometry in which gallium coordinates not only the bridging fluoride, but also an oxygen atom. This does not occur in **22**, which results from the high steric shielding of the oxygen atoms in the $[FAl(phex)_3]^-$ anion. Thus, population analyses were performed on a single point calculation of the geometry taken from the X-ray structure, as well as on an optimized geometry of the X-ray structure without the coordinating 1,2-difluorobenzene molecule (all on BP86/SV(P) level).

Tab. 35: Calculated NBO and PABOON charges points of **22**, free GaF, the isoelectronic CO and the model compound GaFAl(phex)$_3$.

	PABOON charges	**NBO charges**	**Ga-F/C-O [pm]**
22[a]	Ga 0.93	Ga 0.92	208.8
	F -0.48	F -0.90	
	Al 0.30	Al 2.50	
GaFAl(phex)$_3$[b]	Ga 0.89	Ga 0.82	198.4
	F -0.52	F -0.73	
	Al 0.30	Al 2.01	
GaF (BP86)[c]	Ga 0.42	Ga 0.70	179.6
	F -0.42	F -0.70	
CO (BP86)[c]	C -0.11	C 0.47	C-O 114.2
	O 0.11	O -0.47	
GaF (MP2)[d]	Ga 0.94	Ga 0.88	178.1
	F -0.94	F -0.88	
CO (MP2)[d]	C -0.07	C 0.61	C-O 113.7
	O 0.07	O -0.61	

[a] Single point calculation on the X-ray geometry, C_1 symmetry, BP86/SV(P); [b] model compound without coordinated 1,2-difluorobenzene, C_1 symmetry, optimized on BP86/SV(P) level; [c] C_{6v} symmetry, SV(P) basis set; [d] C_{6v} symmetry, TZVPP basis set.

The MP2 geometry of free GaF reproduces the experimental bond distance of 177.4 pm[331] slightly better than the DFT geometry. The same holds for the bond length in CO (exp. 112.8 pm). However, it becomes obvious that the results of the population analyses must be interpreted very cautiously. E.g. the NBO charges of the isoelectronic CO molecule are far too large for a mainly covalent bond and there is even an inversion of the sign when compared with the PABOON values. It is generally accepted that a small negative charge resides on carbon in CO, despite the higher electronegativity of oxygen, due to O→C π donation. In addition, the lower electronegativity of carbon creates a much more diffuse electron cloud, slightly enhancing the dipole moment (which is nevertheless very small, exp.: 0.112 Debye).[121, 333] In rotational spectra of weak complexes of HCl and CO, it was found that the interaction occurs through a hydrogen bond with the carbon atom (thus, carbon should possess a small negative charge).[334] Additionally, a too low covalent Al-F and Al-O bonding character is predicted for the model compound and **22**, as seen by the high partial charges on aluminum and fluorine. MP2-based PABOON values for GaF are far too high, approaching a free ion pair in the gas phase and contradicting the predicted short Ga-F bond of 178.1 pm. In conclusion, the combination of PABOON with BP86/SV(P) seems to deliver reasonable results for the examined systems and has the advantage that the large model compound and the geometry of the crystal structure can be analyzed. For GaF, while a large ionic contribution can be expected due to the differences in electronegativity, there is still some covalent character in the bond. Indeed, the molecule is predicted to be polarized, with partial charges significantly different from +/-1 (+0.42 on gallium and -0.42 on fluorine). Even though the bond lengths differ by 10 pm, the charges of the model compound and geometry of the crystal structure of **22** are consistent, with a high charge on gallium (+0.89, respectively +0.93) that indicates a mainly ionic interaction, in contrast to free GaF. This is in agreement with a valence bond analysis[335] of the crystal structure, which predicts bond valences of 0.31 for the Ga-F bond, which is less than half the value in free GaF in the gas phase (0.73), and 0.62 for the Al-F bond. However, this must be very carefully interpreted due to a lack of reference values for Ga(I). In summary, while the Ga-F bond in **22** has some covalent character, it is probably better described as an ionic compound [1,2-$C_6H_4F_2$Ga][FAl(phex)$_3$]. In other words, even though the [FAl(phex)$_3$]$^-$ is in some compounds clearly coordinating, as indicated by directed Al-F-cation contacts, the coordination can be considered fairly weak.

Tab. 36 shows the results of a topological analysis of the electron density in **22** and several reference compounds (free GaF, the isoelectronic CO and a model compound) according to the AIM (atoms in molecules) theory.[309]

Tab. 36: Calculated electron densities ρ(r) and the negative Laplacians L(r) at the Ga-F and C-O bond critical points (BCPs) of **22**, free GaF and CO in the gas phase and a model compound. $L(r) = -\nabla^2\rho(r)$.

	method	**ρ(r)$_{BCP}$ [e Å^{-3}]**	**L(r)$_{BCP}$ [e Å^{-5}]**	**Ga-F/C-O [pm]**
GaF[a]	BP86/SVP	0.88	-18.32	179.6
	BP86/6-311++G**	0.74	-14.46	183.2
	MP2(full)/6-311++G**	0.74	-16.63	180.6
	MP2(fc)	0.81	-19.28	178.1
CO[a]	BP86/SVP	3.17	-29.40	114.2
	BP86/6-311++G**	3.24	-10.60	113.9
	MP2(full)/6-311++G**	3.17	-18.31	113.8
	MP2(fc)	3.31	-23.86	113.7
22[b]	BP86/SVP	0.40	-5.06	208.8
	BP86/6-311++G**	0.40	-5.06	208.8
GaFAl(phex)$_3$[c]	BP86/SVP	0.47	-7.71	198.4
	BP86/6-311++G**	0.47	-7.47	

[a] C_{6v} symmetry, optimized; [b] single point calculation on the X-ray geometry, C_1 symmetry; [c] model compound without coordinated 1,2-difluorobenzene, C_1 symmetry, optimized.

The calculated L(r) values at the BCP for CO differ from the reference value of -6.6 e $Å^{-5}$ given in the literature (at HF/6-311++G** level).[309] However, other authors showed in a systematic study that the Laplacian is very dependent on the applied method and basis set (with a difference between MP2 and BP86 with the same basis set of more than 30%). Accordingly, they have reported L(r) values for CO between -8.8 (BP86) and -13.1 e $Å^{-5}$ (MP2), albeit with a smaller basis set than the ones shown in Tab. 36. At the same time, the electron density at the BCP was found to be rather method-independent.[336] The same trend is reflected in Tab. 36. L(r) values calculated with BP86/6-311++G** seem to reproduce reported values for CO best, while the electron density at the BCP stays nearly identical for all methods. For free gallium fluoride, the densities at this level are slightly underestimated due to the elongated bond length. It can be deduced that the BP86/SVP and 6-311++G** calculations for **22** and the model compound deliver reasonable properties at the BCP. The results can be interpreted in terms of a lower covalent Ga-F bonding character in **22** when compared with free GaF (BP86/6-311++G** electron density at BCP 0.34 e $Å^{-3}$ lower). However, the covalent contribution is still significant, as purely electrostatic complexes typically have ρ(r) values < 0.1 e $Å^{-3}$ at the BCP.[337] This is in accordance with the trends from population analyses, but judging from the topology of the electron density alone, **22** should be described as a strongly polarized donor-acceptor complex $[1,2\text{-}C_6H_4F_2Ga]^{\delta+}\text{---}^{\delta-}[FAl(phex)_3]$ rather than a salt or a molecular compound.

4.5. Conclusions to chapter 4

The electrophilic cations ICS^+ and $Cl_3C_2S_2^+$ could be isolated as alkoxyaluminate WCA salts (which are stable at room temperature) and were fully characterized. Species of the general type XCE^+ and $X_3C_2E_2^+$ (X = halogen, E = S, O) have so far been unknown in the solid state, except $F_3C_2S_2^+$. While $ClCS^+$ could not be stabilized in the solid state, the cation could be characterized by NMR spectroscopy and may well be accessible, if suitable reaction conditions can be found. As a first test of the stability of $[FAl(phex)_3]^-$, the synthesis of a CCl_3^+ salt of this anion was attempted. While further efforts at characterization failed, a ^{13}C NMR signal was observed, which possibly arose from coordinated CCl_3^+. The compound is even stable at room temperature in solution for short periods of time, hinting at a high stability of the new WCA.

In agreement with conclusions drawn already from the crystal structures of the starting materials in chapter 3, it could be shown that the new alkoxaluminates $[Al(OC(CF_3)_2C_6F_5)_4]^-$ ($[Al(hfpp)_4]^-$) and $[FAl(O(C_6F_{10})C_6F_5)_3]^-$ ($[FAl(phex)_3]^-$) are weakly basic and thus suitable for the stabilization of weakly bound complex cations. As first examples, the complexes $[Ag(P_4)_2][Al(hfpp)_4]$ **19** and $[Ag(S_8)(1,2\text{-}C_6H_4F_2)][FAl(phex)_3]$ **20** could be characterized. In both compounds, the anions are clearly not coordinating to Ag^+, comparable to analogous salts of the $[Al(OC(CF_3)_3)_4]^-$ anion.[12, 13, 129] However, upon introduction of $[Al(OC(CF_3)_3)_4]^-$, crystallographic problems often arise from disorder, which is induced by the rotation of CF_3 units (cf. ICS^+ and $Cl_3C_2S_2^+$ salts above). $[Al(hfpp)_4]^-$ still contains 8 trifluoromethyl groups, but disorder was never detected in structures containing this anion. The same holds for $[FAl(phex)_3]^-$, which contains no CF_3 groups at all. While $[Al(OC(CF_3)_3)_4]^-$ is almost spherical, both new anions exhibit reduced symmetry, inherently reducing the likelihood of pseudo-merohedral twinning (in fact, this type of twinning never occurred in any salt of $[FAl(phex)_3]^-$ or $[Al(hfpp)_4]^-$ except **19**). As a side note, compounds containing the $[FAl(phex)_3]^-$ WCA crystallize quickly from concentrated solutions and tend to form small, but strongly scattering crystals. As already seen from the crystal structures of **12a** and **12b** in chapter 3, this WCA is “Janus-headed”. The basic fluoride ligand can be coordinating or non-coordinating, depending on the level of electrophilicity of the cation and the reaction conditions (solvent). Two modifications of $[FAl(phex)_3]^-$ exist, which differ by the orientation of the perfluorophenyl rings (pointing in the direction of the Al-F bond in the non-coordinating modification and in the opposite direction in the coordinating modification, Fig. 108).

Fig. 108: Space-filling models of the “Janus-headed” $[FAl(phex)_3]^-$ anion, taken from crystal structures. The coordinating modification is shown on the left, the non-coordinating modification on the right. Positions of the basic fluorine atom connected to the central aluminum atom are indicated by arrows and a different shading pattern. The coin shows the most famous representation of Janus, the roman two-faced god of gates and doors.

The steric shielding of the basic fluorine atom by three C_6F_5 units effectively inhibits coordination. However, even when the anion coordinates, cation-fluoride bonds are weak and exhibit significant ionic character due to some residual shielding of the Al-F bond by the phex ligands, as could be shown by the example of $(1,2\text{-}C_6H_4F_2)GaFAl(O(C_6F_{10})C_6F_5)_3$ **22**. In NMR experiments of all compounds containing the $[FAl(phex)_3]^-$ anion, only one anionic species was observed, which means the orientation of the C_6F_5 groups is dynamic in solution (at room temperature). **22** is a remarkable species by itself, as the number of compounds containing only Ga^+, which is not coordinated by strong donor ligands, is limited to $[Ga(1,2\text{-}C_6H_4F_2)_2][Al(pftb)_4]^-$, $[Ga(1,2\text{-}C_6H_4F_2)_2][(pftb)_3AlFAl(pftb)_3]^-$[325] and the poorly characterized, amorphous “GaI”.[330] Additionally, **22** is stable at room temperature and easily available in good yields.

Another new anion, namely $[ClAl(phex)_3]^-$, could be isolated as a trityl salt. Subtraction of the thermochemical volume of the BF_4^- anion (73 $Å^3$)[122] from the crystallographic molecular volume of trityl tetrafluoroborate ($V = 1680$ $Å^3$, $Z = 4$)[276] gives an estimate for the thermochemical volume of the trityl cation (346 ± 9 $Å^3$). With this value, the thermochemical volume of the $[ClAl(phex)_3]^-$ can be estimated as 1363 $Å^3$ (cf. crystal structure of **21**: $V = 20510$ $Å^3$, $Z = 12$). The new WCA could prove suitable for the stabilization of other reactive cations, or as a counterion in catalysis (e.g. $cp_2ZrCl^+[\ ClAl(phex)_3]^-$ in Ziegler-Natta olefin polymerization). Additionally, its formation could only be explained by the presence of the parent Lewis acid $Al(O(C_6F_{10})C_6F_5)_3$ **15** in the reagent, which was the first indication that **15** is stable at room temperature.

5. Summary and outlook

“Perhaps it hasn´t one,” Alice ventured to remark.

“Tut, tut, child!” said the Duchess. ”Everything´s got a moral, if only you can find it.”

It could be shown that the new anions $[Al(hfpp)_4]^-$ and $[FAl(phex)_3]^-$ fulfill all criteria for weakly coordinating anions given in chapter 1: Low basicity, large size and good delocalization of the surface charge. Tab. 37 summarizes the results of extrapolations to estimate the anion sizes from crystal structure data. The new anions are significantly larger than e.g. the $[Al(pftb)_4]^-$ anion[52] and additionally reduce crystallographic problems (twinning and disorder).

Tab. 37: Comparison of estimated thermochemical volumes of different alkoxyaluminate WCAs, based on unit cell volumes and thermochemical volumes of the counterions.[122]

	$[Al(hfip)_4]^-$	**$[FAl(pftb)_3]^-$**	**$[Al(pftb)_4]^-$**	**$[Al(hfpp)_4]^-$**	**$[FAl(phex)_3]^-$**	**$[ClAl(phex)_3]^-$**
V_{therm} [Å^3]	599[52]	609[a]	758[52]	1076[a]	1113[a]	1363[b]

[a] See section 3.4; [b] see section 4.5.

A measure to assess the surface charge distribution is the surface screening charge. Quantum chemical calculations incorporating the COSMO model (*c*onductor-like *s*creening *mo*del)[338, 339] provide a discrete surface around a molecule embedded in a shell of point charges (a virtual conductor). Of this surface, each segment is characterized by the *s*creening *c*harge *d*ensity (SCD) σ, which takes into account the electrostatic screening and back-polarization of the molecule by its surroundings. Fig. 109 shows a comparison of SCD probability distributions of the $[Sb_2F_{11}]^-$ WCA (which is a “traditional” WCA commonly encountered as a counterion in superacidic SbF_5/SO_2ClF),[277] the triflimide $N(SO_2CF_3)_2^-$ (commonly used in electrochemical applications and as counterions in ionic liquids)[99, 100] and four alkoxyaluminates. While the plot for $N(SO_2CF_3)_2^-$ clearly shows the accessibility of the lone electron pairs of oxygen (peak at 0.01 e Å^{-2}), peaks at negative σ in the plot of $[Sb_2F_{11}]^-$ (corresponding to accumulation of positive charge on the surface) stem from the availability of the Sb atoms. Peaks at negative σ are also found in the plots of $[Al(hfpp)_4]^-$ and $[FAl(phex)_3]^-$, resulting from the carbon atoms in the aromatic C_6F_5 rings. Narrow peaks of the $[Al(OR)_4]^-$ anions result from a uniform charge distribution on many fluorine atoms. The onset of the curve when moving from positive to negative σ can be interpreted as a measure for the coordinative strength of a given anion (a smaller value would be associated with lower basicity), and the compared anions can be arranged in the following order (with sinking coordinative strength, in e Å^{-2}): $N(SO_2CF_3)_2^-$ (0.016), $[Sb_2F_{11}]^-$ (0.01), $[Al(hfip)_4]^-$ (0.009), $[Al(hfpp)_4]^-$ (0.009), $[Al(pftb)_4]^-$ (0.007), $[FAl(phex)_3]^-$ (0.007, only the non-coordinating modification with all C_6F_5 units shielding the basic fluorine atom was calculated).

Another method to exemplify the low coordinative strength of the new anions is a comparison of the surface electrostatic potentials (Fig. 110). The accessibility of negative charge (indicated by a negative value of the electrostatic potential) on the central oxygen atoms in $[Al(hfip)_4]^-$ becomes immediately apparent. Additionally, part of the negative charge accumulates on the surfacial fluorine atoms. This effect is most drastic in the comparably small $[Sb_2F_{11}]^-$. In $[Al(pftb)_4]^-$ and the new anions, the oxygen atoms (indicated by red surfaces) are significantly shielded by the ligands and the charge on most fluorine atoms on the surface is lower than in $[Al(hfip)_4]^-$.

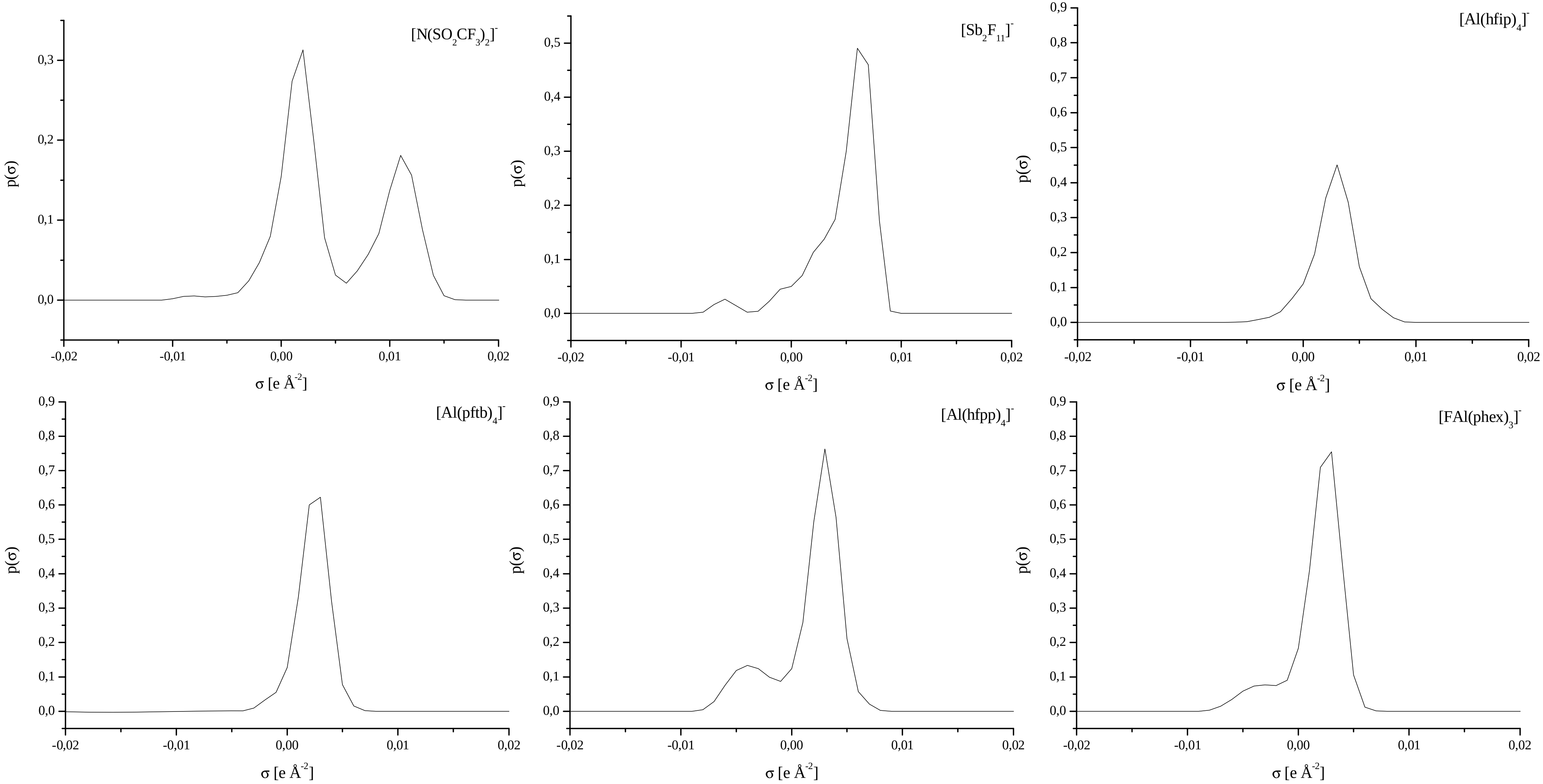

Fig. 109: Probability distribution plots of the screening charge densities σ of alkoxyaluminate WCAs in comparison with $[Sb_2F_{11}]^-$ and $N(SO_2CF_3)_2^-$. Plots based on BP86/SV(P) optimized minimum geometries and BP86/TZVP single-point energies (with COSMO correction).

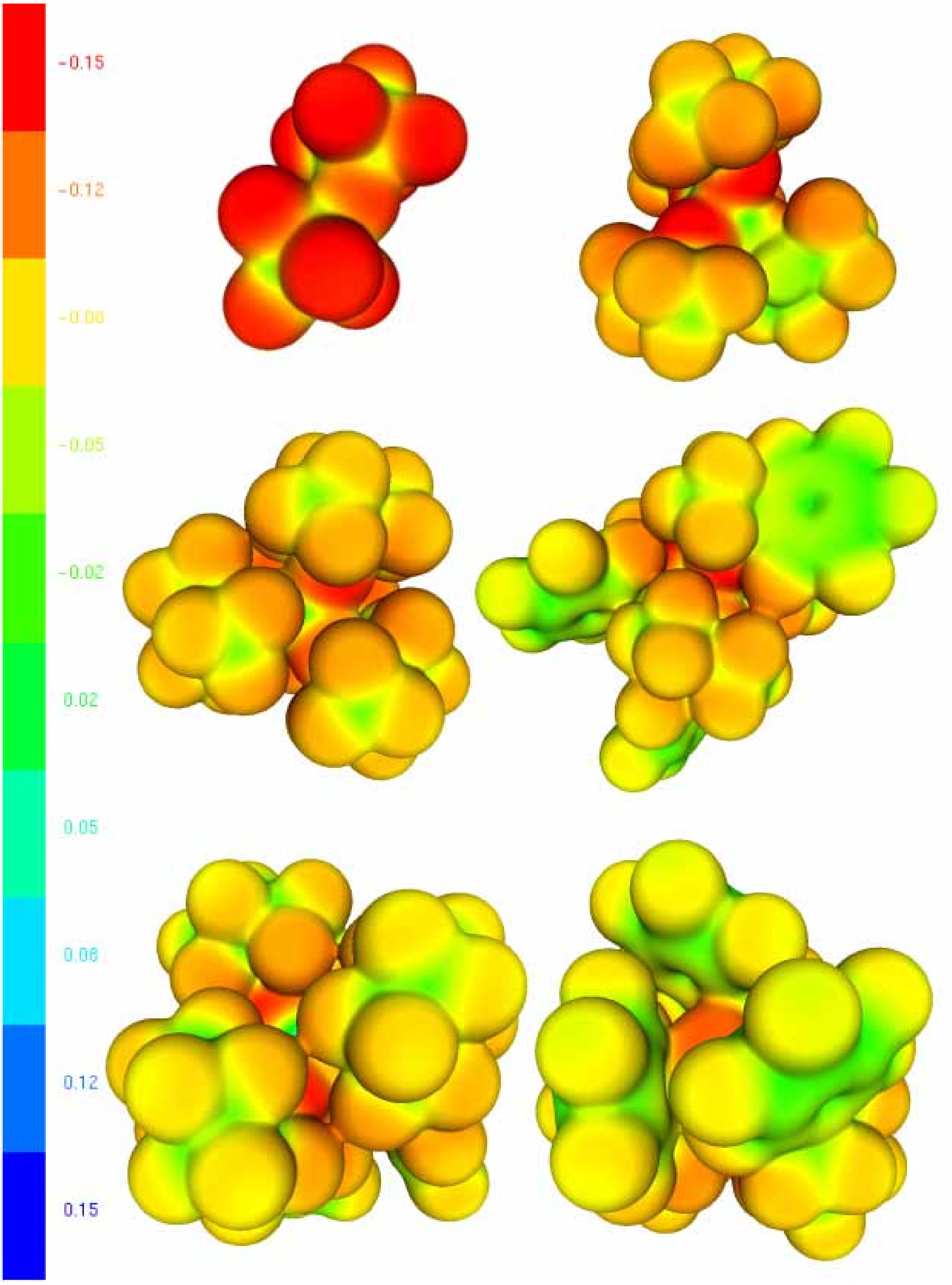

Fig. 110: Electrostatic potentials, mapped on an isosurface of the total electron density (0.005 e (a.u.)$^{-3}$), of alkoxyaluminate WCAs in comparison with $[Sb_2F_{11}]^-$ and $N(SO_2CF_3)_2^-$. Top left: $[Sb_2F_{11}]^-$, top right: $[Al(hfip)_4]^-$, center left: $[Al(pftb)_4]^-$, center right: $[Al(hfpp)_4]^-$ (scaled down), bottom left: $[FAl(phex)_3]^-$ (view on opposite side of the basic fluorine atom), bottom right: $[FAl(phex)_3]^-$ (view on the basic fluorine atom).

While many attempts to find a less tedious synthesis for $[Al(hfpp)_4]^-$ salts have failed, $[FAl(phex)_3]^-$ salts can be obtained in large yields. However, a better synthetic route to salts with this anion is necessary to prevent the formation of epoxide $C_{12}F_{14}O$ and associated loss of 25% of the parent alcohol. First attempts to synthesize the anion from the parent Lewis suffered from lack of a suitable fluoride source. $AgBF_4$ and $LiBF_4$ react too slowly under conditions in which $Al(O(C_6F_{10})C_6F_5)_3$ is stable and various side reactions occur. Ammonium salts of $[FAl(phex)_3]^-$ can certainly be obtained by reacting the Lewis acid with a strong fluoride source such as tetramethylammoniumfluoride. Another possibility might be a reaction with silver tetrafluoroborate in SO_2 (Eq. 38), in which the weak donor could preorganize the molecule, thereby heightening the availability of the Lewis-acidic aluminum atom.

$$\text{"}SO_2{\cdot}Al(phex)_3\text{"} + AgBF_4 \xrightarrow{-\ SO_2} Ag[FAl(phex)_3]$$

phex = $O(C_6F_{10})C_6F_5$

(Eq. 38)

$Al(phex)_3$ **15** is a remarkable species by itself. As a compound which is stable at room temperature and available in a very simple reaction (10 g scale, one day, quantitative yields), it is still one of the strongest Lewis acids with a calculated FIA of 530 kJ mol^{-1}. Apart from possible applications in catalysis which remain to be examined, $Al(phex)_3$ could be a valuable parent compound in WCA syntheses (Eq. 39). Even a small ligand such as a methoxy group could fit in the cage of three C_6F_5 units, forming a fully closed surface. The availability of the Lewis acid allows the quick screening of a large number of possible ligands. Thus, properties of resulting WCAs can be tuned (e.g. alkyl groups should increase the solubility in organic solvents). Additionally, new nuclei can be introduced to facilitate the detection of anion decomposition by NMR, such as ^1H and ^{29}Si.

$$Al(phex)_3 + MOR \longrightarrow M[Al(OR)(phex)_3]$$

phex = $O(C_6F_{10})C_6F_5$; M = Li, Na
R = e.g. Me, CF_3, Ph, $CH(CF_3)_2$

(Eq. 39)

As already shown by the example of $CPh_3[ClAl(O(C_6F_{10})C_6F_5)_3]$, the Lewis acid can also abstract Cl^- from trityl chloride under formation of a WCA salt. This creates new possibilities for the stabilization of electrophilic cations or their adducts with WCAs. Two examples are given in (Eq. 40).

$$\mathrm{Al(phex)_3 + CX_4 \xrightarrow{\qquad} CX_3[XAl(OR)(phex)_3]}$$

$$\mathrm{Al(phex)_3 + XSiMe_3 \xrightarrow{\qquad} Me_3Si[XAl(OR)(phex)_3]}$$

phex = $O(C_6F_{10})C_6F_5$; X = Cl-I

(Eq. 40)

CI_3^+ can be stabilized by alkoxyaluminate WCAs. The shown reactions might be a way to obtain CBr_3^+ and CCl_3^+ salts, which so far only exist with teflate counterions. Reactions with $Al(pftb)_3$ and trimethylfluorosilane lead to a Me_3Si-F-$Al(pftb)_3$ adduct with significant ionic character.[340] However, the $[FAl(pftb)_3]^-$ anion is more strongly coordinating than $[FAl(phex)_3]^-$. Analogous syntheses could be attempted with $Al(phex)_3$, possibly leading to compounds with stronger ionic character or even salts.

The suitability of the new anions for the stabilization of very weakly bound complex cations has already been shown by the examples of $[Ag(P_4)_2][Al(OC(CF_3)_2(C_6F_5))_4]$ **19** and $[Ag(S_8)(1,2\text{-}C_6H_4F_2)][FAl(O(C_6F_{10})C_6F_5)_3]$ **20**. I would like to conclude my thesis with the first example of a Ag-Se_{12} complex, stabilized by $[FAl(phex)_3]^-$ and characterized by X-ray diffraction (with kind permission of the authors).[341] Even though Ag^+ is clearly coordinated by the anion (Ag-F: 242 pm, cf. sum of van-der-Waals radii of Ag and F: 319 pm), silver is still electrophilic enough to bind Se_{12}. Thus, even the coordinating modification of $[FAl(phex)_3]^-$ might be suitable to stabilize further metal complexes with weak bases.

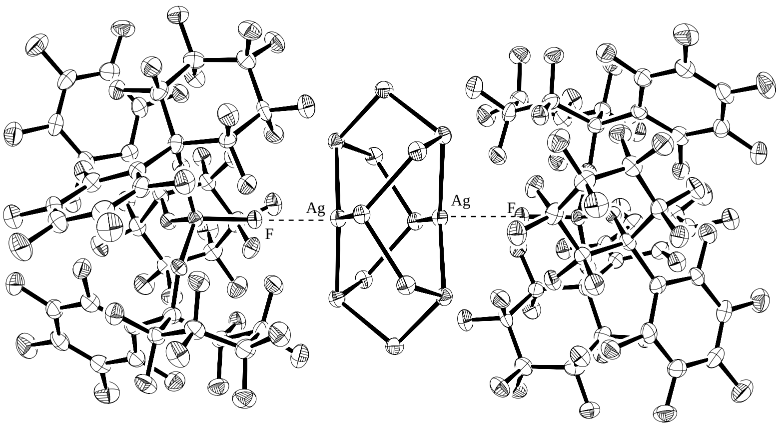

Fig. 111: Crystal structure of the first Ag-Se_{12}-Ag complex, stabilized by the $[FAl(phex)_3]^-$ WCA. The Ag-Se subunit exhibits almost undistorted local D_{3d} symmetry. Thermal ellipsoids drawn at 50 % probability level. R_1 = 3.6 %, wR_2 = 8.0 %.

6. Annex

6.1. Table of numbered compounds

1	$C_6F_5(CF_3)_2COH$ = hfpp-H
2	$C_6F_5(C_6F_{10})OH$ = phex-H
2a	$C_6F_5(C_6F_{10})OH\cdot({}^{n}C_4H_9)_4NBr\cdot H_2O$
3	$LiOC(CF_3)_3\cdot 2THF$
4	$AgO(C_6F_{10})C_6F_5\cdot EtCN$
5	$LiO(C_6F_{10})C_6F_5$
5a	$\{LiO(C_6F_{10})C_6F_5\}_3$
5b	$\{(C_6H_5F)LiO(C_6F_{10})C_6F_5\}_2$
5c	$\{(H_2O)LiO(C_6F_{10})C_6F_5\}_2$
6	$NaO(C_6F_{10})C_6F_5$
6a	$NaO(C_6F_{10})C_6F_5\cdot C_6F_5(C_6F_{10})OH\cdot 2H_2O$
7	$Li[Al(OC(CF_3)_2(C_6F_5))_4]$ = $Li[Al(hfpp)_4]$
8	$Ag[Al(OC(CF_3)_2(C_6F_5))_4]$ = $Ag[Al(hfpp)_4]$
8a	$[Ag(1,2\text{-}C_2Cl_2H_4)_3][Al(OC(CF_3)_2(C_6F_5))_4]$
9	$Na[Al(OC(CF_3)_2(C_6F_5))_4]$ = $Na[Al(hfpp)_4]$
9a	$Na[Al(OC(CF_3)_2(C_6F_5))_4]\cdot 1,2\text{-}Cl_2C_2H_4$
10	$Li[FAl(O(C_6F_{10})C_6F_5)_3]$ = $Li[FAl(phex)_3]$
11	$C_{12}F_{14}O$
12	$Ag[FAl(O(C_6F_{10})C_6F_5)_3]$ = $Ag[FAl(phex)_3]$
12a	$[Ag(CH_2Cl_2)_3][FAl(O(C_6F_{10})C_6F_5)_3]$ = $[Ag(CH_2Cl_2)_3][FAl(phex)_3]$
12b	$[Ag(C_6H_5F)_3][FAl(O(C_6F_{10})C_6F_5)_3]$ = $[Ag(C_6H_5F)_3][FAl(phex)_3]$
13	$Li(O(C_6F_{10})C_6F_5))_2GaCl_2\cdot C_6H_5F$
14	$Li(O(C_6F_{10})C_6F_5))_2GaBr_2\cdot C_6H_5F$
15	$Al(O(C_6F_{10})C_6F_5)_3$ = $Al(phex)_3$
16	$ICS[Al(OC(CF_3)_3)_4]$ = $ICS[Al(pftb)_4]$
17	$Cl_3C_2S_2[Al(OC(CF_3)_3)_4]$ = $Cl_3C_2S_2[Al(pftb)_4]$
18	$CCl_3[FAl(O(C_6F_{10})C_6F_5)_3]$ = $CCl_3[FAl(phex)_3]$
19	$[Ag(P_4)_2][Al(OC(CF_3)_2(C_6F_5))_4]$ = $[Ag(P_4)_2][Al(hfpp)_4]$
20	$[Ag(S_8)(1,2\text{-}C_6H_4F_2)][FAl(O(C_6F_{10})C_6F_5)_3]$ = $[Ag(S_8)(1,2\text{-}C_6H_4F_2)][FAl(hfpp)_3]$
21	$CPh_3[ClAl(O(C_6F_{10})C_6F_5)_3]$ = $CPh_3[ClAl(phex)_3]$
22	$(1,2\text{-}C_6H_4F_2)GaFAl(O(C_6F_{10})C_6F_5)_3$ = $(1,2\text{-}C_6H_4F_2)GaFAl(phex)_3$

6.2. List of abbreviations and units

a, b, c	unit cell axes
a. u.	atomic units
Å	Ångström
AIM	the theory of atoms in molecules
ATR	attenuated total reflection
b	broad (NMR signal)
BCP	bond critical point
b.p.	boiling point
Bu	butyl
cp	cyclopentadienyl
d	doublet (NMR signal)
DFT	density functional theory
e	electron
Et	ethyl
EtCN	propionitrile
F	scattering factor
fc	frozen core
FIA	fluoride ion affinity
F(000)	effective number of electrons in the unit cell
FWHM	full width at half maximum
GA	gas phase acidity
GB	gas phase basicity
GED	gas phase electron diffraction
hfip	hexafluoro^{i}propoxy
hfpp	perfluoro-2-phenyl-^{i}propanoxy
hftb	hexafluoro^{t}butoxy
HF	Hartree-Fock calculation
s	strong (IR band)
HOMO	highest occupied molecular orbital
I	intensity
IL	ionic liquid
K	Kelvin
LUMO	lowest occupied molecular orbital
L	negative Laplacian: $L(r) = -\nabla^2\rho(r)$
LA	ligand affinity
m	medium (IR band)
m	multiplet (NMR signal)
MHz	megahertz
mW	milliwatt
Me	methyl
m.p.	melting point
MP2	Møller-Plesset (second order) calculation
ms	medium strong (IR band)
mw	medium weak (IR band)
NBO	population analysis based on natural bond orbitals
PABOON	population analysis based on occupation numbers
pftb	perfluoro^{t}butoxy
Ph	phenyl
phex	perfluoro-1-phenyl-cyclohexanoxy
pm	picometer
ppm	parts per million
q	quartet (NMR signal)
RT	room temperature

s	singlet (NMR signal)
sh	shoulder (IR band)
t	triplet (NMR signal)
T	temperature
THF	tetrahydrofurane
tol	toluene
U	total energy
U(eq)	isotropic displacement parameter
vs	very strong (IR band)
vw	very weak (IR band)
w	weak (IR band)
WCA	weakly coordinating anion
Z	number of formula units in the unit cell
ZPE	zero point vibrational energy
α, β, γ	unit cell angles
μ	absorption coefficient
δ	chemical shift
ε	permittivity / dielectric constant
θ	scattering angle
ρ	density
σ	standard deviation, also: screening charge density
$\tilde{\nu}$	wave number

6.3. General procedures

6.3.1. Synthetic procedures

All manipulations were carried out in an inert gas atmosphere of argon or nitrogen, using standard vacuum and Schlenk techniques or a glove box (H_2O and O_2 < 1 ppm) to exclude air and moisture. Solvents and liquid reagents were degassed, dried with conventional drying agents (usually P_2O_5 or CaH_2) and distilled afterwards. For some solvents a Grubbs apparatus was used, which utilizes a large solvent reservoir and alumina/catalyst columns to dry and deoxygenate solvents to the desired level of purity. Water contents were checked routinely by Karl-Fischer titration. When a low water content was desired (< 10 ppm), pre-dried solvent was condensed and stored on a suitable drying agent. The solvent was then condensed into the reaction vessel directly from the storage flask. Solid reagents were purified by sublimation (if possible) and stored in airtight vessels or in a glove box. Flasks and reaction vessels containing air- and moisture-sensitive reactions or reagents were sealed with teflon or glass/teflon valves (Schott Produran or J. Young). A cryostat was used to cool reaction vessels and reflux condensers when low temperatures (below 10°C) were desired.

6.3.2. NMR measurements

NMR spectra were recorded in purified deuterated solvents (deuterium content > 99%). Various NMR spectrometers (Bruker AC 250, Bruker AC 200, Bruker Avance 400) as well as different software packages (Bruker XWin-NMR, Bruker Topspin, MestRe-C) were used. Where applicable, a liquid nitrogen evaporator or compressor-fed low-temperature unit was used. Data are referenced against known solvent chemical shifts (^{13}C and ^{1}H), aqueous $AlNO_3$ (^{27}Al), $BF_3 \cdot Et_2O$ (^{11}B) and CF_3Cl (^{19}F). Spectra were recorded at room temperature if not otherwise stated.

6.3.3. IR and Raman spectra

IR samples were prepared as nujol mulls between CsI plates and measured on a Bruker IFS66 or Bruker VERTEX 70 Fourier-transform spectrometer with the OPUS software package. Alternatively, a diamond or ZnSe ATR (attenuated total reflection) cell was used for reflective IR measurements, which were run on a Nicolet Magna-IR 760 Fourier-transform spectrometer with the OMNIC software package. ATR samples were prepared in a glove box under an argon atmosphere. Signal positions and intensities of ATR spectra were corrected for the penetration depth dependence of the frequency, as well as for the refractive index differences between the sample and the window crystal with the advanced ATR correction module of the OMNIC software (using default settings).

Raman samples were prepared in flame sealed glass capillaries in a glove box and recorded on a Bruker RAM II Fourier-transform Raman module (OPUS software package) for the VERTEX 70 spectrometer, equipped with a Nd-YAG laser (excitation wavelength 1064 nm). The laser power output was kept very low (15-50 mW) to prevent sample decomposition and reduce fluorescence. Although the liquid nitrogen cooled germanium detector allows observation of very weak intensities, all spectra were routinely recorded with 1024 or more scans to compensate for the low laser power. Recording of Raman spectra was attempted for all solid products. If no Raman bands are listed for a given compound, the sample did not scatter or the product peaks were obscured by fluorescence. Intensity scales for Raman and IR spectra are in arbitrary units.

6.3.4. Melting points

Melting points were recorded on a Krüss KSPS 1000 digital melting point analyzer. Additionally, the values were double-checked manually with a Laboratory Devices Mel-Temp measuring device. All samples were prepared in flame sealed glass capillaries in a glove box.

6.3.5. Gas phase electron diffraction (GED) study of $C_6F_5(CF_3)_2COH$ (1)

The measurements and refinements were carried out by S. Hayes and R. Berger (group of N. Mitzel, University of Bielefeld). Electron scattering were recorded at room temperature on reusable Fuji imaging plates using a Balzers KD-G 2 Gas-Eldigraph,[342] equipped with a STAIB Instruments electron source, operating at 50 kV with a beam current of 200 nA. Exposed imaging plates were scanned using a commercially available Fuji FLA 1800 scanner, yielding digital 16-bit grey-scale image data. The image data were reduced to total intensities using T. G. Strand’s program PIMAG[343] in connection with a sector curve, which is based on experimental xenon diffraction data and tabulated scattering factors of xenon. Further data reduction, the molecular structure refinement, and the electron wavelength determination (from benzene data) were performed using the ed@ed program (version 2.4).[344] The scattering factors employed were those of Ross et al.[345] Further details about the Bielefeld GED apparatus and methods are to be published elsewhere.[346] Amplitudes of vibration, u_{h1}, and distance corrections for curvilinear perpendicular motion, k_{h1}, were calculated using the program SHRINK,[347] making use of frequency calculations at the B3LYP/6-31G** level of theory,[348, 349] using the Gaussian 03 software package.[350] The GED refinement was performed using the SARACEN method,[351] which uses flexible restraints on parameters for which there is only a little information in the GED data. The restraints were derived from the MP2/TZVPP theoretical geometry, with uncertainties loosely based on the difference between the HF and MP2 geometries. In addition to the geometric parameters, 13 groups of amplitudes of vibration were refined, as was the amplitude for the O–H vibration. These were restrained with uncertainties of 10% of the calculated value.

6.3.6. X-ray structure determination

Single crystals were mounted in high-vacuum grease, perfluoroether oil or motor oil on glass fibers, on top of glass capillaries, on nylon CRYO LOOPS (supplied by Hampton Research) or polyimide MicroMounts (supplied by MiTeGen). Compounds containing the phex ligand were generally mounted in motor oil, because they readily dissolve in perfluoroether oil. Temperature-sensitive compounds were mounted at -30 to -80°C using a custom low-temperature mounting device (Fig. 112).

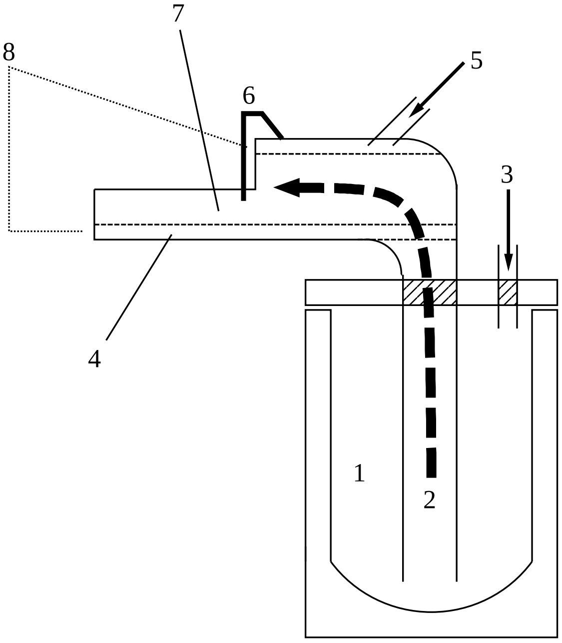

Fig. 112: Low-temperature crystal mounting device. 1: Dewar vessel containing liquid nitrogen; 2: inner tube with cold nitrogen stream; 3: nitrogen gas inlet to pressurize the liquid nitrogen reservoir with valve, controls cold nitrogen stream temperature; 4: outer tube, serves as thermal isolation and pressurized air nozzle, isolated from inner tube; 5: pressurized air inlet (>2 bar); 6: PT100 thermal sensor with digital readout; 7: crystal mounting zone (cold nitrogen stream outlet); 8: pressurized dry air cone, blows atmospheric moisture away from mounting zone, thereby preventing icing of the crystals.

Data were collected on a Stoe IPDS II, a Bruker Kappa APEX II, a Bruker Smart APEX II or a Rigaku R-Axis SPIDER diffractometer using sealed-tube Mo-K_α X-ray sources. During measurements, the crystals were cooled with an Oxford Cryosystems Cryostream model 600 or 700, or a Bruker Kryoflex model 4 low-temperature device at temperatures between 90 and 150 K. Unit cell parameters and measurement strategies were calculated from a least-squares refinement of at least 1000 collected reflections. Structures were solved by the Patterson method, direct methods or dual-space recycling[352] in the SHELXS[353] program or with the charge flipping method as implemented in the PLATON[354] and Superflip[355] programs. Successive interpretation of the difference Fourier maps and refinement against F^2 was carried out within the SHELX97[353] program suite. Unless stated otherwise, all non-hydrogen atoms were assigned anisotropic parameters during the refinement. If all hydrogen atoms were found on the difference Fourier map, they were refined isotropically without positional restraints. If some or all hydrogen positions were not found, all hydrogen atoms were included at calculated positions and refined isotropically based on a riding model. Occasionally, atomic movement in the anions was restricted with SADI, DFIX or DANG constraints.

6.3.7. Quantum chemical calculations

Calculations were carried out with the TURBOMOLE program package (versions 5.7 to 5.10).[356] Calculated compounds were investigated with various density functional (BP86,[357, 358] B3LYP[348, 349, 358]) methods as well as second-order Møller-Plesset (MP2[359, 360]) perturbation calculations. SV(P) and TZVPP[361] basis sets were routinely used and the RI approximation (resolution of identity[359, 360]) was applied where auxiliary basis sets were available. All geometries were optimized in the highest possible point group symmetry. Vibrational frequencies were calculated analytically with the AOFORCE module[362] at the BP86/SV(P) level where possible, for very large systems the spectra were instead calculated numerically with NUMFORCE. The results were used to determine the zero point vibrational energy (ZPE) and to verify that the geometry optimization resulted in a local minimum on the potential energy hypersurface (absence of imaginary frequencies). All energies were corrected by the ZPE except for FIA and LA, which were left uncorrected to obtain values consistent with the recent literature.[266] When thermal corrections to enthalpy and Gibbs free energy were taken into account, the corrections were calculated with the FREEH module, based on the vibrational analysis. Calculations of NMR shifts were performed with the MPSHIFT module[363] (BP86/SV(P) level) or the Gaussian software suite.[350] Corrections to the total energy due to solvation effects were calculated with the COSMO module[338, 339] on the BP86/SV(P) level. Population analyses based on occupation numbers (PABOON)[364, 365] were carried out with the MOLOCH module of TURBOMOLE, whereas NBO (natural bond orbital)[366] population analyses were performed with the RIDFT and DSCF modules (with the "-proper" option). Electrostatic potentials, including core and electronic contributions, were also carried out with RIDFT, after applying COSMO corrections (with ε_r = infinity). Total electron densities were analyzed according to Bader´s *a*toms *i*n *m*olecules (AIM)[309, 337] approach with modified versions of EXTREME,[367] as implemented in the AIMAll[368] and Xaim[369] programs (using the Proaim integration algorithm).[370] In both cases, the results from different methods were compared and found to be within the same ranges for ρ(r) and L(r) at the bond critical points. The chosen methods were BP86/SVP, BP86/6-311++G** and MP2(full)/6-311++G** (single point energies calculated with the Gaussian 03 software package with cartesian 6d/10f definitions of the basis sets[350] on optimized BP86/SV(P) and MP2(fc)/TZVPP geometries taken from TURBOMOLE). Additionally, fully optimized MP2(fc)/TZVPP geometries, calculated with TURBOMOLE 5.10, were analyzed. MP2(full) and DFT calculations from TURBOMOLE proved incompatible with the EXTREME code, probably due to some differing basis set definitions in the core shells. AIMAll and Xaim gave identical results for all methods. However, for the larger molecules only Xaim was used, because it allows to restrict the BCP search to vectors between specified atoms. Analyses of screening charges were carried out with the COSMOthermX program.[371]

6.3.8. Visualization

Molecular graphics from computations and crystal structures without isotropic displacement parameters were plotted with the SCHAKAL-99 program.[372] Crystal structures with thermal ellipsoids were rendered with the program ORTEP-3.[373] Mapping of electrostatic potentials on isosurfaces of the total electron density was performed with the gOpenmol program.[374]

6.4. Syntheses of compounds described in chapter 3

6.4.1. $C_6F_5(CF_3)_2COH$ (1)

2.5 g Mg filings (92.55 mmol) were weighed into a 250 ml round bottom flask fitted with a dropping funnel and reflux condenser (cooled to 0°C). 150 ml diethyl ether were added and the flask suspended in a water bath (10°C). 11.1 ml C_6F_5Br (88.99 mmol) were added dropwise over 30 minutes. The mixture turned turbid, then dark brown from carbon contained in the magnesium. The reaction was then stirred for 16 h at RT. The condenser and flask were cooled to -60°C and gaseous hexafluoroacetone (2 l / 1.23 bar, 109.82 mmol) was condensed into the flask. The flask was allowed to thaw to RT and the mixture was stirred for 12 h. The solvent was removed in vacuo, the product of the Grignard was reaction hydrolyzed with excess aqueous HCl (32%) and the mixture was stirred for 12 h. After removal of HCl / water in vacuo, MgBrCl was removed by filtration and washed twice with 50 ml diethyl ether. The filtrate was separated from the solvent by fractioned distillation. To remove residual diethyl ether, the distillate was again distilled from concentrated H_2SO_4 (b. p. 162°C). Yield: 65 %.
^1H NMR (400 MHz, $CDCl_3$): δ = 4.13 ppm (s). $^{13}C[^1H]$ NMR (101 MHz, $CDCl_3$): δ = 79.1 (m, $^2J_{C,F}$ = 33 Hz), 105.4 (m, $^2J_{C,F}$ = 4 Hz, $^3J_{C,F}$ = 11 Hz), 121.6 (q, $^1J_{C,F}$ = 288 Hz), 138.3 (m, $^1J_{C,F}$ = 253 Hz, $^2J_{C,F}$ = 3 Hz, $^3J_{C,F}$ = 15 Hz), 142.6 (m, $^1J_{C,F}$ = 259 Hz, $^2J_{C,F}$ = 6 Hz, $^3J_{C,F}$ = 13 Hz), 146.3 (d, $^1J_{C,F}$ = 259 Hz) ppm. ^{19}F NMR (376 MHz, $CDCl_3$): δ = -76.2 (t, $^2J_{F,F}$ = 15 Hz), -132.8 (b), -138.4 (b), -148.9 (m, $^3J_{F,F}$ = 23 Hz, $^4J_{F,F}$ = 7 Hz), -160.2 (b) ppm. IR (ZnSe ATR, corrected): $\tilde{\nu}$ = 422 (vw), 449 (vw), 477 (w), 540 (w), 552 (w), 646 (vw), 713 (mw), 733 (m), 744 (mw), 775 (vw), 804 (mw), 944 (m), 956 (m), 988 (m), 1008 (mw), 1110 (m), 1120 (m), 1140 (ms), 1152 (m), 1226 (s), 1275 (ms), 1368 (w), 1420 (w), 1498 (vs), 1533 (ms), 1617 (w), 1654 (mw), 3610 (mw) cm^{-1}.

6.4.2. $C_6F_5(C_6F_{10})OH$ (2)

3.0 g Mg filings (123.43 mmol) were weighed into a 500 ml round bottom flask fitted with a dropping funnel and reflux condenser (cooled to 15°C). 200 ml diethyl ether were added and the flask suspended in an ice bath. 15 ml C_6F_5Br (120.26 mmol) were added dropwise over 30 minutes. The mixture turned turbid, then dark brown from carbon contained in the magnesium. The reaction was then stirred for 16 h at RT. 19 ml perfluorocyclohexanone (116.91 mmol in 20 ml diethyl ether) were added dropwise over 30 minutes. The reaction mixture was refluxed for 4 h and cooled to RT. 30 ml aqueous HCl (32 %) were added and the mixture again refluxed for 2 h. After removal of the solvent and HCl / H_2O in vacuo, the product was isolated by sublimation (10^{-2} mbar, 50°C). Yield: 85 %.

m.p. = 52°C. ^{1}H NMR (400 MHz, $CDCl_3$): δ = 4.20 (t, $J_{H,F}$ = 6.2 Hz) ppm. ^{13}C[^{1}H] NMR (101 MHz, tol-D_8): δ = 78.9 (m, $^2J_{C,F}$ = 26 Hz), 108.1 (b), 109.0 (b), 111.9 (b), 138.0 (d, $^1J_{C,F}$ = 247 Hz), 142.2 (d, $^1J_{C,F}$ = 260), 146.5 (d, $^1J_{C,F}$ = 258) ppm. ^{19}F NMR (376 MHz, tol-D_8): δ = -113.6 (m, $^2J_{F,F}$ = 275 Hz, $^5J_{F,F}$ = 53 Hz), -117.6 (m, $^2J_{F,F}$ = 275 Hz), -121.3 (m, $^2J_{F,F}$ = 284 Hz), -131.1 (m, $^2J_{F,F}$ = 275 Hz), -132.8 (m, $^5J_{F,F}$ = 53 Hz), -135.8 (m, $^2J_{F,F}$ = 275 Hz), -140.6 (m, $^2J_{F,F}$ = 284 Hz), -146.6 (m, $^3J_{F,F}$ = 22 Hz, $^4J_{F,F}$ = 7 Hz), -159.0 (m, $^3J_{F,F}$ = 22 Hz, $^4J_{F,F}$ = 7 Hz) ppm. IR (Diamond ATR, corrected): $\tilde{\nu}$ = 476 (w), 513 (w), 584 (vw), 605 (vw), 622 (vw), 630 (w), 685 (vw), 730 (m), 787 (w), 849 (w), 917 (w), 947 (s), 992 (ms), 1017 (ms), 1034 (mw), 1105 (m), 1116 (m), 1137 (vw), 1155 (w), 1176 (m), 1183 (m), 1213 (s), 1239 (m), 1256 (w), 1307 (m), 1322 (m), 1345 (vw), 1383 (vw), 1405 (w), 1486 (vs), 1536 (m), 1616 (vw), 1651 (m), 3623 (m) cm^{-1}. FT-Raman: $\tilde{\nu}$ = 154 (w), 200 (w), 280 (vw), 291 (vw), 315 (vw), 343 (mw), 376 (m), 412 (vw), 451 (mw), 480 (m), 514 (m), 586 (ms), 630 (vw), 686 (vs), 919 (mw), 1087 (vw), 1139 (w), 1236 (w), 1259 (w), 1299 (w), 1322 (w), 1405 (w), 1652 (mw) cm^{-1}.

6.4.3. $C_6F_5(C_6F_{10})OH\cdot(^nC_4H_9)_4NBr\cdot H_2O$ (2a)

88.8 mg of **2** (0.28 mmol) were mixed with 0.5 g of a reaction mixture obtained in the attempt to synthesize $Li[FAl(O(C_6F_{10})C_6F_5)_3]$ (see 6.4.12). Acetone was added and the mixture stirred at RT for 2 h. After evaporation of the solvent at 80°C the product was recrystallized from $CHCl_3$. Yield (isolated crystals): 21 %.

6.4.4. $LiOC(CF_3)_3\cdot 2THF$ (3)

92 mg $LiBH_4$ (4.23 mmol) were weighed into a 100 ml round bottom flask fitted with a dropping funnel and reflux condenser (cooled to -10°C). 30 ml hexane were added and the flask suspended in an ice bath. 2.4 ml nonafluoro-tert-butanol (17.34 mmol) were added dropwise over 30 minutes (development of hydrogen gas). After stirring for 2 h, the solvent was removed in vacuo, leaving a white powder. **3** was formed by recrystallizing from THF. Yield (before crystallization): 81 %.

^{13}C[^{1}H] NMR (101 MHz, CD_2Cl_2): δ = 122.5 (q, $^1J_{C,F}$ = 292 Hz), 52.8 (m, $^2J_{C,F}$ = 28 Hz) ppm. ^{19}F NMR (376 MHz, CD_2Cl_2): δ = -77.0 (s) ppm. IR (ZnSe ATR, corrected): $\tilde{\nu}$ = 266 (w), 308 (w), 345 (vw), 408 (w), 459 (m), 520 (w), 535 (mw), 571 (w), 667 (vw), 690 (w), 726 (s), 766 (w), 800 (mw), 973 (s), 1008 (m), 1110 (m), 1175 (m), 1198 (m), 1240 (ms), 1261 (s), 1279 (ms), 1304 (ms), 2853 (vs), 2922 (vs), 2956 (vs) cm^{-1}.

6.4.5. $AgO(C_6F_{10})C_6F_5 \cdot EtCN$ (4)

Pentafluorophenylsilver was prepared as described in the literature from AgF and pentafluorophenyltrimethylsilane.[231] 50 mg AgC_6F_5 (0.18 mmol) were weighed into a flask sealed with a greaseless teflon valve. 0.1 ml perfluorocyclohexanone (0.24 mmol) and 20 ml propionitrile were added. After sonicating the mixture for 2 h, the solvent was removed in vacuo. The product was obtained as a white, mildly light-sensitive powder. Yield: 88 %.

^{1}H NMR (400 MHz, CD_2Cl_2): δ = 1.31 (t, $^3J_{H,H}$ = 7.7 Hz), 2.52 (q, $^3J_{H,H}$ = 7.7 Hz) ppm. ^{13}C[^{1}H] NMR (101 MHz, CD_2Cl_2): δ = 10.5 (s), 11.0 (s), 89.3 (b), 125.9 (s) 142.0 (d, $^1J_{C,F}$ = 258 Hz), 145.1 (d, $^1J_{C,F}$ = 260 Hz), 150.6 ppm (d, $^1J_{C,F}$ = 257 Hz). ^{19}F NMR (376 MHz, CD_2Cl_2): δ = -110.1 (m, $^2J_{F,F}$ = 280 Hz, $^5J_{F,F}$ = 20 Hz), -114.9 (m, $^2J_{F,F}$ = 267 Hz), -120.8 (m, $^2J_{F,F}$ = 275 Hz), -131.3 (m, $^5J_{F,F}$ = 20 Hz), -134.6 (m, $^2J_{F,F}$ = 275 Hz), -134.9 (m, $^2J_{F,F}$ = 267 Hz), -139.9 (m, $^2J_{F,F}$ = 280 Hz), -145.0 (m, $^3J_{F,F}$ = 20 Hz, $^4J_{F,F}$ = 10 Hz), -162.1 (m, $^3J_{F,F}$ = 19 Hz, $^4J_{F,F}$ = 7 Hz) ppm.

6.4.6. $LiO(C_6F_{10})C_6F_5$ (5)

90 mg LiH (11.21 mmol) were weighed into a 100 ml round bottom flask fitted with a dropping funnel and reflux condenser (cooled to 15°C). 30 ml diethyl ether were added. 5 g **2** were dissolved in 20 ml diethyl ether and added dropwise over 30 minutes. After refluxing the mixture for 2 h, the solvent was removed in vacuo. The product was obtained as a white powder. Yield: 96 %.

m.p. = 139°C. ^{19}F NMR (235 MHz, CD_2Cl_2): δ = -112.8 (d, $^2J_{F,F}$ = 275 Hz), -116.2 (d, $^2J_{F,F}$ = 273 Hz), -120.8 (d, $^2J_{F,F}$ = 282 Hz), -134.1 (d, $^2J_{F,F}$ = 275 Hz), -135.5 (d, $^2J_{F,F}$ = 273 Hz), -136.6 (b), -140.3 (d, $^2J_{F,F}$ = 282 Hz), -151.1 (b), -160.8 (b) ppm. IR (Diamond ATR, corrected): $\tilde{\nu}$ = 476 (w), 513 (w), 528 (vw), 598 (vw), 606 (vw), 623 (vw), 634 (w), 685 (vw), 731 (m), 752 (vw), 787 (vw), 827 (vw), 849 (w), 916 (mw), 951 (s), 993 (m), 1018 (s), 1036 (mw), 1107 (m), 1140 (w), 1173 (m), 1213 (s), 1240 (ms), 1254 (mw), 1306 (mw), 1321 (m), 1346 (vw), 1385 (vw), 1404 (w), 1485 (vs), 1535 (ms), 1651 (mw) cm^{-1}. FT-Raman: $\tilde{\nu}$ = 146 (w), 156 (w), 198 (w), 279 (vw), 293 (vw), 318 (w), 347 (w), 362 (mw), 376 (ms), 451 (mw), 482 (m), 516 (ms), 586 (s), 630 (vw), 686 (s), 914 (w), 1297 (mw), 1320 (w), 1401 (w), 1652 (w) cm^{-1}.

6.4.7. $NaO(C_6F_{10})C_6F_5$ (6)

2.0 g **2** (4.48 mmol) were dissolved in a saturated solution of NaOH in water and heated to 100°C for 2 h. Water was removed in vacuo and **6** extracted from NaOH with hot toluene. The product crystallized upon cooling of the solvent (colorless crystals).

IR (diamond ATR, corrected): $\tilde{\nu}$ = 102 (ms), 122 (m), 148 (mw), 172 (m), 181 (s), 197 (m), 220 (m), 229 (vs), 256 (mw), 289 (w), 301 (vw), 316 (ms), 326 (mw), 349 (mw), 366 (vw), 390 (w), 411 (w), 432 (w), 471 (m), 482 (mw), 513 (w), 584 (vw), 613 (w), 628 (w), 650 (w), 660 (vw), 730 (ms), 784 (m), 849 (w), 903 (m), 949 (s), 1004 (ms), 1012 (ms), 1035 (w), 1090 (ms), 1137 (m), 1151 (m), 1164 (m), 1181 (mw), 1198 (vs), 1232 (ms), 1250 (w), 1260 (w), 1306 (m), 1382 (vw), 1482 (ms), 1524 (m), 1644 (w), 2961 (vw) cm^{-1}. FT-Raman: $\tilde{\nu}$ = 156 (mw), 200 (mw), 219 (vw), 244 (mw), 268 (vw), 291 (mw), 304 (w), 318 (mw), 350 (m), 358 (mw), 374 (m), 395 (w), 435 (w), 451 (m), 482 (mw), 516 (m), 586 (s), 615 (vw), 632 (vw), 651 (vw), 680 (vs), 730 (vw), 786 (vw), 850 (vw), 900 (w), 948 (vw), 960 (vw), 1008 (vw), 1018 (vw), 1095 (w), 1135 (vw), 1159 (w), 1182 (vw), 1209 (vw), 1224 (w), 1234 (w), 1249 (vw), 1295 (mw), 1309 (mw), 1400 (w), 1527 (vw), 1644 (mw), 2757 (w), 2908 (mw), 2939 (vw), 2966 (vw) cm^{-1}.

6.4.8. $NaO(C_6F_{10})C_6F_5{\cdot}C_6F_5(C_6F_{10})OH{\cdot}2H_2O$ (6a)

3.9 g **2** (8.74 mmol) and 118 mg $NaAlH_4$ were weighed into a 100 ml round bottom flask fitted with a reflux condenser (cooled to 15°C). 50 ml hexane (containing ~100 ppm of water) were added and the mixture was refluxed for 5 h. **6a** crystallized upon cooling of the solvent.

6.4.9. $Li[Al(OC(CF_3)_2(C_6F_5))_4]$ (7)

147 mg $LiAlH_4$ (3.88 mmol) were weighed into a 100 ml round bottom flask fitted with a dropping funnel and reflux condenser (cooled to 15°C). 20 ml n-heptane were added. 3 ml **1** (15.51 mmol) were added dropwise over 30 minutes. The reaction was stirred for 14 h, then refluxed for 2 h. After removal of the solvent in vacuo, the product was obtained as a white powder. Yield: 95 %.

$^{13}C[^1H]$ NMR (63 MHz, CD_2Cl_2): δ = 111.7 (s), 123.1 (q, $^1J_{C,F}$ = 292 Hz), 136.3 (s), 140.0 (s), 146.8 (s) ppm. ^{19}F NMR (376 MHz, CD_2Cl_2): δ = -75.8 (s), -132.8 (b), -154.7 (t, $^3J_{C,F}$ = 21 Hz), -164.3 (t, $^3J_{C,F}$ = 18 Hz) ppm. ^{27}Al NMR (78 MHz, CD_2Cl_2): δ = 27.0 (b) ppm. IR (nujol mull between CsI plates): $\tilde{\nu}$ = 436 (w), 512 (vw), 540 (w), 558 (vw), 571 (w), 636 (mw), 713 (ms), 723 (s), 738 (m), 782 (m), 820 (m), 850 (mw), 869 (w), 951 (s), 979 (ms), 993 (ms), 1019 (s), 1114 (s), 1138 (ms), 1166 (ms), 1206 (vs), 1239 (vs), 1259 (vs), 1301 (ms), 1488 (s), 1530 (ms), 1654 (m) cm^{-1}.

6.4.10. $Ag[Al(OC(CF_3)_2(C_6F_5))_4]$ (8) & $[Ag(1,2\text{-}C_2Cl_2H_4)_3][Al(OC(CF_3)_2(C_6F_5))_4]$ (8a)

3.5 g **7** (2.56 mmol) and 358 mg AgF (2.82 mmol) were weighed into a flask sealed with a greaseless teflon valve. 40 ml CH_2Cl_2 were added and the mixture sonicated for 24 h. LiF and excess AgF were removed by filtration and the solvent was removed from the filtrate in vacuo. The product was obtained as a white powder. Side products were removed by recrystallization of the product from 1,2-dichloromethane (yellow, block-shaped crystals). Yield (isolated crystals): 85 %.

^{13}C[^{1}H] NMR (63 MHz, CD_2Cl_2, main product): δ = 81.3 (b), 111.4 (s), 123.0 (q, $^{1}J_{C,F}$ = 292 Hz), 136.1 (s), 140.1 (s), 146.8 (s) ppm. ^{19}F NMR (376 MHz, CD_2Cl_2, main product): δ = -75.7 (s), -132.8 (s), -154.5 (t, $^{3}J_{C,F}$ = 21 Hz), -164.2 (t, $^{3}J_{C,F}$ = 19 Hz) ppm. ^{27}Al NMR (78 MHz, CD_2Cl_2, main product): δ = 24.6 (b) ppm. IR (nujol mull between CsI plates): $\tilde{\nu}$ = 490 (w), 545 (mw), 566 (mw), 637 (w), 656 (vw), 713 (ms), 722 (ms), 742 (ms), 782 (m), 825 (mw), 843 (mw), 881 (vw), 953 (s), 989 (ms), 1018 (ms), 1125 (vs), 1211 (vs), 1253 (vs), 1289 (ms), 1300 (s), 1314 (s), 1489 (vs), 1533 (s), 1654 (m) cm^{-1}.

6.4.11. $Na[Al(OC(CF_3)_2(C_6F_5))_4]$ (9) & $Na[Al(OC(CF_3)_2(C_6F_5))_4]\cdot 1,2\text{-}Cl_2C_2H_4$ (9a)

235 mg $NaAlH_4$ (4.37 mmol) were weighed into a 100 ml round bottom flask fitted with a dropping funnel and reflux condenser (cooled to 15°C). 30 ml toluene were added. 3.3 ml **1** (17.47 mmol) were added dropwise over 30 minutes. The reaction was stirred for 2 h, then refluxed for 20 h. The solvent was removed in vacuo. The product was extracted from the resulting brown oil with 50 ml pentane. After removal of pentane in vacuo, the product was obtained as a light grey powder containing traces of by-products. The neat product was obtained in the form of **8a** by recrystallization from 1,2-dichloroethane. Yield (isolated crystals): 27 %.

^{19}F NMR (376 MHz, CD_2Cl_2, main products): δ = -76.1 (s), -76.9 (s), -133.1 (s), -134.4 (s), -153.3 (t, $^{3}J_{C,F}$ = 22 Hz), -154.9 (t, $^{3}J_{C,F}$ = 22 Hz), -163.4 (t, $^{3}J_{C,F}$ = 21 Hz), -164.6 (t, $^{3}J_{C,F}$ = 20 Hz) ppm. ^{27}Al NMR (104 MHz, 1,2-$C_2D_4Cl_2$, main products): δ = 24.3 (b), 37.1 (b) ppm. IR (nujol mull between CsI plates): $\tilde{\nu}$ = 236 (w), 257 (w), 331 (w), 365 (w), 387 (m), 395 (m), 425 (w), 438 (mw), 453 (mw), 469 (w), 490 (w), 542 (mw), 569 (mw), 637 (w), 670 (w), 714 (mw), 727 (w), 747 (mw), 770 (mw), 800 (s), 835 (mw), 856 (mw), 878 (mw), 956 (m), 991 (m), 1020 (s), 1101 (s), 1120 (s), 1138 (m), 1155 (mw), 1186 (mw), 1215 (m), 1236 (m), 1260 (vs), 1297 (m), 1316 (m), 1494 (m), 1536 (m), 1656 (mw), 2838 (s), 2881 (s), 2945 (s), 2975 (s) cm^{-1}.

6.4.12. $Li[FAl(O(C_6F_{10})C_6F_5)_3]$ (10)

425 mg $LiAlH_4$ (4.37 mmol) and 20 g **2** (44.84 mmol) were weighed into a 100 ml round bottom flask fitted with a dropping funnel and reflux condenser (cooled to 15°C). 100 ml hexane were added. The reaction was stirred for 12 h, then refluxed for 5 h. The solvent was

removed in vacuo and the product was obtained as a white powder. Yield (product **10** and by-product **11**): 99 %.

^{19}F NMR (376 MHz, CDCl$_3$, main product): δ = -113.9 (m, $^2J_{F,F}$ = 275 Hz, $^5J_{F,F}$ = 53 Hz), -117.9 (m, $^2J_{F,F}$ = 267 Hz), -121.6 (m, $^2J_{F,F}$ = 284 Hz), -131.6 (m, $^2J_{F,F}$ = 275 Hz), -133.5 (b), -135.9 (m, $^2J_{F,F}$ = 267 Hz), -140.7 (m, $^2J_{F,F}$ = 284 Hz), -147.5 (t, $^3J_{F,F}$ = 21 Hz), -159.0 (m, $^3J_{F,F}$ = 22 Hz, $^4J_{F,F}$ = 6 Hz) ppm. IR (mixture containing by-products, ZnSe ATR, corrected): $\tilde{\nu}$ = 675 (vw), 710 (vw), 731 (mw), 752 (w), 768 (vw), 800 (vw), 856 (w), 877 (vw), 910 (mw), 953 (vs), 982 (mw), 1018 (vs), 1074 (mw), 1107 (s), 1138 (m), 1173 (ms), 1207 (vs), 1236 (ms), 1286 (w), 1317 (mw), 1379 (w), 1400 (w), 1419 (w), 1456 (mw), 1481 (vs), 1506 (w), 1535 (ms), 1558 (w), 1576 (vw), 1603 (mw), 1616 (w), 1624 (w), 1635 (w), 1653 (mw), 1684 (vw), 1701 (vw), 1734 (vw), 1772 (vw) cm^{-1}.

6.4.13. Ag[FAl(O(C$_6$F$_{10}$)C$_6$F$_5$)$_3$] (12)

2.062 g **10** (1.14 mmol) and 221 mg AgBF$_4$ (1.14 mmol) were weighed into a flask sealed with a greaseless teflon valve. 10 ml CH$_2$Cl$_2$ were added and the mixture sonicated for 15 minutes. The solution turned dark brown. LiBF$_4$ was removed by filtration and extracted twice with CH$_2$Cl$_2$. After removal of the solvent in vacuo the product was obtained as a light grey powder. Side products were removed by recrystallization (**12a**: from CH$_2$Cl$_2$, **12b**: from C$_6$H$_5$F).

^{19}F NMR (376 MHz, CD$_2$Cl$_2$, assigned to **12**): δ = -113.1 (d, $^2J_{F,F}$ = 285 Hz), -117.6 (d, $^2J_{F,F}$ = 282 Hz), -122.4 (d, $^2J_{F,F}$ = 275 Hz), -131.4 (d, $^2J_{F,F}$ = 285 Hz), -133.1 (t, $^5J_{F,F}$ = 53 Hz), -137.7 (d, $^2J_{F,F}$ = 282 Hz), -141.9 (d, $^2J_{F,F}$ = 275 Hz), -154.3 (t, $^3J_{F,F}$ = 21 Hz), -165.0 (t, $^3J_{F,F}$ = 21 Hz) ppm. ^{19}F NMR (376 MHz, CD$_2$Cl$_2$, assigned to **10**): δ = -114.5 (m, $^2J_{F,F}$ = 280 Hz, $^5J_{F,F}$ = 53 Hz), -118.2 (d, $^2J_{F,F}$ = 275 Hz), -122.0 (d, $^2J_{F,F}$ = 282 Hz), -131.6 (d, $^2J_{F,F}$ = 280 Hz), -132.4 (b), -136.5 (d, $^2J_{F,F}$ = 275 Hz), -141.2 (d, $^2J_{F,F}$ = 282 Hz), -147.5 (b), -159.1 (t, $^3J_{F,F}$ = 21 Hz) ppm. ^{19}F NMR (376 MHz, CD$_2$Cl$_2$, assigned to BF$_3$): δ = -127.7 (b) ppm. ^{27}Al NMR (104 MHz, CD$_2$Cl$_2$): δ = 47.6 (b) ppm. IR (mixture containing by-products, ZnSe ATR, corrected): $\tilde{\nu}$ = 685 (vw), 729 (m), 779 (w), 787 (w), 849 (vw), 916 (mw), 945 (vs), 991 (s), 1016 (s), 1034 (mw), 1105 (m), 1115 (m), 1138 (vw), 1155 (w), 1174 (m), 1211 (vs), 1238 (m), 1255 (w), 1306 (w), 1321 (w), 1348 (w), 1385 (vw), 1404 (vw), 1419 (vw), 1458 (vw), 1485 (vs), 1506 (vw), 1535 (mw), 1558 (vw), 1576 (vw), 1616 (vw), 1626 (vw), 1635 (vw), 1653 (mw), 1684 (vw), 1695 (vw), 1716 (vw), 1734 (vw), 1772 (vw) cm^{-1}.

6.4.14. $Li(O(C_6F_{10})C_6F_5))_2GaCl_2\cdot C_6H_5F$ (13)

700 mg **5** (1.55 mmol) and 68 mg $GaCl_3$ (0.39 mmol) were weighed into a flask sealed with a greaseless teflon valve. 10 ml monofluorobenzene were added and the mixture was sonicated for 15 h. LiCl was removed by filtration and extracted twice with monofluorobenzene. After removal of the solvent in vacuo, the product mixture containing **13** and **5** was obtained as a white powder. **13** was isolated by crystallization from C_6H_5F (colorless cubes, **5** also crystallized in the form of colorless platelets).

^{19}F NMR (188 MHz, tol-D_8, signals clearly assigned to **5** omitted): δ = -112.1 (d, $^2J_{F,F}$ = 285 Hz), -115.4 (d, $^2J_{F,F}$ = 276 Hz), -119.9 (d, $^2J_{F,F}$ = 283 Hz), -130.0 (d, $^2J_{F,F}$ = 285 Hz), -134.8 (d, $^2J_{F,F}$ = 276 Hz), -138.9 (b), -139.2 (d, $^2J_{F,F}$ = 283 Hz), - 145.5 (m, $^3J_{F,F}$ = 23 Hz, $^4J_{F,F}$ = 6 Hz), -157.5 (m, $^3J_{F,F}$ = 23 Hz, $^4J_{F,F}$ = 6 Hz) ppm. IR (mixture of **13** and **5**, ZnSe ATR, corrected): $\tilde{\nu}$ = 471 (w), 492 (vw), 525 (w), 559 (vw), 594 (w), 621 (w), 634 (w), 661 (vw), 688 (vw), 700 (vw), 731 (m), 754 (w), 785 (w), 795 (vw), 852 (vw), 914 (mw), 951 (vs), 991 (s), 1014 (s), 1036 (w), 1101 (m), 1122 (w), 1138 (w), 1169 (m), 1207 (vs), 1232 (ms), 1260 (sh), 1311 (m), 1326 (sh), 1477 (vs), 1506 (w), 1533 (m), 1558 (w), 1653 (m) cm^{-1}.

6.4.15. $Li(O(C_6F_{10})C_6F_5))_2GaBr_2\cdot C_6H_5F$ (14)

680 mg **5** (1.50 mmol) and 116 mg $GaBr_3$ (0.38 mmol) were weighed into a flask sealed with a greaseless teflon valve. 10 ml monofluorobenzene were added and the mixture sonicated for 15 h. LiCl was removed by filtration and extracted twice with monofluorobenzene. After removal of the solvent in vacuo, the product mixture containing **14** and **5** was obtained as a white powder. **14** was isolated by crystallization from C_6H_5F (colorless antiprismatic blocks, **5** also crystallized in the form of colorless platelets).

^{19}F NMR (188 MHz, tol-D_8, signals clearly assigned to **5** omitted): δ = -112.3 (m, $^2J_{F,F}$ = 280, $^5J_{F,F}$ = 50 Hz), -116.0 (d, $^2J_{F,F}$ = 273 Hz), -120.3 (d, $^2J_{F,F}$ = 285 Hz), -131.3 (d, $^2J_{F,F}$ = 280 Hz), -135.3 (d, $^2J_{F,F}$ = 273 Hz), -136.5 (b), -140.1 (d, $^2J_{F,F}$ = 285 Hz), - 147.9 (b), -159.3 (b) ppm. IR (mixture of **14** and **5**, ZnSe ATR, corrected): $\tilde{\nu}$ = 474 (w), 515 (w), 527 (vw), 559 (w), 600(vw), 607 (vw), 624 (vw), 633 (w), 658 (vw), 692 (w), 733 (m), 754 (vw), 793 (w), 852 (vw), 906 (mw), 953 (vs), 989 (ms), 1014 (s), 1036 (w), 1103 (m), 1124 (sh), 1134 (w), 1174 (m), 1209 (vs), 1229 (sh), 1252 (w), 1311 (m), 1383 (vw), 1398 (vw), 1479 (vs), 1506 (vw), 1535 (m), 1558 (vw), 1653 (mw) cm^{-1}.

6.4.16. $Al(O(C_6F_{10})C_6F_5)_3$ (15)

121 mg $AlMe_3$ (2 M solution in hexane, 2.23 mmol) were weighed into a 100 ml round bottom flask fitted with a dropping funnel and reflux condenser (cooled to 15°C). The flask

was cooled to 0°C and 20 ml monofluorobenzene were added. 3.0 g **2** (6.72 mmol), dissolved in 20 ml monofluorobenzene were slowly added dropwise. The reaction was stirred for 3 h at 5°C and the solvent removed in vacuo. The product was obtained as a white powder. Yield: 82 %.

^{19}F NMR (376 MHz, tol-D$_8$): δ = -113.5 (m, $^2J_{F,F}$ = 275, $^5J_{F,F}$ = 54 Hz), -117.5 (d, $^2J_{F,F}$ = 275 Hz), -121.2 (d, $^2J_{F,F}$ = 283 Hz), -131.0 (d, $^2J_{F,F}$ = 275 Hz), -132.8 (t, $^2J_{F,F}$ = 54 Hz), -135.7 (d, $^2J_{F,F}$ = 275 Hz), -140.6 (d, $^2J_{F,F}$ = 283 Hz), -146.4 (m, $^3J_{F,F}$ = 22 Hz, $^4J_{F,F}$ = 7 Hz), -158.9 (m, $^3J_{F,F}$ = 22 Hz, $^4J_{F,F}$ = 7 Hz) ppm. IR (ZnSe ATR, corrected): $\tilde{\nu}$ = 675 (vw), 731 (mw), 756 (sh), 789 (vw), 816 (vw), 835 (vw), 854 (vw), 912 (w), 957 (vs), 984 (m), 1018 (ms), 1045 (vw), 1099 (w), 1128 (w), 1159 (sh), 1174 (mw), 1180 (mw), 1215 (vs), 1232 (m), 1252 (m), 1261 (mw), 1273 (sh), 1306 (w), 1321 (mw), 1479 (vs), 1537 (m), 1651 (w), 1657 (w) cm^{-1}. FT-Raman: $\tilde{\nu}$ = 154 (w), 200 (w), 279 (vw), 291 (vw), 316 (w), 343 (m), 376 (ms), 410 (vw), 435 (vw), 451 (m), 480 (m), 514 (s), 586 (s), 607 (vw), 630 (vw), 686 (vs), 919 (w), 950 (vw), 1139 (vw), 1155 (vw), 1178 (vw), 1236 (vw), 1259 (vw), 1299 (w), 1322 (w), 1405 (vw), 1652 (w) cm^{-1}.

6.5. Syntheses of compounds described in chapter 4

6.5.1. $ICS[Al(OC(CF_3)_3)_4]$ (16)

CI_3^+ was prepared in situ according to the literature[4] by mixing 485 mg $Ag[Al(pftb)_4]$ (0.42 mmol), 239 mg CI_4 (0.46 mmol) and 20 ml dichloromethane at RT in a flask sealed with a greaseless teflon valve. Instantly, precipitation of AgI was observed and the solution turned blood red. 130 µm CS_2 (2.09 mmol) were then added and the solution filtrated. To prevent decomposition, the reaction was kept at -20°C. **16** slowly crystallized from dichloromethane solution at -80°C (orange block-shaped crystals), but additionally formation of black iodine crystals was observed. For further characterization, the solvent and iodine were removed in vacuo at RT.

$^{13}C[^1H]$ NMR (63 MHz, CD_2Cl_2, bulk): δ = 46.1 (s), 78.3 (b), 121.3 (q, $^1J_{C,F}$ = 292 Hz), 145.5 (s), 185.9 (s), 192.5 (s, CS_2) ppm. $^{13}C[^1H]$ NMR (63 MHz, CD_2Cl_2, isolated crystals): δ = 65.9 (s), 78.5 (b), 121.3 (q, $^1J_{C,F}$ = 292 Hz), 149.7 (s) ppm. ^{27}Al NMR (78 MHz, CD_2Cl_2, bulk): δ = 36.0 (b) ppm. IR (nujol mull between CsI plates): $\tilde{\nu}$ = 450 (m), 538 (m), 562 (w), 572 (vw), 727 (vs), 756 (w), 803 (vw), 834 (w), 859 (vw), 974 (vs), 1019 (m), 1173 (m), 1219 (s), 1262 (vs), 1302 (ms), 1354 (m), 1465 (w) cm^{-1}.

6.5.2. $Cl_3C_2S_2[Al(OC(CF_3)_3)_4]$ (17)

645 mg $Ag[Al(pftb)_4]$[53] (0.56 mmol) and 47 µl Cl_2CS (0.61 mmol) were weighed into a flask sealed with a greaseless teflon valve. 10 ml CH_2Cl_2 were added and the mixture was stirred at RT for 12 h. After filtration of formed AgCl and removal of the solvent in vacuo, the product was obtained in the form of orange powder. Yield: 96 %. Crystals were obtained by recrystallization from a highly concentrated CH_2Cl_2 solution at -30°C (yellow platelets).

$^{13}C[^1H]$ NMR (63 MHz, CD_2Cl_2): δ = 79.5 (b), 79.8 (s), 121.6 (q, $^1J_{C,F}$ = 293.1 Hz), 171.2 (s, Cl_2CS), 232.5 (s) ppm. ^{19}F NMR (376 MHz, CD_2Cl_2): δ = -75.3 (s) ppm. ^{27}Al NMR (78 MHz, CD_2Cl_2): δ = 33.8 (b) ppm. IR (nujol mull between CsI plates): $\tilde{\nu}$ = 446 (mw), 537 (mw), 561 (mw), 570 (w), 727 (ms), 756 (w), 810 (m), 831 (mw), 843 (w), 973 (s), 998 (w), 1118 (m), 1172 (m), 1222 (vs), 1246 (vs), 1276 (vs), 1299 (s), 1352 (m) cm^{-1}.

6.5.3. $CCl_3[FAl(O(C_6F_{10})C_6F_5)_3]$ (18)

300 mg **12** (0.21 mmol) were weighed into a flask sealed with a greaseless teflon valve. 5 ml CH_2Cl_2 were added and. 30 µl CCl_4 (0.31 mmol) were condensed onto the solution and the mixture kept at -20°C for 48 h. Precipitation of AgCl was observed. After filtration and

removal of the solvent in vacuo at -20°C, the product is obtained in the form of dark white powder.
$^{13}C[^{1}H]$ NMR (50 MHz, CD_2Cl_2): δ = 96.6 (s, CCl_4), 211.6 (s) ppm (anion signals not observed).

6.5.4. $[Ag(P_4)_2][Al(OC(CF_3)_2(C_6F_5))_4]$ (19)

375 mg **8** (0.26 mmol) and 63 mg P_4 (0.51 mmol) were weighed into a flask sealed with a greaseless teflon valve. 10 ml CH_2Cl_2 were added and the mixture was stirred at RT for 12 h. The reaction was then sonicated for 15 minutes. The solution was concentrated by removing most of the solvent in vacuo. **19** crystallized slowly at -80°C (orange pyrophoric needles).
^{31}P NMR (162 MHz, CD_2Cl_2): δ = -500.5 ppm. ^{19}F NMR (376 MHz, CD_2Cl_2): δ = -76.1 (t, $^{2}J_{F,F}$ = 15 Hz), -133.1 (b), -154.8 (m, $^{3}J_{F,F}$ = 21 Hz, $^{4}J_{F,F}$ = 6 Hz), -164.4 (m, $^{3}J_{F,F}$ = 21 Hz, $^{4}J_{F,F}$ = 6 Hz) ppm. ^{27}Al NMR (104 MHz, CD_2Cl_2): δ = 25.9 (b) ppm. FT-Raman: $\tilde{\nu}$ = 362 (w), 383 (vw), 420 (vw), 458 (m), 599 (vs) cm^{-1}.

6.5.5. $[Ag(S_8)(1,2\text{-}C_6H_4F_2)][FAl(O(C_6F_{10})C_6F_5)_3]$ (20)

0.032 g red selenium (0.41 mmol), 0.013 g S_8 (0.41 mmol) and 0.192 g **12** (0.14 mmol) were weighed into a flask sealed with a greaseless teflon valve. 10 ml 1,2-$C_6H_4F_2$ were added and the mixture was sonicated for 15 minutes. Precipitation of red selenium was observed. The brown solution was filtered and the solvent was removed in vacuo. **20** crystallized slowly from CH_2Cl_2 solution at -20°C (yellow crystals).

6.5.6. $CPh_3[ClAl(O(C_6F_{10})C_6F_5)_3]$ (21)

1.769 g of a product mixture containing $Li[FAl(O(C_6F_{10})C_6F_5)_3]$ (**10**), $Al(O(C_6F_{10})C_6F_5)_3$ (**15**), $LiO(C_6F_{10})C_6F_5$ (**5**) and $C_{12}F_{14}O$ (**11**) were weighed into a flask sealed with a greaseless teflon valve. 272 mg Ph_3CCl and 20 ml CH_2Cl_2 were added and the mixture was stirred at RT for 12 h. After removal of the solvent in vacuo, the resulting brown precipitate was washed twice with pentane. The pentane was removed in vacuo, leaving a yellow powder (1.430 g, probably contained also $CPh_3[FAl(O(C_6F_{10})C_6F_5)_3]$).
^{1}H NMR (200 MHz, $CDCl_3$): δ = 7.59 (d, $^{3}J_{H,H}$ = 9 Hz), 7.8 (t, $^{3}J_{H,H}$ = 9 Hz), 8.23 (t, $^{3}J_{H,H}$ = 9 Hz) ppm.

6.5.7. $(1,2\text{-}C_6H_4F_2)GaFAl(O(C_6F_{10})C_6F_5)_3$ (22)

204 mg (0.14 mmol) of $Ag[FAl(O(C_6F_{10})C_6F_5)_3]$ **12** were weighed into a flask sealed with a greaseless teflon valve. 10 mg (0.14 mmol) elemental gallium and 5 ml 1,2-difluorobenzene

were added and the reaction was activated by sonication (15 minutes). The solution was filtered to remove precipitated elemental Ag. Most of the solvent was removed in vacuo and the product crystallized from the concentrated solution (yellow block-shaped crystals).

IR (ZnSe ATR, corrected): $\tilde{\nu}$ =513 (vw), 534 (vw), 546 (vw), 567 (vw), 596 (vw), 604 (vw), 627 (w), 636 (w), 650 (vw), 671 (vw), 729 (w), 752 (mw), 760 (sh), 841 (w), 850 (w), 910 (w), 933 (sh), 955 (m), 1018 (ms), 1034 (w), 1103 (mw), 1140 (w), 1169 (sh), 1192 (sh), 1207 (ms), 1240 (m), 1271 (ms), 1308 (w), 1319 (w), 1348 (sh), 1383 (vw), 1406 (vw), 1456 (vw), 1487 (s), 1508 (vs), 1533 (m), 1603 (vw), 1620 (w), 1651 (w) cm^{-1}. FT-Raman: $\tilde{\nu}$ = 320 (m), 376 (ms), 451 (m), 487 (s), 588 (vs), 599 (w), 626 (vw), 671 (s), 736 (w), 804 (w), 881 (w), 912 (mw), 1079 (vw), 1295 (w), 1315 (vw), 1407 (w), 1556 (w), 1654 (mw), 2937 (mw), 2908 (mw), 2757 (mw) cm^{-1}.

6.6. Simulated and experimental infrared and Raman spectra of compounds described in chapter 3

Tab. 38: IR spectrum of $C_6F_5(CF_3)_2COH$ **1**.

exp. IR [cm^{-1}][a]	**calc. band [cm^{-1}][b]**
422 (vw)	418 (w)
449 (vw)	443 (w)
477 (w)	462 (w)
540 (w), 552 (w)	536 (vw)
646 (vw)	634 (vw)
713 (mw)	708 (mw)
733 (m)	716 (mw)
744 (mw)	333 (vw) + 418 (w)
775 (vw)	763 (vw)
804 (mw)	795 (w)
944 (m)	407 (w) + 536 (vw)
956 (m)	929 (ms)
988 (m)	980 (m)
1008 (mw)	1010 (mw)
1110 (m), 1120 (m)	1111 (mw)
1140 (ms), 1152 (m)	1139 (mw)
1226 (s)	1226 (s)
1275 (ms)	1254 (vs)
1368 (w)	1358 (m)
1420 (w)	1410 (w)
1498 (vs)	1500 (vs)
1533 (ms)	1532 (ms)
1617 (w)	1621 (w)
1654 (mw)	1639 (mw)
3610 (mw)	3543 (m)

[a] ZnSe ATR, corrected; [b] BP86/SV(P), C_1 symmetry, unscaled.

Tab. 39: IR and Raman spectra of $C_6F_5(C_6F_{10})OH$ **2**.

exp. IR [cm^{-1}][a]	**exp. Raman [cm^{-1}]**	**calc. band [cm^{-1}][b,c]**
	154 (w)	147
	200 (w)	196
	280 (vw)	288
	291 (vw)	298
	315 (vw)	308
	343 (mw)	355
	376 (m)	372
	412 (vw)	400
	451 (mw)	459
476 (w)		469 (vw)
	480 (m)	471
513 (w)	514 (m)	499 (vw)
584 (vw)	586 (ms)	586 (vw)
605 (vw)		609 (vw)
622 (vw)		614 (vw)
630 (w)	630 (vw)	622 (vw)
685 (vw)	686 (vs)	667 (vw)
730 (m)		713 (w)
787 (w)		778 (vw)
849 (w)		825 (vw)
917 (w)	919 (mw)	912 (vw)
947 (s)		948 (m)
992 (ms)		1002 (m)
1017 (ms)		1008 (ms)
1034 (mw)		1028 (w)
	1087 (vw)	1094 (w)
1105 (m)		1106 (vw)
1116 (m)		1116 (vw)
1137 (vw)	1139 (w)	1131 (vw)
1155 (w)		1155 (w)
1176 (m)		1167 (w)
1183 (m)		
1213 (s)		1218 (m)
1239 (m)	1236 (w)	1226 (m)
1256 (w)	1259 (w)	1262 (vw)
1307 (m)	1299 (w)	1287 (mw)
1322 (m)	1322 (w)	1301 (w)
1345 (vw)		1333 (vw)
1383 (vw)		1370 (vw)
1405 (w)	1405 (w)	1371 (vw)
1486 (vs)		1488 (vs)
1536 (m)		1531 (m)
1616 (vw)		1620 (vw)
1651 (m)	1652 (mw)	1632 (mw)
3623 (m)		3542 (m)

[a] ZnSe ATR, corrected; [b] BP86/SV(P), C_s symmetry, unscaled; [c] Raman intensities cannot be reliably predicted with this method, where applicable only IR intensities are given.

Tab. 40: IR spectrum of $LiOC(CF_3)_3 \cdot 2THF$ **3**.

exp. IR [cm^{-1}][a]	**calc. band [cm^{-1}][b]**
266 (w)	261 (vw)
308 (w)	310 (vw)
345 (vw)	342 (vw)
408 (w)	405 (mw)
459 (m)	458 (mw)
520 (w)	517 (vw)
535 (mw)	523 (vw)
571 (w)	567 (vw), 570 (vw)
667 (vw)	667 (vw)
690 (w)	704 (mw)
726 (s)	706 (mw)
766 (w)	742 (w)
800 (mw)	833 (w)
973 (s)	962 (w)
1008 (m)	1020 (w)
1110 (m)	1132 (w), 1134 (w)
1175 (m)	1171 (w), 1173 (w)
1198 (m)	1205 (m), 1218 (vs)
1240 (ms)	1221 (s), 1234 (m)
1261 (s)	1234 (ms)
1279 (ms)	1288 (mw)
1304 (ms)	1310 (w)
2853 (vs)	
2922 (vs)	2933 (m), 2940 (ms)
2956 (vs)	2954 (w), 2970 (w)

[a] Nujol mull between CsI plates; [b] Dimer calculated with BP86/SV(P), C_i symmetry, unscaled.

Tab. 41: IR and Raman spectra of LiO(C_6F_{10})C_6F_5 **5**.

exp. IR [cm^{-1}][a]	**exp. Raman [cm^{-1}]**	**2 IR/Raman [cm^{-1}]**
	146 (w), 156 (w)	-/154 (w)
	198 (w)	-/200 (w)
	279 (vw)	-/280 (vw)
	293 (vw)	-/291 (vw)
	318 (w)	-/315 (vw)
	347 (w)	-/343 (mw)
	362 (mw), 376 (ms)	-/376 (m)
		-/412 (vw)
	451 (mw)	-/451 (mw)
476 (w)		476 (w)/-
	482 (m)	-/480 (m)
513 (w)	516 (ms)	513 (w)/514 (m)
528 (vw)		
598 (vw)	586 (s)	584 (vw)/586 (ms)
606 (vw)		605 (vw)/-
623 (vw)		622 (vw)/-
634 (w)	630 (vw)	630 (w)/630 (vw)
685 (vw)	686 (s)	685 (vw)/686 (vs)
731 (m)		730 (m)/-
752 (vw)		
787 (vw)		787 (w)/-
827 (vw)		
849 (w)		849 (w)/-
916 (mw)	914 (w)	917 (w)/919 (mw)
951 (s)		947 (s)/-
993 (m)		992 (ms)/-
1018 (s)		1017 (ms)/-
1036 (mw)		1034 (mw)/-
		-/1087 (vw)
1107 (m)		1105 (m)/-
		1116 (m)/-
1140 (w)		1137 (vw)/1139 (w)
		1155 (w)/-
1173 (m)		1176 (m)/-
		1183 (m)/-
1213 (s)		1213 (s)/-
1240 (ms)		1239 (m)/1236 (w)
1254 (mw)		1256 (w)/1259 (w)
1306 (mw)	1297 (mw)	1307 (m)/1299 (w)
1321 (m)	1320 (w)	1322 (m)/1322 (w)
1346 (vw)		1345 (vw)/-
1385 (vw)		1383 (vw)/-
1404 (w)	1401 (w)	1405 (w)/1405 (w)
1485 (vs)		1486 (vs)/-
1535 (ms)		1536 (m)/-
		1616 (vw)/-
1651 (mw)	1652 (w)	1651 (m)/1652 (mw)
		3623 (m)/-

[a] ZnSe ATR, corrected.

Tab. 42: IR and Raman spectra of NaO(C_6F_{10})C_6F_5 **6**.

exp. IR [cm^{-1}][a]	**exp. Raman [cm^{-1}]**	**2 IR/Raman [cm^{-1}]**	**exp. IR [cm^{-1}][a]**	**exp. Raman [cm^{-1}]**	**2 IR/Raman [cm^{-1}]**
102 (ms)			1004 (ms)	1008 (vw)	992 (ms)/-
122 (m)			1012 (ms)	1018 (vw)	1017 (ms)/-
148 (mw)	156 (mw)	-/154 (w)	1035 (w)		1034 (mw)/-
172 (m)			1090 (ms)	1095 (w)	-/1087 (vw)
181 (s)					1105 (m)/-
197 (m)	200 (mw)	-/200 (w)			1116 (m)/-
220 (m)	219 (vw)		1137 (m)	1135 (vw)	1137 (vw)/1139 (w)
229 (vs)	244 (mw)		1151 (m)	1159 (w)	1155 (w)/-
256 (mw)	268 (vw)	-/280 (vw)	1164 (m)		1176 (m)/-
289 (w)	291 (mw)	-/291 (vw)	1181 (mw)	1182 (vw)	1183 (m)
301 (vw)	304 (w)		1198 (vs)	1209 (vw)	1213 (s)/-
316 (ms)	318 (mw)	-/315 (vw)	1232 (ms)	1224 (w), 1234 (w)	1239 (m)/1236 (w)
326 (mw)			1250 (w)	1249 (vw)	1256 (w)/1259 (w)
349 (mw)	350 (m), 358 (mw)	-/343 (mw)	1260 (w)		
366 (vw)	374 (m)	-/376 (m)		1295 (mw)	1307 (m)/1299 (w)
390 (w), 411 (w)	395 (w)	-/412 (vw)	1306 (m)	1309 (mw)	1322 (m)/1322 (w)
432 (w)	435 (w), 451 (m)	-/451 (mw)			1345 (vw)/-
471 (m)		476 (w)/-	1382 (vw)		1383 (vw)/-
482 (mw)	482 (mw)	-/480 (m)		1400 (w)	1405 (w)/1405 (w)
513 (w)	516 (m)	513 (w)/514 (m)	1482 (ms)		1486 (vs)/-
584 (vw)	586 (s)	584 (vw)/586 (ms)	1524 (m)	1527 (vw)	1536 (m)/-
613 (w)		605 (vw)/-			1616 (vw)/-
628 (w)		622 (vw)/-	1644 (w)	1644 (mw)	1651 (m)/1652 (mw)
	615 (vw), 632 (vw)	630 (w)/630 (vw)			3623 (m)/-
650 (w)[b]	651 (vw)[b]			2757 (w)[b]	
660 (vw)	680 (vs)	685 (vw)/686 (vs)		2908 (mw)[b]	
730 (ms)	730 (vw)	730 (m)/-		2939 (vw)[b]	
784 (m)	786 (vw)	787 (w)/-	2961 (vw)[b]	2966 (vw)[b]	
849 (w)	850 (vw)	849 (w)/-			
903 (m)	900 (w)	917 (w)/919 (mw)			
949 (s)	948 (vw), 960 (vw)	947 (s)/-			

[a] Diamond ATR, corrected; [b] band of toluene.

Tab. 43: IR spectrum of Li[Al(OC(CF$_3$)$_2$(C$_6$F$_5$))$_4$] **7**.

exp. IR [cm^{-1}][a]	**calc. band [cm^{-1}][b]**	**Li[Al(OC(CF$_3$)$_3$)$_4$] exp. [300]**	**1 exp. [cm^{-1}][c]**
436 (w)	427 (mw)	464 (m)	
512 (vw)	511 (w), 516 (w)		478 (vw)
540 (w)	542 (vw)	539 (m)	540 (vw)
558 (vw)	557 (vw)	546 (mw)	552 (vw)
		562 (mw)	
571 (w)	577 (mw)	572 (m), 582 (m)	
636 (mw)	631 (vw), 636 (vw)		646 (vw)
713 (ms)	708 (mw), 711 (w), 713 (w), 716 (w)		714 (w)
723 (s)	725 (w), 726 (w)	726 (s)	
738 (m)		740 (ms)	734 (m), 744 (w)
782 (m)	772 (w)	756 (m), 760 (m)	775 (vw)
820 (m)	813 (mw), 818 (vw)	798 (m)	804 (mw)
850 (mw)	844 (mw)	844 (ms)	
869 (w)	866 (w)	863 (ms)	
951 (s)	942 (ms), 944 (s)	936 (ms)	944 (mw)
979 (ms)	974 (mw), 976 (mw)	964 (vs)	957 (mw)
993 (ms)	987 (w), 989 (mw)	976 (vs)	988 (mw)
1019 (s)	1016 (w), 1019 (mw), 1021 (w)		1011 (mw)
1114 (s)	1115 (mw), 1118 (ms), 1123 (s)		1110 (mw) 1120 (mw)
1138 (ms)	1136 (m), 1138 (s)		1141 (s)
1166 (ms)	1165 (s)	1184 (ms)	1153 (m)
1206 (vs)	1206 (vs), 1208 (vs), 1210 (s)		
1239 (vs)	1237 (vs), 1244 (ms)	1225 (vs)	1227 (s)
1259 (vs)	1263 (ms)	1243 (s)	
	1264 (vs)	1270 (s)	1276 (m)
1301 (ms)	1289 (vs), 1304 (w), 1309 (m)	1297 (s)	1368 (w)
		1353 (s)	
			1423 (vw)
1488 (s)	1489 (vs), 1492 (s), 1494 (vs)		1498 (ms)
1530 (ms)	1527 (m), 1531 (ms), 1535 (s)		1533 (m)
1654 (m)	1638 (w), 1642 (w), 1644 (w)	1624 (m)	1655 (mw)
			3610 (w)[d]

[a] Nujol mull between CsI plates; [b] BP86/SV(P), C$_1$ symmetry, geometry based on crystal structure, unscaled; [c] ZnSe ATR, corrected; [d] O-H band.

Tab. 44: IR spectrum of $[Ag(1,2\text{-}C_2Cl_2H_4)_3][Al(OC(CF_3)_2(C_6F_5))_4]$ **8a**.

exp. IR [cm^{-1}][a]	**8a calc. band [cm^{-1}][b]**	**$[NEt_4][Al(pftb)_4]$ exp. [cm^{-1}][251]**	**1 exp. [cm^{-1}][c]**
490 (w)	475 (vw)		478 (vw)
545 (mw)	547 (w)	537 (m)	540 (vw)
566 (mw)	551 (w)	562 (mw), 571 (w)	552 (vw)
637 (w)	635 (w)[d]		
656 (vw)	647 (w)		646 (vw)
713 (ms)	715 (w)		714 (w)
722 (ms)	717 (w)	727 (s)	734 (m)
742 (ms)	732 (w)	756 (mw)	744 (w)
782 (m)	767 (w)		775 (vw)
825 (mw)	829 (w)	833 (m)	804 (mw)
843 (mw)	834 (mw)[d]		
881 (vw)	863 (w)[d]		
953 (s)	935 (s)		944 (mw), 957 (mw)
989 (ms)	982 (m)	973 (s)	988 (mw)
1018 (ms)	1015 (m)		1011 (mw)
1125 (vs)	1123 (vs)		1110 (mw), 1120 (mw)
	1149 (mw)		1141 (s)
	1158 (mw)		1153 (m)
1211 (vs)	1209 (vs)	1217 (vs)	
1253 (vs)	1229 (vs), 1281 (vs)	1240 (s), 1254 (s)	1227 (s)
1289 (ms)	1287 (vs)	1277 (vs)	1276 (m)
1300 (s)	1301 (vs)	1299 (s)	
1314 (s)	1301 (vs), 1302 (w)	1353 (ms)	1368 (w)
			1423 (vw)
1489 (vs)	1495 (vs)		1498 (ms)
1533 (s)	1526 (vs)		1533 (m)
1556 (vw)			
1654 (m)	1636 (m)		1655 (mw)
			3610 (w)[e]

[a] Nujol mull between CsI plates; [b] BP86/SV(P), S_4 symmetry, geometry based on crystal structure, unscaled; [c] ZnSe ATR, corrected; [d] bands assigned to the cation; [e] O-H band.

Tab. 45: IR spectrum of Na[Al(OC(CF$_3$)$_2$(C$_6$F$_5$))$_4$] **9**.

exp. IR [cm^{-1}][a]	**8a exp. [cm^{-1}][a]**	**7 exp. [cm^{-1}][a]**	**1 exp. [cm^{-1}][b]**
236 (w), 257 (w), 331 (w)			
365 (w), 387 (m), 395 (m)			
425 (w), 438 (mw)		436 (w)	
453 (mw), 469 (w)			
490 (w)	490 (w)	512 (vw)	478 (vw)
542 (mw)	545 (mw)	540 (w)	540 (vw)
		558 (vw)	552 (vw)
569 (mw)	566 (mw)	571 (w)	
637 (w)	637 (w)	636 (mw)	646 (vw)
670 (w)	656 (vw)		
714 (mw)	713 (ms)	713 (ms)	714 (w)
727 (w)	722 (ms)	723 (s)	734 (m)
747 (mw)	742 (ms)	738 (m)	744 (w)
770 (mw)	782 (m)	782 (m)	775 (vw)
800 (s)	825 (mw)	820 (m)	804 (mw)
835 (mw), 856 (mw)	843 (mw)	850 (mw)	
878 (mw)	881 (vw)	869 (w)	
956 (m)	953 (s)	951 (s)	944 (mw), 957 (mw)
991 (m)	989 (ms)	979 (ms)	988 (mw)
		993 (ms)	
1020 (s)	1018 (ms)	1019 (s)	1011 (mw)
1101 (s), 1120 (s)	1125 (vs)	1114 (s)	1110 (mw), 1120 (mw)
1138 (m)		1138 (ms)	1141 (s)
1155 (mw), 1186 (mw)		1166 (ms)	1153 (m)
1215 (m)	1211 (vs)	1206 (vs)	
1236 (m)		1239 (vs)	1227 (s)
1260 (vs)	1253 (vs)	1259 (vs)	1276 (m)
1297 (m)	1289 (ms)		
	1300 (s)	1301 (ms)	
1316 (m)	1314 (s)		
			1368 (w), 1423 (vw)
1494 (m)	1489 (vs)	1488 (s)	1498 (ms)
1536 (m)	1533 (s)	1530 (ms)	1533 (m)
1656 (mw)	1654 (m)	1654 (m)	1655 (mw)
2838 (s), 2881 (s)[d]			
2945 (s), 2975 (s)[d]			3610 (w)[e]

[a] Nujol mull between CsI plates; [b] ZnSe ATR, corrected; [d] band of residual toluene; [e] O-H band.

Tab. 46: Calculated vibrational spectrum of $C_{12}F_{14}O$ **11**.

calc. band [cm^{-1}][a]	**calc. band of 2 [cm^{-1}][b,c]**	**calc. band [cm^{-1}][a]**	**calc. band of 2 [cm^{-1}][b,c]**
155 (vw), 158 (vw)	147	1006 (mw)	1002 (m)
192 (vw), 200 (vw)	196	1012 (m)	1008 (ms)
286 (vw)	288	1021 (mw)	1028 (w)
294 (vw)	298	1052 (w)	1094 (w)
307 (vw)	308		1106 (vw)[f]
343 (vw)	355	1114 (w)	1116 (vw)
376 (vw)	372	1139 (w)	1131 (vw)
410 (vw)	400	1158 (w)	1155 (w)
438 (vw)	459	1164 (w)	1167 (w)
476 (vw)	469 (vw)	1180 (ms), 1193 (mw)[g]	
485 (vw)	471	1205 (mw), 1209 (mw)[g]	1218 (m)
499 (w)	499 (vw)	1232 (mw)	1226 (m)
547 (w)	586 (vw)	1260 (mw)	1262 (vw)
600 (w), 612 (vw)	609 (vw)	1276 (w), 1280 (mw)	1287 (mw)
616 (w)	614 (vw)	1323 (vw)	1301 (w)
621 (vw)	622 (vw)	1338 (vw)	1333 (vw)
633 (w)			1370 (vw)[f]
654 (w)	667 (vw)		1371 (vw)[f]
710 (mw)[d]	713 (w)[e]	1393 (w)[g]	
771 (w)[d]	778 (vw)[e]	1494 (vs)	1488 (vs)
781 (vw)[d]		1533 (ms)	1531 (m)
	825 (vw)[f]	1619 (vw)	1620 (vw)
863 (vw)[d]		1634 (w)	1632 (mw)
	912 (vw)[f]		3542 (m)
940 (mw)	948 (m)		
963 (s)[d]			

[a] BP86/SV(P), unscaled, all intensities are given because all modes are Raman and IR active due to C_1 symmetry. Because many very weak intensities appear, only those which correspond to modes in **2** or are at least weak were listed for brevity; [b] BP86/SV(P), C_s symmetry, unscaled; [c] Raman intensities cannot be reliably predicted with this method, where applicable only IR intensities are given; [d] modes clearly involving the epoxy function; [e] not observed in the experimental spectrum of **2**; [f] combination modes involving the bridgehead carbon atom. Consequently, these do not appear in the calculated spectrum of **11** because this carbon atom is part of the epoxy function; [g] not observed in spectra of **10**, overlapped by stronger bands of the main product.

Tab. 47: IR and Raman spectra of reaction mixtures of the syntheses of Li[FAl(O(C_6F_{10})C_6F_5)$_3$] **10** and Ag[FAl(O(C_6F_{10})C_6F_5)$_3$] **12**.

10 exp. [cm^{-1}][a]	**12 exp. [cm^{-1}][a]**	**10 exp. [cm^{-1}][a]**	**12 exp. [cm^{-1}][a]**
675 (vw)	685 (vw)	1576 (vw)	1576 (vw)
710 (vw)		1603 (mw)	
731 (mw)	729 (m)	1616 (w)	1616 (vw)
752 (w)		1624 (w)	1626 (vw)
768 (vw)	779 (w)	1635 (w)	1635 (vw)
800 (vw)	787 (w)	1653 (mw)	1653 (mw)
856 (w)	849 (vw)	1684 (vw)	1684 (vw)
877 (vw)		1701 (vw)	1695 (vw), 1716 (vw)
910 (mw)	916 (mw)		
953 (vs)	945 (vs)		
982 (mw)	991 (s)		
1018 (vs)	1016 (s)		
	1034 (mw)		
1074 (mw)			
1107 (s)	1105 (m), 1115 (m)		
1138 (m)	1138 (vw)		
	1155 (w)		
1173 (ms)	1174 (m)		
1207 (vs)	1211 (vs)		
1236 (ms)	1238 (m)		
	1255 (w)		
1286 (w)			
1317 (mw)	1306 (w), 1321 (w)		
1379 (w)	1348 (w), 1385 (vw)		
1400 (w)	1404 (vw)		
1419 (w)	1419 (vw)		
1456 (mw)	1458 (vw)		
1481 (vs)	1485 (vs)		
1506 (w)	1506 (vw)		
1535 (ms)	1535 (mw)		

[a] ZnSe ATR, corrected.

Tab. 48: IR spectra of attempts to synthesize Li[Ga(O(C_6F_{10})C_6F_5)$_4$] **13** and **14**.

exp. 13 [cm^{-1}][a,b]	**exp. 14 [cm^{-1}][a,c]**	**exp. 5 [cm^{-1}][a]**	**exp. 13 [cm^{-1}][a,b]**	**exp. 14 [cm^{-1}][a,c]**	**exp. 5 [cm^{-1}][a]**
471 (w)	474 (w)	476 (w)	1207 (vs)	1209 (vs)	1213 (s)
492 (vw)	515 (w)	513 (w)	1232 (ms)	1229 (sh)	1240 (ms)
525 (w)	527 (vw)	528 (vw)	1260 (sh)	1252 (w)	1254 (mw)
559 (vw)	559 (w)		1311 (m)	1311 (m)	1306 (mw)
594 (w)	600(vw)	598 (vw)	1326 (sh)		1321 (m)
	607 (vw)	606 (vw)	[d]		1346 (vw)
621 (w)	624 (vw)	623 (vw)	[d]	1383 (vw)	1385 (vw)
634 (w)	633 (w)	634 (w)	[d]	1398 (vw)	1404 (w)
661 (vw)	658 (vw)	653 (sh)	1477 (vs)	1479 (vs)	1485 (vs)
688 (vw), 700 (vw)	692 (w)	685 (vw)	1506 (w)	1506 (vw)	
731 (m)	733 (m)	731 (m)	1533 (m)	1535 (m)	1535 (ms)
754 (w)	754 (vw)	752 (vw)	1558 (w)	1558 (vw)	
785 (w)		787 (vw)	1653 (m)	1653 (mw)	1651 (mw)
795 (vw)	793 (w)				
		827 (vw)			
852 (vw)	852 (vw)	849 (w)			
914 (mw)	906 (mw)	916 (mw)			
951 (vs)	953 (vs)	951 (s)			
991 (s)	989 (ms)	993 (m)			
1014 (s)	1014 (s)	1018 (s)			
1036 (w)	1036 (w)	1036 (mw)			
1101 (m)	1103 (m)	1107 (m)			
1122 (w)	1124 (sh)				
1138 (w)	1134 (w)	1140 (w)			
1169 (m)	1174 (m)	1173 (m)			

[a] ZnSe ATR, corrected; [b] from reaction with $GaCl_3$, crystals grown from monofluorobenzene; [c] from reaction with $GaBr_3$, powder obtained after removal of the solvent in vacuo; [d] signals in this region are obscured by signals of coordinated fluorobenzene.

Tab. 49: IR and Raman spectra of $Al(O(C_6F_{10})C_6F_5)_3$ **15**.

exp. IR [cm^{-1}][a]	**exp. Raman [cm^{-1}]**	**calc. band [cm^{-1}][b]**
	154 (w), 200 (w), 279 (vw)	158, 198, 278
	291 (vw), 316 (w), 343 (m)	299, 315, 340
	376 (ms), 410 (vw), 435 (vw)	377, 386, 421
	451 (m), 480 (m), 514 (s)	460, 491, 527
	586 (s), 607 (vw), 630 (vw)	583, 603, 622, 636
675 (vw)	686 (vs)	660 (vw)
731 (mw)		720 (w)
756 (sh)		750 (vw)
789 (vw)		758 (vw)
816 (vw)		800 (vw)
835 (vw)		852 (vw)
854 (vw)		868 (vw)
912 (w)	919 (w)	906 (w)
957 (vs)	950 (vw)	948 (mw)
984 (m)		976 (m)
1018 (ms)		1008 (m)
1045 (vw)		1020 (vw), 1032 (vw)
1099 (w)		1090 (w)
1128 (w)	1139 (vw)	1110 (w)
1159 (sh)	1155 (vw)	1130 (w)
1174 (mw)	1178 (vw)	1152 (w)
1180 (mw)		1162 (w)
1215 (vs)		1186 (s)
1232 (m)	1236 (vw)	1200 (mw)
1252 (m)	1259 (vw)	1218 (m)
1261 (mw)		1226 (mw)
		1246 (m)
1273 (sh)		1264 (mw)
1306 (w)	1299 (w)	1282 (w), 1292 (vw)
1321 (mw)	1322 (w)	1306 (w)
[c]	1405 (vw)	1340 (vw), 1386 (vw), 1404 (vw)
1479 (vs)		1478 (vs)
1537 (m)		1538 (m)
[c]		1612 (w)
1651 (w)		1634 (w)
1657 (w)	1652 (w)	1644 (w)

[a] ZnSe ATR, corrected; [b] calculated with BP86/SV(P), C_1 symmetry, unscaled; [c] no assignment due to very weak bands of 1-fluorobenzene.

6.7. Simulated and experimental infrared and Raman spectra of compounds described in chapter 4

Tab. 50: IR spectrum of ICS[Al(OC(CF_3)$_3$)$_4$] **16**.

exp. IR [cm^{-1}][a]	**calc. band ICS$^+$ [cm^{-1}][b]**	**[NEt$_4$][Al(pftb)$_4$] exp. [cm^{-1}][251]**	**Li[Al(pftb)$_4$] exp. [cm^{-1}][300]**
	304 (vw)		
452 (m)	427 (w)	447 (ms)	464 (m)
537 (m)		537 (m)	539 (m)
			546 (mw)
562 (w)		562 (mw)	562 (mw)
572 (vw)		571 (w)	572 (m), 582 (m)
727 (vs)		727 (s)	726 (s)
			740 (ms)
756 (w)		756 (mw)	756 (m), 760 (m)
805 (vw)			798 (m)
834 (w)		833 (m)	844 (ms)
859 (vw)			863 (ms)
			936 (ms)
			964 (vs)
972 (vs)		973 (s)	976 (vs)
1017 (m)			1017 (mw)
1174 (sh)			1184 (ms)
1221 (s)		1217 (vs)	1225 (vs)
		1240 (s)	1243 (s)
1261 (vs)		1254 (s)	
		1274 (vs)	1270 (s)
1302 (ms)		1298 (s)	1297 (s)
1354 (m)		1353 (ms)	1353 (ms)
1465 (w)	1468 (vs)		

[a] Mull between CsI plates; [b] MP2/TZVPP level, C_{6v} symmetry, unscaled.

Tab. 51: IR spectrum of $Cl_3C_2S_2[Al(OC(CF_3)_3)_4]$ **17**.

exp. IR [cm^{-1}][a]	**calc. band $Cl_3C_2S_2^+$ [cm^{-1}][b]**	**$(Cl_2CS)_2$ [cm^{-1}][375]**	**$[NEt_4][Al(pftb)_4]$ exp. [cm^{-1}][251]**
446 (mw)		443 (m)	448 (m)
537 (mw)		537 (w)	537 (m)
559 (mw)[c]	550 (vw)		
561 (w)			562 (mw)
570 (w)			571 (w)
727 (ms)		683 (w), 702 (mw)	727 (s)
756 (w)	751 (s)	740 (s), 762 (s)	756 (w)
804 (m)[c]	821 (ms)	771 (s), 812 (ms)	
831 (mw)			833 (mw)
973 (s)	978 (w)		973 (vs)
998 (w)			998 (mw)
1111 (m)[c]	1089 (ms)		
1222 (vs)			1217 (vs)
1246 (vs)			1240 (s)
1276 (vs)			1277 (vs)
1299 (s)			1299 (s)
1352 (m)			1353 (ms)

[a] Nujol mull between CsI plates; [b] calculated with BP86/SV(P), C_{2v} symmetry, unscaled; [c] modes of the $Cl_3C_2S_2^+$ cation.

Tab. 52: IR and Raman spectra of $[Ag(P_4)_2][Al(OC(CF_3)_2(C_6F_5))_4]$ **19**.

exp. IR [cm^{-1}][a]	**exp. Raman**	**8a exp. [cm^{-1}][b]**
255 (vw), 283 (vw)	362 (w)	
303 (vw), 314 (vw)	383 (vw)	
326 (w), 418 (w)	420 (vw)	
490 (w)	458 (m)	490 (w)
548 (w)	599 (vs)	545 (mw)
563 (w)		566 (mw)
638 (vw)		637 (w)
		656 (vw)
713 (vw)		713 (ms)
721 (vw)		722 (ms)
743 (w)		742 (ms)
755 (vw)		782 (m)
836 (vw)		825 (mw)
		843 (mw)
		881 (vw)
955 (mw)		953 (s)
992 (w)		989 (ms)
1011 (vw)		
1019 (vw)		1018 (ms)
1123 (mw)		1125 (vs)
1140 (w)		
1167 (vw)		
1202 (vs)		
1216 (m)		1211 (vs)
1248 (m)		1253 (vs)
1269 (vw)		1289 (ms)
1300 (w)		1300 (s)
1309 (w)		1314 (s)
1490 (s)		1489 (vs)
1530 (mw)		1533 (s)
1558 (vw)		1556 (vw)
1655 (w)		1654 (m)

[a] Diamond ATR, corrected; [b] Nujol mull between CsI plates.

Tab. 53: IR and Raman spectra of (1,2-$C_6H_4F_2$)GaFAl(O(C_6F_{10})C_6F_5)$_3$ **22**.

exp. IR [cm^{-1}][a]	**exp. Raman [cm^{-1}][b]**	**calc. band [cm^{-1}][c]**	**10 exp. IR [cm^{-1}][a]**
	320 (m), 376 (ms)	326, 350, 366, 380	
	451 (m), 487 (s)	430, 458, 474, 488	
513 (vw), 534 (vw)		510 (vw), 522 (vw)	
546 (vw), 567 (vw)		578 (w)	
	588 (vs)	588	
596 (vw), 604 (vw)	599 (w)	602 (vw)	
627 (w)	626 (vw)	620 (vw)	
636 (w), 650 (vw)		636 (vw), 652 (vw)	
671 (vw)	671 (s)		675 (vw)
729 (w)	736 (w)	718 (w)	710 (vw), 731 (mw)
752 (mw), 760 (sh)		746 (w), 782 (vw)	752 (w), 768 (vw)
	804 (w)	816	800 (vw)
841 (w), 850 (w)		824 (vw), 838 (vw)	856 (w)
			877 (vw)
910 (w)	912 (mw)	904 (w)	910 (mw)
933 (sh), 955 (m)		936 (sh), 944 (m)	953 (vs)
			982 (mw)
1018 (ms)		1006 (s)	1018 (vs)
1034 (w)		1020 (w)	
	1079 (vw)	1094	1074 (mw)
1103 (mw)		1102 (w)	1107 (s)
		1110 (vw), 1122 (vw)	
1140 (w), 1169 (sh)		1144 (w), 1154 (vw)	1138 (m)
1171 (sh)		1182 (s)	1173 (ms)
1192 (sh)		1196 (sh)	
1207 (ms)		1210 (w)	1207 (vs)
1240 (m)		1222 (vs)	1236 (ms)
1271 (ms)		1268 (w)	
1290 (vw)		1288 (mw)	1286 (w)
1308 (w)	1295 (w)	1304 (vw)	1317 (mw)
1319 (w)	1315 (vw)	1342 (vw)	
1383 (vw)			1379 (w)
1406 (vw)	1407 (w)	1406 (vw)	1400 (w)
			1419 (w)
1456 (vw)			1456 (mw)
1487 (s)		1484 (vs)	1481 (vs)
1508 (vs)		1492 (w)	1506 (w)
1533 (m)		1532 (m)	1535 (ms)

exp. IR [cm^{-1}][a]	**exp. Raman [cm^{-1}]**[b]	**calc. band [cm^{-1}]**[c]	**10 exp. [cm^{-1}]**[a]
1580 (vw)	1556 (w)		1558 (w)
			1576 (vw)
1603 (vw)			1603 (mw)
1620 (w)		1622 (vw)	1616 (w), 1624 (w)
		1636 (w)	1635 (w)
1651 (w)	1654 (mw)		1653 (mw)
			1684 (vw), 1701 (vw)
			1734 (vw), 1772 (vw)

[a] ZnSe ATR, corrected; [b] bands of 1,2-difluorobenzene at 2937, 2908 and 2757 cm^{-1} omitted, bands below 320 cm^{-1} obscured by fluorescence; [c] model compound GaFAl(phex)$_3$, C_1 symmetry, BP86/SV(P). Raman intensities cannot be reliably predicted with this method, where applicable only IR intensities are given.

6.8. Computational data of calculated species described in chapter 3

Tab. 54: Total energies U and zero-point vibrational energies ZPE (in Hartree) of calculated species.

Species[a]	**Sym.**	**U(BP86)**[b]	**U(BP86)**[c]	**U(MP2)**[c]	**ZPE**[d]
$(CH_3)_3COH$	C_1	-233.47834		-233.20677	0.13088
$(CH_3)_3CO^-$	C_3	-232.86352		-232.58993	0.11509
$(CF_3)_3COH$	C_1	-1126.04299		-1125.45696	0.06419
$(CF_3)_3CO^-$	C_3	-1125.49743		-1124.91411	0.05036
$(CF_3)_2(CH_3)COH$	C_1	-828.53031		-828.05123	0.08683
$(CF_3)_2(CH_3)CO^-$	C_1	-827.96189		-827.48421	0.07245
$(CF_3)_2CHOH$	C_1	-789.24391		-788.82109	0.06034
$(CF_3)_2CHO^-$	C_1	-788.67641		-788.25510	0.04572
CH_3COOH	C_1	-228.90903		-228.70227	0.05928
CH_3COO^-	C_1	-228.34477		-228.14087	0.04622
CF_3COOH	C_1	-526.43041		-526.11827	0.03773
CF_3COO^-	C_1	-525.89393		-525.58698	0.02505
Cu^+		-1640.21528			
hfppH	C_1	-1515.93514	-1517.73230	-1514.99338	0.09853
hfpp$^-$	C_1	-1515.39116	-1517.19489	-1514.44774	0.08383
hfppCu	C_1	-3155.88580			0.08751
phexH	C_1	-2029.22080	-2031.62163	-2027.97082	0.12857
phexH	C_s	-2029.21618	-2031.61741	-2027.96564	0.12801
phex$^-$	C_1	-2028.68964	-2031.09506	-2027.43681	0.11439
phexCu	C_1	-3669.16781			0.11702
$C_{12}F_{14}O$ (epoxide)	C_1	-1928.82668			0.11452
AlF_3	D_{3h}	-541.88982	-542.35907	-541.43588	0.00763
AlH_4^-	T_d	-244.78900			0.02345
H_2	D_6h	-1.16995			0.00971
$\{LiOC(CF_3)_3 \cdot 2THF\}_2$	C_i	-3195.30696			0.57049
OCF_2	C_{2v}	-312.80301	-313.17986	-312.62545	0.01379
OCF_3^-	C_{3v}	-412.63727	-413.15530	-412.43651	0.01542

[a] hfpp = $OC(CF_3)_2C_6F_5$, phex = $O(C_6F_{10})C_6F_5$; [b] SV(P) basis set for all elements; [c] TZVPP basis set for all elements; [d] from a vibrational analysis with NUMFORCE or AOFORCE on BP86/SV(P) level.

Tab. 55: Total energies U and zero-point vibrational energies ZPE (in Hartree) of calculated species.

Species[a]	**Sym.**	**U(BP86)**[b]	**U(BP86)**[c]	**U(MP2)**[c]	**ZPE**[d]
Li[Al(hfpp)$_4$]	C_1	-6311.59388			0.35804
[Al(hfpp)$_4$]$^-$	S_4	-6304.09519			0.35465
[Al(phex)$_4$]$^-$	C_1	-8357.20256			0.47444
[FAl(hfpp)$_3$]$^-$	C_1	-4888.54284			0.26817
[FAl(phex)$_3$]$^-$	C_1	-6428.40445			0.35835
[FAl(phex)$_2$]	C_1	-4399.58939			0.24073
[F$_3$Al(hfpp)]$^-$	C_1	-1982.20361		-1980.84852	0.05541
[F$_3$Al(phex)]$^-$	C_1	-2570.69426	-2573.55072	-2568.98875	0.12614
[HAl(phex)$_3$]$^-$	C_3	-6329.14537			0.36228
[H$_2$Al(phex)$_2$]$^-$	C_1	-4301.02451			0.24994
[H$_3$Al(phex)]$^-$	C_1	-2272.91166			0.13737
Al(phex)$_3$	C_1	-6328.44800			0.35731

[a] hfpp = $OC(CF_3)_2C_6F_5$, phex = $O(C_6F_{10})C_6F_5$; [b] SV(P) basis set for all elements; [c] TZVPP basis set for all elements; [d] from a vibrational analysis with NUMFORCE or AOFORCE on BP86/SV(P) level.

6.9. Computational data of calculated species described in chapter 4

Tab. 56: Total energies U and zero-point vibrational energies ZPE (in Hartree) of calculated species.

Species[a]	**Sym.**	**U(BP86)[b]**	**U(BP86)[c]**	**U(MP2)[c]**	**ZPE[d]**
Ag^+	D_{6h}	-146.75968	-146.75985	-145.85066	
AgF	C_{6v}	-246.82307	-246,953201	-246.22101	0.00107
AgCl	C_{6v}	-607.21035	-607.37048	-606.23344	0.00068
AgBr	C_{6v}	-2721.24748	-2721.56144	-2719.12161	0.00048
AgI	C_{6v}	-158.57969	-158.58348	-157.86741	0.00040
OCF_2	C_{2v}	-312.80301	-313.17986	-312.62545	0.01379
OCF_3^-	C_{3v}	-412.63727	-413.15530	-412.43651	0.01542
GaF	C_{6v}	-2024.70778	-2025.08352	-2023.24249	0.00145
CO	C_{6v}	-113.23006		-113.13879	0.00490
$GaFAl(phex)_3$	C_1	-8353.19833			0.35855
$GaAlF_4$	C_{2v}	-2566.67588			0.01083
$GaAlF_4$	C_{3v}	-2566.67001			0.01072
S_8	D_{4d}	-3184.99120	-3186.11937	-3181.72527	0.01087
CI_3^+	D_{3h}	-72.10456	-72.16638	-71.65830	0.00503
CI_4	T_d	-83.86455	-83.92814	-83.29638	0,00500
CS_2	D_{6h}	-834.32063	-833.44808	-833.44809	0.00713
CS	C_{6v}	-436.10807	-435.64984	-435.64984	0.00288
I_2	D_{6h}	-22.92997	-22.93810	-22.65132	0.00047
$CS_2I_3^+$	C_s	-868.40046	-868.73981	-867.13573	0.00879
$CS_2Br_3^+$	C_s	-8556.41019	-8557.67544	-8550.87646	0.00977
$I_3C_2S_2^+$	C_{2v}	-906.43119	-906.80933	-905.13199	0.01329
FCO^+	C_{6v}	-212.61423	-212.86818	-212.48203	0.00865
$ClCO^+$	C_{6v}	-572.99405	-573.28754	-572.49417	0.00726
$BrCO^+$	C_{6v}	-2687.03059	-2687.47792	-2685.38108	0.00756
ICO^+	C_{6v}	-124.36445	-124.50576	-124.14079	0.00705
F_2CO	C_{2v}	-312.80301	-313.18021	-312.62545	0.01241
ClFCO	C_s	-673.13583	-673.55038	-672.58659	0.01078
BrFCO	C_s	-2787.16167	-2787.73052	-2785.46276	0.01023
IFCO	C_s	-224.48163	-224.74260	-224.20411	0.00982
FCS^+	C_{6v}	-535.57812	-535.88076	-535.08517	0.00812
$ClCS^+$	C_{6v}	-895.94765	-896.28775	-895.08744	0.00610
$BrCS^+$	C_{6v}	-3009.98058	-3010.47390	-3007.97100	0.00553
ICS^+	C_{6v}	-447.30934	-447.49611	-446.72548	0.00513

[a] hfpp = $OC(CF_3)_2C_6F_5$, phex = $O(C_6F_{10})C_6F_5$; [b] SV(P) basis set for all elements; [c] TZVPP basis set for all elements; [d] from a vibrational analysis with NUMFORCE or AOFORCE on BP86/SV(P) level.

Tab. 57: Total energies U and zero-point vibrational energies ZPE (in Hartree) of calculated species.

Species[a]	**Sym.**	**U(BP86)**[b]	**U(BP86)**[c]	**U(MP2)**[c]	**ZPE**[d]
F_2CS	C_{2v}	-635.71696	-636.14167	-635.17588	0.01002
ClFCS	C_s	-996.05034	-996.51213	-995.14039	0.00845
BrFCS	C_s	-3110.07648	-3110.69210	-3108.01725	0.00793
IFCS	C_s	-547.39631	-547.70378	-546.75918	0.00756
$Cl_3C_2S_2^+$	C_{2v}	-2252.37645	-2253.21531	-2250.24150	0.01481
$Cl_3C_2S_2^+$	C_1	-2252.36611	-3010.47390	-3007.97099	0.00614
$(Cl_2CS)_2$	D_{2h}	-2712.76956	-2713.76847	-2710.23829	0.01704
$Cl_5C_3S_3^+$	C_s	-3608.77872	-3610.11299	-3605.38075	0.02518
$(Cl_2CS)_3$	C_{3v}	-4069.16537	-4070.65734	-4065.37578	0.02644

[a] hfpp = $OC(CF_3)_2C_6F_5$, phex = $O(C_6F_{10})C_6F_5$; [b] SV(P) basis set for all elements; [c] TZVPP basis set for all elements; [d] from a vibrational analysis with NUMFORCE or AOFORCE on BP86/SV(P) level.

6.10. Gas phase electron diffraction data of $C_6F_5(CF_3)_2COH$ (1)

Tab. 58: GED data analysis parameters of compound **1**.

Dataset	1	2
R_g	6.43%	7.39%
R_d	4.26%	4.48%
Scale Factor, k	0.764(7)	0.750(11)
Correlation Parameter	0.4904	0.4896
Δs / nm^{-1}	2	2
s_{min} / nm^{-1}	24	56
s_{w1} / nm^{-1}	44	76
s_{w2} / nm^{-1}	136	276
s_{max} / nm^{-1}	158	320
Camera Distance / mm	503.5	252.78
Electron Wavelength / pm	5.36	5.37

Tab. 59: Refined atomic coordinates from GED (in Å).

	x	y	z
C1	2.020767	1.464336	0.000000
C2	2.188311	2.244124	1.166422
F3	1.938997	1.740896	2.379888
C4	2.318667	2.117524	-1.217079
F5	2.203637	1.493678	-2.414952
C6	2.903830	4.183048	-0.096109
C7	2.619737	3.575226	1.132292
F8	2.760056	4.264069	2.269702
C9	2.751505	3.447255	-1.277012
F10	3.018661	4.012915	-2.458770
F11	3.315521	5.450530	-0.140916
C12	1.548853	0.000000	0.000000
C13	2.045131	-0.858542	1.205260
F14	2.048225	-2.153628	0.886434
F15	3.302875	-0.521787	1.536674
F16	1.289167	-0.716234	2.300713
C17	0.000000	0.000000	0.000000
F18	-0.513389	-1.224636	0.145562
F19	-0.515218	0.770103	0.968875
F20	-0.438953	0.485527	-1.179660
O21	1.952537	-0.770852	-1.106031
H22	1.655232	-0.336182	-1.913542

Tab. 60: Inter-atomic distances (r_a), amplitudes of vibration (u_{h1}) and distance corrections for curvilinear perpendicular motion (k_{h1}).

	Amplitude	**r_a [Å]**	**u_{h1} (GED)**	**k_{h1}**	**u_{h1} (B3LYP/6-31G**)**
u22	O(21)-H(22)	0.962(10)	0.069(7)	0.003	0.068
u10	C(6)-F(11)	1.333(2)	0.042(2)	0.001	0.043
u16	C(13)-F(14)	1.333(2)	0.044(Tied to u_{10})	0.001	0.045
u19	C(17)-F(18)	1.335(2)	0.044(Tied to u_{10})	0.001	0.045
u11	C(7)-F(8)	1.337(2)	0.042(Tied to u_{10})	0.001	0.043
u12	C(9)-F(10)	1.337(2)	0.042(Tied to u_{10})	0.001	0.043
u4	C(2)-F(3)	1.337(2)	0.043(Tied to u_{10})	0.001	0.043
u18	C(13)-F(16)	1.338(2)	0.045(Tied to u_{10})	0.001	0.045
u20	C(17)-F(19)	1.340(2)	0.045(Tied to u_{10})	0.001	0.045
u17	C(13)-F(15)	1.343(2)	0.045(Tied to u_{10})	0.001	0.045
u21	C(17)-F(20)	1.349(3)	0.046(Tied to u_{10})	0.001	0.046
u6	C(4)-F(5)	1.355(2)	0.044(Tied to u_{10})	0.001	0.044
u7	C(4)-C(9)	1.399(2)	0.045(Tied to u_{10})	0.001	0.045
u8	C(6)-C(7)	1.399(2)	0.045(Tied to u_{10})	0.001	0.045
u5	C(2)-C(7)	1.399(2)	0.045(Tied to u_{10})	0.001	0.045
u9	C(6)-C(9)	1.400(2)	0.045(Tied to u_{10})	0.001	0.045
u15	C(12)-O(21)	1.407(5)	0.047(Tied to u_{10})	0.002	0.048
u1	C(1)-C(2)	1.412(3)	0.046(Tied to u_{10})	0.001	0.046
u2	C(1)-C(4)	1.413(3)	0.046(Tied to u_{10})	0.001	0.046
u3	C(1)-C(12)	1.538(6)	0.053(Tied to u_{10})	0.001	0.053
u14	C(12)-C(17)	1.549(5)	0.053(Tied to u_{10})	0.002	0.053
u13	C(12)-C(13)	1.560(6)	0.054(Tied to u_{10})	0.001	0.054
u193	C(12)-H(22)	1.938(15)	0.097(Tied to u_{110})	-0.003	0.098
u110	F(5)-H(22)	2.04(16)	0.193(20)	0.087	0.194
u201	F(14)-F(16)	2.153(3)	0.054(2)	0.000	0.058
u223	F(18)-F(19)	2.156(3)	0.055(Tied to u_{201})	0.000	0.059
u200	F(14)-F(15)	2.157(3)	0.054(Tied to u_{201})	0.000	0.059
u208	F(15)-F(16)	2.161(3)	0.055(Tied to u_{201})	0.000	0.060
u224	F(18)-F(20)	2.163(3)	0.055(Tied to u_{201})	0.000	0.059
u227	F(19)-F(20)	2.167(3)	0.055(Tied to u_{201})	0.000	0.059
u198	C(13)-O(21)	2.313(10)	0.071(Tied to u_{62})	0.000	0.067
u62	F(3)-C(7)	2.316(3)	0.063(2)	-0.003	0.060
u97	F(5)-C(9)	2.322(4)	0.063(Tied to u_{62})	-0.003	0.059
u192	C(12)-F(20)	2.359(9)	0.073(Tied to u_{62})	-0.001	0.068
u152	C(9)-F(11)	2.365(3)	0.065(Tied to u_{62})	-0.004	0.061
u112	C(6)-F(10)	2.366(2)	0.065(Tied to u_{62})	-0.004	0.061
u111	C(6)-F(8)	2.366(2)	0.065(Tied to u_{62})	-0.004	0.061
u126	C(7)-F(11)	2.368(3)	0.065(Tied to u_{62})	-0.001	0.061
u44	C(2)-F(8)	2.368(2)	0.065(Tied to u_{62})	-0.002	0.061
u81	C(4)-F(10)	2.368(2)	0.065(Tied to u_{62})	-0.002	0.061
u231	F(20)-H(22)	2.368(129)	0.245(fixed)	0.027	0.245
u221	C(17)-O(21)	2.371(10)	0.072(fixed)	0.000	0.072
u187	C(12)-F(14)	2.379(6)	0.071(Tied to u_{62})	-0.001	0.067
u41	C(2)-C(4)	2.386(5)	0.060(Tied to u_{62})	-0.003	0.056
u188	C(12)-F(15)	2.387(6)	0.074(Tied to u_{62})	-0.001	0.070
u23	C(1)-F(3)	2.394(3)	0.065(Tied to u_{62})	-0.001	0.061
u190	C(12)-F(18)	2.400(7)	0.074(Tied to u_{62})	0.000	0.070
u191	C(12)-F(19)	2.404(7)	0.075(Tied to u_{62})	-0.001	0.070
u124	C(7)-C(9)	2.412(5)	0.058(Tied to u_{62})	-0.003	0.055
u43	C(2)-C(6)	2.417(4)	0.059(Tied to u_{62})	-0.003	0.055
u78	C(4)-C(6)	2.417(4)	0.059(Tied to u_{62})	-0.003	0.055
u24	C(1)-F(5)	2.419(4)	0.063(Tied to u_{62})	-0.001	0.059

u189	C(12)-F(16)	2.421(6)	0.074(Tied to u_{62})	-0.001	0.070
u206	F(14)-O(21)	2.431(13)	0.110(Tied to u_{62})	0.008	0.104
u28	C(1)-C(9)	2.465(5)	0.059(Tied to u_{62})	-0.003	0.055
u26	C(1)-C(7)	2.465(5)	0.059(Tied to u_{62})	-0.003	0.055
u35	C(1)-C(17)	2.493(11)	0.078(Tied to u_{62})	-0.001	0.073
u39	C(1)-O(21)	2.493(11)	0.072(Tied to u_{62})	0.000	0.068
u194	C(13)-C(17)	2.521(14)	0.076(Tied to u_{62})	-0.001	0.072
u222	C(17)-H(22)	2.542(115)	0.179(fixed)	0.002	0.179
u83	C(4)-C(12)	2.555(5)	0.069(Tied to u_{62})	-0.004	0.065
u71	F(3)-F(16)	2.582(17)	0.150(Tied to u_{62})	0.048	0.142
u48	C(2)-C(12)	2.606(5)	0.073(Tied to u_{62})	-0.001	0.069
u31	C(1)-C(13)	2.614(9)	0.075(Tied to u_{62})	-0.001	0.071
u98	F(5)-F(10)	2.642(6)	0.113(Tied to u_{217})	-0.001	0.102
u109	F(5)-O(21)	2.643(23)	0.122(Tied to u_{217})	0.021	0.110
u63	F(3)-F(8)	2.649(5)	0.115(Tied to u_{217})	-0.002	0.104
u40	C(1)-H(22)	2.650(100)	0.175(Tied to u_{217})	0.009	0.158
u93	C(4)-H(22)	2.656(155)	0.212(Tied to u_{217})	0.038	0.192
u217	F(16)-F(19)	2.692(54)	0.189(7)	0.015	0.171
u230	F(20)-O(21)	2.699(29)	0.125(fixed)	0.002	0.125
u164	F(10)-F(11)	2.730(3)	0.120(Tied to u_{217})	-0.008	0.109
u215	F(16)-C(17)	2.731(20)	0.133(Tied to u_{217})	0.005	0.120
u140	F(8)-F(11)	2.736(3)	0.120(Tied to u_{217})	-0.003	0.108
u45	C(2)-C(9)	2.775(4)	0.069(Tied to u_{217})	-0.004	0.062
u79	C(4)-C(7)	2.775(4)	0.069(Tied to u_{217})	-0.004	0.063
u70	F(3)-F(15)	2.777(60)	0.230(Tied to u_{62})	0.023	0.216
u195	C(13)-F(18)	2.788(27)	0.140(Tied to u_{217})	0.002	0.126
u225	F(18)-O(21)	2.795(27)	0.151(Tied to u_{217})	0.001	0.136
u37	C(1)-F(19)	2.795(26)	0.142(Tied to u_{217})	0.000	0.129
u203	F(14)-F(18)	2.809(40)	0.247(Tied to u_{217})	0.007	0.223
u33	C(1)-F(15)	2.816(16)	0.145(Tied to u_{217})	0.004	0.131
u216	F(16)-F(18)	2.840(38)	0.240(Tied to u_{217})	0.005	0.217
u25	C(1)-C(6)	2.854(7)	0.068(Tied to u_{217})	-0.004	0.062
u68	F(3)-C(13)	2.875(23)	0.132(Tied to u_{217})	0.027	0.119
u38	C(1)-F(20)	2.891(28)	0.145(Tied to u_{217})	0.000	0.131
u100	F(5)-C(12)	2.909(7)	0.106(Tied to u_{217})	-0.002	0.096
u92	C(4)-O(21)	2.916(16)	0.100(Tied to u_{217})	0.006	0.091
u74	F(3)-F(19)	2.944(78)	0.432(Tied to u_{217})	0.014	0.391
u213	F(15)-O(21)	2.965(17)	0.164(Tied to u_{217})	-0.005	0.148
u67	F(3)-C(12)	2.973(6)	0.121(Tied to u_{217})	0.003	0.110
u51	C(2)-F(15)	3.008(34)	0.183(Tied to u_{217})	0.014	0.166
u196	C(13)-F(19)	3.037(33)	0.132(Tied to u_{217})	-0.001	0.120
u108	F(5)-F(20)	3.044(76)	0.382(Tied to u_{217})	0.005	0.346
u55	C(2)-F(19)	3.072(45)	0.254(Tied to u_{217})	0.007	0.230
u226	F(18)-H(22)	3.085(181)	0.262(Tied to u_{217})	-0.012	0.237
u202	F(14)-C(17)	3.088(22)	0.161(Tied to u_{217})	-0.005	0.145
u49	C(2)-C(13)	3.111(13)	0.098(Tied to u_{217})	0.008	0.088
u199	C(13)-H(22)	3.160(14)	0.097(fixed)	-0.024	0.097
u91	C(4)-F(20)	3.187(48)	0.237(Tied to u_{217})	0.000	0.215
u34	C(1)-F(16)	3.245(10)	0.123(Tied to u_{217})	-0.004	0.112
u52	C(2)-F(16)	3.301(14)	0.144(Tied to u_{217})	0.012	0.131
u53	C(2)-C(17)	3.330(26)	0.184(Tied to u_{228})	-0.005	0.154
u207	F(14)-H(22)	3.330(47)	0.129(fixed)	-0.026	0.129
u88	C(4)-C(17)	3.350(25)	0.161(Tied to u_{217})	-0.010	0.145
u219	F(16)-O(21)	3.461(9)	0.086(Tied to u_{228})	-0.008	0.073
u72	F(3)-C(17)	3.499(46)	0.320(Tied to u_{228})	-0.001	0.269
u105	F(5)-C(17)	3.559(43)	0.293(Tied to u_{228})	-0.011	0.246

u228	F(19)-O(21)	3.564(8)	0.081(3)	-0.008	0.068
u61	F(3)-C(6)	3.599(4)	0.073(Tied to u_{228})	-0.009	0.061
u94	F(5)-C(6)	3.609(4)	0.073(Tied to u_{228})	-0.009	0.061
u59	F(3)-C(4)	3.628(5)	0.073(Tied to u_{228})	-0.007	0.061
u125	C(7)-F(10)	3.629(4)	0.073(Tied to u_{228})	-0.010	0.061
u138	F(8)-C(9)	3.629(4)	0.073(Tied to u_{228})	-0.009	0.061
u82	C(4)-F(11)	3.631(4)	0.073(Tied to u_{228})	-0.010	0.061
u47	C(2)-F(11)	3.632(4)	0.073(Tied to u_{228})	-0.008	0.061
u42	C(2)-F(5)	3.651(5)	0.073(Tied to u_{228})	-0.007	0.061
u209	F(15)-C(17)	3.668(12)	0.088(Tied to u_{228})	-0.010	0.074
u27	C(1)-F(8)	3.670(4)	0.073(Tied to u_{228})	-0.008	0.062
u29	C(1)-F(10)	3.670(4)	0.074(Tied to u_{228})	-0.007	0.062
u197	C(13)-F(20)	3.686(13)	0.089(Tied to u_{228})	-0.008	0.075
u36	C(1)-F(18)	3.687(10)	0.085(Tied to u_{228})	-0.008	0.072
u32	C(1)-F(14)	3.714(9)	0.095(Tied to u_{228})	-0.008	0.079
u229	F(19)-H(22)	3.757(82)	0.202(Tied to u_{228})	-0.006	0.170
u57	C(2)-O(21)	3.769(11)	0.097(Tied to u_{228})	-0.011	0.082
u214	F(15)-H(22)	3.788(79)	0.203(Tied to u_{228})	-0.029	0.170
u90	C(4)-F(19)	3.789(44)	0.259(Tied to u_{228})	-0.018	0.217
u84	C(4)-C(13)	3.833(12)	0.100(Tied to u_{228})	-0.012	0.084
u153	C(9)-C(12)	3.856(6)	0.079(Tied to u_{228})	-0.010	0.066
u204	F(14)-F(19)	3.864(35)	0.217(Tied to u_{228})	-0.013	0.182
u127	C(7)-C(12)	3.890(6)	0.082(Tied to u_{228})	-0.008	0.069
u56	C(2)-F(20)	3.906(44)	0.252(Tied to u_{228})	-0.015	0.212
u86	C(4)-F(15)	3.923(25)	0.217(Tied to u_{228})	-0.004	0.182
u163	C(9)-H(22)	4.006(162)	0.203(fixed)	0.026	0.203
u58	C(2)-H(22)	4.036(94)	0.159(fixed)	-0.011	0.159
u211	F(15)-F(19)	4.057(33)	0.150(Tied to u_{64})	-0.008	0.139
u218	F(16)-F(20)	4.057(20)	0.123(Tied to u_{64})	-0.006	0.114
u64	F(3)-C(9)	4.105(4)	0.069(3)	-0.011	0.064
u210	F(15)-F(18)	4.105(25)	0.131(Tied to u_{64})	-0.013	0.122
u46	C(2)-F(10)	4.106(4)	0.069(Tied to u_{64})	-0.011	0.064
u80	C(4)-F(8)	4.107(4)	0.070(Tied to u_{64})	-0.011	0.065
u95	F(5)-C(7)	4.123(4)	0.070(Tied to u_{64})	-0.010	0.065
u205	F(14)-F(20)	4.155(34)	0.165(Tied to u_{64})	-0.012	0.153
u130	C(7)-F(15)	4.170(31)	0.229(Tied to u_{64})	0.009	0.212
u30	C(1)-F(11)	4.182(7)	0.069(Tied to u_{64})	-0.011	0.064
u69	F(3)-F(14)	4.188(23)	0.132(Tied to u_{64})	0.020	0.122
u134	C(7)-F(19)	4.188(43)	0.267(Tied to u_{64})	-0.005	0.248
u220	F(16)-H(22)	4.217(39)	0.111(fixed)	-0.027	0.111
u76	F(3)-O(21)	4.279(13)	0.110(Tied to u_{64})	-0.015	0.102
u162	C(9)-O(21)	4.289(15)	0.110(Tied to u_{64})	-0.004	0.102
u101	F(5)-C(13)	4.303(17)	0.104(Tied to u_{64})	-0.015	0.097
u161	C(9)-F(20)	4.328(48)	0.261(Tied to u_{64})	-0.011	0.242
u107	F(5)-F(19)	4.350(58)	0.324(Tied to u_{64})	-0.027	0.300
u113	C(6)-C(12)	4.384(7)	0.075(Tied to u_{64})	-0.012	0.070
u50	C(2)-F(14)	4.405(13)	0.098(Tied to u_{64})	-0.001	0.091
u75	F(3)-F(20)	4.419(57)	0.318(Tied to u_{64})	-0.019	0.294
u73	F(3)-F(18)	4.428(51)	0.292(Tied to $u_{66)}$	-0.003	0.271
u128	C(7)-C(13)	4.467(12)	0.110(Tied to u_{64})	-0.002	0.101
u54	C(2)-F(18)	4.496(28)	0.158(Tied to u_{66})	-0.012	0.147
u103	F(5)-F(15)	4.551(36)	0.196(Tied to u_{66})	-0.011	0.182
u132	C(7)-C(17)	4.554(21)	0.165(Tied to u_{66})	-0.015	0.153
u89	C(4)-F(18)	4.564(23)	0.143(Tied to u_{66})	-0.019	0.133
u158	C(9)-C(17)	4.567(20)	0.161(Tied to u_{66})	-0.019	0.150
u106	F(5)-F(18)	4.587(45)	0.259(Tied to u_{64})	-0.017	0.240

u87	C(4)-F(16)	4.612(9)	0.121(Tied to u_{66})	-0.018	0.113
u175	F(10)-H(22)	4.618(169)	0.217(fixed)	0.038	0.217
u131	C(7)-F(16)	4.638(15)	0.146(Tied to u_{66})	0.000	0.136
u66	F(3)-F(11)	4.676(4)	0.082(3)	-0.014	0.076
u99	F(5)-F(11)	4.680(5)	0.081(Tied to u_{66})	-0.016	0.075
u212	F(15)-F(20)	4.715(11)	0.090(Tied to u_{66})	-0.016	0.083
u139	F(8)-F(10)	4.724(4)	0.081(Tied to u_{66})	-0.017	0.075
u85	C(4)-F(14)	4.744(13)	0.118(Tied to u_{66})	-0.022	0.109
u160	C(9)-F(19)	4.746(46)	0.259(Tied to u_{66})	-0.024	0.241
u77	F(3)-H(22)	4.748(56)	0.151(fixed)	-0.026	0.151
u60	F(3)-F(5)	4.797(6)	0.077(Tied to u_{66})	-0.011	0.072
u144	F(8)-F(15)	4.870(40)	0.254(Tied to u_{66})	0.011	0.236
u156	C(9)-F(15)	4.879(36)	0.243(Tied to u_{66})	-0.006	0.226
u135	C(7)-F(20)	4.889(47)	0.250(Tied to u_{66})	-0.022	0.232
u102	F(5)-F(14)	4.895(22)	0.138(Tied to u_{66})	-0.023	0.128
u165	F(10)-C(12)	4.914(5)	0.089(Tied to u_{66})	-0.015	0.082
u136	C(7)-O(21)	4.915(12)	0.103(Tied to u_{66})	-0.017	0.096
u120	C(6)-F(19)	4.917(39)	0.253(Tied to u_{66})	-0.017	0.235
u148	F(8)-F(19)	4.936(53)	0.338(Tied to u_{66})	-0.004	0.315
u141	F(8)-C(12)	4.966(5)	0.090(Tied to u_{66})	-0.012	0.084
u116	C(6)-F(15)	4.983(34)	0.253(Tied to u_{66})	0.000	0.235
u154	C(9)-C(13)	5.001(12)	0.106(Tied to u_{66})	-0.017	0.098
u123	C(6)-H(22)	5.025(149)	0.200(fixed)	0.005	0.200
u137	C(7)-H(22)	5.034(122)	0.182(fixed)	-0.010	0.182
u118	C(6)-C(17)	5.068(12)	0.149(Tied to u_{66})	-0.020	0.139
u121	C(6)-F(20)	5.069(44)	0.250(Tied to u_{66})	-0.020	0.233
u173	F(10)-F(20)	5.070(58)	0.326(Tied to u_{66})	-0.012	0.303
u174	F(10)-O(21)	5.078(18)	0.135(Tied to u_{66})	-0.003	0.125
u122	C(6)-O(21)	5.128(13)	0.112(Tied to u_{66})	-0.014	0.105
u145	F(8)-F(16)	5.195(17)	0.175(Tied to u_{66})	0.008	0.162
u104	F(5)-F(16)	5.261(9)	0.133(Tied to u_{66})	-0.023	0.123
u114	C(6)-C(13)	5.262(11)	0.114(Tied to u_{66})	-0.013	0.106
u142	F(8)-C(13)	5.277(16)	0.135(Tied to u_{66})	0.000	0.125
u65	F(3)-F(10)	5.434(4)	0.075(5)	-0.018	0.066
u96	F(5)-F(8)	5.452(4)	0.076(Tied to u_{65})	-0.018	0.067
u146	F(8)-C(17)	5.535(30)	0.228(Tied to u_{66})	-0.019	0.201
u170	F(10)-C(17)	5.557(30)	0.226(Tied to u_{66})	-0.025	0.199
u157	C(9)-F(16)	5.655(11)	0.135(Tied to u_{66})	-0.023	0.119
u117	C(6)-F(16)	5.669(13)	0.147(Tied to u_{66})	-0.016	0.130
u176	F(11)-C(12)	5.710(7)	0.062(Tied to u_{172})	-0.021	0.072
u129	C(7)-F(14)	5.748(13)	0.097(Tied to u_{172})	-0.013	0.112
u133	C(7)-F(18)	5.788(23)	0.127(Tied to u_{172})	-0.026	0.146
u159	C(9)-F(18)	5.841(19)	0.120(Tied to u_{172})	-0.031	0.138
u172	F(10)-F(19)	5.848(56)	0.252(19)	-0.036	0.292
u149	F(8)-F(20)	5.989(55)	0.272(Tied to u_{150})	-0.032	0.274
u155	C(9)-F(14)	6.013(13)	0.126(Tied to u_{150})	-0.030	0.127
u168	F(10)-F(15)	6.026(32)	0.247(Tied to u_{150})	-0.015	0.249
u150	F(8)-O(21)	6.088(13)	0.107(6)	-0.026	0.107
u183	F(11)-F(19)	6.112(41)	0.262(Tied to u_{150})	-0.026	0.264
u166	F(10)-C(13)	6.145(14)	0.110(Tied to u_{150})	-0.026	0.110
u179	F(11)-F(15)	6.186(25)	0.260(Tied to u_{150})	-0.006	0.262
u186	F(11)-H(22)	6.266(156)	0.208(fixed)	-0.003	0.208
u184	F(11)-F(20)	6.270(46)	0.258(Tied to u_{150})	-0.030	0.259
u151	F(8)-H(22)	6.286(114)	0.181(fixed)	-0.024	0.181
u181	F(11)-C(17)	6.347(13)	0.156(Tied to u_{150})	-0.030	0.157
u119	C(6)-F(18)	6.365(11)	0.125(Tied to u_{150})	-0.034	0.126

u185	F(11)-O(21)	6.416(14)	0.114(Tied to u_{150})	-0.023	0.115
u115	C(6)-F(14)	6.440(11)	0.126(Tied to u_{150})	-0.026	0.127
u177	F(11)-C(13)	6.552(11)	0.116(Tied to u_{150})	-0.021	0.117
u143	F(8)-F(14)	6.589(18)	0.135(Tied to u_{150})	-0.012	0.136
u147	F(8)-F(18)	6.697(35)	0.225(Tied to u_{169})	-0.030	0.204
u171	F(10)-F(18)	6.787(31)	0.216(Tied to u_{169})	-0.039	0.195
u169	F(10)-F(16)	6.892(10)	0.135(8)	-0.034	0.122
u180	F(11)-F(16)	6.909(14)	0.152(Tied to u_{169})	-0.023	0.137
u167	F(10)-F(14)	7.039(17)	0.166(Tied to u_{169})	-0.040	0.150
u182	F(11)-F(18)	7.651(12)	0.175(11)	-0.046	0.145
u178	F(11)-F(14)	7.737(12)	0.172(Tied to u_{182})	-0.037	0.143

6.11. Crystal structure data of compounds described in chapter 3

Tab. 61: Crystal data and structure refinement parameters for compounds **2**, **2a** and **3**.

compound index number	**2**	**2a**	**3**
compound	$\mathbf{C_6F_5(C_6F_{10})OH}$	$\mathbf{C_6F_5(C_6F_{10})OH\cdot({}^nC_4H_9)_4NBr\cdot H_2O}$	$\mathbf{LiOC(CF_3)_3\cdot 2THF}$
sum formula[a]	$C_{12}H_1O_1F_{15}$	$C_{28}H_{39}O_1Br_1F_{15}N_1$	$C_{12}H_{16}F_9Li_1O_3$
T [K]	110(2)	110(2)	95(2)
crystal system	monoclinic	monoclinic	monoclinic
space group	$P2_1/n$	C2/c	$P2_1/n$
a [Å]	12.051(3)	29.328(6)	8.950(2)
b [Å]	15.155(3)	11.145(2)	10.295(2)
c [Å]	15.655(3)	23.694(5)	17.598(4)
α [°]	90	90	90
β [°]	110.91(3)	119.90(3)	96.52(3)
γ [°]	90	90	90
V [$Å^3$]	2670.7(9)	6713.0(2)	1610.9(6)
Z	8	8	4
F(000)	1728	3200	784
ρ (calculated) [g cm^{-3}]	2.219	1.556	1.592
μ [mm^{-1}]	0.283	1.335	0.177
Crystal dimensions [mm]	0.18 x 0.08 x 0.08	0.2 x 0.1 x 0.1	unknown
θ range for data collection [°]	3.03 to 27.46	1.98 to 20.82	6.80 to 24.71
h,k,l index ranges	-13<=h<=15	-28<=h<=28	-10<=h<=10
	-19<=k<=19	-11<=k<=11	-12<=k<=12
	-20<=l<=20	-23<=l<=23	-20<=l<=20
collected reflections	31176	5330	40189
unique reflections	6035	2701	2675
R_{int}	0.0642	0.0986	0.0383
Completeness to θ_{max}	98.6 %	76.7 %	97.6 %
Absorption correction	empirical + spherical	empirical + spherical	empirical + spherical
Data / restraints / parameters	6035 / 0 / 514	2701 / 0 / 434	2675 / 0 / 237
Goodness-of-fit on F^2 (S)	1.046	1.148	1.150
Final R_1 [$I > 2\sigma(I)$]	0.0476	0.0774	0.0306
Final wR_2 [$I > 2\sigma(I)$]	0.1118	0.2074	0.0653
Final R_1 (all data)	0.0665	0.0999	0.0441
Final wR_2 (all data)	0.1218	0.2209	0.0740
Largest peak and hole [e $Å^{-3}$]	0.430 and -0.305	0.385 and -0.382	0.276 and -0.193

[a] Of the monomer, where applicable.

Tab. 62: Crystal data and structure refinement parameters for compounds **4**, **5a** and **5b**.

compound index number	**4**	**5a**	**5b**
compound	**$AgO(C_6F_{10})C_6F_5{\cdot}EtCN$**	**$\{LiO(C_6F_{10})C_6F_5\}_3$**	**$\{(C_6H_5F)LiO(C_6F_{10})C_6F_5\}_2$**
sum formula[a]	$C_{15}H_5O_1F_{15}N_1Ag_1$	$C_{12}O_1F_{15}Li_1$	$C_{18}H_5O_1F_{15}Li_1$
T [K]	100(2)	113(2)	110(2)
crystal system	monoclinic	triclinic	triclinic
space group	$P2_1/c$	P1	$P\bar{1}$
a [Å]	10.319(2)	11.373(2)	7.155(2)
b [Å]	19.050(4)	12.283(3)	11.052(2)
c [Å]	18.071(4)	17.709(3)	11.648(2)
α [°]	90	75.88(3)	94.24(3)
β [°]	93.15(3)	71.54(3)	96.43(3)
γ [°]	90	79.33(3)	99.91(3)
V [$Å^3$]	3547.1(1)	2260.0(8)	897.6(3)
Z	8	2	2
F(000)	2336	1308	536
ρ (calculated) [g cm^{-3}]	2.277	1.993	2.028
μ [mm^{-1}]	1.299	0.251	0.238
Crystal dimensions [mm]	0.4 x 0.3 x 0.3	0.4 x 0.1 x 0.1	0.2 x 0.2 x 0.1
θ range for data collection [°]	6.81 to 24.71	6.81 to 28.28	3.17 to 27.48
h,k,l index ranges	-12<=h<=12	-15<=h<=15	-9<=h<=9
	-21<=k<=21	-15<=k<=16	-14<=k<=14
	-21<=l<=21	-23<=l<=2	-15<=l<=15
collected reflections	44929	29436	31208
unique reflections	5878	18008	4106
R_{int}	0.0442	0.0421	0.0369
Completeness to θ_{max}	97.2 %	97.8 %	99.4 %
Absorption correction	numerical	empirical + spherical	empirical + spherical
Data / restraints / parameters	5878 / 0 / 636	18008 / 3 / 1567	4106 / 0 / 345
Goodness-of-fit on F^2 (S)	1.198	1.030	1.070
Final R_1 [$I > 2\sigma(I)$]	0.0303	0.0621	0.0321
Final wR_2 [$I > 2\sigma(I)$]	0.0523	0.1572	0.0794
Final R_1 (all data)	0.0468	0.0747	0.0403
Final wR_2 (all data)	0.0579	0.1698	0.0830
Largest peak and hole [e $Å^{-3}$]	0.495 and -0.430	0.334 and -0.338	0.459 to -0.282

[a] Of the monomer, where applicable.

Tab. 63: Crystal data and structure refinement parameters for compounds **5c**, **6** and **6a**.

compound index number	**5c**	**6**	**6a**
compound	**$\{(H_2O)LiO(C_6F_{10})C_6F_5\}_2$**	**$NaO(C_6F_{10})C_6F_5\cdot$toluene**	**$NaO(C_6F_{10})C_6F_5\cdot C_6F_5(C_6F_{10})OH$ $\cdot 2H_2O$**
sum formula[a]	$C_{12}H_2O_2F_{15}Li_1$	$C_{18}H_8O_1F_{15}Na_1$	$C_{24}H_5O_4F_{30}Na_1$
T [K]	115(2)	110(2)	110(2)
crystal system	orthorhombic	monoclinic	triclinic
space group	$P2_12_12_1$	$P2_1/c$	$P\bar{1}$
a [Å]	19.170(4)	22.348(5)	9.809(2)
b [Å]	9.839(2)	13.775(3)	10.838(2)
c [Å]	15.696(3)	11.404(2)	15.352(3)
α [°]	90	90	72.75(3)
β [°]	90	92.64(3)	79.15(3)
γ [°]	90	90	73.69(3)°
V [$Å^3$]	2960.4(10)	3506.9(1)	1486.0(5)
Z	8	4	2
F(000)	1824	2008	940
ρ (calculated) [g cm^{-3}]	2.109	1.948	2.159
μ [mm^{-1}]	0.265	0.251	0.283
Crystal dimensions [mm]	0.4 x 0.4 x 0.3	unknown	0.2 x 0.2 x 0.1
θ range for data collection [°]	3.24 to 27.48	4.09 to 23.25	8.79 to 23.26
h,k,l index ranges	-22<=h<=24	-24<=h<=24	-10<=h<=9
	-12<=k<=12	-15<=k<=13	-12<=k<=12
	-20<=l<=19	-12<=l<=11	-17<=l<=15
collected reflections	34916	15069	5236
unique reflections	6687	5009	3345
R_{int}	0.0278	0.0735	0.0514
Completeness to θ_{max}	98.7 %	99.4 %	78.6 %
Absorption correction	empirical + spherical	empirical + spherical	empirical + spherical
Data / restraints / parameters	6687 / 0 / 558	5009 / 0 / 587	3345 / 2 / 551
Goodness-of-fit on F^2 (S)	1.077	1.031	1.784
Final R_1 [I > 2σ(I)]	0.0283	0.0589	0.0758
Final wR_2 [I > 2σ(I)]	0.0617	0.1198	0.0737
Final R_1 (all data)	0.0325	0.1195	0.1049
Final wR_2 (all data)	0.0669	0.1439	0.0770
Largest peak and hole [e $Å^{-3}$]	0.318 and -0.257	0.391 and -0.260	0.831 and -1.383

[a] Of the monomer, where applicable.

Tab. 64: Crystal data and structure refinement parameters for compounds **7**, **8a** and **9a**.

compound index number	**7**	**8a**	**9a**
compound	**$Li[Al(OC(CF_3)_2(C_6F_5))_4]$**	**$[Ag(1,2\text{-}C_2Cl_2H_4)_3]$** **$[Al(OC(CF_3)_2(C_6F_5))_4]$**	**$Na[Al(OC(CF_3)_2(C_6F_5))_4]$** **$\cdot 1,2\text{-}Cl_2C_2H_4$**
sum formula[a]	$C_{36}O_4Al_1F_{44}Li_1$	$C_{43}H_{14}O_4Ag_1Al_1Cl_7F_{44}$	$C_{39}H_6O_4Al_1Cl_3F_{44}Na_1$
T [K]	150(2)	150(2)	100(2)
crystal system	triclinic	orthorhombic	monoclinic
space group	$P\bar{1}$	Fdd2	C2/c
a [Å]	9.608(2)	44.917(9)	14.978(3)
b [Å]	12.214(2)	46.352(9)	16.176(3)
c [Å]	19.738(4)	11.185(2)	41.037(8)
α [°]	83.02(3)	90	90
β [°]	78.49(3)	90	93.67(3)
γ [°]	72.32(3)	90	90
V [$Å^3$]	2156.2(7)	23291(1)	9922(3)
Z	2	16	8
F(000)	1320	14064	5744
ρ (calculated) [g cm^{-3}]	2.104	2.069	1.983
μ [mm^{-1}]	0.282	0.868	0.366
Crystal dimensions [mm]	0.10 x 0.05 x 0.05	0.5 x 0.4 x 0.3	0.3 x 0.3 x 0.2
θ range for data collection [°]	1.75 to 23.04	1.76 to 27.14	1.90 to 24.11
h,k,l index ranges	-9<=h<=10	-57<=h<=57	-11<=h<=17
	-13<=k<=13	-59<=k<=54	-18<=k<=18
	-21<=l<=21	-14<=l<=14	-41<=l<=47
collected reflections	13246	45910	14510
unique reflections	5726	12550	7322
R_{int}	0.0806	0.0524	0.1475
Completeness to θ_{max}	94.5 %	99.3 %	92.7 %
Absorption correction	numerical	numerical	empirical + spherical
Data / restraints / parameters	5726 / 0 / 775	12550 / 1 / 902	14510 / 0 /829
Goodness-of-fit on F^2 (S)	0.894	1.039	0.771
Final R_1 [I > 2σ(I)]	0.0443	0.0367	0.0616
Final wR_2 [I > 2σ(I)]	0.0579	0.0796	0.1365
Final R_1 (all data)	0.0986	0.0473	0.1596
Final wR_2 (all data)	0.0676	0.0832	0.1700
Largest peak and hole [e $Å^{-3}$]	0.219 and -0.240	0.537 and -0.653	0.293 and -0.305

[a] Of the monomer, where applicable.

Tab. 65: Crystal data and structure refinement parameters for compounds **12a**, **12b** and **13**.

compound index number	**12a**	**12b**	**13**
compound	**$[Ag(CH_2Cl_2)_3]$** **$[FAl(O(C_6F_{10})C_6F_5)_3]$**	**$[Ag(C_6H_5F)_3]$** **$[FAl(O(C_6F_{10})C_6F_5)_3]$**	**$Li(O(C_6F_{10})C_6F_5))_2GaCl_2$** **$\cdot C_6H_5F$**
sum formula[a]	$C_{39}H_6O_3Ag_1Al_1Cl_3F_{46}$	$C_{54}H_{15}O_3Al_1Ag_1F_{49}$	$C_{30}H_5O_2Cl_2F_{30}Ga_1Li_1$
T [K]	110(2)	105(2)	103(2)
crystal system	monoclinic	monoclinic	orthorhombic
space group	$P2_1/c$	$P2_1/c$	Fdd2
a [Å]	11.208(2)	11.766(2)	28.370(6)
b [Å]	25.434(5)	25.574(5)	10.831(2)
c [Å]	18.428(4)	19.539(4)	23.403(5)
α [°]	90	90	90
β [°]	93.17(3)	94.24(3)	90
γ [°]	90	90	90
V [$Å^3$]	5245.5(18)	5863(2)	7191(3)
Z	4	4	8
F(000)	3387	3448	4384
ρ (calculated) [g cm^{-3}]	2.234	2.011	2.095
μ [mm^{-1}]	0.952	0.562	1.109
Crystal dimensions [mm]	0.1 x 0.1 x 0.05	0.2 x 0.1 x 0.1	0.2 x 0.2 x 0.1
θ range for data collection [°]	1.37 to 26.37	6.82 to 26.37	2.99 to 27.47
h,k,l index ranges	-14<=h<=14	-14<=h<=14	-36<=h<=36
	-31<=k<=31	-31<=k<=31	-14<=k<=14
	-23<=l<=23	-24<=l<=24	-29<=l<=29
collected reflections	85513	115024	30713
unique reflections	10662	11766	4090
R_{int}	0.0488	0.0859	0.0521
Completeness to θ_{max}	99.5 %	98.1 %	99.6 %
Absorption correction	empirical + spherical	empirical + spherical	empirical + spherical
Data / restraints / parameters	10662 / 0 / 923	11766 / 13 / 1023	4090 / 1 / 317
Goodness-of-fit on F^2 (S)	1.169	1.099	1.050
Final R_1 [$I > 2\sigma(I)$]	0.0585	0.0515	0.0277
Final wR_2 [$I > 2\sigma(I)$]	0.1636	0.1136	0.0530
Final R_1 (all data)	0.0669	0.0975	0.0290
Final wR_2 (all data)	0.1807	0.1340	0.0543
Largest peak and hole [e $Å^{-3}$]	1.811 and -0.667	0.931 and -0.703	0.308 and -0.234

[a] Of the monomer, where applicable.

Tab. 66: Crystal data and structure refinement parameters for compounds **14** and **15**.

compound index number	**14**[b]	**15**
compound	**$Li(O(C_6F_{10})C_6F_5))_2GaBr_2 \cdot C_6H_5F$**	**$Al(O(C_6F_{10})C_6F_5)_3$**
sum formula[a]	$C_{30}H_5O_2Br_2F_{30}Ga_1Li_1$	$C_{36}F_{45}Al_1O_3$
T [K]	110(2)	110(2)
crystal system	monoclinic	monoclinic
space group	Cc	$P2_1/n$
a [Å]	23.505(5)	11.762(2)
b [Å]	10.863(2)	21.807(4)
c [Å]	18.066(4)	16.243(3)
α [°]	90	90
β [°]	128.44(3)	103.31(3)
γ [°]	90	90
V [$Å^3$]	3612.9(13)	4054.1(14)
Z	4	4
F(000)	2136	2632
ρ (calculated) [g cm^{-3}]	2.071	2.232
μ [mm^{-1}]	3.154	0.302
Crystal dimensions [mm]	0.1 x 0.1 x 0.05	0.18 x 0.12 x 0.08
θ range for data collection [°]	6.84 to 23.26	3.06 to 27.48
h,k,l index ranges	0<=h<=26	-15<=h<=15
	0<=k<=12	-28<=k<=28
	-20<=l<=15	-21<=l<=21
collected reflections	5407	49858
unique reflections	2804	9274
R_{int}	0.2018	0.0675
Completeness to $θ_{max}$	93.1 %	99.7 %
Absorption correction	empirical + spherical	empirical + spherical
Data / restraints / parameters	2804 / 2 / 593	9274 / 0 / 766
Goodness-of-fit on F^2 (S)	1.010	1.046
Final R_1 [I > 2σ(I)]	0.0718	0.0526
Final wR_2 [I > 2σ(I)]	0.2008	0.1068
Final R_1 (all data)	0.0861	0.0854
Final wR_2 (all data)	0.2175	0.1206
Largest peak and hole [e $Å^{-3}$]	0.993 and -1.111	0.604 and -0.613

[a] Of the monomer, where applicable; [b] preliminary structure from very weak crystal (probably wrong space group), only isotropic refinement.

Tab. 67: Atomic coordinates (x 10^4) and equivalent isotropic displacement parameters (Å^2 x 10^3) for **2**. U(eq) is defined as one third of the trace of the orthogonalized Uij tensor.

	x	**y**	**z**	**U(eq)**
F(1B)	-52(1)	4145(1)	-606(1)	28(1)
O(1B)	2126(2)	4271(1)	-2331(1)	22(1)
C(1B)	1405(2)	3593(2)	-1188(2)	19(1)
F(1A)	4388(1)	4158(1)	-475(1)	27(1)
C(1A)	5940(2)	3849(2)	-1068(2)	20(1)
F(2B)	468(1)	2979(1)	709(1)	32(1)
C(2B)	808(2)	3570(2)	-566(2)	21(1)
F(2A)	5074(1)	2938(1)	764(1)	32(1)
C(2A)	5351(2)	3692(2)	-459(2)	21(1)
F(3B)	2142(1)	1713(1)	893(1)	34(1)
C(3B)	1057(2)	2953(2)	130(2)	22(1)
F(3A)	6943(1)	1866(1)	920(1)	33(1)
C(3A)	5691(2)	3045(2)	208(2)	22(1)
C(4B)	1899(2)	2310(2)	228(2)	24(1)
F(4A)	8160(1)	2105(1)	-236(1)	37(1)
C(4A)	6637(2)	2509(2)	291(2)	24(1)
F(5B)	2821(1)	2789(1)	-1659(1)	29(1)
F(5A)	7558(1)	3328(1)	-1489(1)	32(1)
C(5A)	7248(2)	2631(2)	-291(2)	25(1)
F(6B)	3(1)	3430(1)	-3120(1)	27(1)
C(6B)	2222(2)	2906(2)	-1082(2)	22(1)
F(6A)	5877(1)	3671(1)	-2933(1)	29(1)
C(6A)	6906(2)	3284(2)	-954(2)	24(1)
F(7B)	-878(1)	4252(1)	-2404(1)	26(1)
C(7B)	1242(2)	4311(2)	-1930(2)	19(1)
F(7A)	4094(1)	3696(1)	-2878(1)	29(1)
C(7A)	5501(2)	4587(2)	-1803(2)	19(1)
F(8B)	489(1)	4792(1)	-3966(1)	30(1)
C(8B)	25(2)	4226(2)	-2720(2)	21(1)
C(8A)	5068(2)	4196(2)	-2786(2)	22(1)
F(9B)	-1347(1)	4893(1)	-4039(1)	31(1)
C(9B)	-206(2)	4945(2)	-3475(2)	22(1)
F(10B)	-4(1)	6452(1)	-3753(1)	35(1)
C(10B)	30(2)	5886(2)	-3080(2)	26(1)
F(11B)	-845(1)	6105(1)	-2771(1)	32(1)
C(12B)	1427(2)	5268(2)	-1545(2)	20(1)
O(1A)	4561(2)	5091(1)	-1739(1)	22(1)
F(14B)	703(1)	5469(1)	-1090(1)	29(1)
F(15B)	2555(1)	5343(1)	-950(1)	28(1)
F(12A)	7059(1)	6531(1)	-2348(1)	32(1)
F(13A)	5245(1)	6556(1)	-2374(1)	29(1)
F(15A)	6676(1)	5717(1)	-877(1)	27(1)
F(13B)	2110(1)	5991(1)	-2622(1)	28(1)
F(12B)	1239(1)	6785(1)	-1890(1)	31(1)
F(10A)	6587(1)	5252(1)	-3567(1)	32(1)
F(4B)	3272(1)	1649(1)	-335(1)	32(1)
F(14A)	7497(1)	4964(1)	-1678(1)	28(1)
F(8A)	4513(1)	4497(1)	-4357(1)	36(1)
F(9A)	3671(1)	5291(1)	-3604(1)	32(1)
C(11B)	1225(2)	5991(2)	-2287(2)	23(1)
C(11A)	6100(2)	6022(2)	-2447(2)	23(1)
C(5B)	2468(2)	2283(2)	-395(2)	24(1)
C(10A)	5652(2)	5617(2)	-3416(2)	27(1)
C(12A)	6466(2)	5307(2)	-1686(2)	21(1)
C(9A)	4703(2)	4902(2)	-3551(2)	25(1)
F(11A)	5214(1)	6267(1)	-4031(1)	33(1)

Tab. 68: Atomic coordinates (x 10^4) and equivalent isotropic displacement parameters (Å^2 x 10^3) for **2a**. U(eq) is defined as one third of the trace of the orthogonalized Uij tensor.

	x	**y**	**z**	**U(eq)**
F(12)	-4742(3)	-4705(6)	-5710(3)	34(2)
F(5)	-3621(3)	-5460(6)	-6284(3)	40(2)
F(7)	-4200(3)	-8701(6)	-5503(3)	38(2)
F(15)	-4626(3)	-5087(6)	-6737(3)	33(2)
F(9)	-4465(3)	-6958(6)	-4904(3)	37(2)
F(14)	-5171(3)	-6576(6)	-7065(3)	34(2)
F(6)	-4971(3)	-8533(6)	-6365(3)	37(2)
F(1)	-4444(3)	-9310(6)	-6791(3)	42(2)
F(11)	-5668(3)	-6992(7)	-6327(3)	39(2)
F(10)	-5381(3)	-5908(7)	-5458(3)	40(2)
O(1)	-3990(3)	-6278(7)	-5561(4)	31(2)
F(2)	-3997(3)	-9768(7)	-7475(4)	51(2)
F(3)	-3378(3)	-8117(8)	-7619(3)	52(2)
F(4)	-3197(3)	-5976(8)	-7010(4)	54(2)
F(8)	-5059(3)	-8333(7)	-5357(3)	44(2)
F(13)	-5497(3)	-4878(7)	-6607(3)	42(2)
C(1)	-4080(4)	-7325(11)	-6513(5)	27(3)
C(12)	-4795(5)	-5997(11)	-6531(5)	29(3)
C(11)	-5061(5)	-5503(11)	-6168(5)	28(3)
C(10)	-5239(5)	-6461(12)	-5847(6)	32(3)
C(4)	-3605(5)	-7889(13)	-7266(6)	37(3)
C(3)	-3921(5)	-8709(11)	-7192(5)	33(3)
C(7)	-4337(5)	-6914(10)	-6117(5)	28(3)
C(2)	-4139(5)	-8424(11)	-6824(5)	34(3)
C(6)	-3742(5)	-6518(13)	-6578(6)	40(4)
C(9)	-4824(5)	-7394(12)	-5483(6)	36(3)
C(5)	-3510(5)	-6809(13)	-6944(6)	40(4)
C(8)	-4581(5)	-7929(11)	-5884(6)	33(3)
N(1)	-3112(4)	-2175(9)	-4214(4)	31(3)
C(1D)	-3152(5)	-1078(10)	-3845(5)	28(3)
C(2B)	-3295(5)	-4439(11)	-4254(5)	32(3)
C(3D)	-3076(6)	1120(11)	-3622(6)	41(4)
C(2D)	-3060(5)	112(11)	-4050(6)	35(3)
C(2C)	-4071(5)	-1917(12)	-5146(5)	35(3)
C(3A)	-1610(5)	-2357(11)	-3473(6)	33(3)
C(4D)	-3604(5)	1210(13)	-3635(6)	43(4)
C(2A)	-2099(5)	-2242(12)	-3447(6)	34(3)
C(1A)	-2569(5)	-2285(11)	-4133(5)	29(3)
C(1C)	-3497(5)	-2074(11)	-4938(5)	28(3)
C(1B)	-3235(5)	-3277(11)	-3928(6)	28(3)
C(4A)	-1109(5)	-2179(14)	-2807(6)	45(3)
C(3C)	-4393(5)	-1865(13)	-5897(6)	42(4)
C(4C)	-4980(5)	-1631(13)	-6139(6)	44(4)
C(3B)	-3339(5)	-5460(11)	-3844(5)	30(3)
C(4B)	-2808(7)	-5696(14)	-3205(7)	59(4)
Br(1)	-2115(1)	-5366(1)	-4460(1)	36(1)
O(2)	-3093(4)	-7246(11)	-4886(5)	33(2)

Tab. 69: Atomic coordinates (x 10^4) and equivalent isotropic displacement parameters (Å^2 x 10^3) for **3**. U(eq) is defined as one third of the trace of the orthogonalized Uij tensor.

	x	**y**	**z**	**U(eq)**
O(1)	944(1)	9483(1)	630(1)	17(1)
F(1)	3896(1)	10129(1)	700(1)	29(1)
F(7)	2986(1)	7018(1)	1748(1)	35(1)
F(4)	353(1)	10183(1)	2043(1)	37(1)
F(3)	3001(1)	11075(1)	1640(1)	34(1)
F(8)	3421(1)	7556(1)	609(1)	32(1)
F(9)	1220(1)	6889(1)	807(1)	31(1)
F(5)	2056(1)	8951(1)	2624(1)	39(1)
F(2)	4441(1)	9387(1)	1840(1)	38(1)
F(6)	95(1)	8105(1)	1980(1)	40(1)
C(1)	1879(2)	9048(2)	1228(1)	19(1)
C(2)	3323(2)	9914(2)	1357(1)	24(1)
Li(1)	160(3)	11186(3)	294(2)	19(1)
C(3)	1101(2)	9077(2)	1980(1)	26(1)
C(4)	2383(2)	7618(2)	1106(1)	23(1)
O(2)	1777(1)	12409(1)	102(1)	22(1)
O(3)	-1187(1)	12093(1)	959(1)	22(1)
C(9)	-794(2)	13030(2)	1564(1)	25(1)
C(8)	1902(2)	13747(2)	347(1)	30(1)
C(10)	-2108(2)	13081(2)	2036(1)	39(1)
C(11A)	-3399(4)	12446(4)	1517(3)	27(1)
C(12)	-2572(2)	11454(2)	1101(1)	27(1)
C(11B)	-2920(20)	11860(20)	1841(12)	50(7)
C(7)	2992(2)	14387(2)	-135(1)	37(1)
C(6)	2844(2)	13563(2)	-855(1)	30(1)
C(5)	2641(2)	12221(2)	-538(1)	28(1)

Tab. 70: Atomic coordinates (x 10^4) and equivalent isotropic displacement parameters (Å^2 x 10^3) for **4**. U(eq) is defined as one third of the trace of the orthogonalized Uij tensor.

	x	**y**	**z**	**U(eq)**
Ag(1)	1645(1)	1941(1)	5414(1)	16(1)
Ag(2)	3651(1)	3252(1)	4847(1)	16(1)
F(17)	1908(2)	3355(1)	6094(1)	21(1)
F(22A)	-395(2)	4395(1)	4010(1)	19(1)
F(13B)	5687(2)	802(1)	6262(1)	20(1)
F(22B)	1611(2)	4347(1)	4450(1)	18(1)
F(26A)	-936(2)	2292(1)	4738(1)	20(1)
F(10B)	4659(2)	3116(1)	6611(1)	21(1)
F(4)	3309(2)	1843(1)	4180(1)	22(1)
F(21)	-2184(2)	4122(1)	4967(1)	22(1)
F(9A)	6235(2)	2887(1)	5480(1)	22(1)
F(26B)	-1894(2)	3147(1)	4126(1)	21(1)
F(25A)	700(2)	2096(1)	3631(1)	21(1)
F(8)	7413(2)	1041(1)	5257(1)	27(1)
F(11B)	4739(2)	2358(1)	7840(1)	29(1)
F(9B)	7197(2)	2032(1)	6093(1)	24(1)
F(23A)	2248(2)	3420(1)	3419(1)	20(1)
F(13A)	3669(2)	847(1)	5839(1)	19(1)
F(24A)	-987(2)	3494(1)	2761(1)	24(1)
F(24B)	638(2)	2860(1)	2415(1)	25(1)
O(14)	1436(2)	2951(1)	4763(1)	13(1)
F(20)	-2918(2)	4456(1)	6279(1)	24(1)
F(25B)	-1302(2)	2201(1)	3203(1)	23(1)
F(18)	1111(2)	3736(1)	7369(1)	22(1)
F(10A)	6665(2)	2994(1)	7017(1)	27(1)
F(23B)	1083(2)	4258(1)	2910(1)	24(1)
F(11A)	6334(2)	1713(1)	7474(1)	27(1)
F(6)	6086(2)	511(1)	2816(1)	30(1)
F(19)	-1303(2)	4268(1)	7519(1)	24(1)
F(5)	3816(2)	1206(1)	2970(1)	26(1)
F(7)	7875(2)	459(1)	4000(1)	30(1)
C(201)	5285(4)	4572(2)	4184(2)	22(1)
O(1)	3862(2)	2250(1)	5497(1)	14(1)
C(101)	-156(4)	732(2)	6151(2)	18(1)
C(23)	1041(4)	3693(2)	3373(2)	17(1)
C(2)	4951(3)	1848(2)	5574(2)	14(1)
C(20)	-1734(3)	4162(2)	6223(2)	17(1)
C(21)	-1334(3)	3968(2)	5535(2)	16(1)
C(3)	5340(4)	1506(2)	4824(2)	16(1)
C(10)	5628(4)	2643(2)	6696(2)	20(1)
N(101)	507(3)	1129(2)	5886(2)	22(1)
C(7)	6756(4)	808(2)	4051(2)	22(1)
C(8)	6484(4)	1129(2)	4712(2)	19(1)
C(102)	-1015(4)	212(2)	6473(2)	23(1)
C(24)	102(4)	3147(2)	3011(2)	19(1)
C(22)	621(3)	3948(2)	4138(2)	15(1)
C(15)	330(3)	3341(2)	4680(2)	14(1)
C(16)	-134(3)	3649(2)	5430(2)	12(1)
C(9)	6024(3)	2340(2)	5943(2)	18(1)
N(201)	4706(3)	4124(2)	4409(2)	24(1)
C(11)	5236(4)	2063(2)	7239(2)	20(1)
C(19)	-936(4)	4077(2)	6851(2)	15(1)
C(5)	4716(4)	1183(2)	3537(2)	19(1)
C(6)	5860(4)	831(2)	3454(2)	22(1)
C(17)	668(3)	3593(2)	6080(2)	16(1)
C(4)	4470(3)	1516(2)	4195(2)	16(1)
C(25)	-288(3)	2557(2)	3537(2)	17(1)

C(18)	283(4)	3796(2)	6771(2)	16(1)
C(26)	-715(3)	2847(2)	4286(2)	16(1)
C(13)	4661(3)	1250(2)	6131(2)	17(1)
C(202)	6083(5)	5146(2)	3889(3)	28(1)
F(12B)	3079(2)	1809(1)	6851(1)	21(1)
F(12A)	4222(2)	967(1)	7371(1)	23(1)
C(12)	4274(4)	1523(2)	6898(2)	18(1)
C(203)	6803(5)	4911(3)	3219(3)	27(1)
C(103)	-1274(5)	-412(2)	5957(3)	30(1)

Tab. 71: Atomic coordinates (x 10^4) and equivalent isotropic displacement parameters (Å^2 x 10^3) for **5a**. U(eq) is defined as one third of the trace of the orthogonalized Uij tensor.

	x	**y**	**z**	**U(eq)**
F(1)	3120(3)	1502(3)	7166(2)	35(1)
F(2)	2513(3)	3328(3)	6940(2)	40(1)
F(3)	1010(4)	1880(4)	6822(2)	46(1)
F(4)	165(3)	3083(3)	7615(2)	41(1)
F(5)	-759(3)	1145(4)	8295(3)	52(1)
F(6)	1096(3)	160(3)	8017(3)	41(1)
F(7)	360(3)	224(3)	9547(3)	43(1)
F(8)	-252(3)	2011(3)	9374(2)	35(1)
F(9)	1972(3)	1594(3)	9687(2)	42(1)
F(10)	2655(3)	416(3)	8878(2)	39(1)
F(11)	4751(3)	785(4)	8221(3)	49(1)
F(12)	6926(3)	1283(5)	8087(3)	71(2)
F(13)	7335(4)	3462(6)	7889(3)	74(2)
F(14)	5414(5)	5175(5)	7706(5)	93(2)
F(15)	3198(4)	4683(3)	7891(3)	55(1)
F(16A)	1045(4)	2621(3)	11223(3)	49(1)
F(16B)	1252(3)	5896(3)	6846(2)	34(1)
F(17A)	126(4)	3406(4)	12256(2)	56(1)
F(17B)	482(3)	7581(3)	6408(2)	40(1)
F(18A)	-1015(4)	5609(6)	11965(3)	78(2)
F(18B)	-1003(4)	6271(4)	6418(3)	47(1)
F(19A)	-561(4)	6449(3)	10653(3)	56(1)
F(19B)	-983(4)	5284(3)	7618(3)	52(1)
F(20A)	-2598(4)	3953(5)	12474(3)	67(1)
F(20B)	-3105(4)	6643(4)	7729(3)	58(1)
F(21A)	-3187(4)	3608(4)	11502(4)	63(1)
F(21B)	-2134(4)	8088(3)	6994(3)	46(1)
F(22A)	-1343(4)	2095(4)	12124(3)	58(1)
F(22B)	-2192(4)	6520(4)	8921(3)	51(1)
F(23A)	-966(4)	2696(4)	10810(3)	48(1)
F(23B)	-2906(4)	8275(4)	8524(3)	49(1)
F(24A)	-2930(3)	5834(4)	11495(3)	52(1)
F(24B)	-667(4)	7831(4)	8977(3)	48(1)
F(25A)	-2013(3)	5195(3)	10428(2)	41(1)
F(25B)	-693(3)	8875(3)	7783(3)	43(1)
F(26A)	2742(3)	3846(4)	9865(2)	41(1)
F(26B)	1527(3)	9008(3)	6578(2)	37(1)
F(27A)	4886(3)	4452(5)	9708(3)	63(1)
F(27B)	3649(4)	9656(3)	6409(3)	46(1)
F(28A)	5160(4)	5686(4)	10721(3)	60(1)
F(28B)	4987(3)	8715(4)	7471(3)	52(1)
F(29A)	3177(4)	6312(4)	11871(3)	57(1)
F(29B)	4071(4)	7053(4)	8768(3)	54(1)
F(30A)	969(4)	5821(4)	12056(3)	51(1)
F(30B)	1949(4)	6349(4)	8988(3)	50(1)
O(1)	1584(3)	3320(3)	8591(2)	31(1)
O(1B)	400(3)	4542(3)	10168(2)	24(1)
O(2B)	390(4)	5991(3)	8382(3)	32(1)
C(1)	2406(4)	2456(4)	8303(3)	21(1)
C(2)	2304(3)	2357(4)	7464(3)	16(1)
C(3)	981(5)	2145(4)	7499(3)	27(1)
C(4)	453(5)	1183(5)	8202(4)	36(1)
C(5)	618(4)	1203(5)	9043(4)	32(1)
C(6)	1977(4)	1400(4)	8962(3)	22(1)
C(7)	3799(4)	2665(5)	8161(3)	27(1)
C(8)	4800(6)	1860(5)	8151(4)	41(1)
C(9)	6002(5)	2113(6)	8055(4)	44(2)

C(10)	6185(6)	3264(7)	7935(5)	56(2)
C(11)	5216(7)	4057(6)	7899(5)	51(2)
C(12)	4070(6)	3778(5)	7987(4)	40(1)
C(12A)	-1969(6)	5075(6)	11198(5)	49(2)
C(13A)	350(5)	4597(4)	10932(3)	29(1)
C(13B)	465(5)	6980(4)	7854(4)	31(1)
C(14A)	-753(5)	5464(5)	11183(4)	35(1)
C(14B)	326(4)	6765(4)	7057(3)	25(1)
C(15B)	-936(7)	6324(6)	7187(4)	46(2)
C(16A)	-2219(6)	3935(7)	11634(4)	48(2)
C(16B)	-2040(6)	7088(6)	7549(5)	42(1)
C(17A)	-1101(7)	3062(7)	11523(4)	49(2)
C(17B)	-1978(5)	7431(5)	8345(4)	40(1)
C(18A)	158(5)	3449(5)	11495(4)	36(1)
C(18B)	-705(4)	7833(4)	8229(3)	25(1)
C(19A)	1668(5)	4852(5)	10936(3)	29(1)
C(19B)	1694(5)	7517(5)	7744(4)	32(1)
C(20A)	2753(5)	4512(6)	10378(4)	37(1)
C(20B)	2098(5)	8430(5)	7135(4)	31(1)
C(21A)	3902(6)	4780(6)	10276(4)	41(1)
C(21B)	3256(5)	8789(4)	7015(4)	35(1)
C(22A)	4017(6)	5420(5)	10804(4)	42(2)
C(22B)	3910(5)	8357(6)	7582(4)	40(1)
C(23A)	2999(6)	5733(6)	11410(4)	47(2)
C(23B)	3489(5)	7501(6)	8216(4)	43(1)
C(24A)	1844(6)	5466(5)	11500(4)	40(1)
C(24B)	2356(6)	7148(6)	8275(4)	38(1)
Li(1A)	24(9)	5822(7)	9457(5)	30(2)
Li(1B)	1137(12)	3354(9)	9714(7)	52(3)
Li(1C)	1259(13)	4671(11)	7902(8)	57(3)
F(31A)	5663(4)	8954(3)	4497(3)	42(1)
F(31B)	2771(3)	12598(3)	2411(2)	36(1)
F(31C)	5226(3)	7757(3)	1467(3)	49(1)
F(32A)	5673(4)	7941(4)	5675(3)	50(1)
F(32B)	2043(3)	13816(3)	3223(3)	44(1)
F(32C)	5696(4)	8483(4)	200(3)	58(1)
F(33A)	7776(4)	7598(4)	4408(4)	61(1)
F(33B)	4910(3)	12189(3)	2774(2)	37(1)
F(33C)	6690(3)	8990(4)	1735(2)	41(1)
F(34A)	6786(4)	6153(3)	5112(3)	51(1)
F(34B)	4305(3)	13990(3)	2576(3)	42(1)
F(34C)	7648(3)	8340(4)	622(3)	51(1)
F(35A)	7560(3)	5943(3)	3606(3)	47(1)
F(35B)	3594(4)	13991(3)	4107(3)	49(1)
F(35C)	7866(4)	10606(4)	640(3)	55(1)
F(36A)	6883(4)	7675(4)	3160(3)	55(1)
F(36B)	5423(3)	13063(4)	3830(2)	44(1)
F(36C)	7282(4)	10199(5)	-317(3)	67(1)
F(37A)	5333(4)	6367(4)	3148(3)	51(1)
F(37B)	4518(3)	11128(3)	4528(2)	41(1)
F(37C)	6026(5)	12073(5)	1(3)	66(1)
F(38A)	4182(4)	6621(3)	5735(2)	43(1)
F(38B)	3659(4)	12334(4)	5320(2)	52(1)
F(38C)	5641(4)	11485(3)	1295(3)	50(1)
F(39A)	5379(3)	5348(3)	4330(3)	39(1)
F(39B)	2155(3)	10867(3)	5171(2)	41(1)
F(39C)	4619(3)	10785(4)	-157(2)	47(1)
F(40A)	3424(3)	8347(3)	5260(3)	45(1)
F(40B)	1584(3)	12684(3)	4939(2)	38(1)
F(40C)	3612(3)	11579(3)	903(3)	43(1)
F(41A)	3185(3)	5201(3)	5533(2)	39(1)
F(41B)	-66(3)	13471(3)	3903(2)	39(1)

F(41C)	1945(3)	10341(4)	2260(3)	49(1)
F(42A)	1016(3)	4557(3)	5728(2)	43(1)
F(42B)	-2238(3)	12940(4)	4023(2)	52(1)
F(42C)	-208(4)	9760(5)	2413(3)	56(1)
F(43A)	-325(4)	5490(4)	4637(3)	54(1)
F(43B)	-2621(4)	10722(6)	4259(4)	90(2)
F(43C)	-494(4)	8513(4)	1422(4)	63(1)
F(44A)	627(4)	7134(4)	3343(3)	53(1)
F(44B)	-706(5)	9105(5)	4338(5)	80(2)
F(44C)	1554(4)	7888(4)	191(3)	57(1)
F(45A)	2716(4)	7837(3)	3144(2)	42(1)
F(45B)	1462(4)	9515(4)	4263(4)	62(1)
F(45C)	3758(4)	8422(4)	36(3)	56(1)
O(3A)	4289(4)	8249(4)	3764(2)	35(1)
O(3B)	3097(3)	10870(3)	3562(2)	27(1)
O(3C)	4284(3)	9683(4)	1941(2)	33(1)
C(25A)	4265(5)	7180(5)	4272(3)	29(1)
C(25B)	2271(5)	11763(5)	3815(3)	33(1)
C(25C)	4282(4)	9660(5)	1171(3)	30(1)
C(26A)	5402(7)	6439(5)	3907(4)	45(1)
C(26B)	2448(7)	11879(6)	4605(4)	48(2)
C(26C)	5471(5)	8750(6)	892(4)	40(1)
C(27A)	6674(5)	6795(6)	3807(4)	39(1)
C(27B)	3748(5)	12095(6)	4574(4)	42(2)
C(27C)	6705(4)	9069(5)	951(3)	26(1)
C(28A)	6752(5)	7073(6)	4563(5)	40(1)
C(28B)	4212(4)	13059(5)	3903(4)	32(1)
C(28C)	6943(5)	10276(6)	441(4)	40(1)
C(29A)	5594(4)	7896(4)	4967(4)	32(1)
C(29B)	4076(5)	12991(4)	3088(4)	31(1)
C(29C)	5801(5)	11204(5)	601(4)	33(1)
C(30A)	4356(6)	7483(5)	5058(4)	39(1)
C(30B)	2747(6)	12784(5)	3164(4)	42(1)
C(30C)	4592(5)	10802(5)	633(4)	33(1)
C(31A)	3081(5)	6672(4)	4393(3)	30(1)
C(31B)	911(5)	11539(5)	3977(4)	37(1)
C(31C)	3035(5)	9343(5)	1154(4)	34(1)
C(32A)	2514(6)	5777(5)	5035(4)	34(1)
C(32B)	627(5)	10450(6)	4133(5)	45(2)
C(32C)	1956(5)	9693(5)	1749(4)	36(1)
C(33A)	1430(5)	5374(5)	5102(4)	36(1)
C(33B)	-549(6)	10163(8)	4217(6)	57(2)
C(33C)	776(5)	9411(6)	1808(5)	47(2)
C(34A)	1261(6)	6693(5)	3909(4)	38(1)
C(34B)	-1514(5)	11068(8)	4157(4)	53(2)
C(34C)	609(5)	8801(6)	1333(4)	43(2)
C(35A)	2355(6)	7095(5)	3803(4)	31(1)
C(35B)	-1306(5)	12089(7)	4052(4)	45(2)
C(35C)	1618(6)	8488(4)	756(4)	36(1)
C(36A)	745(5)	5866(5)	4577(4)	39(1)
C(36B)	-157(4)	12367(5)	3978(3)	31(1)
C(36C)	2808(5)	8767(5)	684(3)	31(1)
Li(2A)	3423(9)	9490(8)	4129(6)	36(2)
Li(2B)	3462(7)	10847(9)	2482(6)	33(2)
Li(2C)	4591(13)	8277(13)	2642(9)	66(4)

Tab. 72: Atomic coordinates (x 10^4) and equivalent isotropic displacement parameters (Å^2 x 10^3) for **5b**. U(eq) is defined as one third of the trace of the orthogonalized Uij tensor.

	x	**y**	**z**	**U(eq)**
F(15)	2168(1)	4398(1)	209(1)	21(1)
F(6)	5123(1)	1415(1)	-4(1)	22(1)
F(14)	-495(1)	3113(1)	302(1)	23(1)
F(7)	5368(1)	3414(1)	223(1)	21(1)
F(11)	3696(1)	4434(1)	-1798(1)	23(1)
F(8)	3213(1)	1236(1)	-2085(1)	23(1)
O(1)	1113(1)	1113(1)	-138(1)	16(1)
F(1)	2516(1)	4267(1)	2270(1)	22(1)
F(5)	3156(1)	67(1)	1361(1)	20(1)
F(9)	5716(1)	2695(1)	-1920(1)	24(1)
F(4)	3879(1)	-133(1)	3565(1)	26(1)
F(2)	3294(1)	3994(1)	4464(1)	27(1)
F(10)	2250(1)	3049(1)	-3185(1)	25(1)
F(30)	-1881(1)	1204(1)	1764(1)	27(1)
F(3)	3944(1)	1786(1)	5183(1)	29(1)
C(1)	2783(2)	2200(1)	1645(1)	15(1)
C(7)	2270(2)	2186(1)	296(1)	14(1)
C(2)	2857(2)	3156(1)	2511(1)	17(1)
C(5)	3537(2)	953(1)	3233(1)	19(1)
C(6)	3144(2)	1095(1)	2072(1)	17(1)
C(3)	3255(2)	3028(1)	3685(1)	20(1)
C(31)	-1936(2)	3094(2)	2836(1)	21(1)
C(8)	4189(2)	2359(1)	-245(1)	16(1)
C(12)	1220(2)	3239(1)	-117(1)	17(1)
C(9)	3972(2)	2374(1)	-1583(1)	18(1)
C(10)	2694(2)	3276(1)	-2024(1)	18(1)
C(4)	3587(2)	1925(2)	4055(1)	21(1)
C(30)	-1756(2)	1877(1)	2824(1)	20(1)
C(32)	-1827(2)	3755(2)	3912(2)	25(1)
C(33)	-1551(2)	3193(2)	4926(2)	29(1)
C(35)	-1484(2)	1275(2)	3806(1)	24(1)
C(34)	-1375(2)	1958(2)	4871(2)	29(1)
Li(1)	-1391(4)	536(2)	191(2)	21(1)
F(12)	-398(1)	2167(1)	-1938(1)	23(1)
F(13)	23(1)	4166(1)	-1735(1)	24(1)
C(11)	829(2)	3188(1)	-1462(1)	18(1)

Tab. 73: Atomic coordinates (x 10^4) and equivalent isotropic displacement parameters (Å^2 x 10^3) for **5c**. U(eq) is defined as one third of the trace of the orthogonalized Uij tensor.

	x	**y**	**z**	**U(eq)**
F(1A)	10004(1)	1502(1)	605(1)	27(1)
F(8B)	5711(1)	4387(1)	4042(1)	32(1)
F(9B)	5213(1)	2416(1)	4105(1)	25(1)
F(4B)	6628(1)	3805(1)	8571(1)	31(1)
O(1B)	5539(1)	931(1)	5464(1)	16(1)
F(1B)	5728(1)	-562(1)	6783(1)	29(1)
F(3B)	6156(1)	1530(1)	9378(1)	30(1)
F(7A)	9607(1)	3580(1)	-543(1)	25(1)
F(2B)	5696(1)	-594(1)	8441(1)	33(1)
F(6A)	8498(1)	3971(1)	-728(1)	28(1)
F(13A)	8862(1)	122(1)	-2313(1)	29(1)
F(2A)	9892(1)	1456(1)	2259(1)	34(1)
F(12A)	7775(1)	669(1)	-2491(1)	34(1)
O(1A)	9416(1)	810(1)	-814(1)	17(1)
F(9A)	9777(1)	2664(1)	-2098(1)	28(1)
F(7B)	6362(1)	4179(1)	5429(1)	34(1)
F(11A)	8017(1)	3264(1)	-2467(1)	35(1)
C(7A)	8873(1)	1631(2)	-607(1)	17(1)
C(1B)	6140(1)	1761(2)	6715(1)	16(1)
F(4A)	7462(1)	1973(2)	2078(1)	46(1)
F(3A)	8639(1)	1730(1)	3048(1)	32(1)
F(10A)	8826(1)	2322(1)	-3247(1)	37(1)
C(2B)	5928(1)	602(2)	7166(1)	20(1)
C(8B)	5880(1)	3178(2)	5323(1)	21(1)
F(6B)	5275(1)	3633(1)	5668(1)	30(1)
C(6B)	6388(1)	2808(2)	7232(1)	18(1)
F(5A)	7518(1)	1948(2)	429(1)	43(1)
C(1A)	8761(1)	1682(2)	383(1)	18(1)
C(2A)	9347(1)	1554(2)	913(1)	19(1)
C(7B)	6061(1)	1773(2)	5720(1)	16(1)
C(4B)	6156(1)	1611(2)	8528(1)	22(1)
F(5B)	6637(1)	3962(1)	6906(1)	31(1)
C(6A)	8134(1)	1828(2)	827(1)	23(1)
C(4A)	8673(1)	1694(2)	2197(1)	24(1)
F(8A)	9164(1)	4519(1)	-2130(1)	36(1)
C(9B)	5788(1)	3099(2)	4337(1)	21(1)
C(5B)	6391(1)	2746(2)	8117(1)	21(1)
C(5A)	8087(1)	1841(2)	1707(1)	27(1)
C(8A)	9023(1)	3089(2)	-926(1)	20(1)
C(3B)	5924(1)	533(2)	8047(1)	22(1)
C(3A)	9305(1)	1541(2)	1793(1)	22(1)
C(9A)	9149(1)	3194(2)	-1902(1)	24(1)
C(10A)	8589(1)	2462(2)	-2442(1)	27(1)
C(11A)	8378(1)	1044(2)	-2101(1)	24(1)
Li(1A)	10388(2)	1064(3)	-813(2)	27(1)
F(15B)	6915(1)	28(1)	5618(1)	25(1)
F(14B)	7300(1)	2109(1)	5528(1)	28(1)
F(14A)	7652(1)	1873(1)	-1065(1)	29(1)
F(15A)	8062(1)	-170(1)	-854(1)	28(1)
F(11B)	6270(1)	2177(1)	3083(1)	31(1)
O(2A)	11017(1)	2499(2)	-1099(1)	25(1)
F(13B)	7386(1)	976(1)	4036(1)	34(1)
F(12B)	6345(1)	104(1)	4094(1)	27(1)
F(10B)	6947(1)	3411(1)	3888(1)	33(1)
C(12A)	8236(1)	1100(2)	-1125(1)	21(1)
C(11B)	6730(1)	1187(2)	4329(1)	23(1)
C(12B)	6757(1)	1283(2)	5318(1)	19(1)

C(10B)	6437(1)	2466(2)	3896(1)	24(1)
O(2B)	8909(1)	2564(2)	4804(1)	25(1)
Li(1B)	5447(2)	-982(3)	5451(2)	23(1)

Tab. 74: Atomic coordinates (x 10^4) and equivalent isotropic displacement parameters (Å^2 x 10^3) for **6**. U(eq) is defined as one third of the trace of the orthogonalized Uij tensor.

	x	**y**	**z**	**U(eq)**
Na(1)	1956(1)	5923(2)	5928(2)	52(1)
Na(2)	1969(1)	4084(2)	7683(2)	51(1)
O(1)	1970(1)	5719(2)	7833(3)	42(1)
O(2)	2005(1)	4289(2)	5784(2)	40(1)
C(1)	2034(2)	6227(4)	8843(4)	37(1)
C(2)	1717(2)	5659(4)	9796(4)	39(1)
C(3)	1046(2)	5448(4)	9487(4)	46(1)
C(4)	698(2)	6349(4)	9051(5)	53(2)
C(5)	1021(2)	7018(4)	8194(5)	52(1)
C(6)	1676(2)	7189(4)	8608(4)	48(1)
C(7)	2705(2)	6384(4)	9220(4)	43(1)
C(8)	3132(3)	5744(5)	8808(5)	65(2)
C(9)	3741(3)	5833(6)	9006(6)	81(2)
C(10)	3958(3)	6606(6)	9648(7)	83(2)
C(11)	3575(3)	7229(5)	10139(6)	73(2)
C(12)	2963(2)	7104(4)	9924(5)	57(2)
C(13)	2064(2)	3785(3)	4787(4)	36(1)
C(14)	1731(2)	4335(4)	3783(4)	42(1)
C(15)	1062(2)	4512(4)	3995(4)	47(1)
C(16)	723(2)	3601(4)	4392(5)	55(2)
C(17)	1070(2)	2961(4)	5303(5)	50(1)
C(18)	1729(2)	2816(4)	4966(4)	45(1)
C(19)	2744(2)	3648(4)	4507(4)	43(1)
C(20)	3160(3)	4326(5)	4959(5)	60(2)
C(21)	3769(3)	4230(6)	4865(6)	80(2)
C(22)	3997(3)	3463(6)	4284(7)	80(2)
C(23)	3609(3)	2818(5)	3763(7)	81(2)
C(24)	2998(2)	2918(5)	3871(5)	62(2)
C(51)	3951(6)	4176(9)	1270(9)	151(4)
C(52)	4381(3)	4773(9)	1755(8)	114(3)
C(53)	4220(4)	5580(9)	2356(8)	110(3)
C(54)	3597(5)	5779(8)	2493(7)	115(3)
C(56)	3384(5)	4294(13)	1331(11)	166(6)
C(57)	4650(6)	6277(10)	2874(10)	201(6)
C(66)	3208(4)	5105(12)	1963(9)	123(5)
F(1)	1990(1)	4776(2)	9934(2)	49(1)
F(2)	1755(1)	6091(2)	10871(2)	49(1)
F(3)	1000(1)	4753(2)	8640(2)	54(1)
F(4)	786(1)	5092(2)	10433(3)	65(1)
F(5)	167(1)	6065(3)	8550(3)	75(1)
F(6)	582(1)	6890(3)	10006(3)	72(1)
F(7)	732(1)	7869(2)	8129(3)	74(1)
F(8)	972(1)	6630(2)	7096(2)	63(1)
F(9)	1953(1)	7699(2)	7781(3)	71(1)
F(10)	1637(1)	7789(2)	9559(3)	64(1)
F(11)	2975(2)	4912(3)	8226(4)	110(2)
F(12)	4112(2)	5183(4)	8575(4)	139(2)
F(13)	4560(2)	6713(4)	9872(4)	120(2)
F(14)	3776(2)	7947(3)	10840(5)	137(2)
F(15)	2624(2)	7747(3)	10478(4)	108(2)
F(16)	1988(1)	5233(2)	3681(2)	51(1)
F(17)	1766(1)	3899(2)	2718(2)	56(1)
F(18)	785(1)	4868(2)	3008(3)	68(1)
F(19)	1008(1)	5215(2)	4830(2)	55(1)
F(20)	615(1)	3054(3)	3421(3)	76(1)
F(21)	195(1)	3865(3)	4800(3)	81(1)
F(22)	1029(1)	3351(3)	6382(3)	68(1)

F(23)	802(1)	2089(2)	5326(3)	73(1)
F(24)	1678(1)	2213(2)	4014(3)	64(1)
F(25)	2016(1)	2305(2)	5833(3)	70(1)
F(26)	2993(2)	5159(3)	5480(4)	98(1)
F(27)	4141(2)	4914(4)	5325(4)	128(2)
F(28)	4593(2)	3373(4)	4164(4)	129(2)
F(29)	3818(2)	2068(3)	3135(5)	144(2)
F(30)	2661(2)	2243(3)	3303(4)	109(2)

Tab. 75: Atomic coordinates (x 10^4) and equivalent isotropic displacement parameters (Å^2 x 10^3) for **6a**. U(eq) is defined as one third of the trace of the orthogonalized Uij tensor.

	x	**y**	**z**	**U(eq)**
F(6A)	33(3)	6820(3)	2225(2)	17(3)
F(11A)	3633(3)	8815(3)	1858(2)	22(3)
F(10A)	2031(3)	9578(3)	2868(2)	21(3)
F(12B)	5813(3)	2256(3)	3486(2)	19(3)
F(4A)	1346(3)	2860(3)	5222(2)	21(3)
F(1B)	6960(3)	6667(3)	1068(2)	17(3)
F(15B)	9345(3)	4321(3)	3053(2)	21(3)
F(13A)	-92(3)	9562(3)	2065(2)	20(3)
F(7A)	1505(3)	6014(3)	1174(2)	18(3)
F(14B)	8898(3)	4670(3)	1656(2)	18(3)
F(012)	2397(3)	8216(3)	456(2)	19(3)
F(10B)	9133(3)	1765(3)	4211(2)	22(3)
F(11B)	8327(4)	588(3)	3591(2)	23(3)
F(8B)	8162(3)	2401(3)	2016(2)	19(3)
O(1A)	3834(4)	6282(3)	1855(3)	12(3)
F(15A)	3312(3)	6963(3)	3503(2)	18(3)
F(2B)	6929(4)	9177(3)	722(2)	21(3)
F(7B)	5119(3)	4498(3)	4096(2)	16(3)
F(5A)	1373(3)	5322(3)	4406(2)	17(3)
F(4B)	6219(4)	8917(3)	3878(2)	22(3)
F(12A)	1463(3)	10389(3)	1013(2)	22(3)
F(6B)	7298(3)	4057(3)	4432(2)	18(3)
F(14A)	1001(3)	7535(3)	3441(2)	18(3)
F(1A)	3616(3)	3984(3)	1669(2)	16(3)
F(3B)	6591(3)	10378(3)	2099(2)	21(3)
F(5B)	6320(4)	6400(3)	4275(2)	20(3)
F(8A)	89(3)	8625(3)	667(2)	21(3)
O(1B)	6023(4)	4633(3)	2283(3)	12(3)
F(2A)	3577(3)	1536(3)	2555(2)	21(3)
F(3A)	2440(4)	901(3)	4335(2)	22(3)
F(13B)	6423(4)	1914(3)	4840(2)	23(3)
C(9A)	1324(6)	6820(5)	1739(4)	10(3)
C(2B)	6858(6)	7132(5)	1806(4)	10(3)
C(5A)	1897(6)	3151(5)	4348(4)	11(3)
C(6B)	6540(6)	6995(5)	3384(4)	11(3)
C(10B)	8236(6)	1833(5)	3617(4)	16(3)
C(3B)	6813(6)	8471(5)	1609(4)	13(3)
C(4B)	6655(6)	9073(5)	2299(4)	17(4)
C(6A)	1910(6)	4461(5)	3897(4)	13(3)
C(1A)	2454(6)	4845(5)	2973(4)	11(3)
C(4A)	2454(6)	2171(5)	3895(4)	14(3)
C(7A)	2540(6)	6277(5)	2384(4)	8(3)
C(1B)	6774(6)	6311(5)	2701(4)	12(3)
C(12B)	8471(6)	4131(5)	2537(4)	15(3)
C(7B)	6903(6)	4803(5)	2828(4)	11(3)
C(5B)	6485(6)	8333(5)	3185(4)	14(3)
C(11B)	6729(6)	2494(5)	3935(4)	13(3)
C(2A)	3014(6)	3797(5)	2547(4)	12(3)
C(3A)	3014(6)	2497(5)	2999(4)	11(3)
C(8A)	2355(6)	8733(5)	2324(4)	16(3)
F(9B)	10203(3)	2156(3)	2482(2)	22(3)
C(11A)	1217(6)	9259(5)	1621(4)	18(4)
C(10A)	2296(6)	7330(5)	2935(4)	11(3)
C(9B)	8782(6)	2612(5)	2658(4)	15(3)
C(8B)	6491(6)	4001(5)	3828(4)	12(3)
C(12A)	1265(6)	8232(5)	1105(4)	12(3)
Na(1)	4675(2)	6499(2)	313(2)	23(3)

O(12)	6422(4)	4429(3)	495(3)	20(3)
O(11)	5625(5)	8199(4)	-560(3)	30(3)
O(99)	8700(30)	5900(30)	-400(30)	278(11)

Tab. 76: Atomic coordinates (x 10^4) and equivalent isotropic displacement parameters (Å^2 x 10^3) for **7**. U(eq) is defined as one third of the trace of the orthogonalized Uij tensor.

	x	**y**	**z**	**U(eq)**
Al(1)	2834(1)	2466(1)	2504(1)	26(1)
O(1)	3241(3)	2999(2)	3222(2)	31(1)
C(1)	3942(5)	2703(4)	3799(3)	32(1)
F(1)	5831(3)	3604(3)	3274(2)	65(1)
O(2)	4206(3)	2149(2)	1815(2)	29(1)
C(2)	4715(6)	3658(5)	3798(3)	44(2)
F(2)	5186(4)	3645(3)	4380(2)	69(1)
O(3)	2207(3)	1317(2)	2827(2)	37(1)
C(3)	5130(6)	1508(5)	3697(3)	48(2)
F(3)	3699(3)	4698(2)	3709(2)	52(1)
O(4)	1576(3)	3861(2)	2357(2)	28(1)
C(4)	2833(5)	2741(4)	4475(3)	32(1)
F(4)	5639(3)	1368(3)	3022(2)	65(1)
C(5)	3173(5)	2130(4)	5092(3)	38(1)
F(5)	6298(3)	1397(3)	3992(2)	61(1)
C(6)	2158(6)	2168(4)	5700(3)	45(2)
F(6)	4544(3)	653(2)	3948(2)	48(1)
C(7)	730(6)	2867(5)	5714(3)	41(1)
F(7)	4557(3)	1466(2)	5131(2)	51(1)
C(8)	360(5)	3492(4)	5127(3)	37(1)
F(8)	2562(3)	1546(3)	6268(2)	62(1)
C(9)	1375(5)	3433(4)	4535(3)	30(1)
F(9)	-260(3)	2956(2)	6299(2)	58(1)
C(10)	5158(5)	2427(4)	1242(3)	27(1)
F(10)	-1023(3)	4201(2)	5127(2)	52(1)
C(11)	5129(5)	3712(4)	1291(3)	32(1)
F(11)	870(3)	4164(2)	3995(2)	39(1)
C(12)	6747(5)	1639(4)	1273(3)	34(1)
F(12)	3964(3)	4436(2)	1051(2)	39(1)
C(13)	4709(5)	2227(4)	571(3)	28(1)
F(13)	6345(3)	3972(2)	959(2)	44(1)
C(14)	4014(5)	1369(4)	563(3)	28(1)
F(14)	4985(3)	3928(2)	1954(2)	48(1)
C(15)	3499(5)	1214(4)	-7(3)	29(1)
F(15)	7301(3)	1902(2)	1781(2)	46(1)
C(16)	3651(5)	1895(4)	-606(3)	34(1)
F(16)	7669(3)	1738(2)	679(2)	46(1)
C(17)	4380(5)	2705(4)	-638(3)	35(1)
F(17)	6761(3)	547(2)	1391(2)	45(1)
C(18)	4895(5)	2854(4)	-62(3)	29(1)
F(18)	3838(3)	641(2)	1110(1)	36(1)
C(19)	1515(5)	541(4)	3170(3)	27(1)
F(19)	2821(3)	386(2)	25(2)	42(1)
C(20)	509(5)	335(4)	2707(3)	33(1)
F(20)	3126(3)	1763(2)	-1158(2)	47(1)
C(21)	539(5)	1072(4)	3836(3)	41(2)
F(21)	4576(3)	3377(2)	-1217(2)	49(1)
C(22)	2670(5)	-625(4)	3313(3)	30(1)
F(22)	5650(3)	3647(2)	-145(2)	44(1)
C(23)	4039(5)	-966(4)	2887(3)	33(1)
F(23)	-660(3)	1269(2)	2658(2)	47(1)
C(24)	5111(5)	-1975(4)	3010(3)	36(1)
F(24)	-32(3)	-551(2)	2957(2)	47(1)
C(25)	4849(5)	-2708(4)	3579(3)	37(1)
F(25)	1241(3)	119(2)	2073(2)	45(1)
C(26)	3491(6)	-2437(4)	3993(3)	36(1)
F(26)	-655(3)	699(2)	4078(2)	44(1)

C(27)	2435(5)	-1429(4)	3854(3)	32(1)
F(27)	17(3)	2222(2)	3737(2)	49(1)
C(28)	515(5)	4432(4)	1952(3)	30(1)
F(28)	1315(3)	896(2)	4353(2)	39(1)
C(29)	532(5)	3638(4)	1391(3)	32(1)
F(29)	4429(3)	-324(2)	2322(2)	51(1)
C(30)	-982(5)	4712(4)	2445(3)	41(1)
F(30)	6437(3)	-2240(2)	2594(2)	52(1)
C(31)	745(5)	5605(4)	1631(3)	30(1)
F(31)	5897(3)	-3682(2)	3707(2)	55(1)
C(32)	1513(5)	6202(4)	1918(3)	32(1)
F(32)	3198(3)	-3135(2)	4544(2)	54(1)
C(33)	1725(5)	7237(4)	1632(3)	39(1)
F(33)	1132(3)	-1239(2)	4295(2)	42(1)
C(34)	1168(6)	7757(4)	1067(3)	39(1)
F(34)	1032(3)	2532(2)	1620(2)	39(1)
C(35)	376(5)	7238(4)	761(3)	36(1)
F(35)	-807(3)	3765(2)	1244(2)	41(1)
C(36)	161(5)	6195(4)	1064(3)	36(1)
F(36)	1424(3)	3789(2)	805(2)	37(1)
F(37)	-2107(3)	5394(2)	2158(2)	47(1)
F(38)	-879(3)	5264(2)	2984(2)	47(1)
F(39)	-1340(3)	3765(2)	2716(2)	52(1)
F(40)	2095(3)	5792(2)	2501(2)	44(1)
F(41)	2498(3)	7720(2)	1944(2)	52(1)
F(42)	1381(3)	8754(2)	790(2)	57(1)
F(43)	-200(3)	7725(2)	201(2)	53(1)
F(44)	-682(3)	5778(2)	750(2)	43(1)
Li(1)	1949(10)	4518(7)	3108(5)	47(2)

Tab. 77: Atomic coordinates (x 10^4) and equivalent isotropic displacement parameters (Å^2 x 10^3) for **8a**. U(eq) is defined as one third of the trace of the orthogonalized Uij tensor.

	x	**y**	**z**	**U(eq)**
Ag(1)	2646(1)	208(1)	3476(1)	52(1)
Cl(1)	2386(1)	-239(1)	2368(1)	58(1)
Cl(2)	2216(1)	20(1)	5110(1)	39(1)
Cl(3)	2697(1)	697(1)	4717(1)	49(1)
Cl(4)	2464(1)	621(1)	1845(1)	46(1)
Cl(5)	3020(1)	-160(1)	4777(1)	62(1)
Cl(6)	3217(1)	304(1)	2581(1)	52(1)
Cl(7)	477(1)	-5015(1)	-747(3)	185(2)
Al(1)	1360(1)	-3839(1)	610(1)	27(1)
O(1)	1246(1)	-3587(1)	-434(2)	39(1)
O(2)	1140(1)	-3844(1)	1886(2)	34(1)
O(3)	1351(1)	-4176(1)	-44(2)	36(1)
O(4)	1713(1)	-3756(1)	1126(2)	34(1)
C(1)	1247(1)	-3363(1)	-1204(3)	34(1)
C(2)	1173(1)	-3478(1)	-2483(3)	36(1)
C(3)	986(1)	-3163(1)	-828(3)	40(1)
C(4)	1551(1)	-3209(1)	-1280(3)	32(1)
C(5)	1600(1)	-2910(1)	-1341(4)	39(1)
C(6)	1879(1)	-2791(1)	-1395(4)	46(1)
C(7)	2128(1)	-2960(1)	-1429(4)	44(1)
C(8)	2093(1)	-3255(1)	-1386(3)	33(1)
C(9)	1811(1)	-3370(1)	-1312(3)	31(1)
C(10)	890(1)	-3841(1)	2573(3)	34(1)
C(11)	984(1)	-3795(1)	3903(3)	37(1)
C(12)	701(1)	-3574(1)	2174(4)	46(1)
C(13)	717(1)	-4129(1)	2532(3)	31(1)
C(14)	411(1)	-4159(1)	2611(4)	45(1)
C(15)	272(1)	-4428(1)	2591(5)	59(1)
C(16)	438(1)	-4672(1)	2545(5)	54(1)
C(17)	739(1)	-4653(1)	2499(4)	40(1)
C(18)	879(1)	-4385(1)	2493(3)	31(1)
C(19)	1367(1)	-4374(1)	-928(3)	31(1)
C(20)	1687(1)	-4359(1)	-1497(3)	36(1)
C(21)	1324(1)	-4675(1)	-357(3)	38(1)
C(22)	1118(1)	-4346(1)	-1871(3)	31(1)
C(23)	1135(1)	-4454(1)	-3036(3)	34(1)
C(24)	907(1)	-4435(1)	-3837(3)	41(1)
C(25)	645(1)	-4308(1)	-3526(4)	45(1)
C(26)	614(1)	-4202(1)	-2382(4)	42(1)
C(27)	844(1)	-4224(1)	-1575(3)	37(1)
C(28)	1908(1)	-3754(1)	2064(3)	35(1)
C(29)	1943(1)	-4075(1)	2525(4)	45(1)
C(30)	2207(1)	-3646(1)	1584(3)	40(1)
C(31)	1816(1)	-3542(1)	3060(3)	38(1)
C(32)	1918(1)	-3564(1)	4242(4)	52(1)
C(33)	1853(1)	-3365(1)	5089(4)	70(2)
C(34)	1680(2)	-3125(1)	4809(5)	79(2)
C(35)	1582(1)	-3093(1)	3658(5)	62(1)
C(36)	1651(1)	-3297(1)	2809(3)	44(1)
C(101)	2245(1)	-441(1)	3612(4)	41(1)
C(102)	2034(1)	-269(1)	4338(4)	43(1)
C(103)	2742(1)	954(1)	3539(4)	45(1)
C(104)	2488(1)	952(1)	2667(4)	45(1)
C(105)	3354(1)	-155(1)	3971(9)	112(3)
C(106)	3385(2)	-17(3)	3008(9)	200(7)
C(107)	74(3)	-5108(4)	-704(15)	228(9)
F(1)	1354(1)	-3689(1)	-2810(2)	48(1)

F(2)	895(1)	-3581(1)	-2551(2)	50(1)
F(3)	1196(1)	-3271(1)	-3310(2)	47(1)
F(4)	1057(1)	-3009(1)	135(2)	49(1)
F(5)	748(1)	-3318(1)	-553(2)	53(1)
F(6)	897(1)	-2979(1)	-1688(2)	50(1)
F(7)	1375(1)	-2721(1)	-1375(2)	53(1)
F(8)	1912(1)	-2503(1)	-1459(3)	72(1)
F(9)	2400(1)	-2844(1)	-1474(3)	66(1)
F(10)	2330(1)	-3427(1)	-1445(2)	42(1)
F(11)	1803(1)	-3660(1)	-1316(2)	35(1)
F(12)	1092(1)	-3528(1)	4088(2)	57(1)
F(13)	1192(1)	-3977(1)	4238(2)	47(1)
F(14)	754(1)	-3828(1)	4646(2)	48(1)
F(15)	879(1)	-3355(1)	1926(2)	55(1)
F(16)	544(1)	-3637(1)	1211(2)	54(1)
F(17)	512(1)	-3480(1)	3025(2)	59(1)
F(18)	228(1)	-3935(1)	2722(3)	63(1)
F(19)	-26(1)	-4441(1)	2634(4)	94(1)
F(20)	307(1)	-4931(1)	2550(4)	88(1)
F(21)	907(1)	-4890(1)	2496(3)	58(1)
F(22)	1174(1)	-4391(1)	2499(2)	35(1)
F(23)	1884(1)	-4267(1)	-699(2)	48(1)
F(24)	1790(1)	-4615(1)	-1887(2)	43(1)
F(25)	1698(1)	-4177(1)	-2413(2)	41(1)
F(26)	1065(1)	-4681(1)	234(2)	43(1)
F(27)	1314(1)	-4888(1)	-1158(2)	48(1)
F(28)	1539(1)	-4736(1)	425(2)	50(1)
F(29)	1381(1)	-4589(1)	-3417(2)	46(1)
F(30)	941(1)	-4543(1)	-4944(2)	56(1)
F(31)	422(1)	-4287(1)	-4315(2)	64(1)
F(32)	357(1)	-4078(1)	-2056(3)	65(1)
F(33)	786(1)	-4121(1)	-478(2)	48(1)
F(34)	1898(1)	-4257(1)	1628(2)	69(1)
F(35)	1741(1)	-4136(1)	3357(2)	53(1)
F(36)	2212(1)	-4133(1)	2957(2)	61(1)
F(37)	2416(1)	-3621(1)	2435(2)	60(1)
F(38)	2315(1)	-3818(1)	733(2)	55(1)
F(39)	2177(1)	-3383(1)	1112(2)	45(1)
F(40)	2089(1)	-3783(1)	4599(2)	68(1)
F(41)	1953(1)	-3394(1)	6197(2)	106(2)
F(42)	1619(1)	-2933(1)	5658(3)	113(2)
F(43)	1415(1)	-2868(1)	3369(3)	86(1)
F(44)	1550(1)	-3239(1)	1704(2)	53(1)

Tab. 78: Atomic coordinates (x 10^4) and equivalent isotropic displacement parameters (Å^2 x 10^3) for **9a**. U(eq) is defined as one third of the trace of the orthogonalized Uij tensor.

	x	**y**	**z**	**U(eq)**
Al(1)	3537(1)	667(1)	993(1)	61(1)
F(15)	4877(3)	2522(2)	1149(1)	75(1)
O(3)	4560(3)	564(2)	1200(1)	67(1)
F(16)	4373(3)	3280(2)	744(1)	80(1)
F(18)	1957(3)	2082(2)	1485(1)	83(1)
F(34)	2534(3)	-1173(2)	814(1)	86(1)
F(26)	5530(3)	502(2)	711(1)	86(1)
O(2)	3078(3)	1658(2)	1042(1)	64(1)
F(35)	2385(3)	-2034(2)	1208(1)	94(1)
F(17)	4402(3)	1975(2)	695(1)	82(1)
F(12)	2727(3)	2689(2)	472(1)	89(1)
F(13)	2657(3)	3728(2)	800(1)	89(1)
F(11)	4573(3)	-903(2)	564(1)	87(1)
F(1)	3484(3)	619(2)	-260(1)	89(1)
O(1)	3513(3)	331(2)	597(1)	66(1)
O(4)	2675(3)	139(2)	1184(1)	64(1)
F(29)	4249(3)	1453(2)	1694(1)	89(1)
F(23)	6368(3)	-599(2)	1545(1)	103(2)
F(4)	1648(3)	-243(3)	331(1)	94(1)
F(14)	1776(3)	2689(2)	847(1)	89(1)
F(2)	4532(3)	716(2)	121(1)	86(1)
F(5)	1981(3)	978(3)	493(1)	91(1)
F(40)	2589(3)	823(3)	1758(1)	97(1)
F(22)	4287(3)	3970(2)	1294(1)	96(1)
F(27)	6299(3)	1412(2)	988(1)	88(1)
F(37)	1050(3)	-806(3)	1085(1)	101(1)
F(38)	1146(3)	59(3)	1477(1)	93(1)
F(6)	1833(3)	719(3)	-21(1)	96(1)
F(36)	3656(4)	-1416(2)	1153(1)	90(1)
F(24)	4991(3)	-603(2)	1639(1)	91(1)
F(44)	3346(4)	-2006(3)	1723(1)	100(2)
F(19)	1818(3)	2753(3)	2052(1)	96(1)
F(25)	5405(3)	-968(2)	1165(1)	97(1)
F(28)	6737(3)	144(3)	991(1)	103(2)
F(39)	1256(3)	-1224(3)	1580(1)	99(1)
F(3)	3441(3)	1572(2)	104(1)	89(1)
F(20)	2841(4)	4034(3)	2263(1)	106(2)
F(10)	4942(4)	-2363(3)	355(2)	112(2)
F(33)	7282(3)	734(3)	1547(1)	111(2)
F(7)	2236(4)	-658(3)	-270(1)	104(2)
F(8)	2629(4)	-2133(3)	-473(1)	123(2)
C(13)	3194(5)	2922(4)	1358(2)	63(2)
F(43)	4089(4)	-1893(3)	2313(1)	122(2)
F(21)	4077(4)	4632(3)	1860(1)	113(2)
F(9)	3975(5)	-3021(3)	-175(2)	140(2)
C(12)	4229(5)	2593(4)	898(2)	67(2)
C(22)	5731(5)	1028(4)	1581(2)	71(2)
C(9)	4045(6)	-1170(4)	315(2)	72(2)
C(19)	5436(5)	462(4)	1291(2)	67(2)
C(10)	3283(5)	2485(4)	1027(2)	64(2)
C(23)	5135(6)	1489(4)	1753(2)	76(2)
F(31)	6563(5)	2630(3)	2337(1)	148(3)
C(1)	3161(5)	195(4)	286(2)	72(2)
F(30)	4804(5)	2468(3)	2144(1)	129(2)
C(4)	3368(6)	-689(4)	166(2)	74(2)
C(28)	2516(5)	-587(4)	1347(2)	67(2)
F(41)	3357(5)	905(3)	2346(1)	135(2)

C(30)	1485(6)	-642(5)	1376(2)	78(2)
C(3)	2145(6)	398(5)	256(2)	80(2)
C(21)	6012(6)	620(4)	997(2)	82(2)
F(32)	7779(5)	1673(4)	2041(2)	147(2)
C(11)	2622(6)	2903(4)	779(2)	75(2)
C(5)	2902(6)	-1060(5)	-102(2)	81(2)
C(32)	2955(6)	132(5)	1878(2)	77(2)
C(7)	3804(8)	-2284(5)	-60(3)	96(3)
C(16)	2968(6)	3679(5)	1969(2)	83(2)
C(31)	2940(6)	-577(4)	1699(2)	76(2)
C(18)	3670(5)	3607(4)	1473(2)	75(2)
C(2)	3642(6)	790(4)	58(2)	75(2)
C(17)	3577(6)	3978(4)	1770(2)	82(2)
C(36)	3317(6)	-1264(5)	1862(2)	81(2)
C(24)	5405(9)	2019(6)	1994(2)	92(3)
C(15)	2450(6)	3024(5)	1865(2)	80(2)
C(20)	5546(7)	-443(5)	1406(3)	86(2)
C(26)	6889(9)	1643(8)	1956(3)	111(3)
C(14)	2558(6)	2674(4)	1577(2)	75(2)
C(29)	2770(7)	-1317(4)	1124(3)	84(2)
C(8)	4246(7)	-1945(5)	199(3)	95(3)
C(27)	6652(7)	1142(5)	1697(2)	88(2)
C(6)	3127(8)	-1834(6)	-214(2)	93(3)
C(25)	6290(11)	2112(6)	2090(3)	110(4)
C(33)	3350(7)	187(6)	2185(2)	94(3)
C(35)	3719(7)	-1208(6)	2173(3)	99(3)
Cl(2)	-20(2)	1876(2)	1370(1)	130(1)
Cl(1)	-127(2)	675(2)	703(1)	121(1)
C(102)	-993(8)	874(11)	944(3)	158(5)
C(101)	-993(9)	1502(10)	1144(7)	257(13)
Na(1)	1513(2)	1194(2)	1061(1)	87(1)
F(42)	4112(4)	-440(4)	2647(1)	126(2)
C(34)	3731(7)	-502(7)	2335(2)	101(3)
Cl(3)	4055(3)	5417(3)	2692(1)	179(2)
C(100)	4775(11)	6220(7)	2647(4)	176(6)

Tab. 79: Atomic coordinates (x 10^4) and equivalent isotropic displacement parameters (Å^2 x 10^3) for **12a**. U(eq) is defined as one third of the trace of the orthogonalized Uij tensor. Parts of the structure are severely disordered.

	x	**y**	**z**	**U(eq)**
Cl(1A)	1577(3)	3436(3)	2533(4)	64(2)
C(19A)	2840(20)	3608(6)	3088(18)	133(10)
Cl(1B)	1670(20)	3521(8)	2432(8)	98(7)
C(19B)	2984(14)	3654(8)	2776(11)	16(5)
Cl(4A)	-231(2)	4568(1)	1214(2)	72(1)
Cl(4B)	-241(5)	4632(2)	668(5)	59(2)
Cl(3A)	-429(4)	4556(2)	2459(3)	44(1)
Cl(5A)	30(20)	4614(18)	3896(17)	105(40)
C(31A)	-380(30)	4571(11)	3550(30)	190(30)
Cl(3B)	14(2)	5191(1)	3178(1)	47(1)
Cl(5B)	-505(3)	4125(1)	3538(2)	90(1)
C(31B)	164(6)	4922(4)	3891(3)	44(2)
Cl(5)	2266(1)	4407(1)	1076(1)	60(1)
Ag(1)	1697(1)	4881(1)	2325(1)	36(1)
Al(1)	3741(1)	6168(1)	2531(1)	20(1)
O(1)	5126(2)	6003(1)	2209(2)	23(1)
F(1C)	4745(2)	7343(1)	1746(1)	30(1)
F(1A)	7308(3)	5320(1)	3843(2)	38(1)
C(1C)	3871(4)	6796(2)	802(2)	23(1)
F(1B)	1017(3)	7261(1)	4047(2)	47(1)
C(1A)	6908(4)	6041(2)	3026(2)	25(1)
C(1B)	3049(4)	7233(2)	3690(2)	28(1)
O(2)	3942(3)	6398(1)	3419(2)	25(1)
F(2C)	6725(2)	7490(1)	1082(2)	39(1)
F(2A)	8507(3)	5879(2)	4794(2)	55(1)
C(2C)	4817(4)	7104(2)	1104(2)	25(1)
C(2A)	7426(4)	5824(2)	3666(3)	31(1)
C(2B)	1944(4)	7488(2)	3756(3)	36(1)
F(2B)	645(3)	8201(2)	3557(2)	71(1)
O(3)	3026(2)	6634(1)	1966(2)	22(1)
F(3C)	7049(2)	7038(1)	-235(2)	40(1)
F(3A)	8779(3)	6936(2)	4619(2)	54(1)
C(3C)	5867(4)	7186(2)	764(3)	29(1)
F(3B)	2320(4)	8720(1)	2810(2)	73(1)
C(3A)	8061(4)	6121(2)	4190(3)	37(1)
C(3B)	1730(5)	7986(2)	3483(3)	50(2)
F(4C)	5285(3)	6431(1)	-865(2)	36(1)
F(4B)	4490(4)	8256(1)	2655(2)	54(1)
C(4C)	6027(4)	6962(2)	96(2)	30(1)
F(4A)	7796(3)	7403(1)	3395(2)	46(1)
C(4A)	8194(4)	6648(2)	4107(3)	39(1)
C(4B)	2575(6)	8252(2)	3107(3)	52(2)
F(5A)	6592(2)	6856(1)	2401(2)	33(1)
F(5B)	4965(2)	7330(1)	3201(1)	34(1)
F(5C)	3305(2)	6259(1)	-230(1)	32(1)
C(5C)	5135(4)	6662(2)	-217(2)	27(1)
C(5A)	7689(4)	6886(2)	3493(3)	36(1)
C(5B)	3653(6)	8014(2)	3026(3)	43(1)
F(6C)	2677(2)	7677(1)	1478(1)	30(1)
F(6A)	8042(2)	5526(1)	1903(1)	31(1)
F(6B)	3839(2)	7016(1)	5141(1)	36(1)
C(6C)	4085(4)	6580(2)	125(2)	25(1)
C(6B)	3878(4)	7522(2)	3315(2)	31(1)
C(6A)	7060(4)	6587(2)	2973(3)	30(1)
F(7A)	7164(2)	6230(1)	1461(1)	31(1)

F(7C)	1765(2)	7389(1)	479(1)	31(1)
F(7B)	5335(2)	6957(1)	4444(1)	33(1)
C(7A)	6183(4)	5753(2)	2396(2)	22(1)
C(7C)	2727(4)	6739(2)	1244(2)	23(1)
C(7B)	3406(4)	6670(2)	3955(2)	25(1)
F(8C)	266(2)	7741(1)	1414(2)	41(1)
F(8A)	7261(3)	5408(1)	550(2)	40(1)
C(8C)	2022(4)	7278(2)	1187(2)	26(1)
C(8A)	6957(4)	5741(2)	1706(2)	25(1)
F(8B)	5375(3)	6305(2)	5597(2)	52(1)
C(8B)	4323(4)	6717(2)	4620(2)	28(1)
F(9C)	1068(2)	7269(1)	2302(1)	33(1)
F(9A)	5480(3)	5698(1)	755(2)	34(1)
F(9B)	5417(3)	5931(1)	4537(2)	41(1)
C(9A)	6424(4)	5435(2)	1051(2)	29(1)
C(9B)	4718(5)	6196(2)	4979(3)	38(1)
C(9C)	832(4)	7285(2)	1570(3)	29(1)
F(10A)	6985(2)	4566(1)	1327(2)	35(1)
F(10C)	-527(2)	6908(1)	704(2)	40(1)
C(10A)	6022(4)	4874(2)	1219(2)	28(1)
C(10C)	-12(4)	6827(2)	1373(2)	31(1)
C(10B)	3681(6)	5832(2)	5167(3)	45(1)
F(10B)	4126(4)	5351(2)	5332(2)	62(1)
F(11A)	5348(3)	4682(1)	653(2)	39(1)
Cl(11)	2939(1)	4282(1)	3291(1)	51(1)
F(11C)	-879(2)	6809(1)	1850(2)	43(1)
C(11C)	649(4)	6294(2)	1380(2)	29(1)
C(11A)	5282(4)	4863(2)	1903(3)	28(1)
F(11B)	3171(3)	6021(2)	5756(2)	55(1)
C(11B)	2740(5)	5782(2)	4530(3)	43(1)
F(12A)	5137(3)	4358(1)	2105(2)	37(1)
F(12C)	-72(2)	5931(1)	1051(2)	37(1)
C(12C)	1816(4)	6316(2)	963(2)	25(1)
C(12A)	5894(4)	5164(2)	2553(2)	27(1)
F(12B)	1757(3)	5547(1)	4772(2)	57(1)
C(12B)	2357(4)	6330(2)	4219(3)	34(1)
F(13A)	4192(2)	5057(1)	1717(2)	33(1)
F(13C)	846(2)	6138(1)	2074(1)	33(1)
F(13B)	3168(3)	5470(1)	4017(2)	45(1)
F(14A)	6890(2)	4872(1)	2721(2)	31(1)
F(14C)	1401(2)	6394(1)	264(1)	31(1)
F(14B)	1802(3)	6552(1)	4775(2)	42(1)
F(15C)	2339(2)	5836(1)	1006(1)	29(1)
F(15A)	5175(2)	5137(1)	3114(1)	29(1)
F(15B)	1545(2)	6252(1)	3658(2)	39(1)
C(41)	839(5)	4185(3)	746(3)	51(1)
F(100)	2863(2)	5629(1)	2545(1)	28(1)

Tab. 80: Atomic coordinates (x 10^4) and equivalent isotropic displacement parameters (Å^2 x 10^3) for **12b**. U(eq) is defined as one third of the trace of the orthogonalized Uij tensor.

	x	**y**	**z**	**U(eq)**
Ag(1)	3748(1)	3261(1)	6121(1)	89(1)
C(107)	3830(4)	2287(2)	6021(3)	61(1)
C(111)	5529(4)	2570(2)	5519(2)	61(1)
C(112)	4932(4)	2483(2)	6097(2)	57(1)
C(108)	3323(4)	2178(2)	5373(3)	71(1)
C(114)	2990(8)	3577(3)	4677(4)	106(2)
C(113)	2108(7)	3866(2)	5651(3)	94(2)
C(110)	5016(4)	2466(3)	4882(3)	87(2)
Al(1)	1472(1)	5823(1)	7775(1)	32(1)
F(1)	2212(2)	5594(1)	8473(1)	38(1)
F(1B)	147(2)	5423(1)	8999(1)	41(1)
F(5B)	1124(2)	3914(1)	7723(1)	53(1)
F(6B)	-355(2)	4216(1)	6888(1)	45(1)
F(7B)	1136(2)	4724(1)	6827(1)	45(1)
F(1A)	3221(2)	6557(1)	8631(1)	45(1)
F(1C)	3176(2)	4864(1)	7656(1)	43(1)
F(14A)	-874(2)	6316(1)	8475(1)	47(1)
F(12B)	-2126(2)	5719(1)	7214(1)	53(1)
F(14C)	3254(2)	6725(1)	7190(1)	44(1)
F(8B)	-289(2)	5498(1)	6268(1)	53(1)
F(15C)	4501(2)	6530(1)	6452(1)	48(1)
F(12C)	1522(2)	6482(1)	6204(1)	50(1)
O(1A)	1179(2)	6484(1)	7898(1)	36(1)
F(2B)	1316(2)	5045(1)	10071(1)	52(1)
F(6A)	2353(2)	7418(1)	8241(1)	50(1)
F(14B)	-1710(2)	5182(1)	8345(1)	48(1)
F(8A)	925(2)	8124(1)	7566(1)	62(1)
F(5C)	5414(2)	6422(1)	7615(1)	51(1)
O(1B)	195(2)	5479(1)	7623(1)	34(1)
F(12A)	-759(2)	6652(1)	7134(1)	51(1)
F(15B)	-1780(2)	4436(1)	7810(1)	48(1)
F(10B)	-2383(2)	4538(1)	6338(1)	55(1)
O(1C)	2279(2)	5741(1)	7065(1)	35(1)
F(2C)	4419(2)	4559(1)	8746(1)	62(1)
F(8C)	1857(2)	5391(1)	5686(1)	57(1)
F(7A)	918(2)	7697(1)	8777(1)	55(1)
F(15A)	-949(2)	7134(1)	8798(1)	52(1)
F(6C)	4765(2)	5550(1)	6146(1)	53(1)
F(13C)	2777(2)	7024(1)	5863(1)	58(1)
F(13B)	-3314(2)	5070(1)	7262(1)	56(1)
F(9A)	1178(2)	7385(1)	7052(1)	54(1)
F(4C)	6629(2)	6091(1)	8697(1)	60(1)
F(11B)	-2472(2)	5345(1)	5986(1)	65(1)
F(9B)	-498(2)	4744(1)	5765(1)	59(1)
C(7A)	851(3)	6801(1)	8419(2)	37(1)
F(7C)	3552(2)	4960(1)	6416(1)	51(1)
F(3C)	6168(2)	5157(1)	9301(1)	68(1)
F(4B)	2193(2)	3540(1)	8825(1)	71(1)
F(2A)	4289(2)	6210(1)	9758(1)	67(1)
F(13A)	-2154(2)	6987(1)	7656(1)	62(1)
F(3B)	2318(2)	4076(1)	10028(1)	69(1)
F(10A)	-950(2)	7646(1)	6808(1)	68(1)
C(2C)	4041(3)	5182(1)	7873(2)	39(1)
C(7C)	3402(3)	5817(1)	6925(2)	35(1)
F(9C)	3357(2)	5325(1)	5104(1)	65(1)
F(11A)	-1120(2)	7883(1)	7867(1)	65(1)
F(5A)	-220(2)	6635(1)	9791(1)	63(1)

C(2A)	2591(3)	6513(1)	9177(2)	41(1)
C(3B)	1222(3)	4755(1)	9496(2)	42(1)
C(9B)	-658(3)	5008(2)	6353(2)	44(1)
C(8C)	3659(3)	5479(1)	6289(2)	41(1)
C(7B)	-137(3)	4965(1)	7670(2)	34(1)
C(9A)	680(3)	7607(1)	7580(2)	47(1)
C(4C)	5548(3)	5316(2)	8738(2)	49(1)
C(6B)	1083(3)	4209(1)	8292(2)	40(1)
C(12C)	3467(3)	6398(1)	6672(2)	39(1)
C(5C)	5773(3)	5787(2)	8437(2)	45(1)
C(1B)	504(3)	4686(1)	8288(2)	33(1)
C(11A)	-1000(3)	6980(2)	7640(2)	48(1)
C(11C)	2607(3)	6520(1)	6053(2)	43(1)
F(11C)	1934(2)	6232(1)	4947(1)	70(1)
C(8B)	18(3)	4720(1)	6954(2)	37(1)
C(2B)	604(3)	4950(1)	8920(2)	35(1)
C(8A)	1209(3)	7378(1)	8263(2)	41(1)
C(1C)	4233(3)	5658(1)	7547(2)	37(1)
F(4A)	919(2)	6318(1)	10909(1)	81(1)
F(10C)	3772(2)	6313(1)	5155(1)	64(1)
C(4B)	1745(3)	4277(2)	9472(2)	48(1)
C(11B)	-2214(3)	5196(2)	7175(2)	44(1)
C(5A)	1486(4)	6381(2)	10336(2)	55(1)
C(3A)	3174(3)	6332(2)	9765(2)	50(1)
C(6A)	906(3)	6556(2)	9742(2)	49(1)
C(1A)	1423(3)	6634(1)	9128(2)	39(1)
F(3A)	3184(2)	6089(1)	10930(1)	83(1)
C(10B)	-1944(3)	5018(2)	6453(2)	47(1)
C(3C)	4675(3)	5017(1)	8453(2)	44(1)
C(10A)	-609(3)	7535(2)	7467(2)	51(1)
C(4A)	2624(4)	6265(2)	10355(2)	57(1)
C(12A)	-483(3)	6797(1)	8354(2)	41(1)
C(12B)	-1446(3)	4945(1)	7759(2)	38(1)
C(9C)	2900(3)	5585(2)	5627(2)	48(1)
C(6C)	5121(3)	5954(1)	7853(2)	40(1)
C(10C)	2802(3)	6166(2)	5432(2)	52(1)
C(5B)	1676(3)	4009(1)	8867(2)	47(1)
C(115)	2993(6)	3881(2)	5239(4)	83(2)
C(117)	1188(7)	3245(3)	4941(6)	107(2)
F(2)	292(5)	2926(2)	4776(4)	201(3)
C(118)	1196(6)	3543(3)	5503(5)	112(2)
C(116)	2047(11)	3246(3)	4524(4)	123(3)
C(101)	4081(6)	3741(3)	7228(3)	87(2)
C(102)	5156(8)	3873(2)	7086(4)	104(2)
C(103)	6053(6)	3572(4)	7328(5)	113(3)
C(106)	3887(6)	3304(3)	7588(4)	98(2)
F(41)	4612(15)	2568(3)	8161(4)	276(8)
C(124)	5978(17)	3149(9)	7650(9)	96(7)
C(125)	4950(20)	3050(8)	7839(12)	117(10)
F(42)	6699(11)	2924(4)	8062(6)	129(7)
C(134)	5649(16)	3160(9)	7786(13)	48(7)
C(135)	4617(18)	2958(9)	7822(15)	40(5)
F(31)	3428(5)	2293(2)	4146(3)	92(3)
F(32)	6568(11)	2714(5)	5538(6)	72(6)
F(33)	5648(9)	2260(5)	4365(5)	90(6)
C(109)	3923(4)	2275(3)	4823(3)	89(2)

Tab. 81: Atomic coordinates (x 10^4) and equivalent isotropic displacement parameters ($Å^2$ x 10^3) for **13**. U(eq) is defined as one third of the trace of the orthogonalized Uij tensor.

	x	**y**	**z**	**U(eq)**
Ga(1)	0	0	2876(1)	21(1)
Cl(1)	424(1)	-1226(1)	3379(1)	35(1)
O(1)	346(1)	799(1)	2294(1)	17(1)
F(1)	607(1)	-1180(1)	1702(1)	23(1)
F(15)	790(1)	1723(1)	3262(1)	25(1)
F(5)	1656(1)	535(1)	3094(1)	27(1)
F(13)	772(1)	4176(1)	3004(1)	36(1)
F(9)	238(1)	2654(1)	1460(1)	28(1)
F(7)	829(1)	847(1)	1271(1)	25(1)
F(3)	1889(1)	-3432(2)	2380(1)	38(1)
F(14)	1372(1)	2473(1)	2745(1)	24(1)
F(2)	1108(1)	-3190(1)	1701(1)	31(1)
F(6)	1420(1)	1825(1)	1660(1)	25(1)
F(8)	884(1)	3315(1)	1052(1)	34(1)
F(11)	1201(1)	4280(1)	2006(1)	33(1)
F(10)	464(1)	4814(1)	1902(1)	36(1)
F(12)	173(1)	3172(1)	2655(1)	30(1)
F(4)	2134(1)	-1518(2)	3081(1)	36(1)
C(9)	703(1)	2872(2)	1546(1)	25(1)
C(2)	1001(1)	-1160(2)	2035(1)	19(1)
C(8)	951(1)	1648(2)	1694(1)	20(1)
C(1)	1127(1)	-122(2)	2357(1)	19(1)
C(7)	827(1)	1070(2)	2291(1)	18(1)
C(10)	754(1)	3859(2)	2010(1)	26(1)
C(11)	641(1)	3331(2)	2610(1)	25(1)
C(5)	1766(1)	-1409(2)	2726(1)	26(1)
C(6)	1512(1)	-314(2)	2717(1)	22(1)
C(3)	1250(1)	-2251(2)	2032(1)	25(1)
C(4)	1641(1)	-2373(2)	2377(1)	27(1)
C(12)	916(1)	2119(2)	2733(1)	21(1)
F(101)	0	0	831(1)	41(1)
C(101)	0	0	245(1)	22(1)
C(102)	106(1)	1074(3)	-31(1)	33(1)
Li(1)	0	0	1647(2)	25(1)
C(103)	106(1)	1064(4)	-618(2)	59(1)
C(104)	0	0	-907(2)	79(3)

Tab. 82: Atomic coordinates (x 10^4) and equivalent isotropic displacement parameters (Å^2 x 10^3) for **14**. U(eq) is defined as one third of the trace of the orthogonalized Uij tensor. Preliminary structure model from weak crystal (only isotropic refinement).

	x	**y**	**z**	**U(eq)**
Ga(1)	-4465(1)	3528(3)	3398(2)	25(1)
Br(02)	-4506(1)	2190(3)	4346(2)	39(1)
Br(1)	-5454(1)	4799(3)	2559(2)	38(1)
F(005)	-5327(10)	-617(15)	1827(12)	42(4)
F(006)	-3940(7)	4760(13)	2096(10)	29(3)
F(007)	-5695(8)	1108(13)	610(9)	27(3)
F(009)	-4044(7)	5311(14)	4984(10)	30(3)
O(1)	-4242(9)	2788(15)	2656(11)	20(4)
F(011)	-4390(9)	361(15)	2994(10)	37(4)
F(013)	-2102(10)	226(17)	7142(14)	46(4)
F(016)	-3013(8)	4137(15)	6719(11)	34(4)
F(017)	-5604(7)	1800(14)	1835(9)	27(3)
F(018)	-2513(9)	2119(14)	7680(11)	36(4)
F(020)	-2707(7)	2438(13)	4538(9)	25(3)
F(022)	-4694(7)	1792(12)	447(9)	24(3)
F(025)	-3755(7)	2778(13)	1607(9)	24(3)
F(026)	-4468(10)	6765(16)	1130(13)	46(4)
F(028)	-6807(8)	5060(16)	-839(11)	37(4)
O(12)	-3571(9)	4379(15)	4013(11)	21(4)
F(8)	-3558(8)	341(15)	1499(12)	38(4)
F(6)	-2983(8)	6075(12)	6095(9)	25(3)
F(7)	-6317(8)	3009(14)	100(10)	30(3)
F(5)	-4789(9)	-651(13)	900(11)	32(3)
F(2)	-2233(9)	451(14)	5535(12)	41(4)
F(1)	-2512(9)	3566(19)	3243(12)	47(4)
F(4)	-3959(10)	-1197(17)	2371(13)	51(5)
F(17)	-5898(8)	7022(16)	-370(11)	38(4)
C(3)	-2655(13)	2460(30)	5310(20)	28(6)
C(4)	-2827(12)	3510(20)	5630(19)	26(6)
C(5)	-3096(13)	4630(20)	4976(16)	15(5)
C(6)	-4818(17)	230(30)	2081(19)	40(7)
C(7)	-5215(15)	1430(30)	1536(19)	32(6)
C(8)	-4262(12)	1950(20)	1385(16)	20(6)
C(9)	-3589(15)	6920(30)	4600(20)	33(7)
C(10)	-6095(13)	4990(20)	-131(16)	22(5)
C(11)	-2510(12)	6440(20)	4660(18)	23(6)
C(12)	-2885(15)	7510(20)	4810(16)	24(6)
C(13)	-2356(13)	5200(20)	5217(15)	19(5)
C(040)	-4657(14)	4770(30)	1314(16)	28(6)
C(046)	-2392(12)	1350(20)	5854(16)	20(6)
C(047)	-3429(15)	5700(30)	5180(20)	33(7)
C(048)	-5089(17)	3690(30)	1085(19)	36(7)
C(049)	-4350(14)	-230(20)	1805(16)	25(6)
C(050)	-2795(13)	3300(20)	6413(17)	21(5)
C(052)	-4703(13)	2450(20)	1714(16)	29(6)
C(060)	-4910(13)	5820(20)	859(18)	22(5)
C(061)	-2556(15)	2200(30)	6941(17)	39(8)
C(062)	-5832(14)	3900(20)	358(18)	25(6)
C(064)	-5642(15)	5950(20)	110(20)	33(7)
C(066)	-2341(13)	1220(20)	6636(18)	25(6)
C(100)	-1928(9)	3678(16)	3279(14)	29(6)
C(101)	-1668(13)	2669(14)	3096(15)	46(8)
C(102)	-1060(14)	2790(30)	3137(17)	80(18)
C(103)	-713(10)	3920(30)	3360(19)	180(50)
C(104)	-972(12)	4930(20)	3542(17)	130(30)

C(105)	-1580(12)	4809(14)	3502(15)	38(7)
F(12)	-2080(7)	4460(13)	4958(10)	28(3)
F(13)	-1869(7)	5427(15)	6146(10)	30(3)
F(10)	-2437(9)	7855(14)	5699(10)	36(4)
F(14)	-3838(10)	7752(15)	4881(12)	42(4)
F(11)	-3059(10)	8389(15)	4242(12)	44(4)
F(15)	-4077(7)	6740(14)	3692(9)	24(3)
F(16)	-2874(8)	6226(15)	3767(10)	31(3)
Li(1)	-3320(20)	3620(30)	3280(40)	28(10)
F(21)	-1846(9)	6897(16)	5004(11)	41(4)
F(20)	-3323(7)	956(14)	2802(10)	33(4)
C(20)	-3857(13)	730(20)	1876(16)	23(5)

Tab. 83: Atomic coordinates (x 10^4) and equivalent isotropic displacement parameters (Å^2 x 10^3) for **14**. U(eq) is defined as one third of the trace of the orthogonalized Uij tensor.

	x	**y**	**z**	**U(eq)**
Al(1)	8489(1)	2916(1)	10732(1)	21(1)
F(9C)	10241(2)	695(1)	12227(1)	33(1)
F(7A)	9527(2)	2810(1)	12834(1)	26(1)
F(1A)	10254(2)	2938(1)	11344(1)	26(1)
F(2B)	4140(2)	3182(1)	8959(1)	30(1)
F(13A)	6331(2)	3899(1)	11540(1)	25(1)
F(1B)	6272(2)	2827(1)	9007(1)	25(1)
F(6B)	9366(2)	4297(1)	10129(1)	24(1)
F(6A)	9572(2)	3607(1)	13651(1)	29(1)
F(7B)	9126(2)	4547(1)	8787(1)	27(1)
F(8B)	10865(2)	3389(1)	9916(1)	29(1)
F(9A)	7858(2)	2892(1)	13808(1)	29(1)
F(9B)	11276(2)	4283(1)	9463(1)	34(1)
F(15A)	8162(2)	4695(1)	11547(1)	33(1)
F(12A)	6356(2)	4674(1)	12378(1)	32(1)
O(1A)	8370(2)	3470(1)	11439(1)	18(1)
F(14A)	8586(2)	4671(1)	12928(1)	36(1)
O(1B)	8542(2)	3128(1)	9731(1)	21(1)
F(8A)	7253(2)	2756(1)	12451(1)	24(1)
F(3B)	3607(2)	4390(1)	9059(1)	35(1)
F(5B)	7491(2)	4925(1)	9282(1)	28(1)
F(11B)	10430(2)	3964(1)	7859(1)	34(1)
F(4B)	5354(2)	5240(1)	9238(1)	31(1)
F(6C)	8365(2)	1485(1)	12224(1)	29(1)
F(7C)	8072(2)	637(1)	11504(1)	32(1)
F(8C)	10450(2)	1637(1)	11861(1)	34(1)
F(1C)	6694(2)	2772(1)	10663(1)	25(1)
F(14C)	7723(2)	803(1)	9687(1)	39(1)
O(1C)	8530(2)	2152(1)	10906(1)	24(1)
F(15C)	7862(2)	1749(1)	9287(1)	34(1)
F(10B)	11555(2)	3237(1)	8505(1)	37(1)
C(9C)	9866(3)	1113(1)	11615(2)	27(1)
C(7C)	7947(3)	1600(1)	10740(2)	22(1)
C(6B)	6716(3)	4463(1)	9177(2)	21(1)
C(7A)	8971(3)	3762(1)	12162(2)	17(1)
C(12C)	8251(3)	1347(1)	9919(2)	29(1)
C(4B)	4698(3)	4221(2)	9077(2)	25(1)
C(11A)	6923(3)	4154(1)	12263(2)	23(1)
C(9B)	10510(3)	3814(2)	9308(2)	25(1)
C(1A)	10260(3)	3883(1)	12136(2)	20(1)
C(12A)	8193(3)	4335(1)	12225(2)	23(1)
C(1B)	7036(3)	3854(1)	9106(2)	19(1)
C(1C)	6610(3)	1654(1)	10646(2)	24(1)
C(8C)	8535(3)	1203(1)	11519(2)	23(1)
C(9A)	7744(3)	3168(1)	13050(2)	21(1)
C(5B)	5582(3)	4643(1)	9158(2)	24(1)
C(2C)	6082(3)	2227(2)	10650(2)	24(1)
C(7B)	8272(3)	3590(1)	9132(2)	19(1)
C(8A)	8975(3)	3340(1)	12931(2)	20(1)
C(2B)	6104(3)	3434(1)	9038(2)	22(1)
C(10B)	10533(3)	3523(2)	8451(2)	27(1)
C(8B)	9288(3)	4072(1)	9338(2)	21(1)
C(3B)	4967(3)	3609(2)	9022(2)	23(1)
F(2A)	12761(2)	4896(1)	12813(2)	49(1)
F(4A)	12468(2)	3023(1)	11353(1)	39(1)
C(5A)	11993(3)	3472(2)	11727(2)	29(1)
F(3A)	13775(2)	4012(1)	12048(2)	47(1)

C(4A)	12649(3)	3969(2)	12081(2)	34(1)
C(3A)	12144(3)	4412(2)	12473(2)	32(1)
F(14B)	7561(2)	2846(1)	8024(1)	28(1)
F(15B)	8002(2)	3759(1)	7649(1)	28(1)
F(12B)	9457(2)	2904(1)	7360(1)	36(1)
F(13B)	9768(2)	2555(1)	8648(1)	30(1)
F(12C)	10131(2)	1799(1)	10035(1)	38(1)
F(5A)	10580(2)	4827(1)	12902(1)	40(1)
F(10A)	7227(2)	4031(1)	13736(1)	36(1)
F(10C)	9783(2)	298(1)	10681(1)	50(1)
F(11A)	5821(2)	3507(1)	12940(1)	35(1)
F(13C)	9728(2)	955(1)	9307(1)	49(1)
F(11C)	11327(2)	884(1)	10880(2)	56(1)
C(2A)	10835(3)	3447(1)	11750(2)	23(1)
C(12B)	8319(3)	3318(1)	8245(2)	23(1)
C(11C)	9584(4)	1254(2)	10006(2)	34(1)
C(10C)	10161(4)	881(2)	10791(2)	35(1)
C(10A)	6913(3)	3718(2)	13008(2)	26(1)
F(2C)	4513(2)	2885(1)	10669(1)	36(1)
F(5C)	6160(2)	576(1)	10515(1)	39(1)
F(3C)	3069(2)	1889(1)	10580(1)	45(1)
F(4C)	3964(2)	744(1)	10497(2)	48(1)
C(3C)	4925(3)	2317(2)	10630(2)	29(1)
C(4C)	4200(3)	1819(2)	10591(2)	33(1)
C(6A)	10980(3)	4368(2)	12502(2)	26(1)
C(11B)	9522(3)	3062(2)	8174(2)	26(1)
C(6C)	5830(3)	1158(2)	10573(2)	30(1)
C(5C)	4653(3)	1239(2)	10556(2)	35(1)

6.12. Crystal structure data of compounds described in chapter 4

Tab. 84: Crystal data and structure refinement parameters for compounds **16**, **17** and **19**.

compound index number	**16**	**17**	**19**
compound	**ICS^+ $[Al(OC(CF_3)_3)_4]^-$**	**$Cl_3C_2S_2^+$ $[Al(OC(CF_3)_3)_4]^{-[b]}$**	**$[Ag(P_4)_2]^+$ $[Al(OC(CF_3)_2(C_6F_5))_4]^-$**
sum formula[a]	$C_{17}O_4Al_1F_{36}I_1S_1$	$C_{19}H_2O_4Al_1Cl_5F_{36}S_2$	$C_{38}H_4O_4Al_1Ag_1Cl_4F_{44}P_8$
T [K]	150(2)	150(2)	100(2)
crystal system	cubic	orthorhombic	triclinic
space group	$P2_13$	$P2_12_12_1$	$P\bar{1}$
a [Å]	14.724(2)	12.091(2)	11.667(4)
b [Å]	14.724(2)	16.423(3)	16.537(6)
c [Å]	14.724(2)	19.313(4)	16.5399(6)
α [°]	90	90	84.67(2)
β [°]	90	90	71.79(2)
γ [°]	90	90	71.79(2)
V [$Å^3$]	3192.0(6)	3834.9(13)	2879.5(2)
Z	4	4	2
F(000)	2160	2408	1816
ρ (calculated) [g cm^{-3}]	2.368	2.159	2.174
μ [mm^{-1}]	1.337	0.718	0.960
Crystal dimensions [mm]	0.3 x 0.3 x 0.3	0.5 x 0.5 x 0.2	0.2 x 0.2 x 0.1
θ range for data collection [°]	1.96 to 26.00	6.81 to 23.25	6.81 to 27.48
h,k,l index ranges	-17<=h<=18 -18<=k<=18 -18<=l<=18	-13<=h<=13 -18<=k<=18 0<=l<=21	-15<=h<=14 -21<=k<=16 -21<=l<=21
collected reflections	25543	10131	40441
unique reflections	2110	5349	12941
R_{int}	0.0604	0.0425	0.0767
Completeness to θ_{max}	99.8 %	96.1 %	98.0 %
Absorption correction	numerical	numerical	empirical + spherical
Data / restraints / parameters	2110 / 41 / 242	5349 / 120 / 605	12941 / 0 / 913
Goodness-of-fit on F^2 (S)	1.063	2.417	0.970
Final R_1 [I > 2σ(I)]	0.0632	0.1323	0.0498
Final wR_2 [I > 2σ(I)]	0.1637	0.3167	0.0827
Final R_1 (all data)	0.0808	0.1505	0.0908
Final wR_2 (all data)	0.1767	0.3291	0.0971
Largest peak and hole [e $Å^{-3}$]	0.646 and -0.460	1.240 and -0.626	0.920 and -0.602

[a] Of the monomer, where applicable; [b] structure must be considered fragmentary.

Tab. 85: Crystal data and structure refinement parameters for compounds **20**, **21** and **22**.

compound index number	**20**	**21**	**22**
compound	**$[Ag(S_8)(1,2\text{-}C_6H_4F_2)]^+$** **$[FAl(O(C_6F_{10})C_6F_5)_3]^-$**	**CPh_3^+** **$[ClAl(O(C_6F_{10})C_6F_5)_3]^-$**	**$(1,2\text{-}C_6H_4F_2)GaF$** **$Al(O(C_6F_{10})C_6F_5)_3$**
sum formula[a]	$C_{42}H_4O_3Ag_1Al_1F_{48}S_8$	$C_{55}H_{15}O_3Al_1Cl_1F_{45}$	$C_{42}H_4O_3Al_1F_{48}$
T [K]	100(2)	110(2)	100(2)
crystal system	triclinic	trigonal	orthorhombic
space group	$P\bar{1}$	$R3_2$	$P2_12_12_1$
a [Å]	10.990(2)	16.246(2)	14.108(3)
b [Å]	15.602(3)	16.246(2)	17.959(4)
c [Å]	17.795(4)	89.729(18)	19.105(4)
α [°]	81.99(3)	90	90
β [°]	72.48(3)	90	90
γ [°]	82.14(3)	90	90
V [Å^3]	2866.8(10)	20510(6)	4840.5(17)
Z	2	12	4
F(000)	1796	9642	3024
ρ (calculated) [g cm^{-3}]	2.153	1.593	2.148
μ [mm^{-1}]	0.858	0.230	0.817
Crystal dimensions [mm]	unknown	0.2 x 0.2 x 0.1 mm	0.08 x 0.06 x 0.06
θ range for data collection [°]	3.02 to 23.26	3.03 to 21.96	6.82 to 26.37
h,k,l index ranges	-12<=h<=12 -17<=k<=17 -19<=l<=19	-17<=h<=17 -17<=k<=17 -94<=l<=94	-17<=h<=17 -18<=k<=22 -21<=l<=23
collected reflections	27714	85931	51771
unique reflections	8168	5568	9720
R_{int}	0.0949	0.1098	0.0550
Completeness to θ_{max}	99.4 %	99.5 %	97.7 %
Absorption correction	empirical + spherical	empirical + spherical	empirical + spherical
Data / restraints / parameters	8168 / 0 / 938	5568 / 0 / 636	9720 / 0 / 872
Goodness-of-fit on F^2 (S)	1.016	1.114	1.053
Final R_1 [$I > 2\sigma(I)$]	0.0488	0.0886	0.0323
Final wR_2 [$I > 2\sigma(I)$]	0.0798	0.2558	0.0554
Final R_1 (all data)	0.0978	0.0978	0.0433
Final wR_2 (all data)	0.0947	0.2635	0.0592
Largest peak and hole [e Å^{-3}]	0.830 and -0.581	1.183 and -0.976	0.473 and -0.519

[a] Of the monomer, where applicable.

Tab. 86: Atomic coordinates (x 10^4) and equivalent isotropic displacement parameters (Å^2 x 10^3) for **16**. U(eq) is defined as one third of the trace of the orthogonalized Uij tensor.

	x	**y**	**z**	**U(eq)**
I	319(1)	9681(1)	4681(1)	86(1)
S	1631(2)	8369(2)	3369(2)	79(1)
C	1046(5)	8954(5)	3954(5)	72(3)
IA	1557(5)	8443(5)	3443(5)	234(6)
Al(1)	-1955(1)	11955(1)	6955(1)	21(1)
O(1)	-2378(4)	10891(3)	6958(3)	78(1)
C(1)	-2856(2)	10168(3)	6674(2)	31(1)
F(2)	-4227(3)	9830(5)	5895(3)	116(2)
F(3)	-3793(3)	11209(4)	5918(4)	108(2)
F(4)	-1497(3)	9691(6)	5984(4)	144(3)
F(5)	-2640(6)	8877(3)	5737(4)	139(3)
F(8)	-3517(4)	8845(3)	7340(4)	116(2)
F(9)	-3101(4)	9869(4)	8245(3)	97(2)
C(2)	-3826(4)	10448(6)	6386(6)	70(2)
C(3)	-2345(6)	9703(6)	5876(4)	67(2)
C(4)	-2896(5)	9482(4)	7468(4)	53(2)
F(1)	-4322(3)	10617(5)	7160(5)	116(2)
F(6)	-2551(4)	10200(4)	5106(3)	85(2)
F(7)	-2070(3)	9096(3)	7573(4)	86(2)
C(2A)	-3411(12)	10447(18)	5828(10)	28(6)
C(3A)	-2160(11)	9402(12)	6500(30)	63(12)
C(4A)	-3474(11)	9990(20)	7507(10)	32(7)
F(1A)	-3070(20)	10400(20)	5090(20)	65(7)
F(6A)	-1500(50)	9270(50)	7490(50)	160(20)
F(7A)	-4090(50)	9990(50)	7770(50)	180(20)
O(2)	-2405(5)	12692(9)	7730(8)	36(3)
C(5)	-3115(3)	13115(3)	8115(3)	45(2)
F(10)	-2823(5)	14522(4)	7481(4)	256(6)
C(6)	-2552(4)	14001(5)	8166(4)	94(6)
F(11)	-1665(5)	13908(6)	8088(6)	90(3)
F(12)	-2691(6)	14473(7)	8917(6)	189(5)
C(6A)	-2844(4)	14106(6)	8308(5)	158(8)
F(11A)	-2014(6)	14056(11)	8706(7)	229(8)
F(12A)	-3500(7)	14440(8)	8867(8)	256(9)

Tab. 87: Atomic coordinates (x 10^4) and equivalent isotropic displacement parameters (Å^2 x 10^3) for **17**. U(eq) is defined as one third of the trace of the orthogonalized Uij tensor.

	x	**y**	**z**	**U(eq)**
Cl(1)	3275(1)	9361(1)	2676(1)	68(1)
Cl(2)	828(1)	11773(1)	2114(1)	109(1)
Cl(3)	2558(1)	11855(1)	1168(1)	127(1)
Cl(4)	-7504(1)	11587(1)	5983(1)	101(1)
Cl(5)	-5798(1)	11717(1)	7022(1)	81(1)
S(1)	2960(1)	11132(1)	2541(1)	75(1)
S(2)	1872(1)	10236(1)	1656(1)	134(1)
Al(1)	-2000(1)	9971(1)	5320(1)	23(1)
O(1)	-934(2)	10026(1)	4748(1)	74(1)
O(2)	-1986(2)	9037(1)	5704(1)	79(1)
O(3)	-3186(1)	10107(1)	4897(1)	81(1)
O(4)	-1862(2)	10684(1)	5946(1)	59(1)
C(1)	-141(1)	9884(1)	4294(1)	39(1)
C(2)	907(1)	9597(1)	4712(1)	487(7)
C(3)	-414(1)	9200(1)	3755(1)	621(3)
C(4)	196(1)	10672(1)	3888(1)	435(6)
C(5)	-1926(1)	8510(1)	6230(1)	53(1)
C(6)	-696(1)	8352(1)	6436(1)	664(3)
C(7)	-2569(1)	8877(1)	6859(1)	1093(2)
C(8)	-2480(1)	7694(1)	6002(1)	74(1)
C(9)	-4155(1)	10033(1)	4568(1)	43(1)
C(10)	-4421(1)	9118(1)	4440(1)	143(2)
C(11)	-4142(1)	10501(1)	3864(1)	406(2)
C(12)	-5052(1)	10417(1)	5050(1)	312(5)
C(13)	-1744(1)	11446(1)	6198(1)	41(1)
C(14)	-2380(1)	12095(1)	5824(1)	145(2)
C(15)	-520(1)	11604(1)	6116(1)	235(2)
C(16)	-2042(1)	11413(1)	6946(1)	183(3)
C(100)	2725(2)	10147(2)	2316(1)	48(1)
C(101)	1996(2)	11329(1)	1828(1)	50(1)
C(102)	-6431(4)	12172(2)	6329(2)	96(1)
F(1)	943(3)	10156(1)	5217(1)	663(3)
F(2)	648(2)	8836(1)	4906(1)	345(2)
F(3)	1677(2)	9663(1)	4216(1)	513(7)
F(4)	-1078(2)	8663(1)	4148(1)	215(2)
F(5)	634(1)	8907(1)	3551(1)	341(2)
F(6)	-958(2)	9745(1)	3307(1)	510(2)
F(7)	-739(1)	11017(1)	3729(1)	395(3)
F(8)	724(2)	10326(2)	3382(1)	390(2)
F(9)	812(2)	11080(1)	4321(1)	502(5)
F(10)	-175(2)	9069(1)	6442(1)	214(2)
F(11)	-308(1)	7852(1)	5948(1)	183(2)
F(12)	-731(3)	8004(1)	7060(1)	296(1)
F(13)	-3514(1)	9229(1)	6623(1)	143(1)
F(14)	-2783(2)	8244(1)	7292(1)	255(2)
F(15)	-1862(2)	9427(1)	7145(1)	179(2)
F(16)	-2195(2)	7080(1)	6398(1)	122(1)
F(17)	-2207(2)	7503(1)	5366(1)	108(1)
F(18)	-3553(1)	7785(1)	6033(1)	130(1)
F(19)	-4846(2)	8831(2)	5037(1)	176(1)
F(20)	-3468(1)	8733(1)	4284(1)	170(2)
F(21)	-5148(1)	9041(2)	3918(1)	221(1)
F(22)	-3579(2)	11186(1)	3951(1)	145(1)
F(23)	-5187(1)	10649(1)	3706(1)	209(1)
F(24)	-3664(2)	10023(1)	3401(1)	361(3)

F(25)	-4820(2)	10182(1)	5705(1)	553(2)
F(26)	-5991(1)	10090(1)	4786(1)	356(5)
F(27)	-4958(2)	11233(1)	4945(1)	196(2)
F(28)	-1967(2)	12845(1)	5934(1)	101(1)
F(29)	-2337(2)	11943(1)	5137(1)	156(1)
F(30)	-3430(1)	12054(1)	6042(1)	171(1)
F(31)	107(2)	10930(1)	6219(1)	125(1)
F(32)	-211(3)	12178(1)	6585(1)	353(1)
F(33)	-260(2)	11899(1)	5478(1)	146(1)
F(34)	-3011(1)	11035(1)	6996(2)	264(1)
F(35)	-1318(2)	11030(1)	7353(1)	160(1)
F(36)	-2162(2)	12168(1)	7183(1)	415(4)

Tab. 88: Atomic coordinates (x 10^4) and equivalent isotropic displacement parameters (Å^2 x 10^3) for **19**. U(eq) is defined as one third of the trace of the orthogonalized Uij tensor.

	x	**y**	**z**	**U(eq)**
Al(1)	2494(2)	2785(1)	7230(1)	17(1)
F(1)	180(3)	2600(2)	5800(2)	30(1)
F(2)	4654(3)	2494(2)	8019(2)	31(1)
F(3)	3175(3)	1939(2)	5380(2)	29(1)
F(4)	1792(3)	4613(2)	8087(2)	26(1)
F(5)	4825(3)	4225(2)	7399(2)	28(1)
F(6)	2361(3)	-499(2)	6911(2)	32(1)
F(7)	-1173(3)	3824(2)	5817(2)	32(1)
F(8)	5170(3)	2549(2)	5118(2)	30(1)
F(9)	372(3)	1971(2)	7538(2)	31(1)
F(10)	3673(3)	5625(2)	9697(2)	33(1)
F(11)	814(3)	3653(2)	5190(2)	31(1)
F(12)	2699(3)	3096(2)	10512(2)	31(1)
F(13)	4150(3)	4848(2)	6353(2)	34(1)
F(14)	3834(3)	-379(2)	7676(2)	35(1)
F(15)	5172(3)	-305(2)	6090(2)	34(1)
F(16)	-317(3)	4343(2)	9121(2)	39(1)
F(17)	2746(3)	5756(2)	8367(2)	32(1)
F(18)	1313(3)	293(2)	4400(2)	33(1)
F(19)	2041(3)	594(2)	8067(2)	31(1)
F(20)	2217(3)	1635(2)	4252(2)	33(1)
F(21)	7357(3)	2608(2)	5208(2)	32(1)
F(22)	6132(3)	4220(2)	6147(2)	32(1)
F(23)	-144(3)	3879(2)	10347(2)	31(1)
F(24)	-2419(3)	4746(2)	7433(2)	33(1)
F(25)	5512(3)	3765(2)	4901(2)	34(1)
F(26)	3717(3)	778(2)	8206(2)	37(1)
F(27)	-248(3)	4882(2)	7500(2)	32(1)
F(28)	1299(3)	4641(2)	6346(2)	39(1)
F(29)	3639(3)	4252(2)	10756(2)	37(1)
F(30)	5325(3)	918(2)	5620(2)	37(1)
F(31)	-4180(3)	4332(2)	8680(2)	38(1)
F(32)	6462(3)	1241(2)	8355(2)	41(1)
F(33)	3620(3)	3693(2)	5372(2)	38(1)
F(34)	-595(3)	5096(2)	6283(2)	33(1)
F(35)	8738(3)	651(2)	7169(3)	44(1)
F(36)	9143(3)	1365(2)	5597(3)	41(1)
F(37)	-668(3)	3168(3)	9569(2)	41(1)
F(38)	5717(3)	462(2)	6791(3)	42(1)
F(39)	1397(3)	-760(2)	5758(2)	38(1)
F(40)	-1389(3)	1602(2)	8789(2)	39(1)
F(41)	1235(3)	2309(2)	10413(2)	32(1)
F(42)	3032(3)	1931(2)	9421(2)	30(1)
F(43)	1357(3)	1760(2)	9261(2)	35(1)
F(44)	-3720(3)	2774(3)	9396(2)	45(1)
O(1)	3346(3)	1735(2)	6962(3)	25(1)
O(2)	1686(3)	3023(3)	8289(2)	25(1)
O(3)	3611(3)	3326(2)	6897(2)	20(1)
O(4)	1357(3)	3119(2)	6710(2)	22(1)
C(1)	184(5)	3621(3)	6706(3)	19(1)
C(2)	3269(6)	464(4)	7696(4)	27(1)
C(3)	4791(5)	3325(4)	6377(4)	20(1)
C(4)	1782(6)	2293(4)	9569(4)	29(2)
C(5)	2(5)	3439(4)	5864(4)	24(1)
C(6)	4986(5)	4165(4)	6564(4)	25(1)

C(7)	137(5)	4571(4)	6717(4)	30(2)
C(8)	4778(5)	3333(4)	5436(4)	25(1)
C(9)	2726(5)	1277(4)	5533(4)	22(1)
C(10)	4954(6)	493(4)	6320(4)	32(2)
C(11)	-1645(6)	2388(4)	8457(4)	28(1)
C(12)	-713(5)	2603(4)	7809(4)	24(1)
C(13)	77(5)	3646(4)	9539(4)	26(1)
C(14)	5871(5)	2592(3)	6577(4)	21(1)
C(15)	1813(5)	-80(4)	5685(4)	25(1)
C(16)	6659(6)	1581(4)	7578(4)	26(1)
C(17)	3530(5)	900(4)	6824(4)	22(1)
C(18)	7068(5)	2272(4)	5993(4)	24(1)
C(19)	-882(5)	3408(4)	7441(4)	22(1)
C(20)	5712(5)	2231(4)	7376(4)	22(1)
C(21)	2796(5)	765(3)	6240(4)	20(1)
C(22)	3225(5)	5020(4)	9557(4)	25(1)
C(23)	2756(5)	5090(4)	8890(4)	23(1)
C(24)	3207(5)	4332(4)	10085(4)	25(1)
C(25)	2273(5)	4469(4)	8741(4)	22(1)
C(26)	1782(5)	444(4)	4994(4)	27(1)
C(27)	-3028(5)	3757(4)	8400(4)	30(2)
C(28)	2232(5)	1132(4)	4928(4)	24(1)
C(29)	-2814(6)	2968(4)	8770(4)	30(2)
C(30)	1494(6)	3169(4)	9126(4)	23(1)
C(31)	8018(5)	1638(4)	6186(4)	30(2)
C(32)	2326(5)	74(4)	6286(4)	24(1)
C(33)	2216(5)	3757(3)	9275(4)	19(1)
C(34)	2704(5)	3726(4)	9948(4)	24(1)
C(35)	7816(6)	1274(4)	6976(5)	31(2)
C(36)	-2093(5)	3970(4)	7750(4)	24(1)
Ag(1)	6931(1)	2793(1)	3028(1)	37(1)
P(1)	3270(1)	3253(1)	3492(1)	42(1)
P(2)	4850(2)	3651(1)	2710(1)	40(1)
P(3)	4199(2)	2810(1)	2169(1)	53(1)
P(4)	5056(2)	2261(1)	3159(1)	31(1)
P(5)	9309(2)	2157(1)	2837(1)	39(1)
P(6)	9912(2)	2742(1)	3679(1)	45(1)
P(7)	10228(2)	3125(1)	2338(1)	38(1)
P(8)	8386(1)	3568(1)	3256(1)	34(1)
Cl(1)	10035(2)	578(1)	1147(1)	71(1)
Cl(2)	7883(2)	2055(2)	1055(1)	74(1)
Cl(3)	2940(2)	1096(2)	2045(2)	75(1)
Cl(4)	5102(2)	1094(1)	562(1)	66(1)
C(101)	3902(8)	659(6)	1041(5)	73(2)
C(102)	9010(40)	980(30)	660(20)	61(10)
C(103)	8630(80)	1090(30)	750(40)	97(14)

Tab. 89: Atomic coordinates (x 10^4) and equivalent isotropic displacement parameters (Å^2 x 10^3) for **20**. U(eq) is defined as one third of the trace of the orthogonalized Uij tensor.

	x	**y**	**z**	**U(eq)**
Ag(1)	5962(1)	7933(1)	7322(1)	34(1)
Al	7041(2)	7552(1)	2272(1)	18(1)
C(1)	8790(6)	9279(4)	3540(4)	22(2)
C(2)	7998(5)	4896(3)	3638(4)	18(2)
C(3)	8522(6)	5029(4)	2720(4)	20(2)
C(4)	8780(5)	5983(4)	2370(4)	20(2)
C(5)	9311(6)	6016(4)	1437(4)	24(2)
C(6)	10546(6)	6176(4)	967(4)	30(2)
C(7)	8447(6)	5961(4)	1017(4)	28(2)
C(8)	8150(6)	9456(4)	1438(4)	22(2)
C(9)	9053(6)	8908(4)	941(4)	22(2)
C(10)	8770(6)	5291(4)	4067(4)	23(2)
C(11)	10003(8)	6197(5)	-236(5)	42(2)
C(12)	8770(7)	6044(4)	201(5)	37(2)
C(13)	10873(7)	6268(5)	146(4)	38(2)
C(14)	7719(6)	10197(4)	225(4)	29(2)
C(15)	8584(6)	9612(4)	-228(4)	32(2)
C(16)	9252(6)	8972(4)	140(4)	27(2)
C(17)	4909(6)	8099(4)	1181(4)	24(2)
C(18)	4574(7)	6687(5)	542(5)	34(2)
C(19)	4296(6)	6678(4)	1350(4)	28(2)
C(20)	4439(5)	7381(4)	1720(4)	20(2)
C(21)	5182(6)	8106(4)	375(4)	29(2)
C(22)	8980(6)	9460(4)	2637(4)	23(2)
C(23)	7482(6)	9637(4)	4062(4)	25(2)
C(24)	9707(6)	6258(4)	2786(4)	22(2)
C(25)	2913(6)	7263(4)	4400(4)	26(2)
C(26)	7859(5)	9237(4)	2355(4)	19(2)
C(27)	6608(5)	9711(4)	2871(4)	22(2)
C(28)	5033(6)	7391(5)	57(4)	33(2)
C(105)	7531(10)	9262(5)	6752(7)	65(3)
C(100)	7071(7)	9047(6)	7559(7)	60(3)
C(101)	7804(8)	8426(6)	7946(5)	57(3)
C(32)	9131(5)	6203(4)	3701(4)	22(2)
C(103)	9386(7)	8332(5)	6697(5)	46(2)
C(102)	8983(8)	8080(5)	7496(6)	52(2)
C(37)	4131(5)	6527(4)	3149(4)	20(2)
C(38)	4033(6)	6600(4)	4023(4)	26(2)
C(39)	2845(6)	8131(4)	3874(4)	25(2)
C(40)	3091(5)	8039(4)	2982(4)	21(2)
C(41)	6361(6)	9452(4)	3777(4)	22(2)
C(42)	4313(5)	7416(4)	2606(4)	18(1)
C(104)	8678(9)	8911(5)	6319(6)	53(2)
C(45)	7503(6)	10101(4)	1044(4)	27(2)
F	7378(3)	7658(2)	1281(2)	22(1)
F(1)	9633(3)	4493(2)	2507(2)	28(1)
F(2)	7675(3)	4728(2)	2438(2)	29(1)
F(3)	9840(3)	4756(2)	4071(2)	32(1)
F(4)	8955(3)	8415(2)	3738(2)	28(1)
F(5)	7299(3)	9272(2)	4823(2)	36(1)
F(6)	3884(3)	5935(2)	1785(2)	31(1)
F(7)	8096(3)	6785(2)	3920(2)	24(1)
F(8)	9960(3)	7087(2)	2523(2)	26(1)
F(9)	6771(3)	5247(2)	3861(2)	25(1)
F(10)	8008(3)	4032(2)	3868(2)	30(1)

F(11)	9714(3)	9638(2)	3720(2)	31(1)
F(12)	7197(3)	5850(2)	1381(2)	29(1)
F(13)	11476(3)	6274(3)	1272(2)	41(1)
F(14)	9746(3)	8239(2)	1237(2)	30(1)
F(15)	8078(3)	5327(2)	4843(2)	30(1)
F(16)	7878(4)	5988(3)	-167(2)	46(1)
F(17)	12082(4)	6419(3)	-267(2)	57(1)
F(18)	10123(3)	8394(2)	-298(2)	38(1)
F(19)	4441(4)	5966(2)	245(2)	43(1)
F(20)	5673(4)	8798(2)	-108(2)	39(1)
F(21)	5136(3)	8821(2)	1431(2)	26(1)
F(22)	6595(3)	10700(2)	1413(2)	34(1)
F(23)	7063(4)	10840(2)	-125(2)	42(1)
F(24)	8762(4)	9671(3)	-1014(2)	43(1)
F(25)	9108(3)	10334(2)	2438(2)	27(1)
F(26)	10106(3)	9030(2)	2280(2)	29(1)
F(27)	7469(3)	10503(2)	4058(2)	34(1)
F(28)	10323(4)	6277(3)	-1034(2)	58(1)
F(29)	10826(3)	5747(2)	2671(2)	27(1)
F(30)	6626(3)	10596(2)	2786(2)	25(1)
F(31)	5587(3)	9553(2)	2658(2)	24(1)
F(32)	3172(3)	8851(2)	2603(2)	26(1)
F(33)	2037(3)	7754(2)	2897(2)	27(1)
F(34)	3032(3)	6188(2)	3189(2)	26(1)
F(35)	5131(3)	5936(2)	2860(2)	24(1)
F(36)	10036(3)	6410(2)	4006(2)	30(1)
F(37)	3845(3)	5806(2)	4430(2)	30(1)
F(38)	5127(3)	6820(2)	4109(2)	27(1)
F(39)	3030(3)	7424(2)	5101(2)	32(1)
F(40)	1805(3)	6909(2)	4545(2)	32(1)
F(41)	1682(3)	8566(2)	4149(2)	31(1)
F(42)	3725(3)	8614(2)	3949(2)	26(1)
F(43)	6154(3)	8613(2)	3983(2)	25(1)
F(44)	5277(3)	9939(2)	4149(2)	27(1)
F(45)	5306(4)	7406(3)	-737(2)	52(1)
O(1)	7732(3)	8356(2)	2558(2)	18(1)
O(3)	7658(3)	6521(2)	2586(2)	18(1)
O(4)	5380(3)	7703(2)	2705(2)	17(1)
S(1)	4801(2)	7967(1)	6113(1)	30(1)
S(2)	3633(2)	7232(1)	7968(1)	29(1)
S(3)	7370(2)	5783(1)	6850(1)	37(1)
S(4)	7583(2)	6906(1)	6097(1)	32(1)
S(5)	3307(2)	7333(1)	6877(1)	31(1)
S(6)	6190(2)	7081(1)	5519(1)	36(1)
S(7)	4498(2)	5999(1)	8199(1)	31(1)
S(8)	6410(2)	6158(1)	7949(1)	33(1)
F(47)	10534(5)	7994(4)	6277(4)	102(2)
F(46)	9387(11)	9054(8)	5554(7)	44(5)
F(49)	9895(8)	7597(5)	7753(6)	91(4)

Tab. 90: Atomic coordinates (x 10^4) and equivalent isotropic displacement parameters (Å^2 x 10^3) for **21**. U(eq) is defined as one third of the trace of the orthogonalized Uij tensor.

	x	**y**	**z**	**U(eq)**
Al(1A)	6667	3333	1316(1)	21(1)
Cl(1A)	6667	3333	1556(1)	27(1)
F(1A)	7697(4)	2143(4)	1471(1)	24(1)
F(15A)	4582(4)	-18(4)	1200(1)	33(2)
F(13A)	5722(4)	2036(4)	982(1)	32(2)
F(12A)	4381(4)	745(5)	959(1)	38(2)
F(14A)	4667(4)	1348(4)	1239(1)	26(1)
F(10A)	5227(5)	-315(5)	945(1)	40(2)
F(6A)	7514(4)	1169(4)	1248(1)	32(2)
O(1A)	6617(5)	2301(4)	1249(1)	21(2)
F(9A)	7365(4)	1827(4)	989(1)	36(2)
F(8A)	7061(4)	362(4)	976(1)	30(2)
F(5A)	4315(5)	133(5)	1462(1)	41(2)
F(2A)	7663(4)	1853(5)	1760(1)	37(2)
F(11A)	5948(5)	905(5)	799(1)	36(2)
F(7A)	6151(4)	-105(4)	1230(1)	35(2)
F(4A)	4342(5)	-112(6)	1747(1)	55(2)
C(12A)	5140(7)	945(8)	1187(1)	26(3)
F(3A)	6016(5)	748(5)	1904(1)	50(2)
C(8A)	6606(7)	820(7)	1195(1)	24(2)
C(9A)	6697(7)	900(7)	1025(1)	24(2)
C(11A)	5265(7)	1111(7)	1020(1)	27(3)
C(6A)	5186(8)	568(7)	1524(1)	29(3)
C(1A)	6014(8)	1115(8)	1443(1)	27(3)
C(5A)	5188(8)	440(8)	1677(1)	33(3)
C(3A)	6847(8)	1408(8)	1681(1)	28(3)
C(2A)	6833(8)	1519(8)	1529(1)	28(3)
C(10A)	5813(8)	673(7)	942(1)	30(3)
C(4A)	6017(9)	843(8)	1756(1)	33(3)
C(7A)	6111(7)	1327(7)	1271(1)	23(2)
Al(1B)	3333	6667	341(1)	26(1)
F(6B)	1367(4)	6682(4)	429(1)	28(1)
F(14B)	4204(4)	9710(4)	393(1)	38(2)
F(5B)	4361(4)	8880(4)	180(1)	28(1)
F(15B)	2854(5)	9607(5)	427(1)	39(2)
F(12B)	3868(5)	10094(4)	672(1)	40(2)
F(7B)	1316(4)	8010(5)	465(1)	38(2)
F(10B)	2072(6)	8963(5)	721(1)	52(2)
F(13B)	4179(5)	8949(5)	654(1)	43(2)
O(1B)	3307(5)	7672(5)	409(1)	33(2)
F(9B)	2453(5)	7053(4)	675(1)	38(2)
F(8B)	1178(5)	7105(5)	714(1)	46(2)
F(4B)	4283(5)	9080(5)	-106(1)	49(2)
F(11B)	2853(5)	8484(5)	853(1)	49(2)
F(1B)	994(5)	7485(5)	205(1)	50(2)
F(3B)	2612(5)	8457(6)	-249(1)	56(2)
C(8B)	1884(7)	7585(8)	479(1)	27(3)
C(11B)	3498(8)	9205(7)	625(1)	28(3)
C(1B)	2691(8)	8247(7)	214(1)	24(2)
C(7B)	2806(8)	8159(8)	386(1)	30(3)
C(6B)	3482(8)	8633(8)	123(1)	31(3)
F(2B)	972(5)	7703(6)	-87(1)	65(3)
C(9B)	2028(7)	7574(7)	645(1)	27(2)
C(4B)	2630(9)	8424(9)	-100(1)	37(3)
C(2B)	1820(9)	7937(8)	139(1)	33(3)

C(10B)	2629(9)	8550(8)	713(1)	36(3)
C(3B)	1802(10)	8004(11)	-22(1)	51(4)
C(12B)	3342(7)	9148(7)	455(1)	21(2)
C(5B)	3469(8)	8698(7)	-31(1)	29(3)
C(37B)	0	0	1174(2)	31(5)
C(39B)	1619(7)	370(8)	1249(1)	27(3)
C(42B)	1383(9)	-1255(9)	1101(1)	36(3)
C(40B)	2333(8)	136(8)	1249(1)	37(3)
C(43B)	660(8)	-1048(8)	1097(1)	29(3)
C(41B)	2221(9)	-645(9)	1178(1)	42(3)
C(38B)	762(8)	-218(8)	1171(1)	26(3)
C(39A)	7694(7)	2682(8)	593(1)	27(3)
C(43A)	6273(8)	1702(8)	442(1)	28(3)
C(40A)	7869(9)	1905(8)	593(1)	35(3)
C(38A)	6890(7)	2582(7)	520(1)	23(2)
C(42A)	6503(8)	1000(8)	436(1)	33(3)
C(37A)	6667	3333	522(2)	25(4)
C(41A)	7282(9)	1080(9)	509(1)	42(3)
Cl(1B)	3333	6667	101(1)	21(2)
F(16B)	3333	6667	518(6)	1(16)

Tab. 91: Atomic coordinates (x 10^4) and equivalent isotropic displacement parameters (Å^2 x 10^3) for **22**. U(eq) is defined as one third of the trace of the orthogonalized Uij tensor.

	x	**y**	**z**	**U(eq)**
Ga(1)	9124(1)	8612(1)	2071(1)	34(1)
Al(1)	11638(1)	7918(1)	2383(1)	13(1)
F(9C)	10820(1)	9569(1)	1811(1)	23(1)
F(100)	10473(1)	8174(1)	2254(1)	18(1)
O(1A)	11768(1)	7814(1)	3279(1)	15(1)
F(8A)	9830(1)	7722(1)	3563(1)	25(1)
F(1B)	10962(1)	5367(1)	3286(1)	27(1)
F(6B)	10161(1)	6555(1)	2590(1)	22(1)
F(8B)	9111(1)	6198(1)	1438(1)	29(1)
F(13B)	11717(1)	6820(1)	520(1)	26(1)
O(1B)	11778(1)	7079(1)	1952(1)	15(1)
F(7B)	10336(1)	5443(1)	2128(1)	25(1)
F(5C)	14215(1)	8140(1)	2108(1)	24(1)
F(1A)	13702(1)	7747(1)	3501(1)	25(1)
F(8C)	10538(1)	9862(1)	726(1)	31(1)
F(14B)	11941(1)	5161(1)	1482(1)	27(1)
F(6C)	11226(1)	8465(1)	868(1)	21(1)
O(1C)	12353(1)	8609(1)	2027(1)	16(1)
F(15B)	12961(1)	6045(1)	1279(1)	26(1)
F(13A)	11041(1)	6657(1)	4166(1)	27(1)
F(2C)	13641(1)	6980(1)	-470(1)	32(1)
F(9B)	10044(1)	7143(1)	1272(1)	25(1)
F(6A)	10675(1)	9075(1)	3473(1)	21(1)
F(10C)	12085(1)	10688(1)	648(1)	35(1)
F(7A)	10929(1)	9055(1)	4612(1)	25(1)
F(7C)	12078(1)	9269(1)	265(1)	26(1)
F(2B)	12026(1)	4969(1)	4308(1)	52(1)
F(4A)	13439(1)	10728(1)	3831(1)	38(1)
F(1C)	12541(1)	8049(1)	-72(1)	25(1)
F(4B)	14619(1)	6267(1)	3356(1)	31(1)
F(3C)	15065(1)	6461(1)	360(1)	36(1)
F(5B)	13554(1)	6727(1)	2324(1)	25(1)
F(10B)	10230(1)	5288(1)	730(1)	28(1)
F(12A)	11312(1)	6791(1)	5278(1)	34(1)
F(3B)	13901(1)	5394(1)	4387(1)	49(1)
F(3A)	15146(1)	10073(1)	3549(1)	47(1)
F(11B)	10062(1)	6321(1)	141(1)	30(1)
F(12B)	11876(1)	5672(1)	186(1)	33(1)
F(12C)	13321(1)	10855(1)	1666(1)	38(1)
F(2A)	15223(1)	8560(1)	3396(1)	37(1)
F(5A)	11931(1)	9945(1)	4027(1)	29(1)
F(13C)	12491(1)	10168(1)	2381(1)	29(1)
F(11A)	10159(1)	7941(1)	5364(1)	35(1)
F(11C)	11330(1)	10955(1)	1609(1)	34(1)
F(9A)	9267(1)	8547(1)	4285(1)	33(1)
C(1B)	12196(2)	6040(1)	2704(1)	17(1)
F(4C)	15320(1)	7077(1)	1653(1)	30(1)
C(9B)	10555(2)	6175(1)	2055(2)	19(1)
C(3B)	12421(2)	5377(2)	3802(2)	30(1)
C(9A)	10027(2)	8117(2)	4151(2)	24(1)
C(6A)	12714(2)	9548(2)	3896(1)	21(1)
C(3A)	14407(2)	8898(2)	3562(2)	27(1)
C(9C)	11231(2)	9726(2)	1190(2)	21(1)
C(8B)	11652(2)	6322(1)	2048(1)	16(1)
C(10A)	10180(2)	7569(2)	4750(2)	26(1)

C(11A)	11125(2)	7167(2)	4682(2)	23(1)
C(6B)	13143(2)	6264(1)	2781(1)	19(1)
C(8C)	11815(2)	9052(2)	919(1)	19(1)
C(10B)	10031(2)	6396(2)	1371(2)	21(1)
C(8A)	10890(2)	8630(2)	4027(1)	19(1)
C(7A)	11853(2)	8230(1)	3883(1)	15(1)
C(5C)	14646(2)	7340(2)	1224(2)	22(1)
C(1C)	13323(2)	8204(2)	1043(1)	18(1)
C(1A)	12718(2)	8770(1)	3832(1)	17(1)
C(2A)	13595(2)	8474(2)	3638(1)	20(1)
C(2B)	11867(2)	5598(2)	3249(2)	21(1)
F(10A)	9468(1)	7067(1)	4760(1)	38(1)
C(7B)	11529(2)	6110(2)	691(2)	22(1)
C(6C)	14061(2)	7905(2)	1451(1)	20(1)
C(2C)	13224(2)	7867(2)	390(1)	20(1)
C(5B)	13718(2)	6042(2)	3328(2)	23(1)
C(3C)	13802(2)	7293(2)	166(2)	23(1)
C(10C)	11844(2)	10422(2)	1282(2)	26(1)
C(11B)	10445(2)	6019(2)	723(2)	24(1)
C(12B)	12033(2)	5910(2)	1382(2)	20(1)
C(11C)	12741(2)	10257(2)	1705(2)	25(1)
C(4A)	14366(2)	9660(2)	3640(2)	29(1)
C(4C)	14521(2)	7027(2)	577(2)	25(1)
C(7C)	12689(2)	8826(1)	1373(1)	17(1)
C(4B)	13362(2)	5595(2)	3848(2)	29(1)
C(5A)	13514(2)	9979(2)	3796(2)	27(1)
C(102)	6864(2)	8723(2)	2418(2)	34(1)
C(101)	7268(2)	8458(2)	3016(2)	33(1)
C(103)	7693(2)	7768(2)	3008(2)	33(1)
C(104)	7728(2)	7359(2)	2407(2)	34(1)
F(14C)	14008(1)	9475(1)	1918(1)	29(1)
F(14A)	12165(1)	8080(1)	5108(1)	26(1)
F(15A)	12724(1)	7217(1)	4427(1)	25(1)
F(15C)	13689(1)	9728(1)	830(1)	31(1)
F(101)	6433(1)	9393(1)	2418(1)	62(1)
F(102)	6467(2)	8588(2)	1236(1)	74(1)
C(12A)	11982(2)	7679(2)	4519(2)	20(1)
C(105)	7329(2)	7622(2)	1803(2)	39(1)
C(12C)	13294(2)	9563(2)	1455(2)	23(1)
C(106)	6889(2)	8316(2)	1813(2)	38(1)

6.13. Publications and conference contributions

N. Trapp, I. Krossing, G. Santiso-Quiñones: $Cu(CO)_2[Al(OCH(CF_3)_2)_4]$ as a benchmark compound to establish in-house electron density studies on stock equipment (Poster). *5th European Charge Density Meeting (ECDM5) in conjunction with DFG 1178 annual report meeting*, Como (Italy) **2008**.

N. Trapp, K. Guttsche, T. Köchner, S. Bulut, P. Klose, H. Scherer, I. Krossing: Entwicklung neuer schwach koordinierender Anionen und starker Lewis-Säuren (Poster). *Tag der Forschung*, Universität Freiburg **2008**.

D. Himmel, N. Trapp, I. Krossing, S. Altmannshofer, V. Herz, G. Eickerling, W. Scherer: Homoleptic silver(I) acetylene complexes (Replique). *Angewandte Chemie, International Edition* **2008**, accepted.

I. Raabe, D. Himmel, S. Mueller, N. Trapp, M. Kaupp, I. Krossing: Stable CI_3^+ salts and attempts to prepare CHI_2^+ and CH_2I^+. *Dalton Transactions* **2008**, *7*, 946.

N. Trapp, H. Böhrer, K. Guttsche, I. Krossing: Entwicklung neuer schwach koordinierender Alkoxyaluminatanionen $Al[OR^f_4]^-$ (Poster). *GDCh Wissenschaftsforum Chemie*, Ulm **2007**.

N. Trapp: One year with the R-Axis Spider (Talk). *Rigaku Small Molecule Crystallography Customer Advisory Board (SMCAB) Meeting*, St. Andrews (Scotland) **2007**.

N. Trapp, K. Guttsche, H. Böhrer, T. Köchner, U. Preiss, I. Krossing: Entwicklung neuer schwach koordinierender Alkoxyaluminatanionen $Al[OR^f_4]^-$ (Poster). *Tag der Forschung*, Universität Freiburg **2007**.

A. Reisinger, N. Trapp, I. Krossing, S. Altmannshofer, V. Herz, M. Presnitz, W. Scherer: Homoleptic silver(I) acetylene complexes. *Angewandte Chemie, International Edition* **2007**, *46(43)*, 8295.

A. Reisinger, N. Trapp, I. Krossing, S. Altmannshofer, V. Herz, M. Presnitz, W. Scherer: Homoleptische Silber(I)-Acetylen-Komplexe. *Angewandte Chemie* **2007**, *119(43)*, 8445.

A. Reisinger, N. Trapp, I. Krossing: $AgOC(CF_3)_3$ - Synthesis and Applications of the First Donor-Free Silver(I) Alkoxide. *Organometallics* **2007**, *26(8)*, 2096.

N. Trapp, I. Krossing, A. Reisinger: Fluorierte Silberalkoxide - Ausgangsstoffe für schwach koordinierende Anionen? (Talk). *Deutscher Fluortag*, Schmitten im Taunus **2006**.

N. Trapp, I. Krossing: Die Reaktion von $Ag^+[Al(OR^F)_4]^-$ mit $Cl_2C{=}S$: $ClCS^+$ und $[ClCS(Cl_2CS)_n]^+$ (n = 1, 2) als $[Al(OR^F)^4]^-$-Salze (Poster). *GDCh Jahrestagung Chemie*, Düsseldorf **2005**.

N. Trapp, I. Krossing: The reaction of $Ag^+[Al(OR^F)_4]^-$ with $Cl_2C{=}S$: $ClCS^+$ and $[ClCS(Cl_2CS)_n]^+$ (n = 1, 2) as $[Al(OR^F)_4]^-$-salts (Poster). *Fall Meeting of the Swiss Chemical Society*, Lausanne (Switzerland) **2005**.

N. Trapp, I. Krossing, I. Raabe: Beiträge zur Chemie mit schwach koordinierenden Anionen (Talk). *Deutscher Fluortag*, Schmitten im Taunus **2004**.

A. Bihlmeier, M. Gonsior, I. Raabe, N. Trapp, I. Krossing: From weakly coordinating to non-coordinating anions? A simple preparation of the silver salt of the least coordinating anion and its application to determine the ground state structure of the $Ag(\eta^2\text{-}P_4)_2^+$ cation. *Chemistry-A European Journal* **2004**, *10(20)*, 5041.

I. Krossing, A. Bihlmeier, I. Raabe, N. Trapp: Structure and characterization of $CI_3^+[Al\{OC(CF_3)_3\}_4]^-$; Lewis acidities of CX_3^+ and BX_3. *Angewandte Chemie, International Edition* **2003**, *42(13)*, 1531.

I. Krossing, A. Bihlmeier, I. Raabe, N. Trapp: Struktur und Charakterisierung von $CI_3^+[Al\{OC(CF_3)_3\}_4]^-$; Lewis-Aciditäten von CX_3^+ und BX_3. *Angewandte Chemie* **2003**, *115 (13)*, 1569.

6.14. Abstract (in german)

Novel Salts of Weakly Coordinating Perfluorinated Alkoxyaluminate Anions and their Parent Lewis Acids - Design, Synthesis and Possible Applications

Dissertation, vorgelegt von Dipl.-Chem. Nils Trapp im Juli 2008

Ionen, die vollständig unkoordiniert in einem Ionengitter vorliegen, sind aufgrund der Coulomb-Kraft nicht vorstellbar. Allerdings ist es möglich, wenige starke durch viele schwache Wechselwirkungen zu ersetzen. Hierfür eignen sich so genannte schwach koordinierende Anionen (WCAs, von engl. *w*eakly *c*oordinating *a*nions). Sie können aufgrund der schwachen Kation-Anion Wechselwirkungen zur Darstellung von Salzen hochelektrophiler Kationen (z.B. $C(CH_3)_3^+$, N_5^+, CI_3^+) und von schwach gebundenen, kationischen Lewis-Säure-Base-Komplexen (z.B. $Ag(P_4)_2^+$, $Ag(S_8)_2^+$) verwendet werden. Mit zunehmender Größe des Anions nähert sich die Gitterenthalpie von WCA-Salzen der Sublimationsenthalpie molekularer Festkörper vergleichbarer Molmasse, d.h. man erreicht „Pseudo-Gasphasenbedingungen“. Zudem eignen sich WCAs für viele industrielle Anwendungen, z.B. als Gegenionen in der Katalyse, in ionischen Flüssigkeiten oder elektrochemischen Prozessen. Um schwache Koordination zu erreichen, muss ein WCA eine niedrige Nukleophilie und Basizität aufweisen. Zusätzlich ist eine hohe chemische Stabilität gegenüber Elektrophilen, Reduktion und Oxidation erwünscht. Dies wird durch eine geringe Ladung, möglichst große Oberfläche und Poly- oder Perfluorierung erreicht. Die vorliegende Dissertation befasst sich mit der Darstellung von Salzen der perfluorierten Alkoxyaluminate $[Al(OC(CF_3)_2C_6F_5)_4]^-$ **1** und $[FAl(O(\textit{cyclo}\text{-}C_6F_{10})C_6F_5)_3]^-$ **2**. Eine Vielzahl neuer Startmaterialien (perfluorierte Alkohole und Alkoxide) wurde dargestellt, die sich u.a. zur Herstellung weiterer WCAs eignen. **1** und **2** sind schwach koordinierend und eignen sich zur Stabilisierung schwacher Lewis-Säure-Base-Komplexe, wie anhand der Verbindungen $[Ag(P_4)_2]$[**1**] und $[Ag(S_8)(1,2\text{-}C_6H_4F_2)]$[**2**] gezeigt werden konnte. Beide neuen Anionen sind größer und unsymmetrischer als bisher bekannte perfluorierte Alkoxyaluminate und verringern systematisch kristallographische Probleme, die bei Salzen symmetrischer Alkoxyaluminate wie $[Al(OC(CF_3)_3)_4]^-$ häufig auftreten (Fehlordnungen, merohedrische Verzwilligung).

Im Zuge der Untersuchungen konnte auch die neue Lewis-Säure $Al(O(\textit{cyclo}\text{-}C_6F_{10})C_6F_5)_3$ **3** synthetisiert und charakterisiert werden. Die Verbindung weist eine *F*luor*i*dionen*a*ffinität

(FIA) von 530 kJ/mol auf und ist somit stärker als die stärkste konventionelle Lewis-Säure SbF_5 (489 kJ/mol). Trotzdem ist **3** als Feststoff bei Raumtemperatur stabil und zusätzlich in einer einfachen Reaktion im 10 g Maßstab darstellbar. **3** ist ein viel versprechendes Startmaterial für neue heteroleptische WCAs $[XAl(O(\textit{cyclo}\text{-}C_6F_{10})C_6F_5)_3]^-$ (X = Cl, Br, MeO, $C(H)(CF_3)_2$, etc.).

Zusätzlich wurden Versuche zur Darstellung von Salzen bisher unbekannter Halothiocarbonylkationen unternommen. Das ICS^+ Salz des schwach koordinierenden Anions $[Al(OC(CF_3)_3)_4]^-$ (**4**) konnte dargestellt und durch Kristallstrukturanalyse charakterisiert werden. Kationen dieses Typs waren bisher in kondensierter Phase unbekannt. Die Synthese des homologen $ClCS^+$ Salzes gelang nicht, stattdessen konnte das Salz $Cl_3C_2S_2[Al(OC(CF_3)_3)_4]$ **5** vollständig charakterisiert werden. Das $Cl_3C_2S_2^+$ Kation kann als Addukt von Thiophosgen an $ClCS^+$ verstanden werden. Anhand von NMR-Untersuchungen wurde aufgezeigt, dass $ClCS^+$ in Lösung im Gleichgewicht vorliegt und möglicherweise durch Wahl geeigneter Reaktionsbedingungen noch in Form eines Salzes charakterisiert werden kann.

Sämtliche Experimente wurden durch systematische quantenchemische Berechnungen begleitet, deren Ergebnisse ebenfalls diskutiert werden.

6.15. Literature references

[1] S. Hollenstein, T. Laube, *J. Am. Chem. Soc.* **1993**, *115*, 7240.

[2] T. Kato, C. A. Reed, *Angew. Chem. Int. Ed. Engl.* **2004**, *43*, 2908.

[3] G. A. Olah, A. M. White, D. H. O'Brien, *Chem. Rev.* **1970**, *70*, 561.

[4] I. Krossing, A. Bihlmeier, I. Raabe, N. Trapp, *Angew. Chem. Int. Ed. Engl.* **2003**, *42*, 1531.

[5] G. J. Schrobilgen, H. P. A. Mercier, M. D. Moran, *ACS Symposium Series* **2007**, *965*, 394.

[6] G. J. Schrobilgen, H. P. A. Mercier, M. D. Moran, C. Steinberg, R. J. Suontamo, *J. Am. Chem. Soc.* **2004**, *126*, 5533.

[7] G. A. Olah, L. Heiliger, G. K. S. Prakash, *J. Am. Chem. Soc.* **1989**, *111*, 8020.

[8] A. E. P. M. Sorrilha, L. S. Santos, F. C. Gozzo, R. Sparrapan, R. Augusti, M. N. Eberlin, *J. Phys. Chem. A* **2004**, *108*, 7009.

[9] E. Marotta, C. Paradisi, *J. Mass Spectr.* **2001**, *36*, 1195.

[10] J. Dyke, N. Jonathan, E. Lee, A. Morris, M. Winter, *Phys. Scripta* **1977**, *16*, 197.

[11] M. Lin, C. Liu, L. Zheng, *Wuli Huaxue Xuebao* **1995**, *11*, 266.

[12] I. Krossing, *J. Am. Chem. Soc.* **2001**, *123*, 4603.

[13] I. Krossing, L. Van Wüllen, *Chem. Eur. J.* **2002**, *8*, 700.

[14] T. Drews, K. Seppelt, *Angew. Chem. Int. Ed. Engl.* **1997**, *36*, 273.

[15] A. Vij, W. W. Wilson, V. Vij, F. S. Tham, J. A. Sheehy, K. O. Christe, *J. Am. Chem. Soc.* **2001**, *123*, 6308.

[16] C. A. Reed, K. C. Kim, R. D. Bolskar, L. J. Mueller, *Science* **2000**, *289*, 101.

[17] A. A. Woolf, H. J. Emeleus, *J. Chem. Soc.* **1950**, 1050.

[18] S. Brownstein, *Can. J. Chem.* **1969**, *47*, 605.

[19] P. A. W. Dean, R. J. Gillespie, R. Hulme, *J. Chem. Soc. D* **1969**, 990.

[20] K. O. Christe, X. Zhang, R. Bau, J. Hegge, G. A. Olah, G. K. S. Prakash, J. A. Sheehy, *J. Am. Chem. Soc.* **2000**, *122*, 481.

[21] R. Minkwitz, C. Hirsch, T. Berends, *Eur. J. Inorg. Chem.* **1999**, 2249.

[22] R. Minkwitz, F. Neikes, *Inorg. Chem.* **1999**, *38*, 5960.

[23] A. J. Edwards, G. R. Jones, R. J. C. Sills, *Chem. Comm.* **1968**, 1527.

[24] S. Seidel, K. Seppelt, *Science* **2000**, *290*, 117.

[25] T. Drews, S. Seidel, K. Seppelt, *Angew. Chem. Int. Ed. Engl.* **2002**, *41*, 454.

[26] M. Bochmann, *Angew. Chem.* **1992**, *104*, 1206.

[27] K. Seppelt, *Angew. Chem.* **1993**, *105*, 1074.

[28] A. G. Massey, A. J. Park, *J. Organomet. Chem.* **1964**, *2*, 245.

[29] K. Fujiki, S.-Y. Ikeda, H. Kobayashi, A. Mori, A. Nagira, J. Nie, T. Sonoda, Y. Yagupolskii, *Chem. Lett.* **2000**, 62.

[30] J. H. Golden, P. F. Mutolo, E. B. Lobkovsky, F. J. DiSalvo, *Inorg. Chem.* **1994**, *33*, 5374.

[31] E. Y.-X. Chen, T. J. Marks, *Chem. Rev.* **2000**, *100*, 1391.

[32] J. van den Broeke, B.-J. Deelman, G. van Koten, *Tetrahedron Lett.* **2001**, *42*, 8085.

[33] K. Fujiki, J. Ichikawa, H. Kobayashi, A. Sonoda, T. Sonoda, *J. Fluorine Chem.* **2000**, *102*, 293.

[34] F. A. R. Kaul, G. T. Puchta, H. Schneider, M. Grosche, D. Mihalios, W. A. Herrmann, *J. Organomet. Chem.* **2001**, *621*, 177.

[35] L. Jia, X. Yang, A. Ishihara, T. J. Marks, *Organomet.* **1995**, *14*, 3135.

[36] L. Jia, X. Yang, C. L. Stern, T. J. Marks, *Organomet.* **1997**, *16*, 842.

[37] G. Rodriguez, P. Brant, *Organomet.* **2001**, *20*, 2417.

[38] M. Bochmann, M. J. Sarsfield, *Organomet.* **1998**, *17*, 5908.

[39] S. J. Lancaster, D. A. Walker, M. Thornton-Pett, M. Bochmann, *Chem. Comm.* **1999**, 1533.

[40] S. J. Lancaster, A. Rodriguez, A. Lara-Sanchez, M. D. Hannant, D. A. Walker, D. H. Hughes, M. Bochmann, *Organomet.* **2002**, *21*, 451.

[41] R. E. LaPointe, G. R. Roof, K. A. Abboud, J. Klosin, *J. Am. Chem. Soc.* **2000**, *122*, 9560.

[42] E. Bernhardt, M. Finze, H. Willner, C. W. Lehmann, F. Aubke, *Angew. Chem. Int. Ed. Engl.* **2003**, *42*, 2077.

[43] D. J. Brauer, H. Buerger, Y. Chebude, G. Pawelke, *Inorg. Chem.* **1999**, *38*, 3972.

[44] M. Finze, E. Bernhardt, A. Terheiden, M. Berkei, H. Willner, D. Christen, H. Oberhammer, F. Aubke, *J. Am. Chem. Soc.* **2002**, *124*, 15385.

[45] G. Pawelke, H. Burger, *Coord. Chem. Rev.* **2001**, *215*, 243.

[46] E. Bernhardt, G. Henkel, H. Willner, G. Pawelke, H. Burger, *Chem. Eur. J.* **2001**, *7*, 4696.

[47] M. Schmidt, A. Kühner, K.-D. Franz, G.-V. Röschenthaler, G. Bissky (Merck Patent GmbH, Germany), Application: 2001-10103189-10103189, **2002**.

[48] M. Schmidt, A. Kühner, H. Willner, E. Bernhardt (Merck Patent GmbH, Germany), Application: 2001-124917-1205480, **2002**.

[49] K. Koppe, V. Bilir, H.-J. Frohn, H. P. A. Mercier, G. J. Schrobilgen, *Inorg. Chem.* **2007**, *46*, 9425.

[50] M. Neukirch, S. Tragl, H. J. Meyer, T. Kueppers, H. Willner, *Z. Anorg. Allg. Chem.* **2006**, *632*, 939.

[51] T. J. Barbarich, S. M. Miller, O. P. Anderson, S. H. Strauss, *J. Mol. Cat. A* **1998**, *128*, 289.

[52] I. Krossing, H. Brands, R. Feuerhake, S. Koenig, *J. Fluorine Chem.* **2001**, *112*, 83.

[53] I. Krossing, *Chem. Eur. J.* **2001**, *7*, 490.

[54] S. M. Ivanova, B. G. Nolan, Y. Kobayashi, S. M. Miller, O. P. Anderson, S. H. Strauss, *Chem. Eur. J.* **2001**, *7*, 503.

[55] T. J. Barbarich, S. T. Handy, S. M. Miller, O. P. Anderson, P. A. Grieco, S. H. Strauss, *Organomet.* **1996**, *15*, 3776.

[56] S. H. Strauss, S. V. Ivanov (Colorado State University Research Foundation, USA), Application: 2000-704252-6335466, **2002**.

[57] M. V. Metz, Y. Sun, C. L. Stern, T. J. Marks, *Organomet.* **2002**, *21*, 3691.

[58] Y. Sun, M. V. Metz, C. L. Stern, T. J. Marks, *Organomet.* **2000**, *19*, 1625.

[59] B. T. King, J. Michl, *J. Am. Chem. Soc.* **2000**, *122*, 10255.

[60] I. Krossing, A. Reisinger, *Eur. J. Inorg. Chem.* **2005**, 1979.

[61] M. Gonsior, I. Krossing, L. Muller, I. Raabe, M. Jansen, L. Van Wullen, *Chem. Eur. J.* **2002**, *8*, 4475.

[62] I. Krossing, I. Raabe, *Angew. Chem. Int. Ed. Engl.* **2001**, *40*, 4406.

[63] M. Gonsior, I. Krossing, *Dalton Trans.* **2005**, 1203.

[64] A. Bihlmeier, M. Gonsior, I. Raabe, N. Trapp, I. Krossing, *Chem. Eur. J.* **2004**, *10*, 5041.

[65] I. Krossing, *J. Chem. Soc., Dalton Trans.* **2002**, 500.

[66] C. A. Reed, *Acc. Chem. R.* **1998**, *31*, 133.

[67] D. Stasko, C. A. Reed, *J. Am. Chem. Soc.* **2002**, *124*, 1148.

[68] T. Jelinek, J. Plesek, S. Hermanek, B. Stibr, *Coll. Czech. Chem. Comm.* **1986**, *51*, 819.

[69] K. Shelly, C. A. Reed, Y. J. Lee, W. R. Scheidt, *J. Am. Chem. Soc.* **1986**, *108*, 3117.

[70] T. Jelinek, P. Baldwin, W. R. Scheidt, C. A. Reed, *Inorg. Chem.* **1993**, *32*, 1982.

[71] S. M. Ivanova, S. V. Ivanov, b. S. M. Miller, O. P. Anderson, K. A. Solntsev, S. H. Strauss, *Inorg. Chem.* **1999**, *38*, 3756.

[72] K.-C. Kim, C. A. Reed, D. W. Elliott, L. J. Mueller, F. Tham, L. Lin, J. B. Lambert, *Science* **2002**, *297*, 825.

[73] T. Kueppers, E. Bernhardt, R. Eujen, H. Willner, C. W. Lehmann, *Angew. Chem. Int. Ed. Engl.* **2007**, *46*, 6346.

[74] E. S. Stoyanov, C. A. Reed, *J. Phys. Chem. A* **2006**, *110*, 12992.

[75] L. J. Mueller, D. W. Elliott, K.-C. Kim, C. A. Reed, P. D. W. Boyd, *J. Am. Chem. Soc.* **2002**, *124*, 9360.

[76] C. A. Reed, K.-C. Kim, E. S. Stoyanov, D. Stasko, F. S. Tham, L. J. Mueller, P. D. W. Boyd, *J. Am. Chem. Soc.* **2003**, *125*, 1796.

[77] C. A. Reed, N. L. P. Fackler, K.-C. Kim, D. Stasko, D. R. Evans, P. D. W. Boyd, C. E. F. Rickard, *J. Am. Chem. Soc.* **1999**, *121*, 6314.

[78] M. Juhasz, S. Hoffmann, E. Stoyanov, K.-C. Kim, C. A. Reed, *Angew. Chem. Int. Ed. Engl.* **2004**, *43*, 5352.

[79] S. V. Ivanov, J. J. Rockwell, O. G. Polyakov, C. M. Gaudinski, O. P. Anderson, K. A. Solntsev, S. H. Strauss, *J. Am. Chem. Soc.* **1998**, *120*, 4224.

[80] H. Willner, personal communication.

[81] E. Molinos, G. Kociok-Koehn, A. S. Weller, *Chem. Comm.* **2005**, 3609.

[82] A. J. Lupinetti, M. D. Havighurst, S. M. Miller, O. P. Anderson, S. H. Strauss, *J. Am. Chem. Soc.* **1999**, *121*, 11920.

[83] T. Kueppers, E. Bernhardt, R. Eujen, H. Willner, C. W. Lehmann, *Angew. Chem.* **2007**, *119*, 6462.

[84] D. M. Van Seggen, P. K. Hurlburt, M. D. Noirot, O. P. Anderson, S. H. Strauss, *Inorg. Chem.* **1992**, *31*, 1423.

[85] H. P. A. Mercier, J. C. P. Sanders, G. J. Schrobilgen, *J. Am. Chem. Soc.* **1994**, *116*, 2921.

[86] D. M. Van Seggen, P. K. Hurlburt, O. P. Anderson, S. H. Strauss, *Inorg. Chem.* **1995**, *34*, 3453.

[87] T. S. Cameron, I. Krossing, J. Passmore, *Inorg. Chem.* **2001**, *40*, 4488.

[88] D. M. Van Seggen, P. K. Hurlburt, O. P. Anderson, S. H. Strauss, *J. Am. Chem. Soc.* **1992**, *114*, 10995.

[89] P. K. Hurlburt, J. J. Rack, J. S. Luck, S. F. Dec, J. D. Webb, O. P. Anderson, S. H. Strauss, *J. Am. Chem. Soc.* **1994**, *116*, 10003.

[90] H. P. A. Mercier, M. D. Moran, G. J. Schrobilgen, C. Steinberg, R. J. Suontamo, *J. Am. Chem. Soc.* **2004**, *126*, 5533.

[91] M. Gerken, P. Kolb, A. Wegner, H. P. Mercier, H. Borrmann, D. A. Dixon, G. J. Schrobilgen, *Inorg. Chem.* **2000**, *39*, 2813.

[92] W. J. Casteel, Jr., P. Kolb, N. LeBlond, H. P. A. Mercier, G. J. Schrobilgen, *Inorg. Chem.* **1996**, *35*, 929.

[93] Z. Zak, A. Ruzicka, *Z. Krist.* **1998**, *213*, 217.

[94] R. Appel, G. Eisenhauer, *Chem. Ber.* **1962**, *95*, 2468.

[95] L. Turowsky, K. Seppelt, *Inorg. Chem.* **1988**, *27*, 2135.

[96] G. Klöter, H. Pritzkow, K. Seppelt, *Angew. Chem.* **1980**, *92*, 954.

[97] S. Seki, Y. Kobayashi, H. Miyashiro, Y. Ohno, A. Usami, Y. Mita, N. Kihira, M. Watanabe, N. Terada, *J. Phys. Chem. B* **2006**, *110*, 10228.

[98] L. A. Dominey, T. J. Blakley, V. R. Koch, *Proceedings of the 25th Intersociety Energy Conversion Engineering Conference* **1990**, 382.

[99] Z. Fei, D. Kuang, D. Zhao, C. Klein, W. H. Ang, S. M. Zakeeruddin, M. Grätzel, P. J. Dyson, *Inorg. Chem.* **2006**, *45*, 10407.

[100] J.-Y. Cheng, Y.-H. Chu, *Tetrahedron Lett.* **2006**, *47*, 1575.

[101] A. I. Bhatt, I. May, V. A. Volkovich, D. Collison, M. Helliwell, I. B. Polovov, R. G. Lewin, *Inorg. Chem.* **2005**, *44*, 4934.

[102] C. G. Frost, J. P. Hartley, D. Griffin, *Tetrahedron Lett.* **2002**, *43*, 4789.

[103] M. Kawamura, D.-M. Cui, S. Shimada, *Tetrahedron* **2006**, *62*, 9201.

[104] A. K. Chakraborti, Shivani, *J. Org. Chem.* **2006**, *71*, 5785.

[105] Y. L. Yagupolskii, T. I. Savina, I. I. Gerus, R. K. Orlova, *Zhurnal Organicheskoi Khimii* **1990**, *26*, 2030.

[106] K. Takasu, N. Shindoh, H. Tokuyama, M. Ihara, *Tetrahedron* **2006**, *62*, 11900.

[107] A. Sakakura, K. Suzuki, K. Nakano, K. Ishihara, *Org. Lett.* **2006**, *8*, 2229.

[108] A. Babai, A.-V. Mudring, *Inorg. Chem.* **2006**, *45*, 3249.

[109] C. Daguenet, P. J. Dyson, *Organomet.* **2006**, *25*, 5811.

[110] W. Dukat, D. Naumann, *Rev. Chim. Min.* **1986**, *23*, 589.

[111] E. Bernhardt, M. Finze, H. Willner, *J. Fluorine Chem.* **2004**, *125*, 967.

[112] J. P. Fackler, C. W. Liu, *Sci. Syn.* **2004**, *3*, 663.

[113] D. Naumann, W. Tyrra, F. Trinius, W. Wessel, T. Roy, *J. Fluorine Chem.* **2000**, *101*, 131.

[114] R. Eujen, B. Hoge, D. J. Brauer, *Inorg. Chem.* **1997**, *36*, 1464.

[115] R. Eujen, B. Hoge, D. J. Brauer, *Inorg. Chem.* **1997**, *36*, 3160.

[116] P. Y. Zavalij, S. Yang, M. S. Whittingham, *Acta Cryst. B* **2004**, *B60*, 716.

[117] S. Tsujioka, T. Mitsui, A. Tarora (Central Glass Co., Ltd., Japan), Application: 2005-359995-2007165125, **2007**.

[118] M. Wachtler, M. Wohlfahrt-Mehrens, S. Stroebele, J.-C. Panitz, U. Wietelmann, *J. App. Electrochem.* **2006**, *36*, 1199.

[119] U. Wietelmann, W. Bonrath, T. Netscher, H. Noeth, J.-C. Panitz, M. Wohlfahrt-Mehrens, *Chem. Eur. J.* **2004**, *10*, 2451.

[120] R. D. Shannon, C. T. Prewitt, *Acta Cryst.* **1969**, *B25*, 925.

[121] D. R. Lide, *CRC Handbook of Chemistry and Physics*, CRC Press, Boca Raton (USA) **2002**.

[122] H. D. B. Jenkins, H. K. Roobottom, J. Passmore, L. Glasser, *Inorg. Chem.* **1999**, *38*, 3609.

[123] H. D. B. Jenkins, J. F. Liebman, *Inorg. Chem.* **2005**, *44*, 6359.

[124] A. Kapustinskii, *Z. Phys. Chem.* **1933**, *B22*, 257.

[125] A. F. Kapustinskii, *Quart. Revs. (London)* **1956**, *10*, 283.

[126] H. K. Roobottom, H. D. B. Jenkins, J. Passmore, L. Glasser, *J. Chem. Edu.* **1999**, *76*, 1570.

[127] C. Shen, R. Hagiwara, T. E. Mallouk, N. Bartlett, *ACS Symposium Series* **1994**, *555*, 26.

[128] H. D. B. Jenkins, K. F. Pratt, *Proc. Royal Soc. London, A* **1977**, *356*, 115.

[129] T. S. Cameron, A. Decken, I. Dionne, M. Fang, I. Krossing, J. Passmore, *Chem. Eur. J.* **2002**, *8*, 3386.

[130] D. D. Wagman, W. H. Evans, V. B. Parker, R. H. Schumm, I. Halow, S. M. Bailey, K. L. Churney, R. L. Nuttall, *J. Phys. Chem. Ref. Data* **1982**, *11*, *Suppl. No. 2*, 392 pp.

[131] S. G. Lias, J. E. Bartmess, J. F. Liebman, J. L. Holmes, R. D. Levin, W. G. Mallard, *J. Phys. Chem. Ref. Data, Supp.* **1988**, *17*, 861.

[132] M. Born, *Z. Phys.* **1920**, *1*, 45.

[133] N. J. Patmore, C. Hague, J. H. Cotgreave, M. F. Mahon, C. G. Frost, A. S. Weller, *Chem. Eur. J.* **2002**, *8*, 2088.

[134] R. Braun, J. Sauer, *Chem. Ber.* **1986**, *119*, 1269.

[135] A. Flohr, H. Waldmann, *J. Prakt. Chem.* **1995**, *337*, 609.

[136] P. A. Grieco, J. J. Nunes, M. D. Gaul, *J. Am. Chem. Soc.* **1990**, *112*, 4595.

[137] A. Kumar, *Chem. Rev.* **2001**, *101*, 1.

[138] S. Saito, in *Lewis Acids in Organic Synthesis, Vol. 1*, Wiley-VCH, Weinheim, **2000**.

[139] S. Moss, B. T. King, A. de Meijere, S. I. Kozhushkov, P. E. Eaton, J. Michl, *Org. Lett.* **2001**, *3*, 2375.

[140] J. J. Rockwell, G. M. Kloster, W. J. DuBay, P. A. Grieco, D. F. Shriver, S. H. Strauss, *Inorg. Chim. Acta* **1997**, *263*, 195.

[141] P. A. Grieco, W. J. DuBay, L. J. Todd, *Tetrahedron Lett.* **1996**, *37*, 8707.

[142] W. J. DuBay, P. A. Grieco, L. J. Todd, *J. Org. Chem.* **1994**, *59*, 6898.

[143] C. Loncaric, K. Manabe, S. Kobayashi, *Adv. Syn. Cat.* **2003**, *345*, 475.

[144] S. D. Ittel, L. K. Johnson, M. Brookhart, *Chem. Rev.* **2000**, *100*, 1169.

[145] W. E. Piers, T. Chivers, *Chem. Soc. Rev.* **1997**, *26*, 345.

[146] W. E. Piers, G. J. Irvine, V. C. Williams, *Eur. J. Inorg. Chem.* **2000**, 2131.

[147] G. Erker, *Acc. Chem. R.* **2001**, *34*, 309.

[148] J. L. Atwood, D. C. Hrncir, R. D. Priester, R. D. Rogers, *Organomet.* **1983**, *2*, 985.

[149] M. R. Mason, J. M. Smith, S. G. Bott, A. R. Barron, *J. Am. Chem. Soc.* **1993**, *115*, 4971.

[150] C. J. Harlan, M. R. Mason, A. R. Barron, *Organomet.* **1994**, *13*, 2957.

[151] N. Bavarian, M. C. Baird, *Organomet.* **2005**, *24*, 2889.

[152] M.-C. Chen, J. A. S. Roberts, A. M. Seyam, L. Li, C. Zuccaccia, N. G. Stahl, T. J. Marks, *Organomet.* **2006**, *25*, 2833.

[153] V. C. Williams, G. J. Irvine, W. E. Piers, Z. Li, S. Collins, W. Clegg, M. R. J. Elsegood, T. B. Marder, *Organomet.* **2000**, *19*, 1619.

[154] J. Zhou, S. J. Lancaster, D. A. Walker, S. Beck, M. Thornton-Pett, M. Bochmann, *J. Am. Chem. Soc.* **2001**, *123*, 223.

[155] P. Wasserscheid, *Chem. unserer Zeit* **2003**, *37*, 52.

[156] P. Wasserscheid, W. Keim, *Angew. Chem. Int. Ed. Engl.* **2000**, *39*, 3772.

[157] T. Welton, *Chem. Rev.* **1999**, *99*, 2071.

[158] P. Bonhote, A.-P. Dias, N. Papageorgiou, K. Kalyanasundaram, M. Graetzel, *Inorg. Chem.* **1996**, *35*, 1168.

[159] A. S. Larsen, J. D. Holbrey, F. S. Tham, C. A. Reed, *J. Am. Chem. Soc.* **2000**, *122*, 7264.

[160] A. Bösmann, G. Francio, E. Janssen, M. Solinas, W. Leitner, P. Wasserscheid, *Angew. Chem. Int. Ed. Engl.* **2001**, *40*, 2697.

[161] Y. Fujita, K. Denpo (Nsk Ltd., Japan), Application: 2005-73727-2006258142, **2006**.

[162] M. B. Shiflett, A. Yokozeki (E. I. Du Pont De Nemours and Company, USA), Application: 2007-US12866-2007143051, **2007**.

[163] J. Qu, J. J. Truhan, S. Dai, H. Luo, P. J. Blau, *Tribology Lett.* **2006**, *22*, 207.

[164] D. Wei, A. Ivaska, *Anal. Chim. Acta* **2008**, *607*, 126.

[165] A. Hengstenberg, P. Tschuncky (Draegerwerk AG, Germany), Application: 2005-102005020719-102005020719, **2006**.

[166] K. Ding, Z. Miao, Z. Liu, Z. Zhang, B. Han, G. An, S. Miao, Y. Xie, *J. Am. Chem. Soc.* **2007**, *129*, 6362.

[167] G. Buhler, C. Feldmann, *Angew. Chem. Int. Ed. Engl.* **2006**, *45*, 4864.

[168] Y.-J. Zhu, W.-W. Wang, R.-J. Qi, X.-L. Hu, *Angew. Chem. Int. Ed. Engl.* **2004**, *43*, 1410.

[169] D. J. Tempel, P. B. Henderson, J. R. Brzozowski, R. M. Pearlstein, H. Cheng, *J. Am. Chem. Soc.* **2008**, *130*, 400.

[170] I. Krossing, J. M. Slattery, C. Daguenet, P. J. Dyson, A. Oleinikova, H. Weingaertner, *J. Am. Chem. Soc.* **2006**, *128*, 13427.

[171] C. Daguenet, P. J. Dyson, I. Krossing, A. Oleinikova, J. Slattery, C. Wakai, H. Weingaertner, *J. Phys. Chem. B* **2006**, *110*, 12682.

[172] N. J. Stone, D. A. Sweigart, A. M. Bond, *Organomet.* **1986**, *5*, 2553.

[173] C. G. Zoski, D. A. Sweigart, N. J. Stone, P. H. Rieger, E. Mocellin, T. F. Mann, D. R. Mann, D. K. Gosser, M. M. Doeff, A. M. Bond, *J. Am. Chem. Soc.* **1988**, *110*, 2109.

[174] B. Grossmann, J. Heinze, E. Herdtweck, F. H. Koehler, H. Noeth, H. Schwenk, M. Spiegler, W. Wachter, B. Weber, *Angew. Chem. Int. Ed. Engl.* **1997**, *36*, 387.

[175] R. J. LeSuer, W. E. Geiger, *Angew. Chem. Int. Ed. Engl.* **2000**, *39*, 248.

[176] F. Barriere, N. Camire, W. E. Geiger, U. T. Müller-Westerhoff, R. Sanders, *J. Am. Chem. Soc.* **2002**, *124*, 7262.

[177] P. G. Gassman, J. R. Sowa, Jr., M. G. Hill, K. R. Mann, *Organomet.* **1995**, *14*, 4879.

[178] P. G. Gassman, P. A. Deck, *Organomet.* **1994**, *13*, 1934.

[179] M. G. Hill, W. M. Lamanna, K. R. Mann, *Inorg. Chem.* **1991**, *30*, 4687.

[180] J. O. Besenhard, *Handbook of Battery Materials*, Wiley-VCH **1998**.

[181] M. Schmidt, A. Kuehner, K.-D. Franz, G.-V. Roeschenthaler, G. Bissky (Merck Patent G.m.b.H., Germany), Application: 2001-10103189-10103189, **2002**.

[182] N. Ignat'ev, P. Sartori, *J. Fluorine Chem.* **2000**, *101*, 203.

[183] F. Kita, H. Sakata, S. Sinomoto, A. Kawakami, H. Kamizori, T. Sonoda, H. Nagashima, J. Nie, N. V. Pavlenko, Y. L. Yagupolskii, *J. Power Sources* **2000**, *90*, 27.

[184] L. M. Yagupolskii, Y. L. Yagupolskii, *J. Fluorine Chem.* **1995**, *72*, 225.

[185] http://www.ionicliquids.de

[186] W. Xu, C. A. Angell, *Electrochem. Sol. St. Lett.* **2000**, *3*, 366.

[187] H. Suzuki, H. Naganawa, S. Tachimori, *Phys. Chem. Chem. Phys.* **2003**, *5*, 726.

[188] H. Naganawa, H. Suzuki, J. Noro, T. Kimura, *Chem. Comm.* **2005**, 2963.

[189] H. P. A. Mercier, M. D. Moran, G. J. Schrobilgen, *ACS Symposium Series* **2007**, *965*, 394.

[190] L. Müller, *Dissertation*, Albert-Ludwigs-Universität (Freiburg), **2008**.

[191] K. O. Christe, B. Hoge, J. A. Boatz, G. K. S. Prakash, G. A. Olah, J. A. Sheehy, *Inorg. Chem.* **1999**, *38*, 3132.

[192] E. Bernhardt, H. Willner, F. Aubke, *Angew. Chem. Int. Ed. Engl.* **1999**, *38*, 823.

[193] G. K. S. Prakash, J. W. Bausch, G. A. Olah, *J. Am. Chem. Soc.* **1991**, *113*, 3203.

[194] F. A. Carey, R. J. Sundberg, *Advanced Organic Chemistry, Vol. Part B: Reactions and Synthesis*, Springer, New York **2007**.

[195] L. L. da Rocha, R. Sparrapan, M. N. Eberlin, *Int. J. Mass Spectrom.* **2003**, *228*, 901.

[196] R. W. Taft, I. A. Koppel, R. D. Topsom, F. Anvia, *J. Am. Chem. Soc.* **1990**, *112*, 2047.

[197] G. W. Caldwell, T. B. McMahon, P. Kebarle, J. E. Bartmess, J. P. Kiplinger, *J. Am. Chem. Soc.* **1985**, *107*, 80.

[198] B. L. Dyatkin, E. P. Mochalina, I. L. Knunyants, *Tetrahedron* **1965**, *21*, 2991.

[199] C. J. Willis, *Coord. Chem. Rev.* **1988**, *88*, 133.

[200] R. D. Chambers, *Fluorine in Organic Chemistry*, Wiley, New York **1973**.

[201] A. Berkessel, J. A. Adrio, D. Huettenhain, J. M. Neudoerfl, *J. Am. Chem. Soc.* **2006**, *128*, 8421.

[202] K. F. Purcell, J. A. Stikeleather, S. D. Brunk, *J. Mol. Spectr.* **1969**, *32*, 202.

[203] R. M. Guidry, R. S. Drago, *J. Am. Chem. Soc.* **1973**, *95*, 759.

[204] O. Schrems, H. M. Oberhoffer, W. A. P. Luck, *J. Phys. Chem.* **1984**, *88*, 4335.

[205] W. J. Middleton, R. V. Lindsey, Jr., *J. Am. Chem. Soc.* **1964**, *86*, 4948.

[206] G. J. Moore, C. F. Smith, C. Tamborski, *J. Fluorine Chem.* **1975**, *5*, 77.

[207] C. Tamborski, W. H. Burton, L. W. Breed, *J. Org. Chem.* **1966**, *31*, 4229.

[208] A. F. Hollemann, N. Wiberg, *Lehrbuch der Anorganischen Chemie*, de Gruyter, Berlin-New York **1995**.

[209] W. Tyrra, D. Naumann, *J. Fluorine Chem.* **2005**, *126*, 1303.

[210] A. Kutt, I. Leito, I. Kaljurand, L. Soovali, M. V. Vlasov, M. L. Yagupolskii, A. I. Koppel, *J. Org. Chem.* **2006**, *71*, 2829.

[211] L. Soovaeli, I. Kaljurand, A. Kuett, I. Leito, *Anal. Chim. Acta* **2006**, *566*, 290.

[212] G. A. Jeffrey, *Cryst. Rev.* **2003**, *9*, 135.

[213] T. Steiner, W. Saenger, *Acta Cryst. B* **1992**, *B48*, 819.

[214] L. G. Hubert-Pfalzgraf, H. Guillon, *Appl. Organomet. Chem.* **1998**, *12*, 221.

[215] M. Veith, S. Weidner, K. Kunze, D. Kaefer, J. Hans, V. Huch, *Coord. Chem. Rev.* **1994**, *137*, 297.

[216] D. C. Bradley, *Chem. Rev.* **1989**, *89*, 1317.

[217] L. G. Hubert-Pfalzgraf, *Coord. Chem. Rev.* **1998**, *178-180*, 967.

[218] J. A. Samuels, E. B. Lobkovsky, W. E. Streib, K. Folting, J. C. Huffman, J. W. Zwanziger, K. G. Caulton, *J. Am. Chem. Soc.* **1993**, *115*, 5093.

[219] D. C. Bradley, H. Chudzynska, M. B. Hursthouse, M. Motevalli, *Polyhedron* **1993**, *12*, 1907.

[220] L. G. Hubert-Pfalzgraf, *New J. Chem.* **1995**, *19*, 727.

[221] D. C. Bradley, H. Chudzynska, M. B. Hursthouse, M. Motevalli, R. Wu, *Polyhedron* **1993**, *12*, 2955.

[222] T. Tsuda, T. Hashimoto, T. Saegusa, *J. Am. Chem. Soc.* **1972**, *94,* 958.

[223] T. Greiser, E. Weiss, *Chem. Ber.* **1976**, *109,* 3142.

[224] M. Hakansson, C. Lopes, S. Jagner, *Inorg. Chim. Acta* **2000**, *304*, 178.

[225] C. Lopes, M. Hakansson, S. Jagner, *Inorg. Chem.* **1997**, *36*, 3232.

[226] H. Schmidbaur, J. Adlkofer, A. Shiotani, *Chem. Ber.* **1972**, *105*, 3389.

[227] A. Reisinger, D. Himmel, I. Krossing, *Angew. Chem. Int. Ed. Engl.* **2006**, *45*, 6997.

[228] A. Reisinger, N. Trapp, I. Krossing, *Organomet.* **2007**, *26*, 2096.

[229] R. E. A. Dear, W. B. Fox, R. J. Fredericks, E. E. Gilbert, D. K. Huggins, *Inorg. Chem.* **1970**, *9*, 2590.

[230] J. A. Samuels, K. Folting, J. C. Huffman, K. G. Caulton, *Chem. Mater.* **1995**, *7*, 929.

[231] W. Tyrra, M. S. Wickleder, *Z. Anorg. Allg. Chem.* **2002**, *628*, 1841.

[232] I. Krossing, M. Gonsior, L. Müller (Universität Karlsruhe (TH), Germany), Application: 2004-EP12220-2005054254, **2005**.

[233] NIST Standard Reference Database **2008**, http://webbook.nist.gov/chemistry/.

[234] H. Plenio, *Chem. Rev.* **1997**, *97*, 3363.

[235] P. M. Jeffries, S. R. Wilson, G. S. Girolami, *J. Organomet. Chem.* **1993**, *449,* 203.

[236] R. D. Shannon, *Acta Cryst. A* **1976**, *A32*, 751.

[237] P. D. J. Grootenhuis, P. A. Kollman, *J. Am. Chem. Soc.* **1989**, *111*, 2152.

[238] G. Wipff, P. Weiner, P. Kollman, *J. Am. Chem. Soc.* **1982**, *104*, 3249.

[239] M. Lutz, M. Haukka, T. A. Pakkanen, M. McPartlin, L. H. Gade, *Inorg. Chim. Acta* **2003**, *345*, 185.

[240] F. Rivals, A. Steiner, *Chem. Comm.* **2001**, 2104.

[241] H. Plenio, R. Diodone, *J. Am. Chem. Soc.* **1996**, *118*, 356.

[242] P. G. Williard, Q.-Y. Liu, *J. Org. Chem.* **1994**, *59*, 1596.

[243] R. Amunugama, M. T. Rodgers, *J. Phys. Chem. A* **2002**, *106*, 9092.

[244] E. S. Meadows, S. L. De Wall, L. J. Barbour, G. W. Gokel, *J. Am. Chem. Soc.* **2001**, *123*, 3092.

[245] B. P. Hay, J. R. Rustad, *J. Am. Chem. Soc.* **1994**, *116*, 6316.

[246] A. Decken, H. D. B. Jenkins, G. B. Nikiforov, J. Passmore, *Dalton Trans.* **2004**, 2496.

[247] E. F. Pearson, W. Gordy, *Phys. Rev.* **1969**, *177*, 52.

[248] S. Ingemann, N. M. M. Nibbering, S. A. Sullivan, C. H. DePuy, *J. Am. Chem. Soc.* **1982**, *104*, 6520.

[249] N. Sato, K. Tanaka, S. Masaki, S. Yamazaki, K. Kimura, A. Nishichi, *J. Polym. Sci. A* **2007**, *45*, 2855.

[250] S. Doering, G. Erker, R. Froehlich, O. Meyer, K. Bergander, *Organomet.* **1998**, *17*, 2183.

[251] I. Raabe, *Dissertation*, Albert-Ludwigs-Universität (Freiburg), **2007**.

[252] H. Plenio, J. Hermann, R. Diodone, *Inorg. Chem.* **1997**, *36*, 5722.

[253] S. Steinhauser, U. Heinz, J. Sander, K. Hegetschweiler, *Z. Anorg. Allg. Chem.* **2004**, *630*, 1829.

[254] The Cambridge Structural Database (CSD), **2008**.

[255] W. Scherer, S. Altmannshofer, personal communication.

[256] E. Bernhardt, M. Berkei, H. Willner, M. Schuermann, *Z. Anorg. Allg. Chem.* **2003**, *629*, 677.

[257] K. C. Williams, T. L. Brown, *J. Am. Chem. Soc.* **1966**, *88*, 5460.

[258] I. D. Brown, *Struct. Bonding Cryst.* **1981**, *2*, 1.

[259] F. H. Allen, O. Kennard, D. G. Watson, L. Brammer, A. G. Orpen, R. Taylor, *J. Chem. Soc., Perkin Trans.* **1987**, *2*, 1.

[260] L. I. Zakharkin, V. V. Gavrilenko, Y. N. Karaksin, *Syn. React. Inorg., Metal-Org., Nano-Met. Chem.* **1971**, *1*, 37.

[261] A. E. Finholt, A. C. Bond, Jr., H. I. Schlesinger, *J. Am. Chem. Soc.* **1947**, *69*, 1199.

[262] I. Krossing, I. Raabe, *Chem. Eur. J.* **2004**, *10*, 5017.

[263] K. O. Christe, D. A. Dixon, D. McLemore, W. W. Wilson, J. A. Sheehy, J. A. Boatz, *J. Fluorine Chem.* **2000**, *101*, 151.

[264] I. Krossing, I. Raabe, *Angew. Chem. Int. Ed. Engl.* **2004**, *43*, 2066.

[265] A. Corma, H. Garcia, *Chem. Rev.* **2003**, *103*, 4307.

[266] L. Müller, D. Himmel, J. Stauffer, G. Steinfeld, J. Slattery, G. Santiso Quinones, V. Brecht, I. Krossing, *Angew. Chem. Int. Ed. Engl.* **2008**, *in press*.

[267] D. Lentz, K. Seppelt, *Z. Anorg. Allg. Chem.* **1983**, *502*, 83.

[268] M. J. Collins, G. J. Schrobilgen, *Inorg. Chem.* **1985**, *24*, 2608.

[269] F. Sladky, H. Kropshofer, O. Leitzke, *J. Chem. Soc., Chem. Comm.* **1973**, 134.

[270] V. C. Williams, W. E. Piers, W. Clegg, M. R. J. Elsegood, S. Collins, T. B. Marder, *J. Am. Chem. Soc.* **1999**, *121*, 3244.

[271] M. Finze, E. Bernhardt, M. Zähres, H. Willner, *Inorg. Chem.* **2004**, *43*, 490.

[272] T. Belgardt, J. Storre, H. W. Roesky, M. Noltemeyer, H.-G. Schmidt, *Inorg. Chem.* **1995**, *34*, 3821.

[273] D. Naumann, W. Tyrra, *J. Chem. Soc., Chem. Comm.* **1989**, 47.

[274] M.-C. Chen, J. A. S. Roberts, T. J. Marks, *Organomet.* **2004**, *23*, 932.

[275] L. Müller, I. Krossing, *in preparation*.

[276] A. H. Gomes de Mesquita, C. H. MacGillavry, K. Eriks, *Acta Cryst.* **1965**, *18*, 437.

[277] G. A. Olah, G. K. S. Prakash, *Carbocation Chemistry*, Wiley-VCH, New York **2004**.

[278] G. A. Olah, *Angew. Chem.* **1973**, *85*, 183.

[279] G. A. Olah, *Friedel-Crafts Chemistry*, Wiley-VCH, New York **1973**.

[280] D. W. A. Sharp, N. Sheppard, *J. Chem. Soc.* **1957**, 674.

[281] R. H. Martin, F. W. Lampe, R. W. Taft, *J. Am. Chem. Soc.* **1966**, *88*, 1353.

[282] R. W. Taft, R. H. Martin, F. W. Lampe, *J. Am. Chem. Soc.* **1965**, *87*, 2490.

[283] J. R. Greene, J. S. Francisco, J. Huang, D. Xu, W. M. Jackson, *J. Chem. Phys.* **2004**, *121*, 5868.

[284] G. A. Olah, G. Rasul, A. K. Yudin, A. Burrichter, G. K. S. Prakash, A. L. Chistyakov, I. V. Stankevich, I. S. Akhrem, N. P. Gambaryan, M. E. Vol'pin, *J. Am. Chem. Soc.* **1996**, *118*, 1446.

[285] G. A. Olah, G. Rasul, L. Heiliger, G. K. S. Prakash, *J. Am. Chem. Soc.* **1996**, *118*, 3580.

[286] H. Vancik, K. Percac, D. E. Sunko, *J. Am. Chem. Soc.* **1990**, *112*, 7418.

[287] J. W. Hudgens, R. D. Johnson, III, B. P. Tsai, S. A. Kafafi, *J. Am. Chem. Soc.* **1990**, *112*, 5763.

[288] G. A. Olah, Y. K. Mo, E. G. Melby, H. C. Lin, *J. Org. Chem.* **1973**, *38*, 367.

[289] C. Douvris, E. S. Stoyanov, F. S. Tham, C. A. Reed, *Chem. Comm.* **2007**, 1145.

[290] R. Minkwitz, S. Schneider, *Angew. Chem. Int. Ed. Engl.* **1999**, *38*, 714.

[291] R. Minkwitz, S. Reinemann, O. Blecher, H. Hartl, I. Brüdgam, *Inorg. Chem.* **1999**, *38*, 844.

[292] W. J. Lafferty, D. R. Lide, Jr., R. A. Toth, *J. Chem. Phys.* **1965**, *43*, 2063.

[293] T. J. Buckley, R. D. Johnson, R. E. Huie, Z. Zhang, S. C. Kuo, R. B. Klemm, *J. Phys. Chem.* **1995**, *99*, 4879.

[294] P. Botschwina, P. Sebald, M. Bogey, C. Demuynck, J. L. Destombes, *J. Mol. Spectr.* **1992**, *153*, 255.

[295] J. M. Dyke, N. Jonathan, A. Morris, M. J. Winter, *J. Chem. Soc., Faraday Trans. 2* **1981**, *77*, 667.

[296] E. Bernhardt, H. Willner, F. Aubke, *Angew. Chem. Int. Ed. Engl.* **1999**, *38*, 823.

[297] Y. A. Tobon, R. M. Romano, C. O. Della Vedova, A. J. Downs, *Inorg. Chem.* **2007**, *46*, 4692.

[298] M. Lantenois, *J. Pharm. et Chim.* **1914**, *10*, 185.

[299] T. Wentink, Jr., *J. Chem. Phys.* **1958**, *29*, 188.

[300] I. Raabe, K. Wagner, K. Guttsche, M. Wang, G. Santiso Quinones, I. Krossing, *submitted to Chem. Eur. J.* **2008**.

[301] M. Hesse, H. Meier, B. Zeeh, *Spektroskopische Methoden in der organischen Chemie*, Georg Thieme Verlag Stuttgart, New York **1995**.

[302] M. Gonsior, I. Krossing, *Chem. Eur. J.* **2004**, *10*, 5730.

[303] M. Kaupp, O. L. Malkina, V. G. Malkin, *Chem. Phys. Lett.* **1997**, *265*, 55.

[304] G. Diderrich, A. Haas, M. Yazdanbakhsch, *Chem. Ber.* **1977**, *110*, 916.

[305] B. Krebs, H. H. Beyer, *Z. Allg. Anorg. Chem.* **1969**, *365*, 199.

[306] J. Antel, K. Harms, P. G. Jones, R. Mews, G. M. Sheldrick, A. Waterfeld, *Chem. Ber.* **1985**, *118*, 5006.

[307] A. Waterfeld, R. Mews, *Chem. Ber.* **1985**, *118*, 4997.

[308] M. L. DeLucia, P. Coppens, *Inorg. Chem.* **1978**, *17*, 2336.

[309] R. F. W. Bader, *Atoms in Molecules. A Quantum Theory*, Oxford University Press, Oxford **1994**.

[310] H. W. Roesky, M. Thomas, J. Schimlowiak, P. G. Jones, W. Pinkert, G. M. Sheldrick, *J. Chem. Soc., Chem. Comm.* **1982**, 895.

[311] J. L. M. Abboud, I. Alkorta, J. Z. Davalos, J. F. Gal, M. Herreros, P. C. Maria, O. Mo, M. T. Molina, R. Notario, M. Yanez, *J. Am. Chem. Soc.* **2000**, *122*, 4451.

[312] J. L. M. Abboud, M. Herreros, R. Notario, M. Esseffar, O. Mo, M. Yanez, *J. Am. Chem. Soc.* **1996**, *118*, 1126.

[313] M. Di Vaira, L. Sacconi, *Angew. Chem.* **1982**, *94*, 338.

[314] A. P. Ginsberg, W. E. Lindsell, K. J. McCullough, C. R. Sprinkle, A. J. Welch, *J. Am. Chem. Soc.* **1986**, *108*, 403.

[315] T. Groeer, G. Baum, M. Scheer, *Organomet.* **1998**, *17*, 5916.

[316] M. Peruzzini, L. Marvelli, A. Romerosa, R. Rossi, F. Vizza, F. Zanobini, *Eur. J. Inorg. Chem.* **1999**, 931.

[317] H. Östmark, S. Wallin, N. Hore, O. Launila, *J. Chem. Phys.* **2003**, *119*, 5918.

[318] I. G. Dance, K. J. Fisher, G. D. Willett, *Inorg. Chem.* **1996**, *35*, 4177.

[319] P. Liu, C. Han, Z. Gao, F. Kong, Q. Zhu, *J. Phys. Chem. B* **1999**, *103*, 3337.

[320] H. W. Roesky, M. Witt, *Inorg. Syn.* **1986**, *24*, 72.

[321] I. Krossing, personal communication.

[322] Z. Xie, R. Bau, A. Benesi, C. A. Reed, *Organomet.* **1995**, *14*, 3933.

[323] K.-C. Kim, C. A. Reed, G. S. Long, A. Sen, *J. Am. Chem. Soc.* **2002**, *124*, 7662.

[324] R. J. Wehmschulte, J. M. Steele, J. D. Young, M. A. Khan, *J. Am. Chem. Soc.* **2003**, *125*, 1470.

[325] J. Slattery, I. Krossing, personal communication.

[326] G. Gerlach, W. Höhnle, A. Simon, *Z. Allg. Anorg. Chem.* **1982**, *486*, 7.

[327] W. Höhnle, G. Gerlach, W. Weppner, A. Simon, *J. Solid State Chem.* **1986**, *61*, 171.

[328] D. G. Tuck, *Polyhedron* **1990**, *9*, 377.

[329] H. Schmidbaur, *Angew. Chem. Int. Ed. Engl.* **1985**, *24*, 893.

[330] M. L. H. Green, P. Mountford, G. J. Smout, S. R. Speel, *Polyhedron* **1990**, *9*, 2763.

[331] R. E. Wasylishen, D. L. Bryce, C. J. Evans, M. C. L. Gerry, *J. Mol. Spectr.* **2000**, *204*, 184.

[332] J. W. Hastie, R. H. Hauge, J. L. Margrave, *J. Fluorine Chem.* **1973**, *3*, 285.

[333] J. S. Muenter, *J. Mol. Spectr.* **1975**, *55*, 490.

[334] P. D. Soper, A. C. Legon, W. H. Flygare, *J. Chem. Phys.*, *74*, 2138.

[335] I. D. Brown, *Acta Cryst. B* **1977**, *B33*, 1305.

[336] J. Wang, Z. Shi, R. J. Boyd, C. A. Gonzalez, *J. Phys. Chem.* **1994**, *98*, 6988.

[337] C. F. Matta, R. J. Boyd, *The Quantum Theory of Atoms in Molecules*, Wiley-VCH, Weinheim **2007**.

[338] A. Schafer, A. Klamt, D. Sattel, J. C. W. Lohrenz, F. Eckert, *Phys. Chem. Chem. Phys.* **2000**, *2*, 2187.

[339] A. Klamt, G. Schüürmann, *J. Chem. Soc., Perkin Trans. 2* **1993**, 799.

[340] I. Krossing, L. Müller, D. Himmel, personal communication.

[341] T. Köchner, personal communication.

[342] W. Zeil, J. Haase, L. Wegmann, *Z. Instr.* **1966**, *74*, 84.

[343] S. Gundersen, S. Samdal, T. G. Strand, H. V. Volden, *J. Mol. Struct.* **2007**, *832*, 164.

[344] S. L. Hinchley, H. E. Robertson, K. B. Borisenko, A. R. Turner, B. F. Johnston, H. Rankin, M. Ahmadian, J. N. Jones, A. H. Cowley, *Dalton Trans.* **2004**, 2469.

[345] A. W. Ross, M. Fink, R. Hilderbrandt, in *International Tables for Crystallography, Vol. C*, Kluwer Academic Publishers, Dordrecht, **1992**, p. 245.

[346] R. J. F. Berger, N. W. Mitzel, *in preparation*.

[347] V. A. Sipachev, *J. Mol. Struct.* **1985**, *121*, 143.

[348] A. D. Becke, *J. Chem. Phys.* **1993**, *98*, 5648.

[349] C. Lee, W. Yang, R. G. Parr, *Phys. Rev. B* **1988**, *37*, 785.

[350] M. J. Frisch, G. W. Trucks, H. B. Schlegel, G. E. Scuseria, M. A. Robb, J. R. Cheeseman, J. A. Montgomery, T. Vreven, K. N. Kudin, J. C. Burant, J. M. Millam, S. S. Iyengar, J. Tomasi, V. Barone, B. Mennucci, M. Cossi, G. Scalmani, N. Rega, G. A. Petersson, H. Nakatsuji, M. Hada, M. Ehara, K. Toyota, R. Fukuda, J. Hasegawa, M. Ishida, T. Nakajima, Y. Honda, O. Kitao, H. Nakai, M. Klene, X. Li, J. E. Knox, H. P. Hratchian, J. B. Cross, V. Bakken, C. Adamo, J. Jaramillo, R. Gomperts, R. E. Stratmann, O. Yazyev, A. J. Austin, R. Cammi, C. Pomelli, J. W. Ochterski, P. Y. Ayala, K. Morokuma, G. A. Voth, P. Salvador, J. J. Dannenberg, V. G. Zakrzewski, S. Dapprich, A. D. Daniels, M. C. Strain, O. Farkas, D. K. Malick, A. D. Rabuck, K. Raghavachari, J. B. Foresman, J. V. Ortiz, Q. Cui, A. G. Baboul, S. Clifford, J. Cioslowski, B. B. Stefanov, G. Liu, A. Liashenko, P. Piskorz, I. Komaromi, R. L. Martin, D. J. Fox, T. Keith, M. A. Al-Laham, C. Y. Peng, A. Nanayakkara, M. Challacombe, P. M. W. Gill, B. Johnson, W. Chen, M. W. Wong, C. Gonzalez, J. A. Pople, Gaussian 03 (Revision C.02), **2004**, Gaussian Inc.

[351] N. W. Mitzel, D. W. H. Rankin, *J. Chem. Soc., Dalton Trans.* **2003**, 3650.

[352] G. M. Sheldrick, T. R. Schneider, *NATO Sci. Ser. I: Life & Beh. Sci.* **2001**, *325*, 72.

[353] G. M. Sheldrick, SHELXL-97 - Program for crystal structure refinement, **1997**, University of Göttingen, Germany.

[354] A. L. Spek, PLATON - A Multipurpose Crystallographic Tool, **2008**, Utrecht University, The Netherlands.

[355] L. Palatinus, G. Chapuis, *J. App. Cryst.* **2007**, *40*, 786.

[356] R. Ahlrichs, M. Bär, M. Häser, H. Horn, C. Kölmel, *Chem. Phys. Lett.* **1989**, *162*, 165.

[357] J. P. Perdew, K. Burke, Y. Wang, *Phys. Rev. B* **1996**, *54*, 16533.

[358] A. D. Becke, *Phys. Rev. A* **1988**, *38*, 3098.

[359] F. Weigend, M. Haser, *Theor. Chem. Acc.* **1997**, *97*, 331.

[360] F. Weigend, M. Haser, H. Patzelt, R. Ahlrichs, *Chem. Phys. Lett.* **1998**, *294*, 143.

[361] A. Schäfer, C. Huber, R. Ahlrichs, *J. Chem. Phys.* **1994**, *100*, 5829.

[362] P. Deglmann, F. Furche, R. Ahlrichs, *Chem. Phys. Lett.* **2002**, *362*, 511.

[363] M. Kollwitz, J. Gauss, *Chem. Phys. Lett.* **1996**, *260*, 639.

[364] C. Ehrhardt, R. Ahlrichs, *Theor. Chim. Acta* **1985**, *68*, 231.

[365] R. Heinzmann, R. Ahlrichs, *Theor. Chim. Acta* **1976**, *42*, 33.

[366] A. E. Reed, R. B. Weinstock, F. Weinhold, *J. Chem. Phys.* **1985**, *83*, 735.

[367] F. W. Biegler-Koenig, R. F. W. Bader, T. H. Tang, *J. Comp. Chem.* **1982**, *3*, 317.

[368] T. A. Keith, AIMAll (Version 08.05.04), **2008**, http://aim.tgkristmill.com.

[369] J. C. Ortiz Alba, C. B. Jané, Xaim - X Atoms in Molecules (Version 1.0), http://www.quimica.urv.es/XAIM/.

[370] F. W. Biegler-Koenig, R. F. W. Bader, T. H. Tang, *J. Comp. Chem.* **1982**, *13*, 317.

[371] F. Eckert, A. Klamt, COSMOtherm, Version C2.1, Release 01.05, **2005**, COSMOlogic GmbH & Co. KG.

[372] E. Keller, SCHAKAL-99 for MS-Windows, **1999**, http://www.krist.uni-freiburg.de/ki/Mitarbeiter/Keller/schakal.html.

[373] L. J. Farrugia, *J. Appl. Cryst.* **1997**, *30*, 565.

[374] L. Laaksonen, *J. Mol. Graphics* **1992**, *10*, 33.

[375] C. A. Frenzel, K. E. Blick, C. R. Bennet, K. Niedenzu, *J. Chem. Phys.* **1970**, *53*, 198.